Gaze stabilization in mice : visuo-vestibular adaptation and predictive motor signaling during locomotion

Filipa França De Barros

THÈSE DE DOCTORAT

UNIVERSITÉ DE PARIS

Spécialité Neurosciences

École Doctorale Cerveau Cognition Comportement nº158

Présentée par

Filipa França de Barros

Pour obtenir le grade de

Docteure de Université de Paris

Sujet de la thèse

Gaze stabilization in mice: visuo-vestibular adaptation and predictive motor signaling during locomotion

Stabilisation du regard chez la souris : adaptation visuo-vestibulaire et signalisation prédictive pendant la locomotion

Soutenue publiquement le 04 Septembre 2020

Devant le jury composé de

Pr. Thérèse Collins	Université de Paris	Présidente du jury
Dr. Megan Carey	Fondation Champalimaud	Rapporteure
Dr. Muriel Thoby-Brisson	Université de Bordeaux	Rapporteure
Dr. Andrew Murray	Sainsbury Wellcome Center	Examinateur
Pr. Hans Straka	Ludwig Maximilian University of Munich	Examinateur
Dr. Pierre Pouget	Institut du Cerveau et de la Moelle épinière	Examinateur
Dr. Mathieu Beraneck	Université de Paris	Directeur de thèse

Statement

The *Université de Paris*, former *Université Paris Descartes*, was the home institution of the candidate. The work was directed by Dr. Mathieu Beraneck, group leader of the Spatial Orientation team of the Integrative Neuroscience and Cognition Center, the laboratory of the candidate. The candidate was a student at the doctoral school *École Doctorale Cerveau Cognition Comportement (ED 158)* and received a total of 200 hours of training provided by the *Institut de Formation Doctorale*.

The candidate participated in obtaining, interpreting, analyzing and discussing the results as well as writing the published works featured in this thesis. The work was also presented in the form of oral communications, in local national meetings, and posters were presented in two international meetings (FENS International Forum of Neuroscience 2017 and the Society for Neuroscience meeting 2019).

This work, developed between October 2016 and March 2020, was funded by the French entities: *Agence Nationale de la Recherche* (ANR, ANR-15-CE32-0007) *Centre national d'Études Spatiales* (CNES), and the *Centre National de la Recherche Scientifique* (CNRS).

II

Virtus unita fortius agit

Acknowledgements

'Virtus unita fortius agit'. I chose this sentence to start my thesis manuscript because it is the motto of my alma matter and it has always been present in my life during my academic years. 'The strength is in the union'. Little did I know that, after handing in my thesis, this sentence would gain a whole new meaning. At the beginning of 2020, a world pandemic emerged and has shown the power of being united, for good and for bad. The coronavirus defies global health by quickly spreading and affecting population worldwide. However, this difficult period, has showcased some of the best traits of humankind and has demonstrated how people can stand together, even while miles apart.

During my PhD, I was lucky enough to be part of a united front, full of people whose support and strength enabled me to make this thesis possible. I couldn't have done it without you; thank you for making me stronger.

I want to start by thanking all the jury members of this thesis for having accepted the invitation to read and evaluate my work. Particularly, I want to express my gratitude to my thesis follow up committee, Megan Carey and Pierre Pouget. Your time and advice during these years were very much appreciated.

Thank you Mathieu for enabling me to make one of my dreams come true. I'm extremely grateful to you for having believed in me and giving me this opportunity. Your continuous guidance, support and scientific advice were fundamental during these years. I will miss our conversations and being a part of the amazing team you have created. I'll forever cherish the wonderful memories I'm taking with me. De tout coeur, merci.

To the Spatial Orientation team, an authentic dream team, it was a pleasure to work with all of you! Michele, thank you for your humor, the scientific discussions and advice and for taking me along in a parabolic flight, a dream come true! Desdemona, thank you for sharing with me your scientific expertise and rigor that I certainly appreciated and will take with me. David, merci pour nôtres discussions et pour tes conseils sur les manips d'immunohistochimie. François, thank you for the laughs we shared (and for the surgical tools too!). To the most recent additions to the team, Jules and Flavia, I hope that you have the best time being members of this team; it was great getting to know you and I wish you good luck.

A big thank you to everyone at the former CNPP lab, new INCC, for making me feel welcomed since the first day and for having such a great work environment.

Un grand merci to a very special former member of this team, Julie. It was your guidance during the master that built in me a solid foundation for the PhD and I won't forget how supportive you were. It was a lot of fun having you back at the lab for our second paper together and I'm keeping that video as a souvenir of the times we shared.

An enormous thank you to Marin, the amazing 'mouse surgeon' that taught me all the intricate surgeries and inspired me to learn how to code. Your help and expertise were crucial for our project and I wish you the very best in your next endeavors.

To my fellow 'locogazers'. François, I enjoyed collaborating with you and I thank you for your dedication to our project and for your time (and humor!) and all the meetings we have. Denis, thank you for being at the origin of this project that was such a key part of my thesis. Julien, thank you for joining too, you're a great colleague and your expertise is very valuable.

Hélène, merci beaucoup de m'avoir accueilli dans ton labo et de m'avoir montré la belle cité de Marseille. Si j'ai apprécié mon temps à l'INT c'était grâce à toi ; je me suis senti très bienvenue et j'ai adoré les manips qu'on a fait ensemble. C'était vraiment un plaisir de faire ta connaissance.

To my colleagues Louise and Louis, thank you so much for our conversations, jokes, messages, parties and overall support. Your presence during these years was fundamental and you brightened up my days. I hope that in the future we continue working together and share more amazing moments. Louis, you were my first PhD colleague in the team and I was very happy to know that I was going to share the lab with your during these years. Our trip to Chicago was fantastic and I wish we can meet there again and have breakfast at Yolk! To Louise, thank you for your synchronized girl power, for always being there, our conversations about series and, of course, for joining our project.

I'm really thankful for Merouann and Susie, for going through this PhD experience with me from the get-go. Sharing the struggles with someone that understood made a big difference. To my brother in arms, Merouann; thank you for sharing with me the ups and downs of this journey and for becoming a true friend in the process. I'm sure great things await you! Susie, meeting you was wonderful, thank you for our lunch time and hallway conversations and for introducing me to raclette. Hope that in the future we can go on a ski trip together!

A very warm thank you to all my friends at Maison du Portugal. You made our residence feel like a home. Muito obrigada aos amigos que nesta casa fiz e que levo comigo para a vida. Em especial, àqueles que fiz enquanto membro do comité de residentes.

Quero também fazer um agradecimento muito especial à minha *alma mater*, a Universidade do Porto. Foram os anos passados nesta Universidade invicta que, para além de me ter permitido conhecer pessoas fantásticas, me formou e ajudou a trilhar este caminho em busca do conhecimento.

A toda a minha família um enorme obrigada por, com o vosso carinho, me terem dado forças ao longo destes anos. Muito obrigada André por desde o início me teres apoiado na decisão de fazer o doutoramento em Paris, mesmo sabendo o que isso implicaria. Obrigada por seres sempre o meu companheiro de viagem. Obrigada Raquel por partilhares comigo várias brincadeiras e me ajudares a pôr as situações em perspetiva quando assim o precisava. Estou muito orgulhosa de estares quase a ser veterinária; a vocação que foi feita à tua medida!

Muito obrigada aos meus pais que sempre estiveram presentes e acreditaram em mim, apostando desde cedo na minha educação. Obrigada Papi por sempre me ensinares a lutar pelos meus sonhos e me mostrares que o ‘não consigo’ não deve existir no nosso vocabulário. Obrigada Mami por toda a dedicação, as horas passadas na mesa da sala a rever a matéria para os testes da Miranda e por sempre me motivares a ser a melhor versão de mim. O vosso apoio incondicional foi o que me possibilitou chegar até aqui.

Abstract

Visual information is crucial to animal species to act on, interact with and orientate in their environment. Gaze stabilization allows adequate visual acuity by ensuring that the visual scene is held stationary on the retina, even during movement. Sensorimotor systems are responsible for gaze stabilization through the use of complementary inputs that ultimately move the eye in space and/or the head in space.

This thesis first reports studies of two brainstem-converging sensorimotor pathways that enable gaze stabilization in mice. Specifically, it investigates how visual (OKR) and vestibular (VOR) reflexes adapt in response to a long-term visual perturbation. This was performed by means of a 2 weeks visuo-vestibular mismatch protocol in freely-behaving mice (França de Barros et al., 2019). At a first instance, we demonstrated that the long term visuo-vestibular mismatch protocol lead to plasticity outside the cerebellum, namely in the direct VOR pathway (Carcaud et al., 2017). Neural changes occurred in the synaptic transmission and intrinsic properties of central vestibular neurons. Next, the adaptation and recovery dynamics of the OKR and VOR reflexes were compared in two mismatches that differed in the amount of retinal slip (França de Barros et al, in preparation[1]). We found that the two conditions were comparable, both leading to larger changes in the VOR than in the OKR. The dynamic of these plastic changes was largely frequency-dependent, with a delayed recovery for frequencies lower than 1Hz. Overall, these data provide evidence for sequential cascades of plasticity in the OKR/VOR pathways.

In addition to classical sensorimotor pathways, recent evidence demonstrated in Xenopus tadpoles the role of predictive motor signaling in helping minimize visual disturbances during locomotion. This thesis proceeds by exploring whether that predictive signal, coupling eye movements to locomotion, is phylogenetically preserved in mammals (França de Barros et al. in preparation[2]). Using a precollicular and premamillary decerebrated head-fixed adult mouse preparation, we found consistent correlation between treadmill locomotion evoked in dark and conjugated eye movements. To determine the influence of the cervical and lumbar spinal locomotor CPGs on the eye's motor nuclei, the activity of spinal and abducens motor nerves was recorded simultaneously *ex vivo* in isolated brainstem-spinal cord preparations of neonatal mice. Rhythmic coupled discharge was found between limb and abducens motor nerve activities during fictive locomotor bouts elicited by electrical or

pharmacological stimulation. To map the neuronal pathway that couples the cervical CPG and the abducens nuclei, rabies virus (RV) was injected in the lateral rectus muscle of adult mice. We found infected (RV+) motoneurons (revealed by ChAT labelling) in the ipsilateral abducens nucleus as well as RV+ interneurons along the cervical spinal cord. This study for the first time demonstrated that a cervical CPG-driven efference copy directly couples eye movements with forelimb movement during vigorous locomotion in mice.

Furthermore, this thesis features a collaboration with the group of Saaid Safieddine at *Institut Pasteur* where AAV-mediated gene therapy was used to durably restore the auditory and vestibular functions of a mouse model of Usher 1 syndrome. USH1$^{-/-}$ mice display profound deafness and locomotor dysfunction suggesting vestibular disorders. In this study, our team measured the vestibule-ocular reflexes from canal and otolith origin of treated or non-treated Knock-out USH1$^{-/-}$ mice using videoculography. While USH1$^{-/-}$ mice failed to evoke compensatory eye movements, injected USH1$^{-/-}$ mice exhibited responses that were close to those of wild-type. Hence, the AVV-mediated gene therapy was able to restore the vestibular function. This seminal study has since led to several ongoing collaboration with other groups at Pasteur institute all aiming at developing new therapeutic lines for patients suffering from inner ear pathologies.

Overall, this thesis provides insight to the functional complementarity of reflexive pathways participating in gaze stabilization as well as their adaptation to different behavioral and environmental contexts.

Keywords: gaze stabilization, VOR, OKR, vestibular, brainstem, sensorimotor, efferent copy, central pattern generators, motor-to-motor coupling.

Résumé

L'information visuelle est cruciale pour que les espèces animales agissent, interagissent et s'orientent dans leur environnement. La stabilisation du regard permet une acuité visuelle adéquate en garantissant que la scène visuelle est maintenue immobile sur la rétine, même pendant le mouvement. Les systèmes sensorimoteurs sont responsables de la stabilisation du regard grâce à l'utilisation d'entrées complémentaires qui finissent par déplacer l'œil dans l'espace et / ou la tête dans l'espace.

Cette thèse présente toute d'abord des études qui concernent les deux voies sensorimotrices convergentes du tronc cérébral qui permettent la stabilisation du regard chez la souris. Plus précisément, nous étudions comment les réflexes d'origine visuelle (réflexe optocinétique ou OKR) et vestibulaire (réflexe vestibulo-oculaire ou VOR) s'adaptent en réponse à une perturbation visuelle persistante. Cela a été réalisé au moyen d'un protocole de conflit visuo-vestibulaire de 2 semaines chez des souris libres de leurs mouvements (França de Barros et al., 2019). Dans un premier temps, nous avons démontré que le protocole de conflit visuo-vestibulaire à long terme conduit à une plasticité en dehors du cervelet, notamment dans la voie directe du VOR (Carcaud et al., 2017). Des modifications plastiques ont été mises en évidence dans la transmission synaptique entre les afférents vestibulaires et les neurones vestibulaires centraux d'une part, et dans les propriétés intrinsèques de certains neurones vestibulaires centraux d'autre part. Ensuite, la dynamique d'adaptation et de récupération des réflexes OKR et VOR a été comparée dans deux mésappariements qui différaient dans la quantité de glissement rétinien (França de Barros et al., en préparation[1]). Nous avons constaté que les deux conditions étaient comparables, entraînant toutes deux des changements plus importants dans le VOR que dans l'OKR. La dynamique de ces changements plastiques est très largement dépendante de la fréquence, avec une récupération retardée pour les fréquences inférieures à 1 Hz. Dans l'ensemble, ces données fournissent des données expérimentales concernant les cascades séquentielles de plasticité dans les voies réflexes de stabilisation du regard et montrent les interdépendances fonctionnelles entre le VOR et l'OKR.

En plus des voies sensorimotrices classiques, des preuves récentes ont démontré chez les têtards de Xénope le rôle de la signalisation motrice prédictive dans la réduction des perturbations visuelles pendant la locomotion. Nous avons exploré si ce signal prédictif, couplant les mouvements oculaires à la locomotion, est phylogénétiquement

conservé chez les mammifères (França de Barros et al., en préparation [2]). En utilisant une préparation précolliculaire et prémamillaire décérébrée de souris adultes, maintenue tête fixe, nous avons montré que la locomotion entraînée par le tapis roulant provoque des mouvements des yeux bilatéraux et conjugués. Pour déterminer l'influence des CPG (Central Pattern Generator) locomoteurs des rachis cervical et lombaire sur les noyaux moteurs de l'œil, l'activité des nerfs moteurs rachidiens et abducens a été enregistrée simultanément ex vivo dans des préparations isolées de tronc cérébral et de moelle épinière de souris néonatales. Une décharge couplée rythmique a été trouvée entre les activités du membre et du nerf moteur abducens lors d'épisodes locomoteurs fictifs provoqués par une stimulation électrique ou pharmacologique. Pour cartographier la voie neuronale qui couple le CPG cervical et les noyaux abducens, le virus de la rage (RV) a été injecté dans le muscle droit latéral des souris adultes. Nous avons trouvé des motoneurones infectés (RV^+) (révélés par le marquage ChAT) dans le noyau abducens ipsilatéral ainsi que des interneurones RV + le long de la moelle épinière cervicale. Cette étude a pour la première fois démontré qu'une copie d'efférence pilotée par le CPG cervical couple directement les mouvements oculaires avec le mouvement des membres antérieurs pendant une locomotion soutenue chez la souris.

Aditionellement, cette thèse présente une collaboration avec le groupe de Saaid Safieddine de l'Institut Pasteur où la thérapie génique médiée par l'AAV a été utilisée pour restaurer durablement les fonctions auditives et vestibulaires d'un modèle murin du syndrome d'Usher 1. Les souris $USH1^{-/-}$ présentent une surdité profonde et un dysfonctionnement locomoteur suggérant des troubles vestibulaires. Dans cette étude, notre équipe a mesuré par vidéoculographie les réflexes vestibulo-oculaires d'origine canalaire et otolitique de souris Knock-out $USH1^{-/-}$. Alors que les souris $USH1^{-/-}$ non injectées n'ont pas réussi à évoquer des mouvements oculaires compensatoires, les souris $USH1^{-/-}$ injectées ont présenté des réponses proches de celles de type sauvage. Par conséquent, la thérapie génique médiée par AVV a pu restaurer la fonction vestibulaire. Cette étude a conduit à plusieurs collaborations avec groupes de l'Institut Pasteur visant tous à développer de nouvelles lignes thérapeutiques pour les patients souffrant de pathologies de l'oreille interne.

Globalement, les travaux présentés dans cette thèse permettent de mieux comprendre les complémentarités fonctionnelles des voies réflexes impliquées dans les mécanismes de stabilisation du regard ainsi que leurs adaptations à différents contextes comportementaux et à des changements de l'environnement.

Mots-clés : stabilisation du regard, réflexe vestibulo-oculaire, réflexe optocinétique, tronc cérébral, sensorimoteur, copie d'efférence, générateur central du patron locomoteur, couplage moteur.

Preface

Gaze stabilization helps to ensure visual acuity by holding the visual scene stationary on the retina. The convergence of visual, vestibular and proprioceptive inputs and their integration in brainstem structures is known to generate active gaze stabilization.

Within this framework, this thesis aims at two distinct but complementary goals: 1) to study the adaptability and kinematics of gaze stabilizing reflexes after the visual and vestibular inputs undergo a long-term perturbation; 2) to decipher if mammals, in addition to the classical sensorimotor pathways, use predictive motor signaling during locomotion to stabilize gaze.

The first goal originated three projects. During my first year at the laboratory, as a master's intern, the team had an ongoing project that consisted in studying the effects of a long-term visuo-vestibular perturbation on the direct VOR pathway (Carcaud et al., 2017). The design of this protocol allowed not only for *in vivo* video-oculography recordings of the gaze stabilizing reflexes, but also for *in vitro* electrophysiological recordings of central vestibular neurons. This dataset, to which I contributed both with behavioral and electrophysiological data, was finalized in the first few months of my PhD. For this study, mice were exposed during 2 weeks to a visuo-vestibular (VVM) mismatch that consisted of a helmet-like device fixed onto their heads. With this VVM device, mice could freely behave in their cages while constantly being exposed to a VOR motor learning protocol. When the device was removed at the end of the protocol, a 50% decrease of the VOR gain was registered. Flocculus shut down experiments combined with VOR and OKR tests showed that this decrease was located outside the flocculus/paraflocculus complex. The neuronal mechanisms of this reduction were further investigated in MVN neurons of brainstem slices using afferent stimulations and patch-clamp recordings. The stimulation of the VIIIth nerve demonstrated that the amplitude of the evoked EPSCs were decreased in adapted mice. Additionally, the analysis of membrane properties of MVN neurons showed that a subpopulation of vestibular neurons (type A) presented a decrease in spontaneous discharge and excitability. In sum, this study shows that a long-lasting visuo-vestibular mismatch leads to changes in synaptic transmission and intrinsic properties of central vestibular neurons in the direct VOR pathway. Hence, our results provide direct evidence to the hypothesis of consolidation of long-term VOR changed in the brainstem.

Long-term sensory conflict protocols are a valuable means of studying motor learning. Therefore, the next goal for this thesis was to further optimize the VVM protocol used in the aforementioned study (França de Barros et al., 2019). By being fixed on mice heads, this device creates an enduring sensory conflict making it a great tool for long-term learning experiments. This helmet-like structure respects the anatomy of the snout of mice and therefore allows barbering, feeding and drinking behaviors. Several aspects like the production, cost, material and final weight of the device were optimized to render an improved methodology. The production passed from manual to serial through the use of a 3D printer which consequently lowered the cost of production as well as a bigger reproducibility rate between different experimenters and laboratories. The material used for its production was also switched to a poly lactic plastic that enabled a lighter weight. Subsequently, the steps for device assembly and surgery animal care related to this innovative VVM protocol were detailed and published in a written and audiovisual form so that it became available to any other laboratory that could benefit from it (Article 2. Long-term Sensory Conflict in Freely Behaving mice).

The concluding project of the first goal of this thesis studied the kinematics of recovery of the gaze stabilizing reflexes after a long-term sensory conflict. In this project both the optokinetic and vestibulo-ocular reflexes were tested on the removal of the VVM device as well as 1, 2, and 6 after. We found that VOR changes persist for at least 2 days after the end of the VVM protocol. Additionally, we report for the first time that the OKR is affected as well; its responses suffer from a 30% decrease on the day of the end of the protocol, and report on the recovery dynamics of both VOR and OKR after the end of the VVM protocol. Using sinusoidally-modulated stimulations, the decreases in VOR and OKR were found to be frequency-selective with larger reductions for frequencies <0.5Hz. Nonetheless, the OKR decrease is more transient since all the tested conditions rapidly recover their initial gains. Hence, our data are compatible with the hypothesis of sequential cascades of plasticity in the OKR/VOR pathways.

To identify the signals driving VOR and OKR reductions, we compared the responses of mice exposed to a high-contrast and no-contrast VVM. The VVM protocol in Carcaud et al., 2017 used exposure to a high-contrast pattern during training sessions to evoke a strong error signal that would drive motor learning of the VOR. In this study, apart from that high-contrast pattern VVM device, we also applied a no-pattern model of this device without any pattern on it. Surprisingly, we found no major differences between both types of devices in neither the magnitude of the decrease of the response nor in the recovery dynamics. The no-pattern device tended to produce milder adaptation, but few of these differences reached significance. This result suggests that rather than an error

signal (retinal slip), it is more the decorrelation absence of visual feedback which would be responsible of the reduction in OKR and VOR (Chapter III- Results; Article 3).

The second goal of this thesis is rendered in the project named “LOCOGAZE”, an acronym for “Evolutionary and developmental neurophysiological substrates for gaze stabilization strategies during locomotion in vertebrates”. This work, granted by the French National Agency for Research (ANR), initially involved 2 collaborating laboratories: Institut de Neurosciences Cognitives et Integratives d'Aquitaine (INCIA, Bordeaux) and our lab, the Integrative Neuroscience and Cognition Center (INCC, Paris). A collaboration was also made with the Institut de Neurosciences de la Timone (INT, Marseille), where I carried on the rabies virus experiments. These teams worked to characterize, in the mouse, the influence of an efference copy generated in the spinal locomotor network on gaze stabilization (França de Barros et al, in preparation). It was the INCIA team that in 2008 (Combes et al., 2008) first reported in Xenopus tadpoles a predictive feed-forward signaling from the spinal locomotor CPGs engaged in eye movement during fictive swimming. Since this was discovery done in semi-intact head-fixed tadpoles, it raised the question of whether this spino-extraocular pathway is conserved through phylogeny in mammals. This thesis aimed at investigating the existence of this pathway in mice and to characterize it (Article 4. Locomotor CPG-driven efferent copy couples eye movements with forelimb locomotion in mice). We did so through a multimethodological approach that combined semi intact preparations, *ex vivo* as well as *in vivo* experiments.

A precollicular and premammillary decerebrated head-fixed adult mouse preparation was used to unmask this efferent copy in a behaving mouse. We found consistent correlation between treadmill locomotion evoked in dark and conjugated eye movements. The trot-like locomotion bouts lasted between 10-40s and evoked conjugated horizontal eye movements with slow phases between 5-10º amplitude and 1-5Hz frequency range. Additionally, to determine the influence of the cervical and lumbar spinal locomotor CPGs on the eye’s motor nuclei, the activity of spinal and abducens motor nerves was recorded simultaneously *ex vivo* in isolated brainstem-spinal cord preparations of neonatal mice. Rhythmic coupled discharge was found between limb and abducens motor nerve activities during fictive locomotor bouts elicited by electrical or pharmacological stimulation. The isolated activation of cervical or lumbar CPG activity revealed that cervical but not lumbar network output is sufficient to drive abducens nerve discharge. We used rabies virus to map the neuronal pathway that pairs the cervical CPG with the abducens nuclei. Injections in the lateral rectus muscle of adult mice marked motoneurons in the ipsilateral abducens nucleus and interneurons in the

cervical spinal cord, revealing a direct pathway connecting the cervical spine to oculomotor neurons.

Overall, the original studies conducted by our team during this thesis provide insight to the functional complementarity of reflexive pathways participating in gaze stabilization as well as their adaptation to different behavioral and environmental contexts.

Finally, this thesis features a collaboration with *Institut Pasteur* (Article 5. Local gene therapy durable restores vestibular function in a mouse model of Usher syndrome type 1G) where adeno associated virus (AAV)-mediated gene therapy was used to restore the auditory and vestibular functions of an Usher syndrome type 1(USH1) mouse model (Emptoz et al., 2017). USH1 patients suffer from congenital profound deafness and balance disorders and, currently, there is no available treatment for this pathology. In this study, the scaffold protein *sans*, which is involved in the morphogenesis of the inner ear hair cells, was restituted in USH1 mice by the delivery of its cDNA through an AAV. This restored the functionality of stereociliary bundles and consequently improved hearing thresholds and regained the locomotor and postural behaviors. However, the demonstration of the restauration of vestibular function was lacking. To that end, the restoring of the vestibular function was evaluated by measuring the specific vestibulo-ocular responses. No compensatory eye movements were registered in USH1$^{-/-}$ mice, and various tests indicated a total loss of function of both semicircular canals and otolithic organs. On the other hand, AAV-treated USH1$^{-/-}$ mice responses to the same tests were indistinguishable from wild-type mice hence, indicating the vestibular function had been restored. This result, based on video-oculography, provided the definitive evidence of the efficacy of the treatment on vestibular-specific pathways. We could further show that this restauration was persisting for more than a year after the single treatment injection, indicating the potential of this therapy for long term healing. This seminal study has since led to several ongoing collaborations between my group and groups at *Pasteur Institute*. It demonstrates how the expertise developed to gain basic knowledge about vestibular function can be translated into studies which aim at developing new therapeutic lines for patients suffering from inner ear pathologies.

Table of contents

List of abbreviations

AAV	Adeno-Associated Virus
aCSF	artificial Cerebrospinal Fluid
ANOVA	Analysis of Variance
AHP	After Hyperpolarization
AOS	Accessory Optic System
AVOR	Angular Vestibulo-Ocular Reflex
BT	Burst-Tonic
cDNA	Complementary Deoxyribonucleic Nucleic Acid
CNS	Central Nervous System
CPG	Central Pattern Generator
CR	Corneal Reflection
CVS	Challenge Virus Standard
DNA	Deoxyribonucleic Nucleic Acid
DSCT	Dorsal Spinocerebellar Tract
DSRGC	Direction Selective Retinal Ganglion Cell
DTN	Dorsal Terminal Nucleus
DVN	Descending Vestibular Nucleus
EH	Eye-Head
EOM	Extraocular Muscles
EPSC	Excitatory post-synaptic currents
ES	Eye movement-sensitive
FTN	Floccular Target Neurons
GFP	Green Fluorescent Protein
HVOR	Horizontal Vestibulo-Ocular Reflex
IP	Intraperitoneal
IR	Infrared
IV	Intravenous
KO	Gene knockout
LED	Light-emitting Diode
LOIN	Last Order Interneuron

LTD	Long-Term Depression
LTN	Lateral Terminal Nucleus
LVN	Lateral Vestibular Nucleus
LVST	Lateral Vestibulo-spinal Tract
MET	Mechanoelectrical transduction
MLF	Medial Longitudinal Fasciculus
MLR	Mesencephalic Locomotor Region
MN	Motoneuron
MOR	Maculo-Ocular Reflex
MR	Medial Rectus
MRF	Medullary Reticular Formation
MTN	Medial Terminal Nucleus
MVN	Medial Vestibular Nucleus
MVST	Medial Vestibulo-Spinal Tract
NOT	Nucleus of the Optic Tract
nAChR	Nicotinic Acetylcholine Receptor
NPH	Nucleus Prepositus Hypoglossi
NRTP	Nucleus Reticularis Tegmenti Pontis
N-T	Naso-Temporal
OFR	Ocular Following Response
OKAN	Optokinetic After Nystagmus
OKN	Optokinetic Nystagmus
OKR	Optokinetic Reflex
OVAR	Off Vertical Axis Rotation
PBS	Phosphate Buffer Saline
PC	Purkinje Cells
pCO_2	partial pressure of carbon dioxide
PFA	Paraformaldehyde
PLA	Poly Lactic Acid
PNS	Peripheric nervous system
PVP	Position-Vestibular-Pause neurons
RGC	Retinal Ganglion Cells
RNA	Ribonucleic Acid
RT	Room Temperature

RV	Rabies Virus
SC	Superior Colliculus
SEM	Standard Error of the Mean
SLR	Subthalamic locomotor region
SVN	Superior Vestibular Nucleus
T-N	Temporo-Nasal
TVOR	Translational Vestibulo-Ocular Reflex
USH1	Usher Syndrome type 1
VAF	Variance Accounted For
VCR	Vestibulocollic
VN	Vestibular Nucleus
VO	Vestibular-Only
VOR	Vestibulo-Ocular Reflex
VSCT	Ventral Spinocerebellar Tract
VSR	Visuo-spinal reflex
VVM	Visuo-Vestibular Mismatch
WT	Wild Type
1ºVN	First order Vestibular Neuron
2ºVN	Second order Vestibular Neuron

List of figures

List of tables

Chapter I –

Introduction

1. Eye movements in vertebrates

All vertebrate species, regardless of their visual acuity, share the need to avoid motion blur, this is, to stabilize gaze (Walls, 1962). They do so because the visual system directly perceives what the eyes see and proceeds to stabilize them in response to expected (self-generated) or unexpected (other-generated) movements. Hence, gaze stabilization is the capability of maintaining the orientation of the eyes in space during head or body movements so the visual scene remains still in the retina (Angelaki, 2004; Cullen, 2012). Gaze stabilization is ubiquitous in vertebrates. In mammals, it largely depends on the combination of head-on-body and eye-in-head movements.

Visual encoding in vertebrates is constrained by two main characteristics: the anatomy of the eye and the type of eye movements (M. F. Land, 2013). Anatomically, an element that defines the eye of an animal is the presence of a fovea; a small (<1% of the retina's area) and central pit in the retina that encompasses the highest density of retinal ganglion cells (Büttner & Büttner-Ennever, 2006). This unique characteristic provides the capacity to encode high visual acuity and is present in humans, primates and some reptiles (Slonaker, 1897). It is important to note that most mammals lack this foveal specialization, *i.e*, they're nonfoveate or afoveate mammals (Chalupa & Williams, 2008). Some of them, like cats, have a functionally comparable *area centralis,* while rabbits have a 'visual streak' (Rapaport & Stone, 1984). Mice bear neither a fovea nor one of the equivalent specialized areas (Slonaker, 1897) and recent studies show that their retinal ganglion cells, instead of being densely focalized in one region, are heterogeneously spread on the retina according to their functional properties, to allow better representation of the different stimulus characteristics (Warwick et al., 2018). Having no fovea hinders the performance of eye movements that require high spatial resolution and or a specialized circuitry like smooth pursuit and vergence (John S. Stahl, 2004).

Another important anatomical point is the location of the eyes on the skull (**Figure 1**). The eyes can be placed more or less laterally or frontally relatively to the center of the skull. For example, the eyes of primates are frontally-positioned (0º between the eye axis and center of the skull) and thus, due to the big binocular overlap, a large visual field can be perceived (M. F. Land, 2013). This positioning, together with the presence of a fovea, allows higher primates to visualize in detail at near and far distance, as well as enabling stereoscopic vision. On the other end, are animals with laterally placed eyes. The greater spacing between both eyes implies bigger angles between the head axis and optical axes. Therefore, lateral-eyed species tend to have a smaller binocular

overlap than frontal-eyed ones. However, the orbit convergence (degree to which the bony orbital margins face the same direction) is also a preponderant factor in rendering binocular overlap since it also takes into account the vertical orientation (Heesy, 2004). Mice, based on an interocular distance of 1cm and an optical convergence of 38,3º, have a binocular field of 40º (Drager, 1978; Heesy, 2004; Samonds et al., 2019). The monocular field of mice is much bigger, attaining 104º (Samonds et al., 2019). Functionally, this allows mice to perceive a larger field, thus enabling the detection of a predator approaching from various angles.

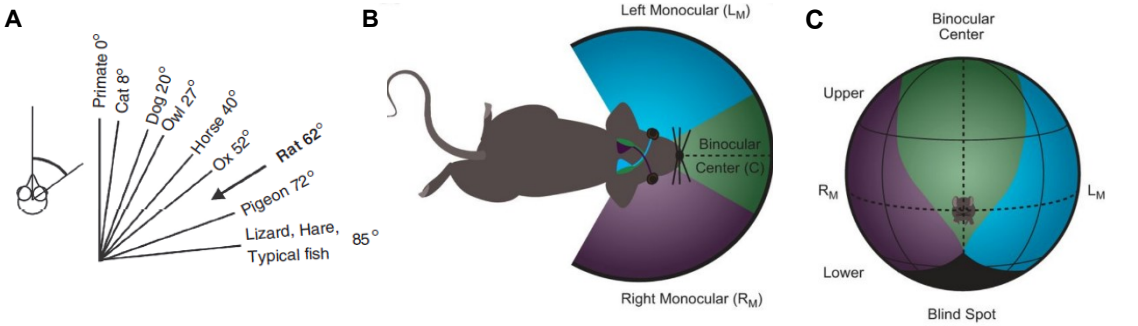

Figure 1. Position of the eyes in respect to the visual field. A- Schematic of the angle created between the eye axis and the center of the skull in several vertebrate species. Adapted from Land 2013. B- Schematic of the distribution of the monocular (Left, LM; Right- RM) and binocular fields in the mouse. Adapted from Samonds et al., 2019. C- Due to the lateral and upward-tilted placement of the eyes of mice, their binocular overlap is bigger in the upper area (green). Dotted lines represent the vertical and horizontal midlines. Adapted from Samonds et al., 2019.

Oculomotor capacities of animals can be described by the features of the eye movements and their purpose. Quantitatively, they can be described by their angular rotation (in degrees) or by the velocity at which the movement is executed (degrees/second; º/s). In the beginning of the 20th century, Raymond Dodge (Dodge, 1903) classified the eye movements into 5 groups. 3 of these movements are done to voluntarily shift or redirect gaze to a certain target: saccades, smooth pursuit and vergence. The 2 others are reflexive eye movements that are performed to stabilize gaze: the vestibulo-ocular reflex and the optokinetic reflex. It is important to note that vergence and smooth pursuit are only present in animals with frontal vision (*e.g.*, cats, primates, humans). Nevertheless, all vertebrates share the ability to make saccades and the same two gaze stabilizing reflexes (M. Land, 2019).

First, this section will briefly describe each class of eye movements (**Figure 2**). Then, the mechanistical control and the effectors of these movements, the extraocular muscles, will be presented.

1.1. Types of eye movements

Saccades

The word saccade derives from the French adjective '*saccadée'* meaning a jerky or twitchy kind of movement. Saccades are performed to switch the eye from one fixation point to another so that gaze is set to a target of interest. This type of gaze shifting eye movements are brief and very rapid. In humans they can reach peak velocities almost 1000 º/s (Bahill et al., 1975) and 1500º/s in mice (Wang et al., 2015) . Only the amplitude and direction of saccades can be voluntarily changed. The execution, *i.e.,* velocity and duration of the movement, solely depend on the location and distance of the target and can't be voluntary adjusted. Even though saccades are performed voluntarily and are often evoked by visual stimuli, they can also be made in the dark and be triggered by auditory or tactile stimuli (Büttner & Büttner-Ennever, 2006).

Smooth pursuit

Smooth pursuit movements work to maintain the image of a moving target. These slow and smooth eye movements help to attenuate the blurring that would occur if the target's image wasn't steady on the fovea. Smooth pursuit eye movements are voluntary but require a moving target to initiate them. The eye adapts its tracking speed to the moving target with reaching speeds up to 50º/s (Barnes & Collins, 2008). An example of this type of eye movement is when tracking the trajectory of an airplane flying in the sky. Afoveate animals do not have smooth pursuit eye movements (John S. Stahl, 2004) .

Vergence

Vergence movements are eye movements that angularly rotate the eyes so that different depths of the visual surroundings can be seen. These are deconjugate eye movements, that is, the eyes move in the different direction or by different amounts so that the centering of the visual target in each fovea is assured (Squire, 2008). The eyes can either converge if the target is close or diverge if the target is far. Vergence movements are the slowest of the gaze shifting movements, the velocity of pure vergence is <20 deg/s.

Gaze stabilizing eye movements

These eye movements are reflexive and work to hold the images locked to retina either during head movement (vestibulo-ocular reflex) or visual scene movement (optokinetic reflex). These reflexes are widespread in vertebrate species (M. Land, 2019) including mice, the animal model used in this thesis.

Optokinetic reflex

The optokinetic reflex (OKR) keeps the images stable on the retina during movement of the visual surroundings. It consists of slow compensatory eye movements (slow phases) and, when the eye reaches the end of the orbit, a quick resetting (quick phase) movement is done to reposition the eye on the center of the orbit. Since this reflex depends on the transduction of the surrounding visual stimuli and requires many relays in the central nervous system, it is more efficient for relatively slow motions (lower speeds, lower frequencies) of the visual scene.

Vestibulo-ocular reflex

The vestibulo-ocular reflex (VOR) stabilizes the position of the eye in space by producing a compensatory eye movement in the opposite direction of the head movement. VOR preferentially prevents image blur on the retina at mid- to high-frequency head movements as a result of the acceleration-sensitivity of vestibular endorgans. It has a shorter latency than OKR (7-15ms for semicircular-canal transmitted signals in humans (Johnston & Sharpe, 1994)).

The gaze stabilizing reflexes in mice were studied in most of the works of this thesis. Therefore, both OKR and VOR will be presented in detail (see 2. Gaze stabilization). The next section focuses on the neuronal and muscular elements that executes the eye movements, the extraocular eye muscles and related extraocular motor nuclei.

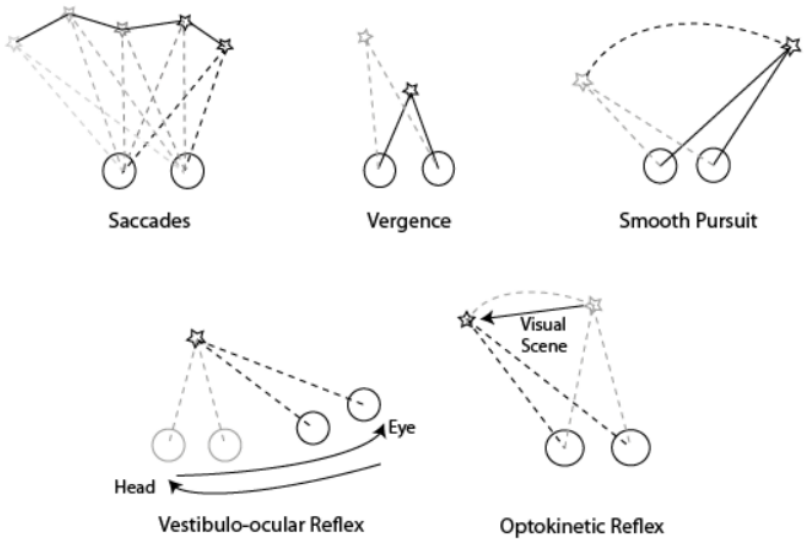

Figure 2. Types of eye movements. Circles represent the eyeballs, stars the visual target with dashed lines pointing towards them. Credit Filipa FdB.

1.2. Extraocular muscles

Voluntary and reflexive eye movements can be performed by contracting the extraocular muscles (EOMs). There are 7 EOMs located within the eye's orbit, extrinsically located in the eye. Depending on their function, they can be categorized in muscles that move the superior eyelid (the *levator palpebrae superioris* muscle) or in muscles that control the eye movements. The location in the orbit and innervation pattern of the EOMs is congruous between mammalian species but there are slight individual muscle differences between frontal-eyed and lateral-eyed species (Spencer & Porter, 2006). Mice, a lateral-eyed species, show a standard EOM organization (Bohlen et al., 2019) with slight particularities that will be discussed along this section.

The six EOMs that control the eye movement can be categorized depending on their path from origin to attachment on the eyeball (**Figure 3**). That is, muscles that have a direct path are denominated as recti (Latin word for 'straight') and muscles that have an angular path to the eyeball are referred to as oblique.

Recti EOMs

There are 4 recti muscles: superior rectus, inferior rectus, medial rectus and lateral rectus. They all share a common tendinous ring (annulus of Zinn) placed at the back of the orbit to which they attach differently according to their nomenclature and pass anteriorly to attach at the equivalent part in the sclera, the external membrane surrounding the eye. For example, the lateral rectus muscle originates at the lateral part of the tendinous ring and attaches to anterolateral part in the sclera. Due to their importance for horizontal gaze stabilizing reflexes, the work developed in this thesis will often refer to the medial and lateral recti muscles.

Oblique EOMs

The two oblique muscles are the superior oblique and inferior oblique. The inferior oblique, unlike the recti and the superior oblique muscles, originates from the maxillary bone in the medial wall of the orbit (Spencer & Porter, 2006). Mice in particular have more prominent oblique muscles with insertion points that are different from the ones of frontal-eyed species (Bohlen et al., 2019).

Accessory EOMs

Apart from the standard EOMs, some vertebrates have accessory EOMs called retractor bulbi. In mice, the retractor bulbi muscle surrounds the optic nerve and lies internally to the recti muscles (R. S. Smith et al., 2001). Its function is to retract, or intort, the eye in the globe in response to corneal stimulation. These muscles are of special

interest in the framework of this thesis and their relevance will be discussed further on (Article 4). In phylogeny, the presence of the retractor bulbi is related to species that possess a nictitating membrane (Spencer & Porter, 2006) . The nictitating membrane, or third eyelid, is a transparent membrane that has mainly a protective and humidifying function to the eye, without disturbing vision. The contraction of the retractor bulbi pulls the eye inside the orbit which makes the nictitating membrane to unravel in front of the eye (Büttner-Ennever, 2006). In the mouse, the synergistic action of the retractor bulbi and the nictitating membrane putatively helps cleaning potential debris from the ground that can easily reach the eye. Primates and humans have a vestigial form of this membrane in the corner of the eye called *plica semilunaris* (Spencer & Porter, 2006).

1.3. Extraocular motor nuclei

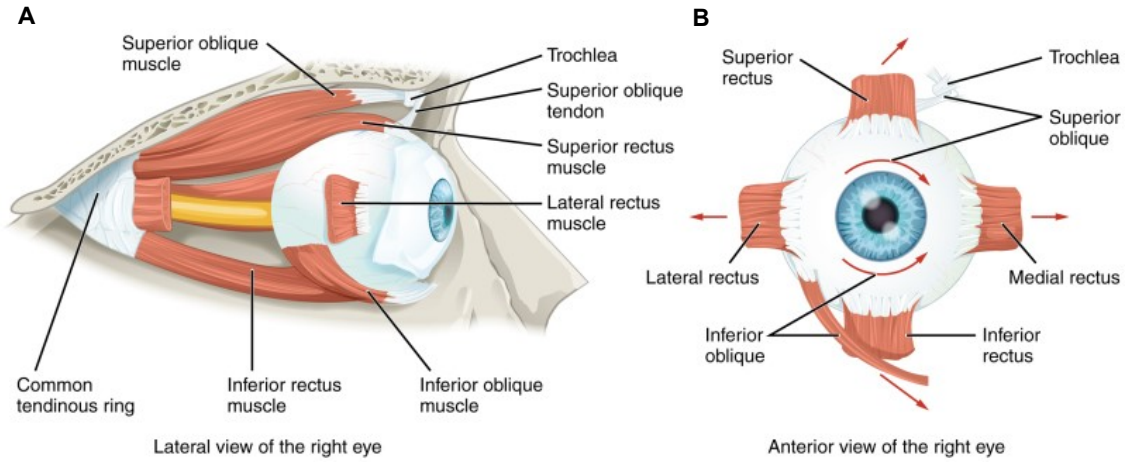

Figure 3. Extraocular muscles. A-Relative position of the muscles in the eye and B- directionality (red arrows) of their movements. From: Ludwig and Czyz, 2019.

The eye muscles referred above must be innervated by motoneurons in order for them to move, *i.e.*, contract and relax. These motoneurons are organized into 3 nuclei: the oculomotor (III); the trochlear (IV) and the abducens (VI). Each one of these motoneurons can innervate one or several eye muscles (**Table 1**).

The motoneurons of these nuclei can be broadly divided into 2 groups. One group is made of large motoneurons located in the middle of the nucleus and that innervate rapid contracting muscle fibers with a single neuromuscular terminal. The other group is composed by small-sized motoneurons that are situated in the periphery of the nucleus and innervate slow, fatigue-resistant eye muscle fibers through several neuromuscular terminals. This group is in charge of maintaining the extraocular muscle tone (Büttner-Ennever, 2006).

Table 1. Innervation of the extraocular motoneurons. N/a.= not applicable.

Extraocular muscle innervation side	Cranial nerve nuclei		
	Oculomotor nucleus (iii)	**Trochlear nucleus (iv)**	**Abducens nucleus (vi)**
Ipsilateral	Inferior rectus, Medial rectus and Inferior oblique	n/a	Lateral rectus
Contralateral	Superior rectus	Superior oblique	Medial rectus (through the internuclear neurons)

In sum, the previous sections reported the different types of eye movements that are present in vertebrates as well as the EOMs responsible for their execution. The work in this thesis studies the eye movements performed in mice, an afoveate species. More particularly, it focuses on the gaze stabilizing eye movements performed on the horizontal plane thus, that rely on the oculomotor and abducens nuclei for their execution. The next part details the gaze stabilization mechanisms, pathways and coding strategies in mammals and, more importantly, in mice.

2. Gaze stabilization

Visual information is crucial to most animal species to act on, interact with and orientate in their environment. Visual acuity is crucial to adequately process the details of the composition of our surroundings. To achieve it, the position of the eye in space must be oriented towards the desired object so that images are held stationary on the retina. This is accomplished through gaze stabilizing reflexes.

The two existing gaze stabilizing reflexes are performed either during head movement (VOR) or during visual scene movement (OKR) and are driven by the integration of vestibular and visual inputs, respectively.

2.1. The vestibulo-ocular reflex

2.1.1. The vestibular system

A brief historical context along with a functional description is here made, followed by the neuroanatomy of the structures that play a role in the vestibular function.

Brief historical context

The anatomy of the inner ear began to be studied in the mid-16th century with the elaboration of *De Humani Corporis Fabrica* (Andreas Vesalius, 1543). This was a very important work regarding the anatomy of the human body as it precisely located and examined several organs. The inner ear was described in this book by Grabiele Fallopio who divided it into two areas: the labyrinth, composed of the semicircular canals and otolithic organs, and the cochlea. After, in 1795, Antonio Scarpa described the inner ear fluids and vestibular ganglion and by the beginning of the 19th century, most of the inner ear anatomy was described (Wiest, 2015). The description of the vestibular apparatus as sense organ independent from hearing, began in the mid-19th century. The first scientist to report the role in postural control and balance was Pierre-Marie Flourens, who discovered that lesioning the semicircular canals of pigeons made them lose balance and uncapable to control their heads position (Yildirim & Sarikcioglu, 2007). Later in 1861, Prosper Ménière described a group of patients that had suffered from damage to the inner ear and were experiencing vertigo and did the parallel with Flourens work. Most probably, these patients suffered from what is known nowadays by Ménière syndrome; a fluctuant inner ear disease which functional basis remain poorly known that provokes vertigo, tinnitus and, with time, hearing loss (Wiest, 2015).

Finally, in 1874 and 1875 three different scientists concluded that semicircular canals were organs that sensed head rotations. Josef Breuer (Joseph Breuer, 1873) continued Flourens' work on the semicircular canals of birds and noted the eye

movements that came with their stimulation (**Figure 4**); Ernst Mach (Ernst Mach, 1873) conceived a chair that rotated patients in several axes and noted their sensations during vertical and horizontal rotations; Alexander Crum Brown (Alexander Crum Brown, 1874) had patients in a rotating table and blindfolded them while positioning the table in different planes (Jay M. Goldberg et al., 2012a). In 1906, Robert Bárány used caloric stimulation of the external ear in his patients and noticed that they felt vertigo and nausea. He postulated that this effect was due to a convection effect of the water (hot or cold) that was being administered against the endolymph. This observation granted him the Nobel Prize in 1914. The Barany test, or caloric stimulation test, is a clinical vestibular test used currently to point the presence of labyrinthic malfunction (Robert Bárány, 1907).

Up to the beginning of the 20th century researcher's focus was on the peripheral vestibular organs. That changed when Lorente de Nó, in 1926, studied the morphology of the vestibular nerve in the central nervous system as well as the connections involved in the VOR (Lorente de Nó, 1933). Baloh and Honrubia, Lorente de Nó's students, in the 1970s, invented electronystamography. With the use of computers, they were able to control the stimulus being given and record the output quantitatively using a set of tests to asses vestibular function (Jay M. Goldberg et al., 2012c). This technique was the precursor of videoculography, one of the key techniques in vestibular research of the 20st century.

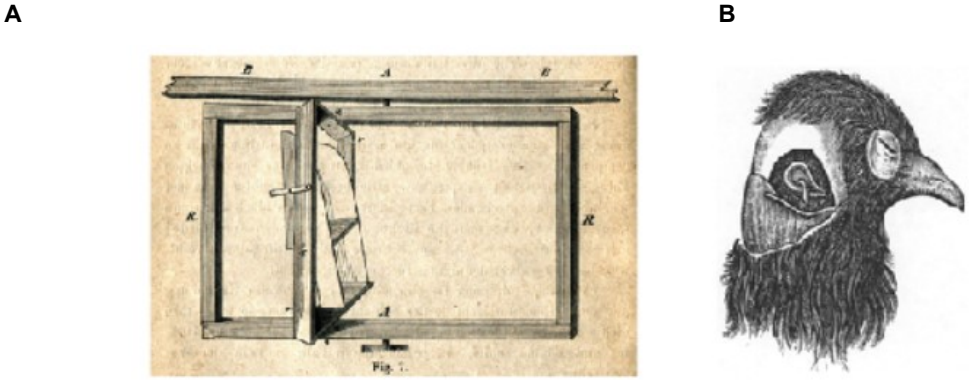

Figure 4. Vestibular history landmarks. A- Ernst Mach's rotational chair used to test human subjects. B- Joseph Breuer's experiments on the lesioning of semicircular canals of pigeons. From Wiest 2015.

Functional description

As seen above, the recognition of the properties of the vestibular apparatus as an organ different from the cochlea came about fairly late. This is probably because, under normal circumstances, vestibular sensations remain completely unobtrusive (Jay M.

Goldberg et al., 2012d). The vestibular system partakes in a wide range of fundamental behaviors, from the maintenance of visual acuity to postural control and spatial orientation. It does so by transmitting information about head motion and position in regard to gravity. However, in the case of a pathology in the peripheral or central vestibular system, dizziness or vertigo sensations arise (Bittar et al., 2013).

The vestibular system stabilizes gaze by detecting motion of head in space. As it will be described in this chapter, apart from the inputs coming from the vestibular labyrinth, it also processes inputs coming from other regions like the cerebellum, cerebral cortex and spinal cord. These inputs converge on the vestibular nuclei where an appropriate premotor command is generated.

2.1.2. VOR pathway overview

Eye movements counteract in equal but opposite direction the movement of the head in space. They do so through the vestibular system that responds to angular (rotational) as well as to linear (translational) movements of the head in space. The angular acceleration is sensed by the ampullae of semicircular canals that will generate the angular vestibulo-ocular reflex or AVOR. On the other hand, the linear acceleration is sensed by the otolithic organs that will generate the translational vestibulo-ocular reflex or TVOR (Angelaki & Cullen, 2008). Lorente de Nó, in 1933 (Lorente de Nó, 1933), was the first to describe the 3-neuron reflex arc that enables the direct VOR pathway. The first projection goes through afferent fibers (1ºVNs, first order vestibular neurons), from the peripheral vestibular apparatus, to the vestibular nuclei complex (2ºVNs, second order vestibular neurons). From there, the 2ºVNs will project to eye motor nuclei that will contact the EOM which contraction will execute the eye movements. Although this pathway exists for both AVOR and TVOR, it has been shown that there is a bigger lag in response of the TVOR. This implies that TVOR could be mediated by more complex polysynaptic pathways and is not as effective as the AVOR in stabilizing gaze (Angelaki, 2004). The reflex studied in this thesis was the AVOR which from now on, for simplification purposes, will be referred to as VOR. This reflex is an interplay between push and pull movements of the lateral and medial recti EOMs.

The VOR has a circuit anatomy that has been thoroughly characterized (Boyden et al., 2004). For explanatory purposes, let's consider the example illustrated in the figure above (**Figure 5**) where the subject's head moves towards the left, producing compensatory eye movements (VOR) to the right. This angular movement will make the endolymph flow in the horizontal semicircular canals on both sides of the head, which will deflect the hair cells in their ampullae to the same side. This will excite (depolarize)

the hair cells that have their kinocilium on the same side of the movement of the head, in this case, the horizontal canal of the left side. Hence, there will be an increase in the discharge of the left vestibular afferents that will propagate to the ipsilateral vestibular nuclei. From there, the intorsion/contraction of the antagonistic muscle pair will happen as follows:

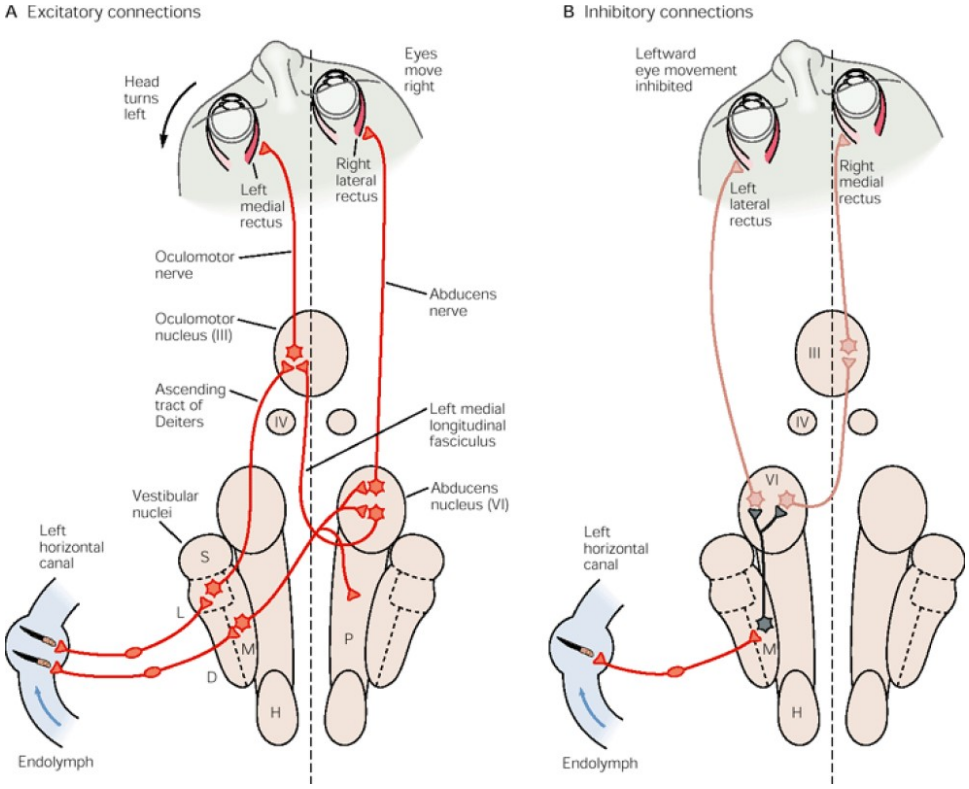

Figure 5. Schematic of the VOR pathway. In response to a counterclockwise head movement, the eyes will move clockwise. Depiction of the A- Excitatory connections (red) and B: Inhibitory connections (pink) coming from the left horizontal canal. (M) medial vestibular nucleus; (L) lateral vestibular nucleus; (D) descending vestibular nuclei; (S) superior vestibular nuclei; (P) prepositus hypoglossi; (H) nucleus prepositus hypoglossi; (III) oculomotor nucleus; (IV) trochlear nucleus; (VI) abducens nucleus. From (Kandel, 2013).

-In this example, the rightward eye movement will be excited (**Figure 5**, A). Thus, the contraction of the right lateral rectus will be achieved by the innervation coming from the left MVN neurons that decussate and project to the contralateral (right) abducens nucleus. At the same time, the left medial rectus will be contracted through the activation of the oculomotor nuclei neurons. Projections to these neurons can come either from the LVN through the ascending tract of Deiter's or from the contralateral abducens nucleus through the internuclear neurons that form the medial longitudinal fasciculus (MLF).

-Simultaneously, the leftward eye movement is inhibited (**Figure 5**, B). Ipsilaterally, vestibular afferents excite neurons in the MVN which in turn will inhibit left abducens

neurons and interneurons (MLF) projecting to the oculomotor nucleus. Additionally, this head movement will also inhibit the hair cells with their kinocilium oriented oppositely to the movement, in this case, the right horizontal canal. Therefore, due to their discharge decrease, the right medial rectus and the left lateral rectus will be inhibited.

This simultaneous inhibition/excitation allows a push and pull motion of the eye muscles. The antagonistic pair of medial/lateral recti muscles eye muscles acts synergistically and enables the execution of conjugate eye movements on the horizontal plane. In the VOR, these eye movements are of the same magnitude and speed but in opposite direction of the head movements. Hence, stabilizing gaze in response to head/body movements.

On the next section, the direct VOR pathway composed of a 3-neuron arc will be anatomically and physiologically characterized by the structures that participate and modulate its response (**Figure 6**). First, the peripheral system, containing the 1ºvestibular neurons (1ºVNs), followed by the central vestibular nuclei, where the 2° VNs are located.

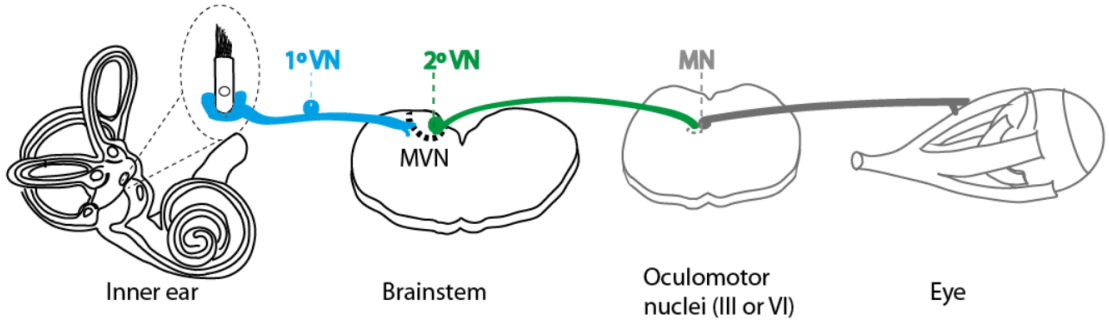

Figure 6. Schematic of the VOR, a 3-neuron arc reflex. From the peripheral vestibular apparatus, the afferent fibers (1ºVN) run to the vestibular nuclei complex (2ºVN) and then to the motoneurons on the oculomotor nuclei (3ºMN) to move the eyes. Credit Filipa Fdb.

2.1.3. Peripheral vestibular system

The vestibular system can be categorized into two subsystems: the peripheral and the central vestibular system. They are divided that way because, as their nomenclature suggests, they are distributed either peripherally, on the inner ear, or centrally, within the central nervous system.

In mammals, the peripheral vestibular system consists of 5 pairs of organs: 3 semicircular canals (horizontal, anterior and posterior) and 2 otolithic organs (saccule

and utricle) (**Figure 7**). They reside in the temporal bone and lie symmetrical on each side of the head. The bony and membranous labyrinths make up the inner ear; the bony labyrinth protects and holds the membranous labyrinth that contains a system of ducts and sacs filled with fluid. Extracellular fluids surround these structures; the perilymph bathes the space between the bony and membranous labyrinths (low in K+ and high in Na+) and the endolymph fills up the membranous labyrinth (high in K+ and low in Na+) (Khan & Chang, 2013). The membranous labyrinth is not only formed by the semicircular canals, saccule and utricle but also by the cochlea, the organ responsible for hearing. The cochlea will not be further discussed in this section since it is not part of the vestibular system.

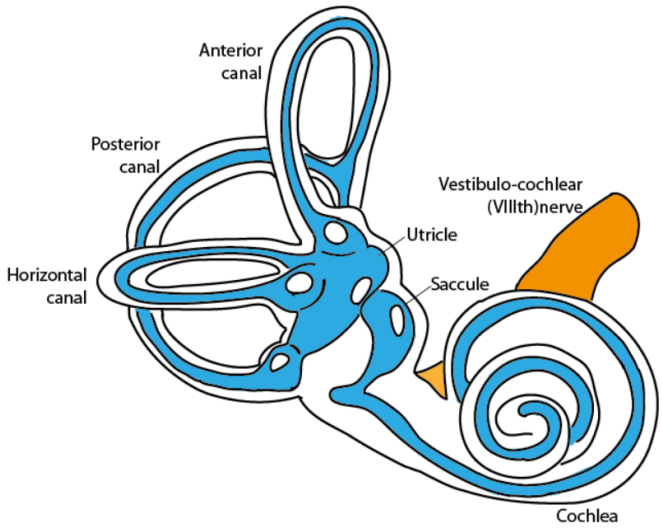

Figure 7. Peripheral vestibular system. Credit: Filipa FdB

Utricle and saccule: the otolith organs

The utricle and saccule sense gravity and the linear acceleration of the head when, for example, tilting or translational movements occur. The utricle detects these displacements mostly in the horizontal plane and the saccule mainly in the vertical plane through their sensory neuroepithelia, the maculae (J. M. Goldberg & Fernandez, 1975; Lim & Brichta, 2012). The epithelia have a flat, dott-like structure and coating them is a gelatinous membrane containing the otoliths, or otoconia. It's these small (3-30 μm in humans) and characteristic calcium carbonate 'stones' (otolith means 'ear stone' in Greek) that provide the otolith organs their name. Each otolithic organ has a striola, a structural landmark made of small otoconia that divide in two halves each otolith organ. In the utricle, the hair cells are oriented towards the striola while in the saccule they are

pointing away (Lindeman, 1969; Purves, 2004). This differential arrangement enables several patterns of stimulation given by the direction of the head tilts. These signals will in turn be transmitted to the CNS through a dedicated branch of the vestibulocochlear nerve (see Vestibular nerve). When linear forces act in the macular plane there is a tangential displacement of the otolithic membrane relative to the sensory epithelia.

The superior vestibular nerve innervates the utricle, as well as the superior and lateral canals. The inferior vestibular nerve innervates the posterior canal and the saccule.

The semicircular canals

Semicircular canals sense angular acceleration (J. M. Goldberg & Fernandez, 1975). Due to their relative perpendicular positioning they detect movement in three orthogonal planes, thus covering 3D space. In humans, the horizontal canal is positioned 25º to the axial plane and the anterior and posterior canals are aligned 45º in regard to the sagittal plane and 90º between each other (Blanks et al., 1975) (**Figure 8**). These values change between animal species; in C57Bl/6J mice, the canals are positioned similarly to humans: 32,6º for the horizontal canals relatively to the axial plane (Calabrese & Hullar, 2006). This 3-dimensional positioning is completed by the fact that, since each peripheral vestibular endorgan has its symmetrical counterpart on the other side of the head, there is a coupling of conjugate canals for the movement in a given plane, *i.e*., a canal on one side will have a parallel canal on the other side. For example, the left anterior canal is paired with the right posterior and vice versa. The horizontal canals lie parallel to each other on both sides of the skull.

Each canal has at one of their extremities an ampulla, a bulb-shaped sac that contains the sensory neuroepithelium called the crista ampullaris. In turn, the crista is

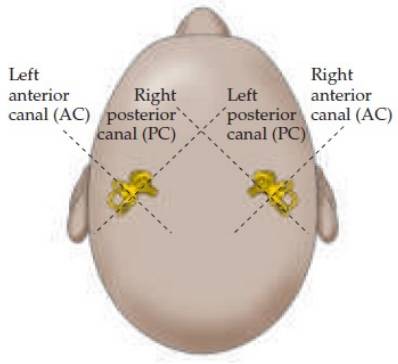

Figure 8. Aerial view of the semicircular canals. They make a 45º angle with the sagittal plane. From Purves, 2004.

covered by the cupula, a gelatinous substance that creates a barrier in the ampulla that prevents endolymph from getting in (Jay M. Goldberg et al., 2012b; Khan & Chang, 2013).

Hair cells

The mechanoreceptors of the peripheral vestibular system are the hair cells. They are responsible for the transduction of the movement sensed by the vestibular organs into a change of afferent discharge. Hair cells make up the neuroepithelia of the otolithic organs (macula) and the semicircular canals (crista ampullaris). Trough attachment to the neuroepithelium, hair cells have a mechanical pole on their apical surface and a synaptic pole at their basal surface (Eatock, 2000). Stereocilia are arranged by size, being that the biggest one stands next to the kinocilium. There are proteins that run obliquely and connect the shortest to the tallest adjacent stereocilia called tip links. Globally, hair cells translate the mechanical energy applied to the apical part in a synaptic signal. In detail, stereocilia are anatomically polarized so, the movement of the hair bundle towards a given kinocilium will depolarize the hair cell, leading to increase transmitter release and excitation of the vestibular nerve fiber. On the contrary the movement of the stereocilia away from a given kinocilium results in hyperpolarization of that hair cell and decrease in the firing of vestibular nerve neurons (Lim & Brichta, 2012).

In a mouse labyrinth, there are around 10000 vestibular hair cells (Eatock & Songer, 2011) which have been classified in two classes: type I and type II (**Figure 9**). Type I are piriform or amphora-shaped and are surrounded by a synaptic calyx ending,

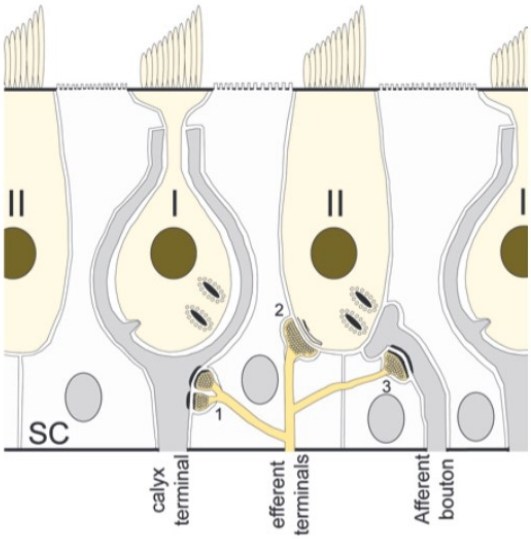

Figure 9. Depiction of type I and II hair cells. Type I hair cells are represented with their single afferent fiber innervation. Type II hair cells are shown with bouton terminals from various afferents. Both types of cells are innervated by single efferent fibers. Supporting cells (SC) of the neuroepithelium. From Holt et al 2011.

coming from a single afferent fiber; they are only present in the vestibular organs (Eatock & Songer, 2011). They are commonly located at the center of the otolithic macula and at the top of the crista (Fernández et al., 1988). Type II are more ubiquitous since they're found in both vestibular and auditory organs (Lysakowski, 1996); they are column-shaped and have multiple connections to their afferent fibers. They are located at the periphery of the macula and at the basal part of the crista (Fernández et al., 1988).

These hair cells are contacted by the peripheral processes of the vestibular nerve neuron's that convey the information to the central vestibular nuclei. In turn, both type I and II hair cells also have efferent synaptic boutons at their basal surface. These vestibular efferents, coming from the brainstem, are thought to provide a positive feedback loop to vestibular afferents; a high discharge of the afferents would cause an increase of discharge of the efferents that would in turn stimulate back the afferents (Sadeghi et al., 2009). However, this is only a hypothetical role for the efferent vestibular system and there are more theories that aim at explaining its function. Despite the efferent morphology and location being well described, there are few recordings from efferent vestibular neurons and a lack of understanding of this circuitry. Therefore, the exact functional role of the efferent vestibular system in mammals remains elusive (Mathis et al., 2018).

The work presented in the first part of this thesis (Article 1, Article 2 and Article 3) concentrates on the direct VOR pathway whose modulation directly depends on the vestibular afferents. Therefore, ahead (see 2.1.3.1. Two vestibular-encoding channels) it's discussed how different hair cell/afferent combinations could be rendering two distinct vestibular channels for head motion (Cullen, 2012; Eatock & Songer, 2011) signals.

Vestibular nerve/ 1º VN

In order to render a 3D depiction of head/body acceleration (angular and linear), the vestibular afferents innervate the vestibular endorgans (Dickman & Angelaki, 2002; Rabbitt, 1999). The inputs coming from the hair cells flow to the central vestibular system through the vestibulocochlear or VIIIth cranial nerve.

This sensory nerve is made of two branches, the vestibular (vestibular inputs) and the cochlear (auditory inputs) branches. The vestibular branch is made of bipolar neurons whose soma forms the vestibular or Scarpa's ganglion. These neurons simultaneously innervate the peripheral (hair cells) and central vestibular system (cerebellum and brainstem). According to the vestibular organ they innervate, it is possible to subdivide the nerve into a superior and inferior region. The superior part of the VIIIth nerve is composed by afferences coming from the crista ampullaris of the

anterior and horizontal canals and the utricle (Hain, 2007). The inferior part is made of fibers that innervate the saccule as well as the crista ampullaris of the posterior semicircular canal (Fernandez & Goldberg, 1976). Before entering the brainstem, the auditory and vestibular branch unite to once again separate at the pontomedullary junction. (Khan & Chang, 2013).

The vestibular nerve branch encodes both linear an angular acceleration, 2 different sensory modalities that are carried separately. The projections of this nerve to the central vestibular system are explained in the following section (2.1.4. Central vestibular nuclei).

2.1.3.1. Two vestibular-encoding channels

As described above, vestibular afferents receive inputs coming from the neuroepithelia of the inner ear, product of their polarization due to the detection of acceleration in a given spatial plane. However, vestibular-nerve fibers aren't all the same and the output, depending on which type of fiber is carrying it, will be different. At rest, in the squirrel monkey, vestibular afferents have a mean discharge of 100 spikes/s (Goldberg, 2000) but, the spacing between their action potentials varies. Thus, vestibular afferents are classified as regular or irregular based on their resting discharge profile. This classification is shared among mammals (Goldberg et al., 1987) but also lower vertebrates (Boyle & Highstein, 1990). This is a convenient distinction not only because fibers differ on their resting potentials but also on their response dynamics, response sensitivity as well as on their axon diameter (Goldberg, 2000). Thus, it can be a useful way to identify which type of fiber is being stimulated during experiments.

Keeping in mind their discharge pattern, they can also be classified based on the morphology of their endings in the neuroepithelium: 1) bouton fibers, or B-regulars, that provide bouton endings to type II hair cells; 2) calyx fibers, or C-irregulars, that give calyx endings to type I hair cells; 3) dimorphic or D-irregular that provide both calyx and bouton endings to type I hair cells (Jay M. Goldberg et al., 2012c).

Irregular afferents have bigger axon diameter, have a phasic-tonic response dynamic, high conductance speed and are more responsive to high amplitude (natural) vestibular stimuli. Regular afferents have smaller fiber diameter and their terminals are located in a more peripheric area, have a tonic response and have better detection thresholds (Cullen, 2019)(**Figure 10**).

Thus, evidence suggests that there are two different peripheral vestibular 'channels' conveying information to the central vestibular system: the irregular channel, that better responds to natural head acceleration and use a precise-spike timing code;

and the regular channel that preferentially carries small-amplitude stimuli via a firing rate code (Cullen, 2012; Eatock & Songer, 2011).

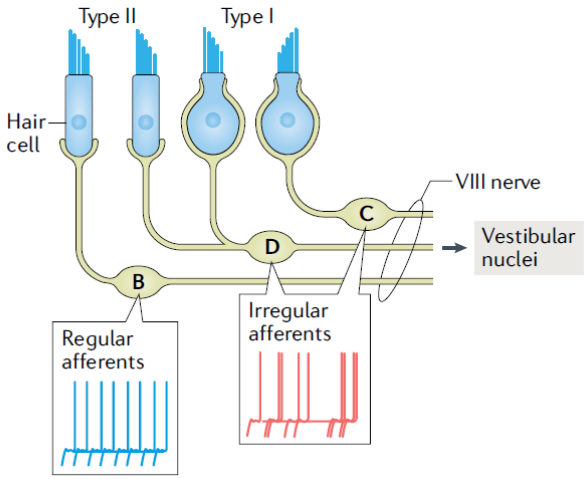

Figure 10. Hair cell types and respective afferent innervation. Regular afferents innervate type II hair cells while irregular afferents can contact type I hair cells or both type I and II simultaneously. Adapted from Cullen 2019

2.1.4. Central vestibular nuclei

Anatomy of the vestibular nuclei complex

The vestibular nerve fibers innervate a group of nuclei located on the dorsal part of the brainstem. In mammals, vestibular nuclei are bilateral complexes located on the floor of the fourth ventricle. The vestibular nuclei complex is made of four nuclei: the superior vestibular nucleus (SVN), the medial vestibular nucleus (MVN), the lateral vestibular nucleus (LVN or Deiter's) and descending (also called inferior or spinal) vestibular nucleus (DVN). Adjacent to these four main nuclei, there are other small cell groups: *e, x, y, z* (Brodal & Pompeiano, 1957). However, these cell groups are not recognized in all vertebrates and they don't receive direct vestibular afferents. The only exception is the y-group that receives direct vestibular afferents coming from the saccule (Highstein & Holstein, 2006). The e-group (efferent-group), doesn't seem to receive primary vestibular afferents but the neurons of this efferent vestibular nucleus send their axons back to the peripheral vestibular organs (J. M. Goldberg & Fernández, 1980).

This anatomical division also corresponds to a functional one. Globally, every nuclei, except the LVN, receives direct vestibular nerve afferents (Carleton & Carpenter, 1984). The SVN receives afferents from the 3 semicircular canals. The LVN receives otolithic afferents as well as canalar, specially from the vertical component. The DVN receives otolithic and canalar afferents from the posterior canal (Highstein & Holstein,

2006). The MVN, the nucleus studied in one of the works of this thesis, appears to be topographically organized. Neurons on the rostro-lateral part of MVN receive afferents from the semicircular canals, mainly from the horizontal canal, and the flocculus. This area is also called magnocellular area due to the larger size of this neurons. The caudal part of the MVN receives vestibular otolithic fibers. These neurons project to the oculomotor nuclei and is the nucleus where inputs relative to hVOR are mainly processed (Epema et al., 1988; Highstein & Holstein, 2006).

Therefore, it was here that the neuronal changes after visuo-vestibular mismatch were studied in one of the works of this thesis (see Article 1 (Carcaud et al., 2017)).

2.1.4.1. Afferent convergence on 2°VNs

The central vestibular nuclei complex integrates afferents inputs so that the head/body movements are correctly detected and adequate postural reflexes as well as compensatory eye movements are generated (Dickman & Angelaki, 2002). This integration could be carried out at a 1:1 ratio, *i.e.*, one vestibular neuron receives vestibular afferents coming from one of the vestibular endorgans or, on a X:1 ratio, where vestibular afferents coming from several endorgans converge in the same single vestibular neuron. This matter of individualization or convergence of vestibular information lies at the epicenter of multisensory transformation (Simpson & Graf, 1985).

On average, each 2ºVN receives 4-5 vestibular afferent fibers (cat, Mitsacos et al., 1983). Most of this converging projections are thought to originate from the same sensory organ (monosynaptic convergence). For example, in the frog, more than 80% of the 2ºVNs are monosynaptically innervated by one afferents coming from one of the 3 semicircular canals (H. Straka et al., 1997). Therefore, the detection of a movement in a given plane by the vestibular endorgans is directly translated onto this first synapse. However, as said in the section above, the vestibular nerve separately carries 2 different sensory modalities (linear and angular accelerations) coming from the vestibular endorgans. Since body/head movements are a combination of both modalities, there must be a simultaneous interplay of between them in order to output the adequate premotor command. This is attained by the convergence of several afferents coming from different vestibular organs in the same neuron (2ºVN). For example, in cats, around 30% of vestibular neurons simultaneously receive inputs from the anterior/posterior semicircular canal and utricle/saccule and 15% from the horizontal canal and utricle/saccule and another 1/3 receive converging inputs from both utricle and saccule (Uchino et al., 2005). In monkeys, around 50% of VN neurons (otolith and canal neurons)

are also seen to have a mixed modulation and respond to both rotation and translation movements (Dickman & Angelaki, 2002).

It therefore appears that 2°VN are not simple relay of the information encoded in the vestibular periphery, but a key player in integrating vestibular information originating from different vestibular endorgans; see 2.1.5. Central vestibular coding/ 2ºVNs below.

2.1.4.2. Non-vestibular afferences in the vestibular nuclei complex

In mammals, the main excitatory input that the vestibular nuclei complex receives is the vestibular input (J. M. Goldberg & Fernández, 1980; Sadeghi et al., 2009) described above. However, secondary vestibular neurons also receive several other non-vestibular afferences: commissural afferences form the contralateral vestibular complex, visual, proprioceptive, cerebellar or even cortical afferences. An overview of the main contributions of these non-vestibular afferences is reviewed below.

Vestibular nuclei are bilateral complexes that have reciprocal projections between each other, with the exception of the LVN that doesn't have any projection to the opposite nuclei (rabbit, (Epema et al., 1988)). Commissural projections are classically described as a dominantly inhibitory system.

The caudal parts of the MVN and DVN also receive direct proprioceptive projections that come from the entire spinal cord as well as from the neck. Anatomically, in the rat, retrograde tracing from the vestibular nuclei allowed to show that these sensory afferences come from the ipsilateral C2-C3 spinal cord (Bankoul & Neuhuber, 1990) and from the dorsal horn of C1-C6 (McKelvey-Briggs et al., 1989). These projections from the spinal cord to the VN play an important role on the control of posture and orientation of the body in space.

Vestibular nuclei are also innervated by direct cortical afferences coming from: premotor cortex, cingulate cortex, vestibular cortex, parietoinsular vestibular cortex and temporal superior cortex (Highstein & Holstein, 2006)

Visual afferences are also delivered to the vestibular nuclei. The error message (retinal slip) created when the visual scene moves in the retina, is processed in the VN. This error message is conveyed by several structures: the accessory optic system (AOS) and the cerebellum. Part of the work of this thesis focuses on the OKR, whose pathway involves the detection of the error message that is conveyed to the VN. The detailed pathway of this relay is described in part 2 (2.3. The optokinetic reflex).

A part of the cerebellum is implied in the control of the activity of the vestibular nuclei. The vestibular cerebellum, or vestibulocerebellum, is phylogenetically the oldest

part of the cerebellum (Purves, 2004). It consists of two caudal lobes (the flocculus and paraflocculus) and two portions of the cerebellar vermis (the nodulus and uvula). Axons coming from the VIIIth nerve as well as from the vestibular nuclei complex project to the vestibulocerebellum (Carpenter, 1988). The vestibular nuclei complex is connected to the vestibulocerebellum by the inferior cerebellar peduncles (juxtarestiform body).The nodulus and uvula (cerebral vermis), by projecting to the LVN are able to influence the vestibulo-colic reflexes (stabilize head in space) and vestibulo-spinal reflexes (stabilize trunk, neck and limbs for posture control). The flocculus/paraflocculus modulates the dynamic properties of the VOR (H. Cohen et al., 1992). The main cerebellar afferences of the MVN neurons are ipsilateral projections that come from the flocculus and uvula. The floccular target neurons (FTN) are MVN neurons that are direct targets of inhibition by Purkinje cells from the ipsilateral flocculus (Babalian & Vidal, 2000). Since they integrate cerebellar and vestibular inputs, FTNs are key players in VOR modulation (Carcaud et al., 2017) .

Ultimately, all the different inputs described above converge on the vestibular nuclei's neurons (2ºVN) that will integrate them to produce an adapted motor response.

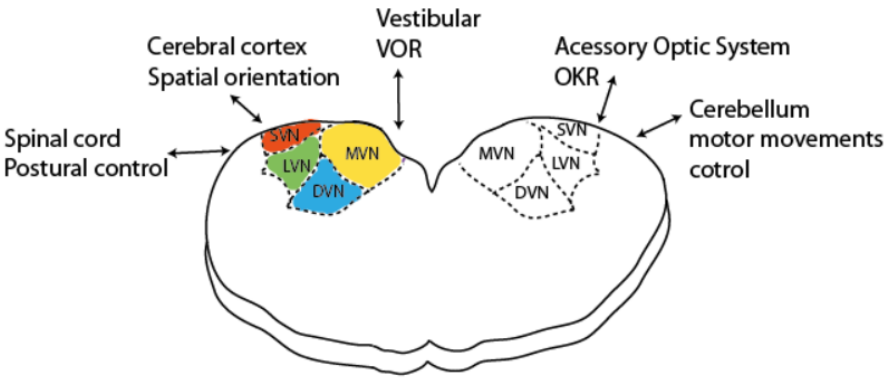

Figure 11. Brainstem slice and vestibular nuclei complex representation. Examples of the different vestibular and non-vestibular projections to- and from- the brainstem are represented with double-sided arrows. Credit Filipa FdB

2.1.4.3. Frequency-dependent pathways

Following the rational that regular and irregular afferents show differences in their firing patterns, one could think that this is reflected on the way each one of them encodes head motion. In fact, the coding of the head motion by the vestibular afferents depends on the range of the stimuli at stake. Experiments on this field mainly stand on the supposition that head motion is encoded in a linear way (Cullen, 2012). This is, the total

response to two or more stimuli will be the addition of the responses to each stimulus individually (Cullen, 2019). In this aspect, research has thus focused its attention to how different frequencies are encoded during early vestibular processing (Cullen, 2012). At low frequencies (the ones usually tested in laboratories, between 0.1 and 5 Hz for mice), the vestibular afferents are in phase with the velocity and acceleration applied. However, when frequencies start to increase a higher sensitivity is seen in the gain as well as an anticipation of the response, that translates into a phase lead. This is known as high-pass tuning; that is, the higher the frequency applied, the higher the response modulation (gain and phase) will be (Cullen, 2019). This differential coding of frequency is seen when comparing irregular afferents that have higher gains and phase leads than regular afferents.

Figure 12 (Cullen, 2019) summarizes the high-pass tuning properties that both regular and irregular afferents possess. The frequencies shown in these graphs are a result of only a small fraction of the frequencies that are performed in natural everyday life head movements. As it's shown on the middle panel, the range of rotational velocities done by monkeys and humans are much bigger than the ones tested in the lab (darker purple strip). This is one of the main constraints: the frequencies, to which afferents are more sensitive to, can't (or at least so far) be tested in laboratorial conditions. A mouse reaches as high as 15 Hz (Beraneck et al. 2008; Carriot et al., 2017) during yaw movements (humans reach 20 Hz) which, in a vestibular turntable, is hard to reach. Thus, limiting the neurons to the linear range response. Regular afferents send detailed information by firing rate and have better detection thresholds (respond to a wider range of frequencies) while irregular afferents are more precise in the spike timing and have and overall higher gain sensitivity. Regular afferents transmit more information (on average 2x more) about head motion than irregular afferents that are better at distinguishing or detecting different head stimuli by their precise spike timing (Cullen, 2019). Therefore, both afferents send parallel and complementary information; irregular afferents carry high frequency stimuli and gains while regular afferents give the exact timing of the stimuli for a give frequency. The VOR information is thought to go through regular afferents while irregular afferents would dominantly transmit information to the vestibulo-spinal reflex pathways (VSR) (Cullen, 2019).

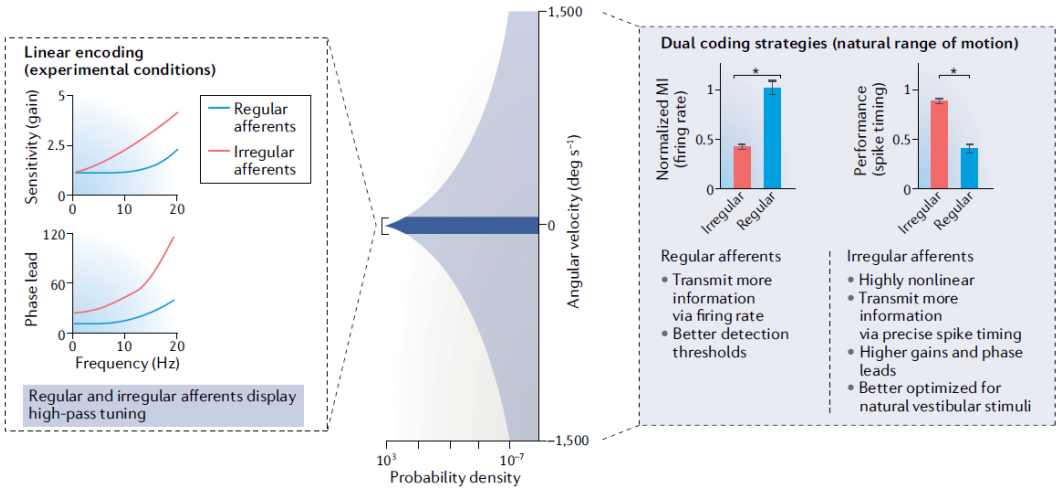

Figure 12. Frequency-dependence of vestibular coding. From Cullen 2019

2.1.5. Central vestibular coding/ 2ºVNs

Central vestibular neurons (2ºVN) are the epicenter of multisensory integration and are key in the processing of vestibular inputs. The outcome of the integration of these signals will be the pre-motor command that will generate the movement of eye in space and/or the head in space.

In vivo characterization of 2ºVNs

Experiments in head-restrained alert monkeys classified 2ºVN neurons in 3 classes: position-vestibular-pause neurons (PVP), vestibular-only neurons (VO) and eye-head (EH) neurons. This classification was based on 2ºVN responses to passive head rotation as well as sensitivities to eye motion (Fuchs & Kimm, 1975; Lisberger & Miles, 1980; Tomlinson & Robinson, 1984). PVP and EH neurons encode horizontal head velocity during passive body movement as well as input eye movements without head movement. Specifically, PVP neurons respond to eye position and pause the firing during saccades and are responsible for VOR generation. The other class of neurons, VO neurons, only responds to passive head rotations but not to eye movements and, when the goal is to generate active head motion, the VO neuron response is suppressed (Cullen, 2019). This class of neurons most likely mediates the vestibulo-spinal reflex (Roy & Cullen, 2001; Scudder & Fuchs, 1992) and projects to higher brain areas to ultimately output balance and orientation signals (Büttner & Lang, 1979).

Parallelly, 2ºVNs were also characterized in alert mice during horizontal body rotations (vestibular stimulations) (M. Beraneck & Cullen, 2007). The response of most (approximately 2/3) of the neurons found was comparable to VO neurons since they

were sensitive to the body rotations but not to the eye movements. Additionally, eye movement-sensitive (ES) neurons, much like PVP neurons, encoded head/body velocity and eye position information during passive rotations.

In vitro characterization of 2ºVNs

When characterized *in vitro*, in slices and isolated brain preparations, 2ºVNs can be classified as type A and type B (when referring to rodents and guinea pig) or tonic and phasic (when referring to frog). This classification is not based on their connectivity but on their electrophysiological features at rest (Beraneck et al., 2003). It has been shown that MVN neurons can be classified according to their action potential afterhyperpolarization (AHP) and interspike intervals (Serafin et al., 1991; Beraneck et al., 2003). Type A neurons have a single and large-amplitude AHP that slows down its depolarization (I_A-like rectification). Type B MVN neurons have a biphasic (first fast then slow AHP) and smaller AHP. Proportionally, in adult mice, there are more type B neurons (80%) than type A (20%) (Eugene et al. 2007).

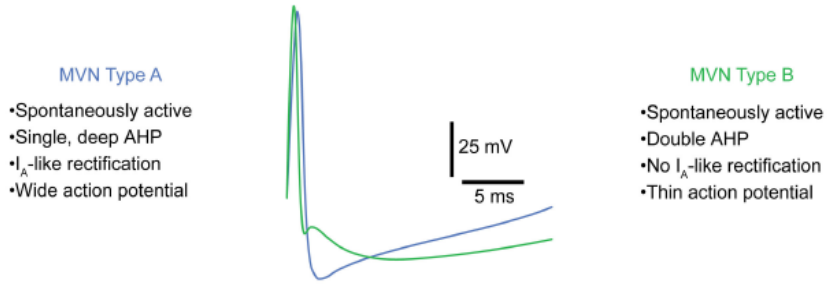

Figure 13. Static properties of 2ºVNs. Blue- type A and green-type B neurons. From Beraneck and Idoux 2012.

In sum, two different parallel channels mediate the processing of the sensory signals coming from vestibular afferents to extraocular motor nuclei. These channels must encompass a wide range of head/body motion and are frequency tuned, *i.e.*, each of them preferentially responds to a certain range of motion frequencies. This is a common feature across vertebrates where 2ºVNs are classified as type A and type B in rodents or tonic and phasic, respectively, in frog (Beraneck et al., 2007; Beraneck & Straka, 2011).

2.2. Vestibular projections

From the vestibular nuclei, information will flow through different vestibular pathways involved in gaze stabilization reflexes, posture and neck reflexes, and orientation.

The MVN receives inputs from the horizontal semicircular canals in order to ascend to control the VOR or descend and control the vestibulo spinal reflex (VSR). The SVN receives inputs from the anterior and posterior semicircular canals in order to send up its axons to the EOMs and control the VOR. The LVN receives inputs from the whole vestibular system and sends its fibers down to the spinal cord and forming the lateral vestibular tract to control the VSR and the vestibulocollic reflex (VCR). The DVN receives inputs from the otolithic organs and projects to the cerebellum as well as to the other 3 vestibular nuclei (Khan & Chang, 2013).

The vestibulospinal system controls the extensor or anti-gravity muscles to maintain posture and balance during linear and angular acceleration. The vestibulospinal system is organized in tracts. There are two major pathways that link the vestibular nuclei with the spinal motoneurons: the medial vestibulo-spinal tract (MVST) and the lateral vestibulo-spinal tract (LVST). The MVST originates in the MVN and LVN and connects to cervical spinal cord motoneurons (α and γ), controlling head and neck muscles. The LVST derives from the ipsilateral LVN, extending all along the spinal cord and controlling the extension of head, neck and limbs (Büttner-ennever & Gerrits, 2004). One of the works of this thesis uses a decerebrated mouse preparation. There, in the absence of the corticospinal inputs, the vestibulospinal pathway allows for the muscular tonus and postural control that enables the mouse to run.

2.2.1. VOR as a proxy for vestibular function

Balance is of the outmost importance in someone's life. The loss of balance signifies the inability to stabilize gaze and translates to disorientation, gait difficulties, high anxiety and potentially social exclusion (Bittar et al., 2013). Thus, pathologies that affect the vestibular system can be severely debilitating. Dizziness or vertigo is one of the most common sensations related to the vestibular system and it affects 20 to 30% of the world population (Bittar et al., 2013). Vertigo is the erroneous perception of object- or self-motion and it's caused by a mismatch between somatosensory, visual and vestibular inputs. Therefore, it is a multisensory syndrome that can occur when one of the mentioned inputs has a dysfunction (Dieterich, 2007). The pathological origin can be connected to the peripheral or central vestibular system (Ohio & Neuroscience, 1999) as well as having a genetic origin.

A work performed during this thesis has studied a genetic disorder, the Usher1 syndrome (USH1) that causes profound deafness and vestibular troubles. In this study, VOR was used as a proxy of vestibular function before and after a genetic therapy was implemented. The measurement of VOR allowed to infer that the offered treatment was

able to restore a functional vestibular response. The combining of gene therapies with vestibular tests is a promising alliance for a new approach to treat vestibular-related disorders. Please, see Article 5.for more information about this study.

The projections from the vestibular nuclei to the oculomotor centers are indubitably of interest since gaze stabilization is a focal point of this thesis. Apart from the VOR, whose response and modulation was described so far, the OKR pathway is also going through the vestibular nuclei. The following sections will be dedicated to the OKR pathway and functional aspects.

2.3. The optokinetic reflex

The optokinetic reflex pathway relies on the visual system. OKR response is activated when the head is fixed in space but the visual surroundings are moving. It outputs slow compensatory eye movements that follow the visual scene to avoid retinal slip and quicker eye movements that serve to recenter the eye in the orbit (saccades). The occurrence of these ‘slow’ and ‘quick’ eye movements is referred to as optokinetic nystagmus (OKN) (Büttner & Büttner-Ennever, 2006).

In the OKR pathway, the processed input is a signal that encodes visual motion on the retina. This visual signal will ultimately be transformed into an oculomotor command. First, the detection and transmission of the visual input, trough the retinofugal projections, into higher brain areas will be described. Then, the full OKR pathway will be overviewed.

The movement of the visual scene on the retina is detected by retinal ganglion cells (RGCs) whose axons form the optic nerve. The optic nerves of each eye meet at the level of the optic chiasm, which allows the partial decussation of the axons. From there, retinofugal axons (axons originating from the retina) project to different parts of the brain, taking either the geniculo-striatal the retinotectal, hypothalamic pathway or the accessory optic pathway.

The OKR pathway relies on the accessory optic system (AOS). Neurons that belong to the AOS and to the nucleus of the optic tract (NOT) are sensitive to the displacement of the image on the retina in a specific direction; the ON-type direction-selective retinal ganglion cells (ON-DSRGCs) (Oyster et al., 1972; Schiller, 2010). In mammals, ON-DSRGCs , going through the AOS, can project to two different brainstem regions: 1) nucleus of the optic tract/dorsal terminal nucleus (NOT/DTN) or 2) medial terminal nucleus/lateral terminal nucleus (MTN/LTN)(Dhande et al., 2013; Oyster et al., 1972). Electrophysiology experiments performed in rabbits demonstrated that the NOT/DTN detect motion in the horizontal (temporo-nasal) direction and the LTN and

MTN detect vertical motion (Soodak & Simpson, 1988). Moreover, the reduction of RGCs innervating the NOT and DTN impaired the horizontal OKR (Badea et al., 2009).

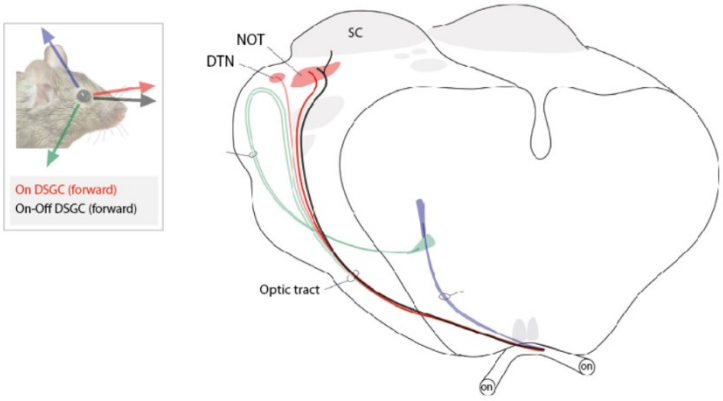

Figure 14. Circuit from the optic nerves (on) to the components of the AOS structures involved in compensatory horizontal eye movements. Red- circuitry of ON DSGCs; from the retina through the optic nerves they connected to the NOT (nucleus of the optic tract) and DTN (dorsal terminal nucleus). Black line- ON-OFF DSGCs connect to the NOT and superior colliculus (SC). Adapted from Dhande&Huberman 2014.

After the visual input has been conveyed to the pretectum, it is sent to the cerebellum and the vestibular nuclei complex so that an oculomotor command can be generated. Considering that clockwise OKR stimulation drives the right eye in the N-T direction and the left eye in the T-N, the OKR pathway would go as follows: the clockwise movement will mainly activate the DSGCs of the left retina. These DSGCs innervate the right NOT and DTN (Dhande & Huberman, 2014). The neurons from the NOT respond preferentially to horizontal movements of the image on the retina in the temporo-nasal direction at a slow velocity, while the DTN of the AOS preferentially respond to vertical movements (Dhande & Huberman, 2014). After the signal reaches the NOT/DTN it will go to the precerebellar nuclei, either through the nucleus reticularis tegmenti pontis (NRTP) or through the inferior olive (IO) and reach the floccular PC (FTN). Following the scheme stimulation, the right eye is activated in the naso-temporal direction. For these signals there are direct projections from the NOT/DTN to the NPH. So, the N-T direction doesn't (directly) require the cerebellum for its response. Once in the NPH or MVN the premotor neurons can convey the signal directly to the ipsilateral or contralateral abducens nucleus (Kodama & du Lac, 2016). Overall, in the clockwise direction, the left abducens will be inhibited (T-N) and the right abducens will be excited (N-T).

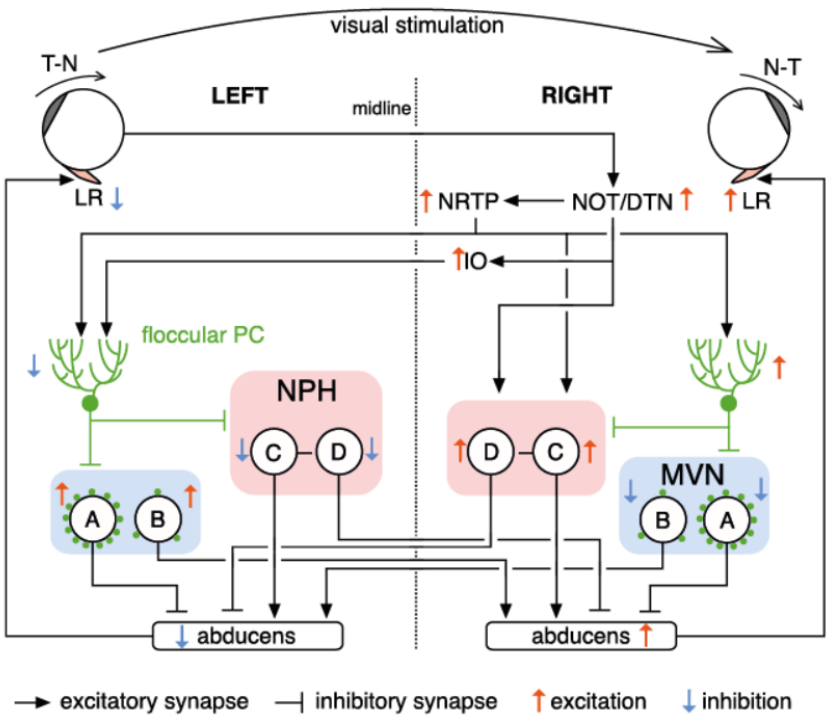

Figure 15. OKR circuitry. A- MVN inhibitory premotor neuron; B-MVN excitatory premotor neuron. C, NPH excitatory premotor neuron. D, NPH inhibitory premotor neuron. For simplicity, only nuclei and cell types likely to play major roles in the OKR to the clockwise visual stimulation are shown; commissural projections and pathways to the oculomotor nucleus and the medial rectus are omitted. LR, lateral rectus; NOT, nucleus of optic tract; DTN, dorsal terminal nucleus; NRTP, nucleus reticularis tegmenti pontis; IO, inferior olive; PC, Purkinje cell; NPH, nucleus prepositus hypoglossi; MVN, medial vestibular nucleus. Adapted from Kodama and du Lac 2016.

2.3.1. Direct and indirect components

As stated above, the OKN is composed by fast resetting movements and slow compensatory eye movements. The generation of slow eye movements by the OKN can be divided into two components: the 'direct' and the 'indirect' phases (B. Cohen et al., 1977). The 'direct' component, closely related to the ocular following response (OFR)(Inoue et al., 1998; Miles, 1998), which is linked to smooth pursuit mechanisms and happens right after the optokinetic stimulus begins. It is seen as the increase of slow-phase responses at the moment when an optokinetic stimulus is presented. On the other hand, the 'indirect' or 'velocity storage' component consists in a more progressive increase of slow-phase eye movements along the presentation of the optokinetic stimulus (Büttner & Büttner-Ennever, 2006). The 'indirect' phase of the OKN relies on the visual inputs that come from the retina specifically from retinal ganglion cells that, with their large visual fields, can detect the visual scene. This component involves a

delayed and exponential increase that ultimately attains a steady state. In other words, the velocity storage component requires a 'loading' of velocity. It is important to note that, even though it's possible to transmit the 'indirect' phase only through the brainstem, there is a cortical control component in these pathways (Büttner & Büttner-Ennever, 2006). For example, humans that have cortical blindness do not have optokinetic responses (Verhagen et al 1997).

Mice, being animals with laterally placed eyes, have no smooth pursuit eye movements and have an OKN that mainly consists of the 'indirect' component that relies on retinal ganglion cells (Büttner & Büttner-Ennever, 2006; Oyster et al., 1972). Contrarily, in humans the stronger component is the 'direct' pathway, while the 'indirect' component is mostly missing (Simons and Buttner 1985). Nevertheless, mice have a low and "leaky" velocity storage when compared to other rodents, including rats (absence of OKAN response, (Laurens & Angelaki, 2011; John S. Stahl, 2004)).

However, mice show similar qualitative kinematic OKR features as compared to humans (onset latency, acceleration at stimulus onset, imperfect velocity buildup during the stimulation, rapid deceleration at stimulus offset and steady gaze-holding), with the difference being in the quantitative aspect (Kodama & du Lac, 2016).

2.3.2. Functional aspects of the OKR

The OKR optimally works at low-frequency ranges due to the fact that RGCs are efficient at relatively slow motion of the visual scene (± 3º/s in mice; (Dhande et al., 2013)). While most vertebrates have an OKR, the underlying neuronal mechanisms have changed along evolution. The quality and occurrence of this reflex is variable among vertebrates; velocity and amplitude of the eye movements as well as the range of velocities for which they are able to compensate vary (Masseck & Hoffmann, 2009). An interesting common feature of the OKR response among these species is the asymmetry in its response depending on which direction each eye is moving to: nasal-to-temporal (naso-temporal, N-T) or to the temporal-to-nasal (temporo-nasal, T-N) direction. In most species, including mice, the T-N direction has higher responses to the stimulus (Büttner & Büttner-Ennever, 2006) than the N-T. Recent evidence fortifies that the OKR pathway in mice is also direction-selective; the acceleration response in the T-N direction largely relies on the ipsilateral floccular complex (Kodama & du Lac, 2016) and not the N-T. Therefore, the OKN response for the T-N should involve the flocculus more specifically, FTNs, that are the only neurons floccular Purkinje cells that project out from the flocculi.

Several hypotheses have been proposed to explain this asymmetry. Some of them include: the need of a retinal specialization (*e.g.* fovea) for having a symmetric response

(Tauber & Atkin, 1968); the decussation pattern of RGCs as a determinant of symmetry (Fukuda & Tokita, 1957), as well as the binocular field overlap for a higher symmetry in the OKR response (Ter Braak, J.W., 1936). In mammals, unlike other vertebrate species, these 3 theories apply. For example, in primates and humans, who have a fovea, complete ipsilateral projections from the retina and almost a full overlap of the binocular field have a symmetric monocular OKR. On the other hand, rodents don't have a retinal specialization, only few ipsilateral projections (Masseck & Hoffmann, 2009). However, this asymmetry doesn't prevent mice from having great OKR gains, with relatively good responses up to <10º/s (John S. Stahl, 2004).

As seen, the OKR is a rather intricate reflex; it depends on the integration of visual inputs but shares the last neuronal components with the vestibulo-ocular reflex, making these 2 reflexes acting synergistically in physiological conditions. Moreover, even though this reflex is present among all vertebrates, the OKR neuronal circuits have diverged with evolution due to the differences in the visual system between species (Masseck & Hoffmann, 2009).

2.4. Convergence of OKR and VOR: functional complementarity

OKR and VOR are working conjunctly to stabilize gaze in vertebrates. The many similarities between the function and structure of vestibular endorgans in vertebrates (fishes, amphibians, birds, mice, primates) show how well-preserved it is among vertebrates (Hans Straka et al., 2016). At the same time, even though OKR is also present among vertebrates, its performance has a bigger variability between vertebrate species due to the different characteristics of the visual system (*e.g.* presence/absence of a retinal specialization, lateral-eyed/frontal-eyed) among them (Masseck & Hoffmann, 2009).

During everyday life, OKR and VOR cooperate so gaze stabilization has an optimized oculomotor performance. They do so by each one specializing in different working ranges: OKR, due to RGCs neuronal features, is more sensitive at slow motion; VOR is more effective at detecting velocities at higher head/body accelerations (Schweigart et al., 1997). This complementarity is also present in the response to constant velocities where only OKR can respond to constant velocities while VOR can't (Soodak & Simpson, 1988).

The dependence in gaze stabilizing reflexes changes through life. In mice, OKR gains in juveniles (postnatal days 21-26) are higher than in adult mice, while VOR gains behave in the opposite manner (Mathieu Beraneck et al., 2014). This indicates that, at a younger age, mice strongly rely on vision to stabilize gaze (Faulstich et al., 2004).

Furthermore, there is evidence that there are multiple mechanisms of plasticity operating with different time courses so that oculomotor performance is optimized. Training based on visuo-vestibular mismatch differentially affect each gaze stabilizing reflex. For example, experiments done in mice showed that a 30min of visual-vestibular mismatch training session induced VOR gain to decrease while OKR gain increased (Faulstich et al., 2004). Additionally, the persistence of these changes can also vary according to the adaptation protocol. In the next section, the capability of change of the VOR and OKR is further explored.

The OKR and VOR share part of the neuronal circuitry. Both reflexes have in common the adaptive controller of the circuitry *i.e*., the flocculus and VN, as well as what is being controlled *i.e.*, the oculomotor system and eyes (Ito, 2006). The responsiveness of each reflex to a certain type of stimulus (OKR- visual; VOR-vestibular), allows to differently shape the oculomotor responses.

In light, when the animal moves, both VOR and OKR are simultaneously evoked and act synergistically. VOR acts instantly and with a small latency in which the visual inputs can't correct for imperfections due to the time that retinal processing would take. Therefore, VOR must output a quick eye movement in response to a slow input, doing so by operating in an open-loop or feed-forward way. Parallelly, when the goal is to follow the movement of the visual scene, OKR moves the eye in the same direction, also to avoid retinal slip and maintain visual acuity. Here, the OKR visual signal is used in a closed-loop or feedback control. Feedback and feed forward control, common concepts among the works of this thesis, will be discussed in more detail in 5.1. Feedback vs Feed forward control.

Being a reflexive response to head movements, VOR works in the dark since the feedback from the visual system is not an essential part for its execution. However, developmental and pathological changes could occur and affect the correct performance of this reflex. When the VOR is not fully compensatory, the error message (retinal slip) is sent back to the VN and flocculus through the climbing fibers. The detection of the retinal slip is done through the OKR circuitry that will in turn serve for the correction of the VOR. Here is where motor learning comes into play by modulating OKR/VOR and restoring accurate gaze stabilization. This process is known as OKR/VOR adaptation, discussed in the following section.

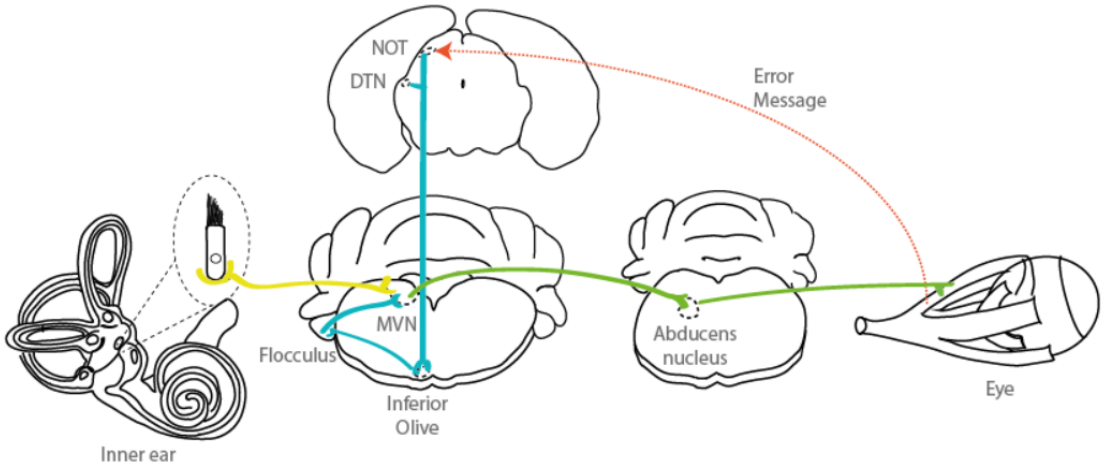

Figure 16. OKR and VOR pathways. The schematic of the convergence of these pathways uses traces to underline the commonalities and particularities of each pathway. Traces: yellow - vestibular nerve; blue – projections from the NOT and DNT to the cerebellum (OKR pathway); green – projections of the MVN to the eye muscle. Credit Filipa FdB.

3. Motor learning in gaze stabilizing reflexes

3.1. Gaze stabilizing reflexes as motor learning models

Gaze stabilizing reflexes are a model system used in worldwide laboratories. Both OKR and VOR have several advantages that make them great models to study motor learning: inputs can easily be controlled, the motor outputs are quantifiable with precise methods. As it can be appreciated in the previous section (VOR and OKR pathway), VOR circuitry is less intricate, and therefore better known, than OKR making it a vantage point for the study of VOR. However, because it relies on only one sensory modality, OKR is usually preferred in cerebellum-related studies (Kodama & du Lac, 2016; Wada et al., 2014).

Hence, there are 3 main concepts that are inherent to VOR motor learning (Jay M. Goldberg et al., 2012c): 1) the removal/lesion of the flocculus removes the capacity of VOR to adapt (Lisberger, 1984; Shutoh et al., 2006); 2) both the lability and reversibility depend on the time frame on which the learning is performed; 3) it requires the comparison of visual and vestibular input (Collewijn & Grootendorst, 1979).

OKR and VOR motor learning paradigms can easily be performed and quantified in the laboratory. Experimentally, the goal is to produce a retinal slip, frequently attained using a high-contrast visual stimulus (*e.g.* a black and white striped or checked pattern). In the case of VOR, this is done by pairing image and head motion; either the head is moved in the same direction as the visual stimulus (gain-down) or in the opposite direction (gain-up). In both cases, a retinal slip will be evoked since the image will be blurred in the retina due to a mismatch between the visual and vestibular information. The retinal slip will act as an error signal indicating that the eye movements are not completely compensatory and will ultimately drive motor learning to modify the VOR (Shin et al., 2014). This process is known as VOR adaptation. On the other hand, OKR adaptation experiments are performed by rotating the visual stimulus, usually a drum/cylinder with a high-contrast pattern, around the animal. Training sessions consist of combinations of sinusoidal drum rotations at different frequencies and combined directions (N-T or T-N) (Faulstich et al., 2004; John S. Stahl, 2004).

Commonly, these VOR and OKR adaptation paradigms consist of repetitive passive head-fixed training sessions with different inter trial intervals (Boyden & Raymond, 2003). One of the projects of this thesis (Carcaud et al., 2017) developed a protocol that allows for continuous VOR adaptation, product of natural head movements in freely-behaving mice. A similar experimental paradigm, which inspired our approach, was performed in primates where VOR adaptation was induced through the long-term use of prisms (Berthoz et al., 1981; Nagao et al., 2013).

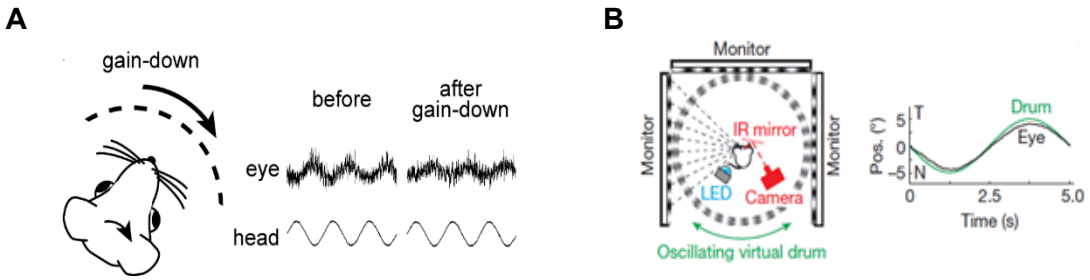

Figure 17.Motor learning paradigms. Left- VOR gain-down stimulus generates a decrease in the VOR response. Adapted from Boyden and Raymond 2003. Right- OKR motor learning set up with example recordings. Adapted from Liu et al., 2016.

3.2. The driving error signal for motor learning: theories

Even though the direct VOR pathway does not involve the cerebellum, the adaptation of this reflex depends on this structure. An error signal is generated (retinal slip) when eye movements are not perfectly compensating for head movements. This error message will create adaptive processes that will result in a change of the response of VN neurons thus, calibrating the VOR (Medina, 2011). The cerebellum is known to be key in the calibration of VOR (Boyden et al., 2004) yet, two hypotheses provide contrasting roles for it in this process, sharing as a common ground an implication of Purkinje cells (PC) of the vestibulocerebellum (flocculi).

First, Masao Ito (Ito, 2002) proposed that the Purkinje cells are themselves the site of plasticity. After going through the inferior olive and the climbing fibers, the error signal would change the efficacy of the synapse between parallel fibers and PC by long-term depression (LTD). The PC neurons would inhibit the VN and change the VOR response. Following this hypothesis, motor learning would only stop when the climbing fibers don't carry any error message. Hence, in this hypothesis, the cerebellum acts as the storage site of the learned motor memory.

Later, in 1981, Miles and Lisberger (Miles & Lisberger, 1981) proposed a new theory of the neural basis of VOR adaptation. This hypothesis was fueled by the

observation that, in awake monkeys, passive-head rotation caused PC to send a gaze-related message (Lisberger & Fuchs, 1978). In a gain-up scenario, there is a decrease in PC activity that causes LTD at the synapse with the VN (Medina, 2011). In this theory, PC neurons carry the error signal to the site of plasticity, the VN. Hence, the role of the cerebellum is to transmit the signal that will drive plasticity in the brainstem. Recent studies (McElvain et al., 2010) came to strengthen this theory by proving that LTD could be induced at the synapse between the vestibular nerve and the VN. Although the hypothesis of a long-term retention of adaptive memory in the brainstem has been suggested and given support from several theoretical studies (Yamazaki et al., 2015, Clopath et al., 2014, Menzies et al., 2010, Masuda and Amari, 2008, Porrill and Dean, 2007), it doesn't have yet any experimental support *in vitro* and the underlying mechanisms therefore remain elusive.

3.3. Short-term and long-term adaptation

After being learned, motor memories can become less labile through consolidation. This consolidation requires a fundamental change in the way that memory is encoded and is achieved by switching from a short-term plasticity mechanism to a durable mechanism (Boyden et al., 2004). Thus, different time windows could reflect different brain structures involved in the retention of the learned memory.

For short-term adaptation the cerebellum is known to be responsible for its retention (Boyden et al., 2004; Carey, 2011). However, long-term retention of motor learning resides outside the cerebellum. Flocculi shut down studies showed that VOR adaptation is suppressed on the short-term (1h) but not on the long-term (72h) (Kassardjian, 2005). Additionally, OKR motor learning has also been proven to depend on the short-term in the cerebellum (flocculus) and transfer to another site, possibly the brainstem (Shutoh et al., 2006). Other theoretical studies have considered the brainstem as a putative site for long-term adaptation (Menzies et al., 2010; Porrill & Dean, 2007). Still, the neural mechanisms as well as in vitro support are missing to fully prove this theory. One of the studies of this thesis adds experimental support for the retention of motor learning in the brainstem; we show that synaptic transmission and intrinsic properties of MVN neurons change after long-lasting visuo-vestibular mismatch (Carcaud et al., 2017).

3.4. Mice as model systems for oculomotor plasticity

The mouse was disregarded as a vestibular laboratory model up until the early 2000s and was outshined by other animal models. The uprising of videoculography (reviewed in Methods 2. Video-oculography) as a laboratory tool to assess eye

movements demonstrated the efficacy of gaze stabilizing reflex in the mouse. Additionally, molecular genetic techniques enable the creation of mutant mice with desired characteristics (*e.g.*, fluorescent neurons, KO lines). Mice have robust eye movement responses to visual and vestibular inputs and the synergy of both reflexes during self-motion almost outputs gain unity (J. S. Stahl et al., 2000; van Alphen et al., 2001). Apart from the anatomical similarities, it was proven that mice have VOR responses and features comparable to those of humans and monkeys [VOR: (John S. Stahl, 2004); OKR: (Kodama & du Lac, 2016)] hence, making it possible to study in the same animal model behavior and its underlying neuronal elements (M. Beraneck & Cullen, 2007), taking advantage of the genetical tools available. Furthermore, adaptive plasticity of gaze stabilizing reflexes has been proven in the mouse and has become one of the main animal models to study cerebellum related plasticity (Faulstich et al., 2004; Kodama & du Lac, 2016).

4. Locomotion

4.1. Overview

The motor system englobes several networks of the nervous system that are responsible for the organization of vital functions such as respiration, chewing and locomotion (Grillner, 2003). Locomotion is the motor action that enables the movement of an animal in the environment. Walking, crawling, swimming or even flying are ways of locomotion that allow different animal species to perform essential everyday life tasks like hunting for food, running away from danger or interacting with other animals. In the evolution of vertebrate species, different locomotion ways appeared in function of the development of the appendicular system.

Locomotion is a subject that has long fascinated scientists. The concept of locomotor pattern was first portrayed with the development of chronophotography by Étienne-Jules Marey and Eadweard Muybridge in the 1880s. They both captured animals and humans in motion using consecutive stop-motion pictures. Despite the big diversity of behaviors, locomotion studies in numerous animals showed that the main characteristics of the locomotor cycle are common to every species (Falgairolle et al., 2006).

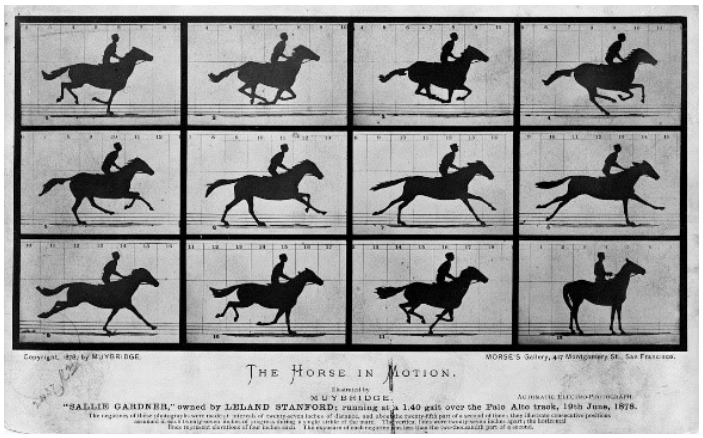

Figure 18. Muybridge's 'The Horse in Motion', 1878. Sequence of pictures taken to solve the debate whether all four feet of a horse were off the ground at the same time. Source: Library of Congress Prints and Photographs Division.

4.2. Elements of the locomotor system

4.2.1. Spinal cord

The spinal cord is part of the CNS and is the relay of motor commands from the brain to the muscles as well as sensory inputs from the periphery. The spinal cord

contains the neurons (motoneurons) that perform motor actions as well as the interneuronal network capable of generating rhythmic locomotion.

Cylindrical and slender, the spinal cord ranges from the end of the brainstem to the lower part of the vertebral column. Shape-wise, it has bilateral symmetry with the ventral median fissure and dorsal medial septum creating a dentation in the cylinder (Sengul & Watson, 2012). In the mouse, the spinal cord is divided in 34 segments: 8 cervical (C1 to C8), 13 thoracic (T1 to T13), 6 lumbar (L1 to L6), 4 sacral (S1 to S4) and 3 coccygeal (Co1 to Co3). The beginning of the thoracic and end of the cervical as well as the beginning of the lumbar and end of the thoracic spinal cord can be distinguished by the cervical (C5 to T1) and lumbosacral enlargements (L2 to L6), respectively.

It is made of grey and white matter and its proportions vary along the different parts of the spinal cord. The white matter owes its color to the abundance of myelinated fibers and is located on the outermost region, composed of ascending and descending tracts as well as glial cells. The bundles of nerve fibers that run along the white matter are called tracts or fasciculi and are named in regard to their origin and destination (for example, vestibulospinal, corticospinal). The grey matter is mostly made of neurons and their processes and, in a transverse section (schematic representation below, **Figure 19**), they form a shape that resembles a butterfly. The dorsal and ventral horns categorize the grey matter, dividing it into an area of mostly sensory (dorsal) neurons or interneurons and motoneurons (ventral) (Sengul & Watson, 2012).

The division of the grey matter of the spinal cord into ten layers was proposed by Rexed in 1952. The first lamina is at the top part of the dorsal horn and progressively their counting goes until the ventral horn and ends with the tenth lamina around the central canal. Laminas 1 to 6 make up the dorsal horn, lamina 7 stands intermediate and 8 and 9 make the ventral horn.

The axonal projections of neurons exit the spinal cord through the dorsal and ventral roots. The dorsolateral sulcus is the entry point of the dorsal roots. Dorsal roots are formed by the axons of sensory neurons on the dorsal horn of the grey matter. In turn, ventral roots emerge from the ventrolateral sulcus and are mostly made of efferent motor fibers.

4.2.2. Motor units

Locomotion is achieved by the activation of muscle fibers through motoneurons. In the spinal cord, motoneurons are located in the ventral horn, in layer IX of Rexed (1952). There, motoneurons project their axons directly to a muscle and innervate some of its fibers, creating a motor unit. Fibers of the same motor unit share their contractile

characteristics that render either slow or fast (2 subtypes) motor units. In turn, the activation of motoneurons is done through interneurons. Interneurons are one of the three functional classes of spinal neurons (sensory, motor and interneurons) and are thought, due to their short axons, to innervate neighboring neurons (Purves, 2004). They can belong to numerous motor or reflex pathways and thus activate motoneurons in many ways to effectuate a given movement.

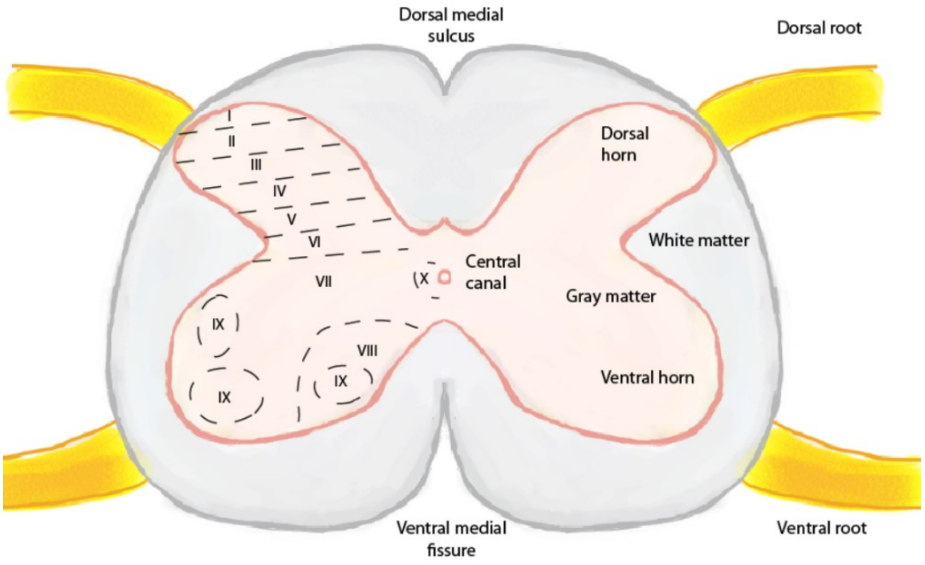

Figure 19. Schematic representation of a transversal spinal cord slice. Left- Rexed's laminae classification. Right- areas of the spinal cord is regards to white and grey (dorsal and ventral horns) matters. Credit Filipa FdB.

4.2.3. Central Pattern Generators

In the early 20th century, Sherrington and Graham Brown were responsible for most of the advances in the comprehension of the neuronal substrates that allow for the generation of locomotion. Sherrington showed in the spinal dog that a 'scratch-reflex' persisted and suggested that it was due to an internally generated rhythmic movement (Sherrington, 1906). Graham Brown showed in a transected spinal cord cat preparation (with cut spinal cord and dorsal roots) that the flexion and extension movement of hindlimbs could still be evoked. Since there was no sensory feedback or descending input, he concluded that the neuronal networks of the spinal cord contained the 'machinery' to generate rhythmic movements. Thus, the spinal cord possessed the neuronal networks (microcircuits) responsible for the generation of locomotion. These neuronal networks are the so-called central pattern generators (CPGs). CPGs are groups of interneurons that produce coordinated motor output through the rhythmic

activation of neurons. They activate and rhythmically coordinate certain motoneurons that will produce an intended response/movement while inhibiting the ones that counteract it. There is also research in the most diverse non-mammalian species from the drosophila (Hückesfeld et al., 2015) to the Xenopus (Picton et al., 2018), that have brought insights to CPG involved in other types of locomotion.

CPGs are located throughout the CNS and serve not only for generating voluntary behaviors, like locomotion, but also for behaviors that are basally happening without the subject realizing them. For example, breathing is a rhythmic motor behavior that is controlled by a brainstem CPG that continuously works to exchange air with rhythmic inspirations and expirations (preBötzinger complex, (Gray et al., 2001; J. C. Smith et al., 1991).

The CPGs responsible for locomotion are located in the spinal cord. Research done on isolated spinal cord mice preparations combined with lesions, electrophysiology, pharmacology and neuroanatomy defined the T13-L2 as the hindlimb CPG location in this model (Cazalets et al., 1995). The C7-T1 region is pointed to be host of the forelimb control generators (Ballion et al., 2001). These 2 CPGs are interconnected to allow the adequate coordination of the anterior and posterior members. During locomotion, CPGs are responsible for: 1) generating the rhythm and reiteration (cycles); 2) the flexor/extensor alternance of a limb as well as 3) contralateral alternation of limbs.

The locomotor pattern can be adjusted to the external environment, for example in the case of an obstacle or if the animal starts running from a predator. Sensory feedback reaches the CPG to alter the duration of the phases of that particular response and gives feedback to motoneurons. CPGs are turned on by descending commands from brain regions and sensory feedback from limb proprioceptors. These commands not only activate the CPGs but also control the level of activation. They can either come from corticospinal or subcortical areas. They are also called pyramidal and extrapyramidal, respectively, due to the pyramidal cells of the cerebral cortex that in these pathways send their axons to the motoneurons in the spinal cord and will be briefly described in the following section (see 4.4.1. Descending command systems for locomotion).

Nevertheless, in vertebrates, the exact functioning and genetic content of the neurons that make up the CPGs are not yet underpinned. In vertebrates, locomotor CPGs have been studied using electrophysiological recordings and microscopy imaging in genetically modified mice. That is so because the identification of CPG neurons is based on their transcription factors. The putative CPG interneurons are classified as v0, v1, v2 and v3 (Goulding, 2009).

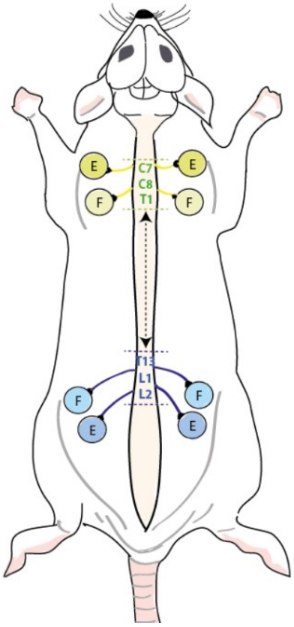

Figure 20. Schematic representation of the location of the CPGs in the cervical and lumbar spinal cord of the mouse. Representative connection of the CPG to the flexor (F) and extensor (E) muscles. Credit Filipa FdB.

4.3. The locomotor cycle

4.3.1. Phases of the locomotor cycle

In 1911, Thomas Graham Brown, one of the precursors of the locomotor field, published the 'Intrinsic Factors in the act of progression in the Mammal' (Brown, 1911). There, he wrote one of the first definitions of a locomotor cycle:

'Whilst the act of progression is being performed, the several limbs exhibit rhythmic movements of flexion and extension. When any limb is in contact with the ground, it extends, and thus serves to propel the animal forwards. At the end of this act the limb is lifted from the ground by a movement of flexion, is carried forward and finally is again placed upon the ground to repeat the cycle'. Graham Brown, 1911.

Over-ground locomotion in limbed animals requires rhythmic sequential cycles of limb flexion and extension. A locomotor cycle begins with liftoff – swing phase –and ends when the same limb goes back to its starting point after executing the stance phase. The swing phase consists in the propulsion of the limb using, mainly, the flexor muscles. After that, when the limb touches ground again, the body is propelled using the extensor muscles during stance phase.

This description of the locomotor cycle is based on the movement and displacement of a certain limb, but it must be noted that locomotion requires a narrow coordination between ipsilateral and contralateral limbs thus involving a considerable number of synergistic and antagonistic actions. By varying the duration over time of each of the locomotor phases, the patterns of locomotion change thus, creating different types of gaits. A gait is classically defined by the time that the stance phase takes. Data from kinematic recordings linked to electromyographic recordings allowed to enrich the locomotor pattern by characterizing the different gaits (Abourachid, 2003; Lemieux et al., 2016).

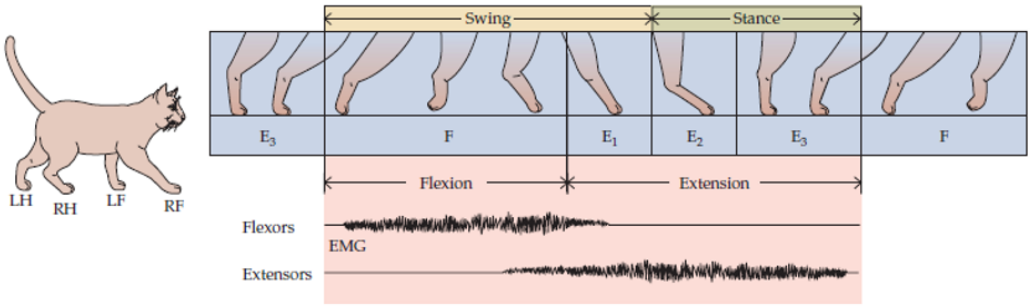

Figure 21. The phases of the locomotor cycle. On the swing phase the limb is flexed and leaves the ground propelling to the stance phase where the limb is extended, touching the ground. During swing the leg is mostly flexed (F) and during stance the paw is extended (E1, E2, E3). As seen in the EMG (orange panel), during the swing phase, there is a small overlap between flexion and extension. LF- left forepaw, RF- right forepaw, LH- left hind paw and RH-right hind paw. Adapted from Purves et al 3rd edition.

4.3.2. Types of gaits

According to their stance pattern (the cycle begins with the footfall of a reference limb and ends with the footfall of the same limb), the gaits of quadrupeds have been classified as symmetrical or asymmetrical. If half of the locomotor cycle was enough to describe the locomotor pattern, the cycle was considered to be symmetrical. Conversely, if half of the cycle was insufficient to describe the locomotor cycle, the gait is asymmetrical. However, depending on desired type of study, this classification has some constraints. For example, the actions of the other limbs had to be done during that stance and it obliges to pick a reference foot that must be the same throughout the entire experiment, which sometimes is not possible since the animal changes gait (Abourachid, 2003). Nevertheless, this classification has been used to demonstrate a wide range of locomotor gaits in several quadrupedal species (Abourachid et al., 2007) that likely share among the same neuronal circuitry (Orlovsky et al., 1999).

In the mouse, the locomotor repertoire has recently been classified by Lemieux and colleagues (Lemieux et al., 2016) using kinematic recordings and graph analysis. Using the step frequency, swing and stance duration, they identify the following locomotor patterns: lateral walk, trot, half-bound, full-bound, hop, transverse gallop, rotary gallop and out-of-phase walk. Based on locomotion being a dynamic process, they further classify these gaits into attractor and transitional. Attractor gaits were the preferentially used gaits at which the locomotor network has the tendency to go to. At low speeds (15 cm/s) – out-of-phase walk –, at intermediate speeds (45 cm/s) – trot – and full-bound for high speeds (90 cm/s). Transitional gaits were the ones used to switch between two types of gaits: lateral walk, hop, rotary and transverse gallops (Lemieux et al., 2016).

As it can be seen in **Figure 22**, in mice, changes in locomotor speeds are related to changes in the sequence of the movements. Naturally, if the locomotor speed increases, it will reduce the time needed to complete a cycle as well as the amount of time where the limb is in contact with the ground (Purves, 2004). During the lower speeds (out-of-phase walk) the hind and front limbs are out of phase, whereas in the fastest speeds (full-bound) both sets of limbs are synchronized, *i.e.*, in phase. In the intermediate speeds (trot) both the hindlimbs are out of phase but in phase with the contralateral hindlimb (diagonal) (Lemieux et al., 2016).

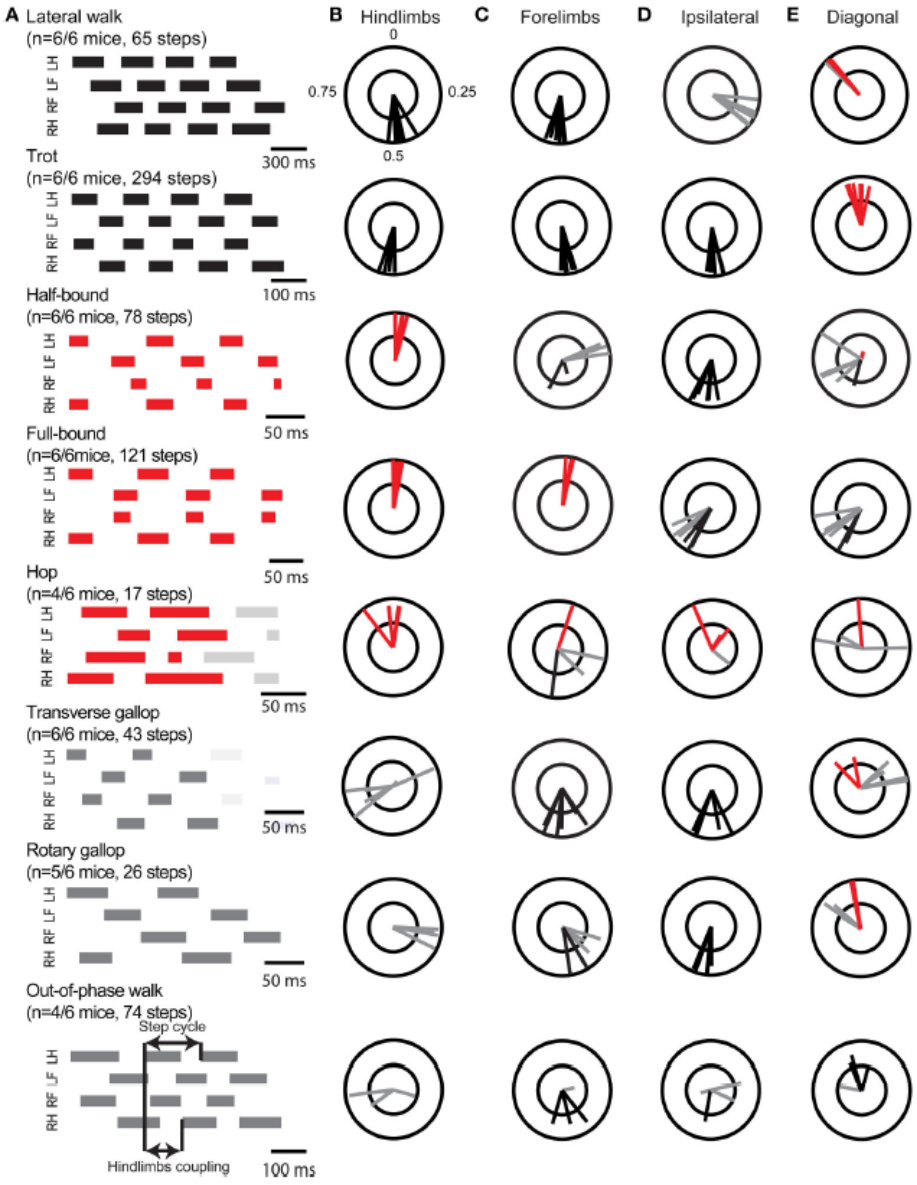

Figure 22. Types of gaits in the mouse. A- Duration of the stance phase (thick lines) of: LH- Left hindlimb, LF- left front limb, RF- right front limb and RH- right hindlimb. Mean phase coupling between B-hindlimbs; C- Forelimbs; D- Ipsilateral and H- contralateral front and hindlimb. From Lemieux et al 2016.

4.4. Neural control of locomotion

When a motor output is determined by the brain it excites the spinal circuits to accomplish it. In turn, after integrating the descending commands and the exafference sensory inputs (net sensory signals encoded by sensory organs, see below), the spinal motoneurons perform the movement and send feedback to the supraspinal structures via ascending pathways. Therefore, the control of locomotion involves a tripartite system

where supraspinal, spinal and afferent sensory stimuli interplay. The organization that underlies the genesis of locomotion is particularly well-preserved in vertebrates.

4.4.1. Descending command systems for locomotion

The supraspinal level

Information coming from the cortex can take two projection pathways: direct pathways of voluntary movements of cortical origin, or pyramidal system, and indirect pathways of motricity of sub-cortical origin, or extra-pyramidal system. The corticospinal pathway begins with the pyramidal neurons in the cerebellar cortex that directly project to the spinal neurons after having decussated at the level of the bulb. This pathway comprises two tracts: the lateral corticospinal tract and the anterior corticospinal tract. Most neurons take the lateral corticospinal tract, that controls distal limb musculature, this is, fine and precise movements. The anterior corticospinal tract controls axial musculature, that is, gross movements. The subcortical pathway makes a relay at the level of the hypothalamus and the basal ganglia before entering the spinal cord. Then, the fibers coming from the basal ganglia project to locomotor regions either: subthalamic locomotor region (SLR), mesencephalic locomotor region (MLR) or medullary reticular formation (MRF) (L. H. Kim et al., 2017). These regions are conserved in vertebrate species (Rossignol et al.,2016) and were identified due to their capability of eliciting different locomotor gaits when electrically stimulated (cats – Ryczko & Dubuc, 2013; mice – Josset et al., 2018; Roseberry et al., 2016).

From that point, information can be sent through the pons via the reticulospinal tract that receives inputs form the ascending tracts and controls extensor muscles. The rubrospinal tract originates in the red nuclei of the brainstem, receives inputs from the cerebellum and coordinates flexor muscles. Locomotor gait is the product of sensory afferent inputs and the supraspinal pathways described above. However, little is known about how the descending pathways regulate gait.

The spinal level

When the motor command is at the spinal stage, the CPGs transform this tonic command in an organized pattern of rhythmic motor activity by conveying it to the motoneurons that will integrate it and initiate locomotion. Motoneurons will not only send to the muscles this command but they are also a big relay of the integration of the motor output (Hultborn & Kiehn, 1992). The descending inputs from the motor cortex, basal ganglia and brainstem determine the outputs from the locomotor CPG. However, this output can also be shaped by the proprioceptive and vestibular pathways that converge in the CPG (Goulding, 2009).

4.4.2. Ascending command systems for the regulation of locomotion

Cerebellum

The supraspinal elements are not only in charge of initiating locomotion but also of its regulation. The cerebellum is a key structure in the regulation of these locomotor interactions. Lesions in the cerebellum make a disorganized locomotion with variable step lengths, an incorrect foot placement as well as balance troubles like increase of the postural oscillations. For example, Purkinje cell degeneration (pcd) mutant mice exhibit gait ataxia characterized by an impaired front-hind interlimb and whole-body coordination (Machado et al., 2015).

The spinocerebellum (vermis and medial part of the cerebellar hemispheres) integrates inputs of spinal excitatory neurons that are rhythmically active during walking: the dorsal spinocerebellar tract (DSCT) and the ventral spinocerebellar tract (VSCT) (Fedirchuk et al., 2013). The DSCT carries inputs from the proprioceptive afferents and updates the cerebellum of about the actual limb movement (Bosco & Poppele, 2001). The VSCT neurons are modulated by the locomotor CPG without being dependent of the sensory information coming from the limbs. The role of this tract is to convey to the spinocerebellum an efferent copy of the rhythm generated by the locomotor CPG (Gustafsson & Lindström, 1973).

By creating a spinocerebellar loop, these tracts modulate the activity of CPGs with the external environment. The spinocerebellum encompasses the expected movement (VSCT) and compares it with the performed one (DSCT). Then, it will adjust the motor command by indirectly controlling the activity of the spinal CPGs and the motoneurons by the descending vestibulospinal, rubrospinal and reticulospinal pathways.

Sensory afferences

Despite CPGs being able to produce rhythmic motor output without sensory feedback, the locomotor pattern is modulated by sensory inputs in order to correctly respond to a changing environment(Rossignol et al., 2006). The generation of a movement not only implies a motor command but also a set of sensory information that will interact with the supraspinal and spinal stages to adapt the performed movement to proprioceptive and external obstacles. Furthermore, these inputs can initiate or stop locomotion. Proprioceptive afferences are key in regulating locomotion by controlling the transition between the stance and swing phases of the cycle as well as the degree of activation of the muscles (Whelan et al., 1995). Cutaneous sensory inputs are an important CPG modulator. Cutaneous afferents are the mechanoreceptors that encode

touch; they can initiate, stop as well as modulate ongoing locomotion (Panek et al., 2014). For example, when the moving limb finds an obstacle in its environment, cutaneous afferents can trigger corrective responses (Rossignol et al., 2006). Acoustic and vibration stimuli have also been found to initiate locomotion, for example, auditory startle responses that create a generalized motor response.

It is important to note that the weight of the sensory component is different between species and changes with the speed of locomotion. If very fast movements are being executed, sensory feedback is unable to act due to lack of time. Therefore, the adjustments have to be done in a predictive (feedforward) mode (Purves, 2004). This point will be further elaborated in the following section.

Vestibular nuclei determine the level of postural tonus to maintain balance in an animal along locomotion by permanently adjusting the balance between contraction of flexor and extensor muscles. Therefore, the lateral vestibular nuclei, phasically active during locomotion, projects to the center of the spinal cord on the interneurons and extensor motoneurons, inducing an increase of the antigravity muscles during the stance phase. Inversely, the red nucleus and the pontine reticular formation project to the neurons innervating the flexor muscles, acting preferentially for the regulation of the swing phase (Rossignol et al 2006). This functional balance between these structures is revealed in lesional experiments in the cat or following an intercollicular transection that gives a rigidity of decerebration (hyperextension) after the suppression of the influence of the red nucleus (Sherrington, 1906).

5. Predictive motor signaling for gaze stabilization

5.1. Feedback vs Feed forward control

Locomotion allows animals to explore their environment using goal-directed as well as reflexive motor commands that must adapt to the external environment. To do so, animals need to change their gait and gaze through the integration of sensory information (proprioceptive, cutaneous, vestibular, etc.) while the movement is ongoing. This process is called sensorimotor integration and aims at optimizing and correcting the motor output. One of the most important features of sensorimotor integration is the precise timing during which the action needs to be executed. Depending on whether the sensory input/perturbation was expected or not, two different types of control will occur.

If, for example, a mouse is walking on its cage and an external force is of a sudden applied, the sensory signals will be sent to the CNS so that the movement is adapted to this unexpected event. This post-occurrence correction embodies feedback control. However, this probably won't prevent the mouse from stumbling. A disadvantage of feedback control is the delay involved in the processing of the sensory inputs, in this case. It involves the detection by the respective sensory afferent, the sending to the nervous system and the production of a response that will be sent to motoneurons so that muscles can be flexed/extended. Nevertheless, if the mouse is just standing up or exploring the environment, sensory feedback is key.

Now, let's consider that the mouse is running in its cage and transitions from a ground full of sand bedding to one that is covered in paper tissue. In this case the perturbation is anticipated before its initiated. Here, the mouse can anticipate the change in terrain ahead and optimize, for example, joint angle combinations and/or interlimb coordination. Therefore, correction of movement begins before the actual perturbation arises. This type of control is referred to as feed forward control. Feed forward control is often automatic and involuntary (Purves, 2004). For locomotor control, the cerebellum has been hypothesized to provide a forward model that is able to predict the sensory consequences of limb movements. For example, ataxic Purkinje cell degeneration mice appear not to have the capacity to predict and actively cancel the sensory consequences of snout and tail movements which is the possible cause of their impaired limb coordination (Machado et al., 2015).

5.2. Efference copy

Locomotion is a complex behavior that involves the activation of nervous system structures at several levels as well as several effector muscles. Consequently, during

this behavior, sensory systems are constantly receiving different stimuli, both from an environmental (exafference) origin as well as the actual sensory prediction that is internally being produced from that expected movement (reafference). To be able to process the stimuli that translate important contextual changes, animals need to distinguish the external stimuli from the internally generated ones. Corollary discharges or efference copies are neural representations of the actual motor output that is sent to a sensory system, decreasing or cancelling the reafference component (**Figure 23**). This predictive feed-forward mechanism has been detected in several animal species and acts on various behaviors like human speech (Whitford et al., 2017), vocalization (Kelley & Bass, 2010), visuomotor processing in flies (Fujiwara et al., 2017; A. J. Kim et al., 2015). One of the most popular examples is not being able to tickle ourselves (Blakemore et al., 1998); briefly, this happens because there is a prediction of the sensory consequences of these movements and this signal will cancel the sensory response to the auto-generated stimulation (Blakemore et al., 1998).

Corollary discharge and efferent copy are not synonyms, even though they are been used as so for a long time. A corollary discharge is a neural representation of an ongoing motor task that is sent to a different brain area with no inherent temporal pattern. On the other hand, an efferent copy is an exact replica of the motor output that is directly sent to the desired effector. Furthermore, a corollary discharge can exert its influence at any point, while efference copies usually act on the early stages of the sensory processing (Hans Straka et al., 2018).

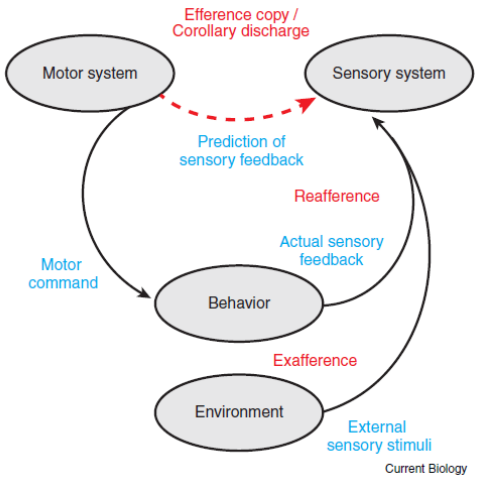

Figure 23. Schematic of the relationships between motor and sensory systems during the production of behavior. From Straka 2018.

5.2.1. Efference copy in motor systems: gaze stabilization

The maintenance of visual acuity during locomotion is achieved by gaze stabilizing eye movements. Classically, this ability has been exclusively attributed to reflexive eye movements (VOR and OKR). However, efference copies have also been shown to have an important role in minimizing visual disturbances during locomotion (Combes et al., 2008). They do so by connecting spinal cord CPGs to gaze stabilization areas in a feed forward manner. This motor-to-motor coupling is based on the idea that the timing and amplitude of head/body movement can be predicted due to the patterned fashion of rhythmic locomotion (Hans Straka et al., 2018).

The demonstration of the participation of efferent copies on gaze stabilization has been provided in experiments on Xenopus tadpoles (Combes et al., 2008; Lambert et al., 2012). In these studies, it was reported that the neural signals produced by locomotor spinal cord CPGs are sent to the brainstem extraocular motor nuclei. Using electrophysiology, a paired spino-extraocular discharge was seen to occur during undulatory swimming in semi-intact preparations but also during fictive swimming of isolated brainstem spinal-cord preparations (Combes et al., 2008). Soon later, using *in vitro* and *in vivo* experiments, the spinal origin of this efference copy was traced as well as the putative map of the ascending trajectory of this command from the spinal CPG to the medial rectus motoneurons. Additionally, conjugated eye movements were found to counteract the head movement performed during swimming in the opposite direction. During externally applied motion (turntable stimulation) tadpoles exhibited VOR to compensate for the inherent visual disturbances. On the other hand, during real locomotion (self-motion) the VOR was suppressed and it was the spinal locomotor efference copies that evoked compensatory eye movements (Lambert et al., 2012). Hence, this suggests that there are two different mechanics involved for gaze stabilization during self-generated or externally applied movements (Hans Straka & Chagnaud, 2017).

Despite the many ways in which locomotion can be expressed (undulatory, bipedal, quadrupedal), it has been stated in the previous sections of this thesis, that all tetrapod vertebrates, including mammals, share most of the basic motor elements involved in locomotion, *e.g.*, the CPGs. Therefore, one can suspect that this motor-to-motor coupling would not only be present in amphibians but also in other vertebrates like mammals, birds and reptiles. Thus, in an evolutionary context, it's interesting to explore existence of such an efference copy signaling on higher vertebrates.

6. Aims of the thesis

In this thesis, gaze stabilization in mice was studied by experimenting on two classical pathways, the optokinetic and vestibulo-ocular pathways, and by deciphering a novel pathway from the cervical spinal cord to the brainstem where a predictive feedforward efferent copy is relayed (**Figure 24**). Using a multimethodological approach, this thesis aims at gaining insights about how the brain combines different sensorimotor inputs to ensure the homeostasis of gaze stabilization in different contexts.

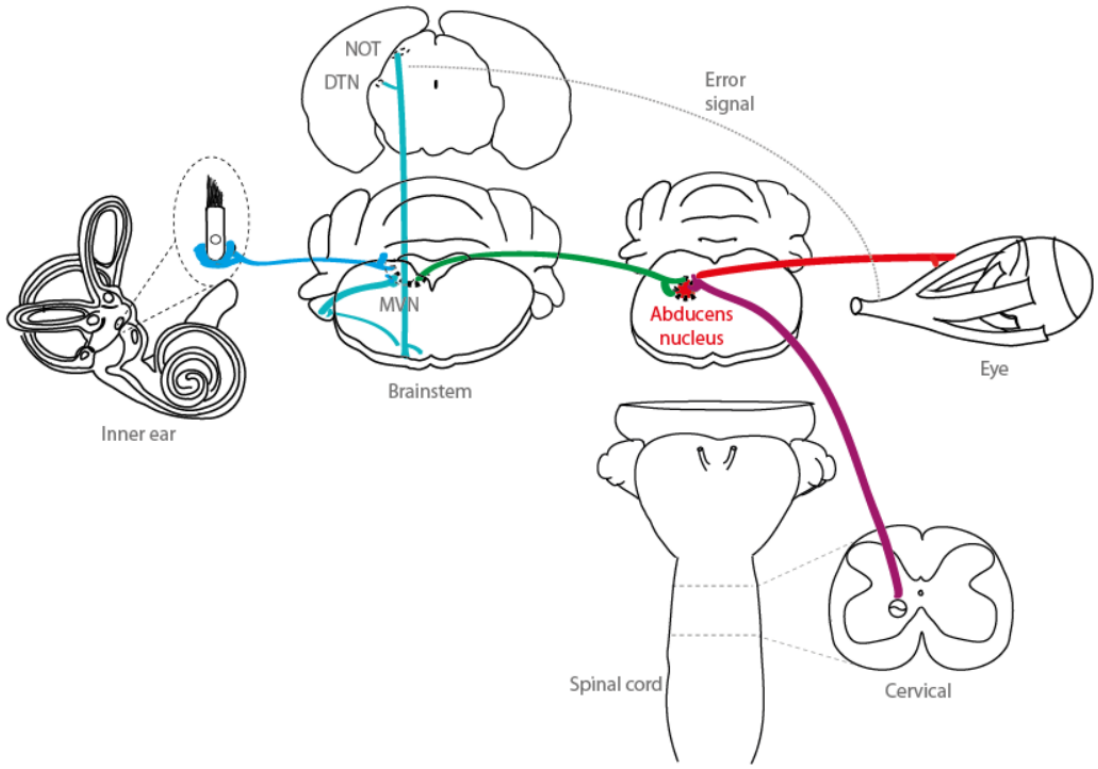

Figure 24. Conceptual scheme of the pathways studied in this thesis. VOR (Light blue and green line), OKR (turquoise and green lines), efferent copy from the locomotor CPGs (purple line) converge on the abducens nucleus (red) so that a premotor command that will move the eye can be generated. Credit Filipa FdB

One of the main goals was to investigate how visual and vestibular inputs complete each other, and how the brain adapts to conflicting sensory signals. We wanted to understand the effects of a long-term visuo-vestibular mismatch perturbation on gaze stabilizing reflexes (OKR and VOR). We did so by employing an innovative visuo-vestibular mismatch (VVM) protocol designed by my team where mice have a helmet-like device fixed onto their heads for 14 days. First, with this VVM protocol we aimed at quantifying the decrease of the VOR as well as to study the neuronal mechanisms of this reduction (Article 1. Long-Lasting Visuo-Vestibular Mismatch in Freely Behaving Mice Reduces the

Vestibulo- Ocular Reflex and Leads to Neural Changes in the Direct Vestibular Pathway). To achieve this, we used patch-clamp electrophysiology as well as videoculography experiments. Due to the versatility of this protocol, we felt compelled to share the detailed methodology for its use for other studies (Article 2).

For the last study of this project, we aimed at studying the influence of visual signals in the tuning of mice gaze stabilizing reflexes (Article 3). To do so, we investigated the consequences of the VVM on: 1) the OKR responses; 2) the kinematics of both OKR and VOR during up to 10 days after the removal of the device (recovery period); 3) the frequency-dependency of the recovery of the responses and 4) the comparison between the recovery of OKR and VOR.

The second project of my thesis investigates how these sensory-based pathways could, in the context of active behavior, be supported by non-sensory, predictive motor signaling. In this study we defy the traditional understanding that gaze stabilization during locomotion is exclusively attained by sensory inputs. More specifically, this thesis aimed at deciphering and characterizing the existence of a spino-extraocular pathway that minimizes visual disturbances during locomotion in mice. The experiments performed for this project were a collaboration between 3 teams across France (Bordeaux, Marseille and Paris) that enabled the use of an array of different techniques (semi-intact preparations, *ex vivo* and *in vivo* recordings). The results of this project are presented in Article 4.

The expertise gained during these fundamental research projects was applied in a collaborative study that aimed at treating auditory and vestibular disorders using adeno-associated virus (AAV) gene therapy (Article 5). Here, we measured compensatory eye movements in AAV-treated and non-treated Usher syndrome type 1 (USH1) mice. Like their human counterparts, USH1 mice suffer from congenital profound deafness and balance disorders. Using videoculography, we were able to evaluate the success of this treatment by measuring their vestibular function. Studies like this will help explore new possibilities for the treatment of inner ear pathologies.

Chapter II -

Methodology

1. Visuo-vestibular mismatch protocol

This protocol was initially developed by Dr. Mathieu Beraneck in 2014 and, since then, several papers have been published using this methodology (see Carcaud et al., 2017; França de Barros, Carcaud, & Beraneck, 2019; Idoux, Tagliabue, & Beraneck, 2018, França de Barros et al 2020 in preparation). The aim of the following protocol is to induce a sensory conflict for long-term learning studies in mice. The uniqueness of this protocol resides in the fact that the VVM device induces a remarkable gain-down decalibration of the visual and vestibular reflexes while mice are naturally behaving in their cage. Thus, filling the gap between in vivo and in vitro experiments in the study of VOR motor learning in mouse. The technical description of the animal care, device assembly, surgery for the device implantation as well as reflex measurements are detailed below. The advantages and limitations of this protocol will be further discussed on chapter IV (Motion in mice: vestibulo-ocular and optokinetic pathways through time).

Animals

Male wildtype (WT) C57BL/6J (Janvier, Le Genest Saint Isle, France), with ages comprised between 3-4 weeks, were used. Mice were housed in the *Animalerie des Saints Pères, Université de Paris*, fed *ad libitum* standard rodent chow and kept in a 12h light /12h dark cycle. While the protocol was ongoing, the weight of each mice was registered daily (the document holding the weight of a group is available in annex X). This procedure was approved by the ethical committee for animal research of the *Université de Paris* and follows the European guidelines for animal well-being (European Communities Council Directive 2010/63/EU).

Device assembly

For this protocol, two elements were necessary: a headpost, to be implanted on the mouse's skull, and a VVM device that is fixed onto the headpost.

The VVM devices as well as the headposts were produced in a 3D printer using poly lactic acid (PLA) plastic (**Figure 25**). This material rendered a final device that was lighter than the one previously used by my group (before 3g, now 0.9g). Additionally, in comparison to the translucid plastic used before, PLA ensured that no coherent image was seen by the mouse since the material was opaque, only letting light in. The device's design was made so that the facial morphology of the mouse was respected and daily habits (feeding, drinking, social interactions) could be performed without trouble. The specification files for 3D printing are provided in the paper.

After its production, additional 3 mm vertical stripes were drawn with nail polish onto some of the device's external surface to create the 'pattern' device. The stripes on the 'pattern' device created a high contrast and fixed visual signal during self-generated head movements. Hypothetically, every time the mouse would move and perform VOR, since the image on the retina is locked during movement (black stripes), an error message would happen (retinal slip). Contrarily, the ´no-pattern´ device only prevents the mouse of seeing a coherent image on the retina and, putatively, no or little retinal slip would be generated.

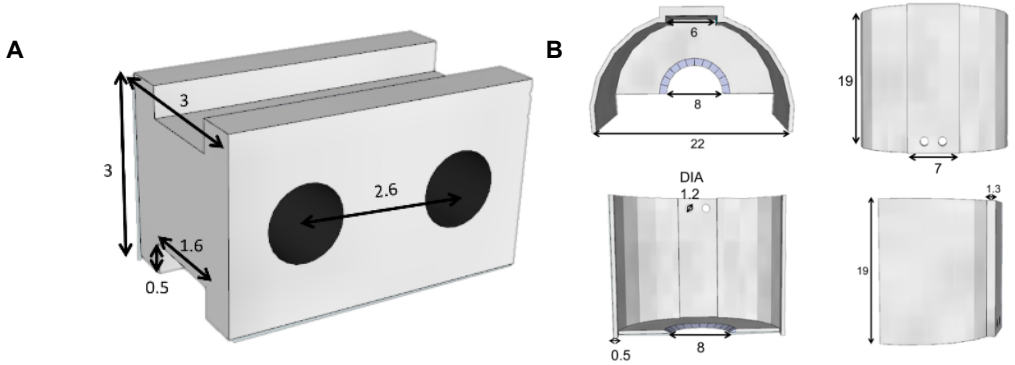

Figure 25. Headpost and adaptation device. A- Headpost and B- device size specifications and rendering. From França de Barros *et al*., 2019.

Headpost implantation surgery

The headpost implantation surgery was a crucial stage for ensuring that the rest of the protocol could go on uneventfully. If the headpost was not implanted properly, there was the risk of the mouse ripping off the implant during the adaptation phase or even while it was contained in the tube during the tests of the reflexes. This would cause the immediate stop of the protocol. Therefore, I meticulously ensured that the headpost was secured properly so it would last until the very end of the protocol. A more detailed description as well as a video of the procedure can be found on the methods paper on the Journal of Visualized Experiments (França de Barros et al., 2019).

Mice were anesthetized throughout the whole procedure with isoflurane gas (induction: 2.5-3%; maintenance: 1.5-2.0%). The head was shaved using an electric razor and lidocaine hydrochloride (2%, 2 mg/kg) was applied subcutaneously on that region for local anesthesia. An incision of about 1.5 cm following the course of the skull's midline was made to expose the skull. After, the periosteum was carefully removed using a scalpel and great care was taken for the skull not to bleed since that would compromise the next steps. The headpost was then glued to the skull between lambda and bregma landmarks and cemented to improve the fixation and protect the headpost. Once dried

(±3 min), the lose skin from the initial incision was sutured at the back of the ears. Post-surgery, the animals were placed under read warm light to avoid hypothermia and moistened food was placed on the cage's floor to facilitate access. When mice regained consciousness, they were housed in groups of 3 or 4 to motivate daily social interactions.

Device fixation and adaptation period

The helmet-like structure was attached to the headpost with small screws. Before releasing the animal back on the cage (**Figure 26**), it was verified that the device was well-secured and no pressure was being applied on the snout. Right after the fixation of the device mice ran on the cage trying to remove the device, often bumping into the cage's walls and not being able to reach for food and water. Therefore, special attention was given on the 48h after the fixation by providing moistened food and hydrogel water on the cage's ground. After the fixation of the device, and until the rest of the protocol, mice were daily surveilled, and a qualitative scale of well-being was applied. This scale was based on the animal's body weight alterations (indication of sufficient feeding and drinking), physical appearance (*e.g.,* grooming and wounds) and social behavior. If on any given day they scored higher than 4 points on that scale, mice were immediately removed from the protocol.

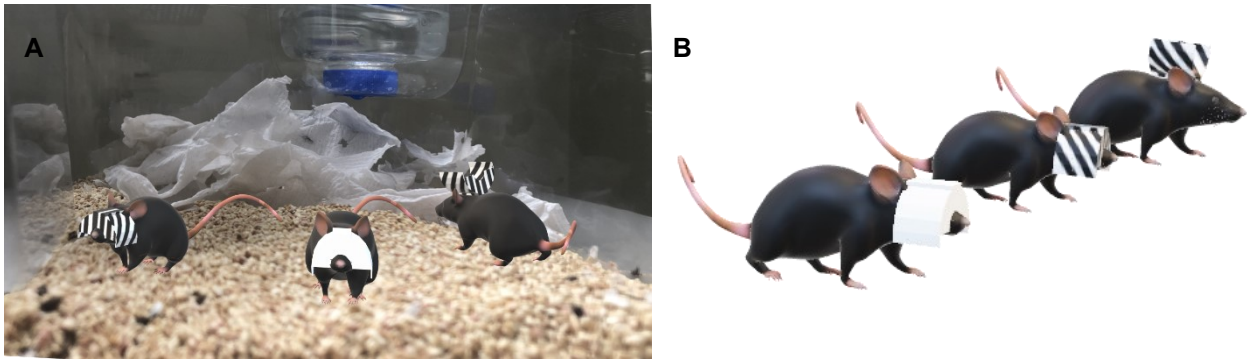

Figure 26. 3D reconstruction of mice wearing the device, on their cages (A). B- Side view of the 3 VVM conditions: No-pattern, Pattern and Sham. Credit FdB

Video-oculography tests

The mouse wore the device for 14 days and video-oculography tests were thereafter performed (**Figure 27**). The OKR and VOR were tested right after the removal of the device as well as 2, 6 and 10 days after.

The mouse's body was placed inside a small plexiglass restraining tube and its head, that stood outside of the tube, was fixated to the table by two screws that were fixed onto a metallic bar. This restraint method stood was incorporated on the vestibular

platform that stood on top of the vestibular turntable's platform. Mice stood at a 30º nose-down position to imitate their natural head position were their horizontal canals are aligned to the yaw plane. Miosis was induced by using pilocarpine so that the size of the pupil became trackable during experiments in dark. During VOR tests a black box was placed on top of the turntable to prevent the mouse from seeing any light (<0.02 lux). HVOR recordings consisted in a first sinusoidal angular rotations around the vertical axis at 0,5Hz and velocities in range 20-50˚/s as well as stimulations at 0,2, 0,5, 1 and 2Hz at a peak velocity of 30˚/s. Like for the VOR recordings, apart from the optokinetic projector and the computer screen, all sources of light were turned off during OKR. The optokinetic stimulation consisted of a white-dotted pattern (25.000 white dots), on a black background, that was projected on a plastic white dome. The pattern rotated for 1 minute at a set of constant speeds (2,5; 5; 7 and 10 ˚/s) in both clockwise and counterclockwise directions of at different frequencies (0,2; 0,33; 0.5; 1 Hz) at a fixed speed of 10º/s.

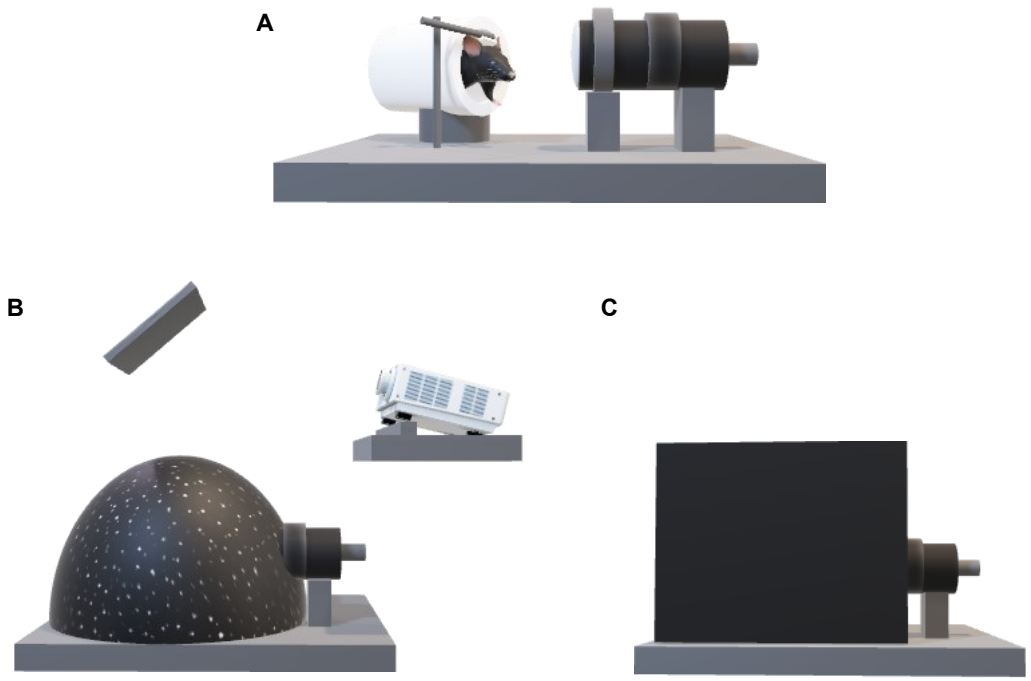

Figure 27. Visual and vestibular reflex tests. A- Mouse in turntable; B- OKR set up, with a dome surrounding the animal and a projector to induce optokinetic stimulation; C-VOR set up consisted in a box surrounding the animal and camera to completely isolate the animal and test the reflex in complete darkness. Credit Filipa FdB.

2. Video-oculography

Video-oculography is a technique that has been developed in the mouse in the early 2000's (van Alphen et al., 2001) to replace the use of mini-search coils which significantly impaired the eye movements, leading to reduced gains. Video-oculography, being non-invasive, allowed to faithfully record eye movements and qualified mice as a model for oculomotor studies.

There are numerous types of eye tracking systems: video-oculography; eye coil; bio-adhesive phosphorescent particles (Katoh et al., 2015); magnets (Payne and Raymond 2015).

Video-oculography eye-tracking system

The type of eye-tracking system used in our experiments was video-oculography. This choice was preferred to the eye coil due to the fact that it's non-invasive, not involving any further surgeries. In our visuo-vestibular mismatch experiment, during the adaptation period, mice wear a device on their heads that would impede the monitoring of the condition of the coils during that period. In case of removal, there would be no possibility to re-apply the coils since that could potentially change the response of the reflexes tested. In our other set of experiments mice are subject of a fairly long and delicate procedure (decerebration lasts for approximately 2h) that the addition of time for the insertion of eye coils would compromise the viability of the preparation.

The eye tracking system used in all our experiments is a commercially available ISCAN system (ETL-200, ISCAN, Burlington, MA). This system is originally developed for used in primates but adapted to mice by adding a macro lens that allows for a shorter working distance (100 mm) and a smaller horizontal field (4.2 mm). A point to consider is that mice have an extremely curved cornea and no visible sclera. This makes the corners of the eyes a tricky region to record for these types of automated systems (Stahl et al, 2000). Such obstacle is overcome by the use of IR LEDs (infra-red emitters) stuck laterally to each camera by a shaft that allows for optimal adjustment. The IR were positioned underneath the horizontal midline of the eye so that the light emitted would reflect on the cornea and make this structure visible for detection. The corneal reflection (CR) was the reference immobile point that allowed the recording of the pupil displacement during experiments. The CR is taken as a reference point also because by being a fixed point in the eyeball, if displacement of the camera or mouse were to occur, the video system would not read out any value. The ISCAN system, through the use of

algorithms based on contrast, detects the center of the CR and pupil with only a small delay of 30ms.

Calibration of the video-oculography system

In monkeys and other foveate species, calibration of the video-oculography set up can be performed by training the animal to fixate a specific point. However, mice, as an afoveate species, can't be trained to fixate its gaze towards a target. Therefore, different alternatives have to be found to achieve the calibration of the oculography system.

As mentioned above, the signals that are registered by the ISCAN video system are the linear positions of the pupil and CR. However, one must keep in mind that the eyeball is not a flat surface and, therefore, these positions must be converted from linear translation to angular rotation. When the pupil position is subtracted from the CR position, it only yields the rotational component. Consequently, any difference between the axis of the eyeball and the axis of the camera must be additionally accounted for (Stahl et al., 2000). The calibration is done using the following equation, where Rp is the radius of rotation of the pupil:

$$E = \arcsin (CR\text{-}P) / R_p$$

A custom-made calibration platform (**Figure 28**) was designed to facilitate the calibration since, in both experiments where video-oculography was used, cameras were fixed onto a platform and could not be rotated around the mouse. Mice were restrained in the tube and headfixed; the center of the pupil was set so that it would be in the center of the camera and the proximity of both was regulated for the image to be in-focus. The eye image was set as big as possible on the screen and taken as a reference point for setting the cameras for the binocular recordings. Image thresholds and IR illumination were then set to finalize the tracking parameters. Then, in order to find the Rp value, the camera was rotated 20º (-10º to +10º) around the mouse, who remained still in the restraining tube. This procedure was repeated several times and only accounted for when the mouse eye was motionless.

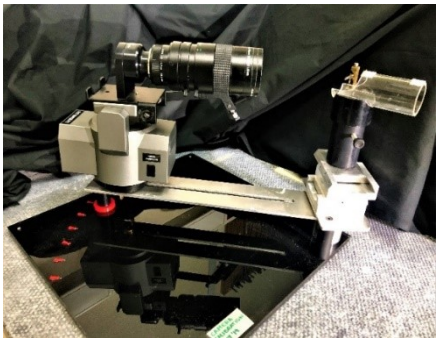

Figure 28. Video-oculography calibration set up.

2.3. Quantification of OKR and VOR

The two main quantitative factors that characterize gaze stabilization reflexes are the gain and phase. The gain is the ratio between the eye and the stimuli movement. The phase is the temporal synchrony between the eye movement and the stimulus.

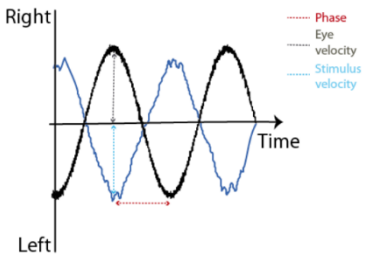

Figure 29. Raw traces of a VOR test. The eye (blue trace) and the turntable (black trace) positions are shown over time. The phase (red), eye velocity (grey) and stimulus velocity (light blue) are represented with arrows.

$$Gain = \frac{eye\ velocity\ (deg^{-1})}{stimulus\ velocity\ (deg^{-1})}$$

A perfect compensation of the occurring stimulus (head movement – VOR; visual – OKR) will compute a gain of 1 and a phase of 0º (Goldberg et al., 2012b). These values are shaped by the type of stimulus *i.e*, its velocity, frequency and, in the case of OKR, the contrast. The gain values also have an age-related component that is influenced by the EOMs themselves, declining with age (Peterka et al., 1990). Quantitatively, they can range anywhere from 0 to 1, in case of the gain, and from -90 to +90º, in case of the phase.

Other parameters, derivative from gain and phase, have been used to describe these reflexes in more detail. For example, in OKR, the onset latency –time interval between the beginning of the stimulus and the beginning of the response – and the deceleration.

3. Decerebrate mouse preparation

In 1906, Charles Scott Sherrington performed the first known decerebration experiments in cats to study sensorimotor systems. These experiments aimed at Sherrington passed on his knowledge to Graham Brown, his student, who in 1911 recorded locomoting decerebrate cats on a custom-made motorized treadmill. Sadly, this research that Graham Brown conducted on the Cardiff Institute of Physiology was never published. Decades later, in 1973, videos of these recordings were analyzed by Lundberg and Philips who described the movements performed by the cats on the treadmill (Jones et al., 2011). Ultimately, decerebrate preparation became famous in the locomotion field when in 1966 Shik and collaborators showed that when a precollicular, premammillary cat had an area below the inferior colliculus stimulated (mesencephalic locomotor region or MLR), it could locomote. Decerebrated preparations are also used in the study of fields like respiration (Fung et al.1994) or exercise physiology (Bedford et al., 1992) and have potential to serve a vast group of applications.

Here, the overall goal of the use of this preparation was to isolate the physiological output of the spino-extraocular command. By decerebrating our subjects of study, the descending commands coming from the motor cortex, and other superior brain regions, are excluded. Thus, the decerebration potentially unmasks a pathway that is activated during locomotion and it is independent of descending control.

Anesthesia induction and tracheotomy

The mouse was first anesthetized in an isolation chamber with 3% isoflurane gas delivery for 4 minutes. After tilting the induction chamber to verify the righting reflex, the mouse was transferred to the surgery table on a covered heating pad (38ºC). A nose cone was placed on the snout and mouth to maintain anesthesia with 1.5-2% (vol/vol) isoflurane with medical grade oxygen (SomnoSuite, Kent Scientific) at 0,4 L/min. A rectal probe was placed to ensure the temperature stayed around 38ºC (Physiosuite, Kent Scientific), the head was shaved with hair clippers and the eyes were covered with ophthalmic gel to avoid dryness. The head fur was shaved to prepare beforehand for the decerebration procedure. The mouse was then flipped to its dorsal side and the fur surrounding the neck was shaved using small clippers. A sterile working area was obtained by rubbing the shaved skin with iodine solution as well as with 70% alcohol. The front paws were then taped to the table, a pulse oximeter with a heart rate monitor (MouseSTAT, Kent Scientific) was attached to a hindlimb and the other was left uncovered to verify the pinching reflex along the surgery. Using a pair of fine forceps, the skin immediately below the chin was lifted and, with round scissors, a small cut was

made so that the blade of the scissors could get underneath the skin and make an incision until the sternum. Using blunt forceps, the superficial adipose tissue was excavated, and the skin was opened laterally by carefully separating the skin and conjunctive tissue on each side. Due to the small size of the mouse anatomy, at each step it was important to aim for a clear and visible surgical working area so that every incision could be made precisely to avoid bleeding (**Figure 30**).

To expose the trachea, the salivary glands were detached from one another as well as the sternohyoid muscle trachea. Using fine Graefe forceps, two 4-0 suture threads were passed underneath the trachea, set parallel side to side and the more caudal thread was loosely knotted. The tracheotomy was then performed, using a pair of micro scissors, by cutting only the upper half of the fibrous membrane between two cartilages horizontal to the trachea. Despite cutting between two tracheal rings, the trachea was never fully segmented in two since, due to the cartilaginous nature of the tissue, that would result in the loss of the tensional forces and cause the tracheal cannula to slide out the trachea. The air delivery mode was then quickly switched to ventilator mode (150mL/min) on the respiration system (SomnoSuite, Kent Scientific). The trachea was held using fine forceps and the plastic endotracheal tube (connected to the ventilator) was inserted into it to allow for artificial ventilation along the rest of the procedure. The more caudal suture thread was tied on the trachea and the more rostral was knotted on a small insertion in the tracheal tube to improve the hold. The isoflurane level was lowered to 1.5% after verifying that the peak CO_2 levels (higher than 2.5%) and heart rate [417±17 in an anesthetized *vs* 580±18 in awake mouse (Ho et al., 2011)] had stabilized. The peakCO_2 levels measure, in the systemic circulation, how well the alveoli in the lungs are diffusing the CO_2, *i.e.*, ventilating. Their values were monitored along the procedure so that they'll stay around 2.5-4%. The absence of response to toe pinch was also checked at this point.

To avoid excessive bleeding during decerebration, the supply of blood to the brain was stopped. To do so, the left and right carotids (thick pulsating walls) were dissected using blunt forceps and two 6-0 soy suture threads, spaced out a few millimeters between them, were tied off around each carotid. The vagus nerve lies adjacent to the carotid and ligation or crushing would prevent proper breathing together with vagus stimulation effects (heart rate and digestive tract). Therefore, the carotid (thicker pulsating walls) was dissected away from the vagus nerve (white fibrous appearance) and special care was taken not to damage it. Then, an electric cauterizer (Change-a-tip cautery, Bovie Medical) was used to cauterize each carotid on the space between the two knots. The incision initially made along the neck's midline was closed back using

nylon suture thread; to further ensure that the tube would stay immobile during the experiment it was tied underneath the chin. Lastly, to prevent dehydration, a subcutaneous 0,3 mL injection of sterile lactated Ringer's solution (Braun Medical) was administered.

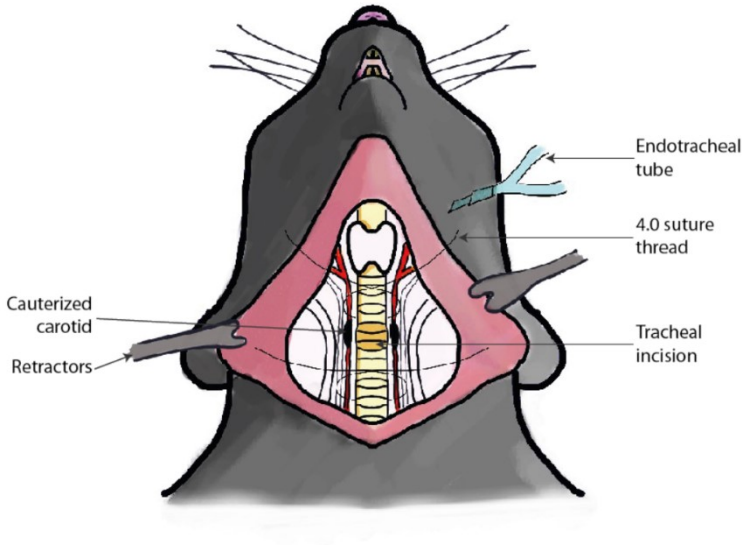

Figure 30. Illustration of the tracheotomy step of the decerebration protocol. Credit: Filipa FdB.

Craniotomy and decerebration

After the tracheotomy procedure was terminated, the tape fixing the limbs to the table was removed and the mouse was flipped with its ventral side down. The mouse was turned over simultaneously with the endotracheal tube so that ventilation wouldn't be disrupted. Ophthalmic gel was then re-applied. The mouse was placed in a stereotaxic frame and, using a pair of blunt scissors, an incision was made along the skin of the head to expose the skull. Connective tissue on that area was detached from the bone and, using a micro-drill (Foredom, David Kopf Instruments), the skull was gently scored along the limitation of the parietal bones; once they were loose, they were removed in one piece. The sagittal suture was then scored at the lambda and bregma crest and carefully removed after immediate cauterization of the superior sagittal sinus (**Figure 31**). Any small bleeding was stopped using hemostatic gelatin sponges (Spongostan, Ethicon). Decerebration was performed at the confluence of the sagittal and transverse sinus, at a 40±5º angle relative to the midline. On that location, a quick slicing motion was made with a nº10 scalpel that ran deep until the intersection between the thalamus and the basal forebrain so that the mammillary bodies were not damaged.

This incision separated the brain in two regions, creating a precollicular premammillary decerebration. Then, the more rostral brain tissue was removed to ensure that all connections were shut down. A microspatula was run superficially along the middle so that the cortical left and right hemispheres would detach and could be neatly taken away from the skull. The rest of the rostral structures (thalamus, caudate nucleus) were removed carefully using a microspatula, without going too low not to damage the optic nerves. Hemostatic sponges were used to clean blood in the skull cavity. Those sponges were after removed and replaced by fresh ones before the skin on the skull was sutured. Usually, right after decerebration was performed, the pCO2 levels would go down but rose up again after the mouse was placed on the treadmill. Finally, another subcutaneous injection of Ringer's lactate (0.3 ml) was applied and the isoflurane was turned off.

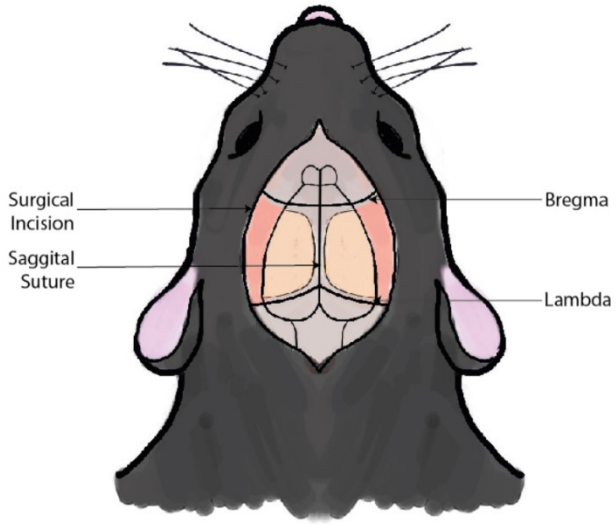

Figure 31. Aerial view of a decerebration in preparation. Credit: Filipa FdB.

Treadmill locomotion

Still on the surgery table, the pulse oximeter was removed as well as the stereotaxic frame and custom-made ear bars were placed. Then, the intubated and decerebrated mouse was transferred to the treadmill, the added ear bars were fixed onto a transparent custom-made platform and the stereotaxic hold was completed with a mouthpiece (**Figure 32**). The ventilation parameters were again verified at this point to confirm that the displacement from the surgery table to the treadmill didn't alter the correct position of the ventilation tubes. The mouse was then left for 20-30min with a hairdryer as an indirect heat source (more on the importance of the body temperature on the preparation on this comment section), time during which the videoculography set up

began to be set up (section: videoculography during locomotion). Muscular tonus and pCO2 levels rose again, indicating that the mouse soon would start to locomote. Therefore, any remaining ophthalmic gel was removed with a cotton swab and the fur around the eye was gently brushed to have a non-occluded eye.

If all the procedures up to this point were successful, with good ventilation and no major blood loss, there was a high probability that the mouse would locomote. If that was the case, the mouse would last from 1 to 3 hours on the treadmill. The procedure would end either with spontaneous death (usually 1-1,5h after the start) or, by an IP injection of Dolethal (Vethoquinol, France). If the mouse survived the procedure up to this point but during its first hour on the treadmill didn't present a sustained locomotion, it was sacrificed and excluded from the experiment.

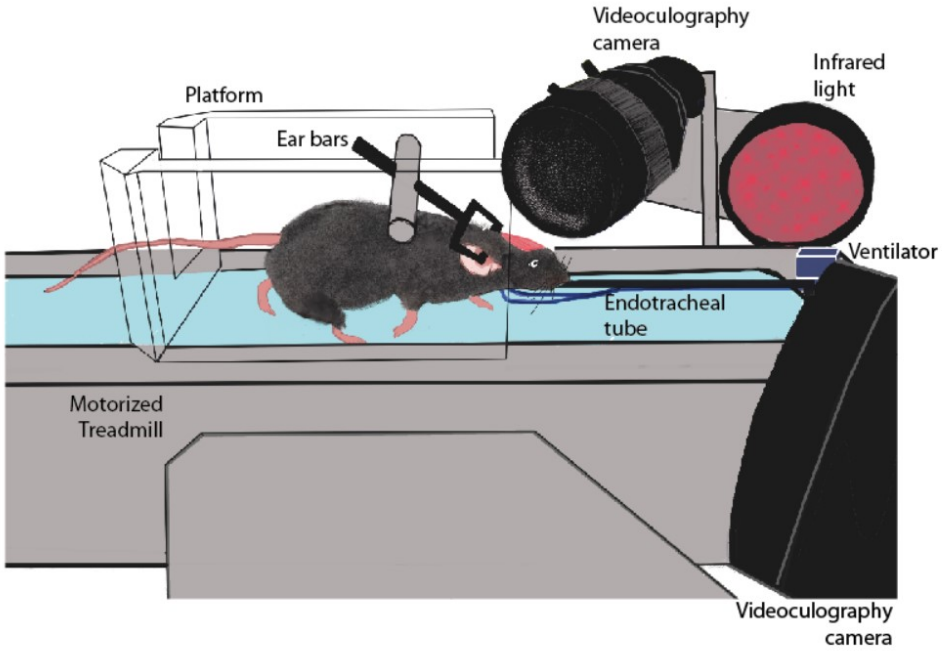

Figure 32. Schematic of a mouse in the motorized treadmill during an experiment. Credit Filipa FdB

Videoculography during locomotion on the motorized treadmill

The set up for recording eye movements during locomotion consisted in: an infrared video system for recording the eyes (ETL-200 rodent eye tracking lab, Iscan); an infrared video camera to record the movement of the limbs (Grasshopper3, Point Grey) and a motorized treadmill (LE8708TS, Panlab, Harvard Apparatus) all fixed onto a metallic platform. The infrared video system consisted in two cameras, one per eye, with a sampling rate of 120 Hz and using Spike2 software. The detection, recording methods and calibration of the eye movements was performed as previously described

in (2. Video-oculography section). The treadmill was connected to Spike2 software so that its activation as well as speeds would be registered. The IR video camera used to record the limbs was paired to Spike2 with a trigger so that, when the video was launched, there would be marks on the recording of the exact time at which certain frame was taken and posterior off-line pairing of both could be done. Its sampling rate was set to 100 Hz.

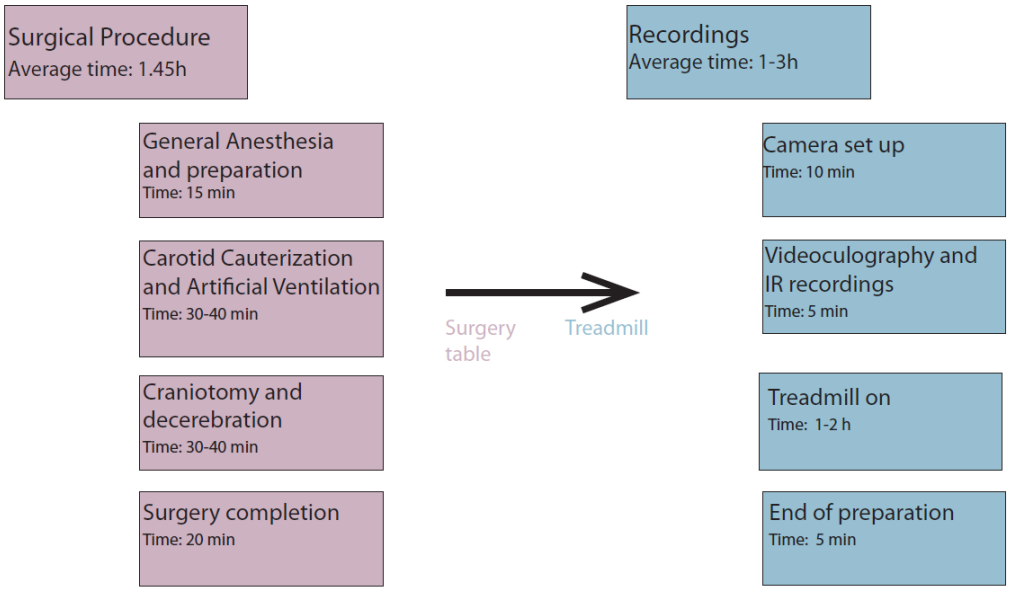

Figure 33. Workflow and timings of a successful decerebrated mouse preparation and recording.

Eye and limb movement offline quantification and analysis

Locomotor cycles were tracked using a 3D markerless pose estimation software (DeepLabCut, Mathis et al., Nature Neuroscience 2018). DeepLabCut is a fairly recent free software that was developed to track animal behavior without the use of physical markers. It works through the use of deep neural networks (thus, requiring a NVIDIA GPU) that require minimal training data. This software gave the trajectory of a mouse's limbs in time. For example, on a video of the mouse running in the treadmill for 1 minute, since our camera had a 100Hz sampling rate, would output 6000 frames in total. With the use of DeepLabCut, from all these frames, only 30-60 frames would need to be manually tracked, instead all of them.

Horizontal and vertical pupil and CR were sampled at 1KHz digitally recorded (CED power1401 MkII) with Spike2 software and were analyzed offline together with the limb

movement using DataView (W.J.Heitler, University of St.Andrews, version 11.3.2). The parameters analyzed were the amplitude, frequency and phase of the eye movements. Since the original responses obtained were expressed as position over time, they were first converted from position to velocity by calculating the derivative of each trace. Then, a threshold was set to detect any deflection from- and to- 0. Peak-to-peak amplitude was obtained from those intervals and the absolute maximum peak of each deflection was set to be an event frequency. The phase was calculated between left and right eye as well as left or right eye and front or hindlimb. To calculate the phase between the two eyes, the right eye was arbitrarily always set as the reference. To calculate the phase between eye and limb, the limb was the reference point since it's the spinal cord CPG that, hypothetically, would drive the eye movement. Statistical analysis was performed using GraphPad Prism (GraphPad Software, San Diego, CA) and the results were given as mean values ± SEM, unless mentioned otherwise. Results were considered to be statistically significant whenever $p<0.05$ ($^{*}p < 0.05$; $^{**}p < 0.01$; $^{***}p < 0.001$; $^{****}p < 0.0001$; ns: non-significant).

Three possible preparations resulted from this procedure. 1 – No eye movements nor locomotion, with a mouse that showed no muscular tonus and frequently died spontaneously not long after being in the treadmill; these are the largest in number because it took a big amount of preparations for the procedure to be optimized. 2 – No eye movements but some spontaneous locomotion; in these preparations, the eyes looked 'dead', covered by the milky layer shown in **Figure 34**. 3 – Eye movements while locomoting. These were the only type of preparations analyzed.

Circular data was computed using Oriana 4.0 software (Kovach Computing Services, Wales). Temporal relationships between the movement of left and right eyes or, an eye movement and a locomotor phase, were evaluated by the circular phase analysis of pooled data. The mean direction of the vector 'μ' and its length 'r' indicate, respectively, the preferential phase and strength of the coupling between both parameters (Bacqué-Cazenave et al., 2018). Therefore, this type of analysis allowed to show the dispersion of data as well as the phase relationships. Phase distributions were tested using the Rayleigh's uniformity test (p) and the phase values were given as a single grand mean of all the individual phase means of each mouse. The circular data results were expressed as (μ,r,p).

Key parameters and troubleshooting

At the first preparations performed, mice presented sort of white milky layers **Figure 34** covering the eyeballs. This completely prevented the videoculography

recordings since neither the pupil nor the corneal reflection could be detected. I found that the cause of those layers could be dehydration. Therefore, hydration was key throughout the procedure.

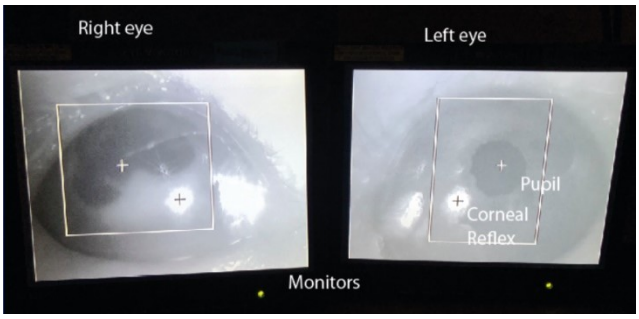

Figure 34. Eyes of a decerebrated preparation during videoculography recordings.The right eye was not recorded due to the 'milky' white layer while the left eye was in great shape and recorded.

Once on the treadmill, the maintenance of the physiological body temperature of the mouse (between 38-39ºC) was also crucial for its survival. Once decerebrated, the mouse didn't have the capacity to autoregulate it's body temperature. Therefore, an external source of heat had to be applied. A hairdryer was found to be the best option for this. We also tried a lamp that didn't interfere with the IR light but, the only possible location on our set up was too far away to be feasible. Heat was applied on the mouse using low potency with a hairdryer and, once the mouse presented acceptable body temperatures, if was turned off. This procedure was repeated every time the temperature values went down.

The general goal of decerebrating our preparations was to remove the descending commands from the cortex to the abducens in order to show that these inputs were not needed to drive these eye movements during locomotion. Also, to ensure that the eye movements recorded were in fact reflexive and not driven by visual stimuli, almost all of the visual cortex (less than half of the V1 and the LM remained) was removed. There are several kinds of decerebration: lower – the cut is made above the upper border of the pons –, middle – the cut is made through the red nucleus –, and upper – the cut is made so that the cortical area is removed. The type of decerebration performed in this experiment was a precollicular and premammillary decerebration. This type of decerebration was chosen since we wanted to remove motor cortex and visual inputs preserve the key structures responsible for locomotion maintenance.

4. Transneuronal tracing of MNs and LOINs using Rabies Virus

Rabies virus as a transneuronal tracer

Rabies virus (RV) is a great tool to understand the connectivity and, ultimately, the functioning of neuronal networks. After determining *in vivo* (decerebrate preparation) and *in vitro* (brainstem-spinal cord preparation) that there was abducens discharge when the spinal networks were being activated, we wanted to identify the chains of connectivity between the spinal cord and the extraocular muscles. Therefore, in the context of this thesis, RV transneuronal tracing was used to map the neuroanatomy of the spino-extraocular pathway involved in the relay of the efferent copy (**Figure 35**). All these experiments were performed in Marseille, at the *Institut de Neurociences de la Timone* (INT), were I had the opportunity to work with Helene Bras, an expert researcher on the use of rabies virus. Patrice Coulon also provided some guidance during the initial experiments. It is important to state that all precautions were taken to ensure a safe manipulation of the RV including manipulation of the virus inside a Biosafety level 2 facility as well as my vaccination against the virus at the anti-rabies center of *Institut Pasteur* (Paris) before starting the experiments.

RV is a retrograde tracer, *i.e.*, it moves from synapse to soma. They identify the synaptic connections between *directly* connected neurons, being able to progress from first-order to last-order neurons. There are several advantages in the use of viruses as tools for neuronal tracing: RV can jump across synapses; they self-replicate in the recipient neurons so, when the infection reaches the secondary neuron, the virus multiplies again and replicates; the number of synapses it crosses relies on the time the virus is left to migrate.

Rabies Virus replication and inoculation

The rabies virus is a reliable tool for transneuronal tracing. Its unidirectional retrograde migration enables the mapping of entire neuronal networks, only spreading between immediately connected neurons. The virus can be injected either in the muscles or in the CNS; if the injection is intramuscular the virus will spread only through motoneurons hence why it's a fantastic tool to study motor systems.

After infection with CVS RV, it usually takes 1 week for animals to present the symptoms of the disease (Gabriella Ugolini, 2010) even though some changes in behavior start happening after 3 days (personal observation from our studies: mice were a bit slower and more prostrated). This is ethically an advantage since, during that time,

the virus can cross 7 synapses which is enough for what most of the motor network studies aim at.

RV is a single-strand RNA virus with negative sense polarity and it's the type species of the Lyssavirus genus (*Lysa* is a goddess in the Greek mythology that represented rage and madness) of the Rhabdoviridae family (*rhabdos* in Greek means rod, the shape of these viral particles). It consists of a light genome (<12 kb) that encodes five proteins (nucleoprotein, phosphoprotein, matrix protein, glycoprotein and polymerase). Trimers of glycoprotein form spikes on the outer envelope of the virus. This glycoprotein is crucial for binding and internalization of the virus [deletion of this protein from the genome prevents diffusion of the virus in the host, (Mebatsion et al., 1996)). Replication of the virus occurs in the cytoplasm, where the viral genome is first transcribed to produce complementary mRNA, then translated to viral proteins and finally replicated to give more infectious particles (Gabriella Ugolini, 2011). Thus, it is in the cytoplasm that the machinery of active viral infection is found. These are spherical eosinophil inclusions where viral RNAs are being formed (Nikolic et al., 2019). RV is only absorbed in the inoculated portion of the muscle; specifically, in the neuromuscular junction (probably by nAChR) and doesn't spread between adjacent muscle fibers (Gabriella Ugolini, 2010). Therefore, between different experiments it is important to target, with the same amount of virus, the same region of the muscle. In mice, unlike other rodent species and primates, intramuscular infection of motoneurons is as susceptible to happen as primary sensory neurons.

RV strains can be classified as: street or fixed. The street strains directly come from animals that have been infected. Fixed strains are more stable 'street' strains that were repeatedly passed in mice and are the ones used in transneuronal tracing experiments. An example of a fixed strain is the Challenge Virus Standard (CVS), the subtype CVS-11 strain of RV was the one used in these experiments (Coulon et al., 2011). The virus was grown in baby hamster kidney cells and concentrated as described by (Gaudin et al., 1992). Please note that several studies have already confirmed the ability of this virus to map motor networks after peripheral injection in both rodents (Ruigrok et al., 2008; G. Ugolini, 1995) and primates (Grantyn et al., 2002; Gabriella Ugolini et al., 2006).

Rabies virus inoculation procedure

The CVS-11 RV aliquots were stocked at -80ºC and thawed right before use. Mice were anesthetized by an IP. injection of ketamine (Imalgene, 60 mg/kg) and xylazine (Rompun, 10 mg/kg) and deep anesthesia was confirmed by lack of response

to interdigital pinching. The left extraocular muscles were exposed through an incision on the skin covering the mouse's eye, surrounding fatty tissue was removed and absorbable hemostatic gelatin sponges were used to curtail bleeding (Spongostan, Ethicon). After its identification, the left lateral rectus (LRM) was isolated from the rest of the extraocular muscles using small hooks with sutures that gently pulled the muscle away. Then, an injector canula (gauge 33) linked to a 10 µL Hamilton syringe through a catheter was inserted into the LRM. To improve the probability of uptake of the virus by the muscle, the same portion of the LRM with a neuromuscular junction in its location was aimed for in every experiment. With the needle inside the muscle, RV (1 µL) was slowly injected and the needle was left in place for an extra minute to minimize leaking by reducing abrupt changes in muscle pressure and to ensure all the virus had been administrated. Once the syringe was removed the skin was closed using monofilament suture and mice were put back on their cages under a red light.

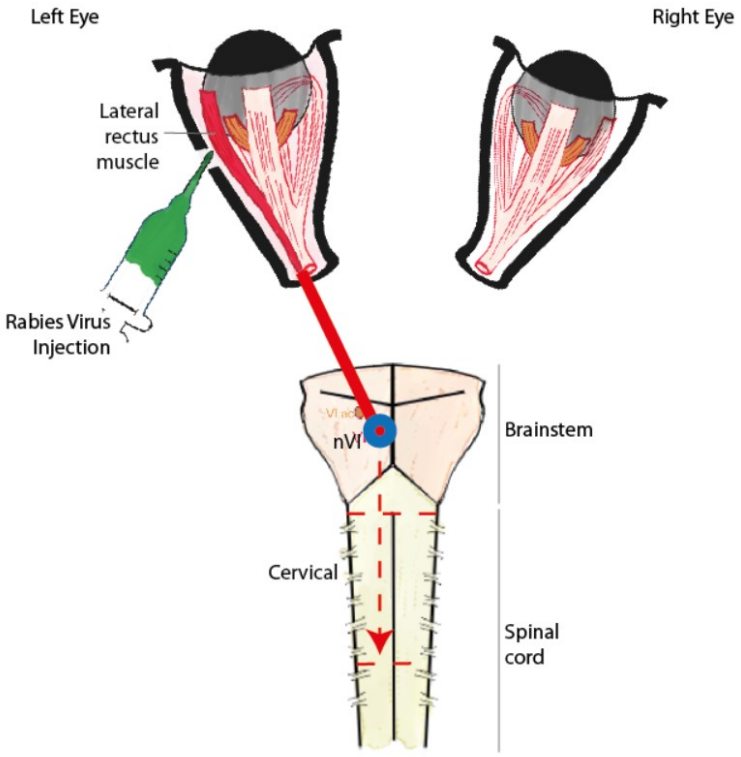

Figure 35. Schematic of the protocol of rabies virus injection and migration. Credit: Filipa FdB.

Rabies virus inoculation time window

In order to restrict the RV-infection to the interneurons monosynaptically connected to the MN of the LRM, the first question tackled in these experiments was to narrow down the inoculation time. If the dose and detection methods are equal, transneuronal transfer

is purely time-dependent. Typically, first-order neurons take 2 days to be infected and the next neuronal steps take 12h or more to be infected. Therefore, three inoculation windows were tested: 72h, 67h and 57h. When mice were sacrificed 72h post-inoculation, the virus had already traveled two synapses, (disynpatic) justified by the presence of infected neurons in the cerebellum. When a 57h inoculation time was tested, the virus barely migrated trough the LRM, presenting almost to infected neurons on the abducens. When the inoculation time was lowered to 67h, the RV+ neurons were restricted to the brainstem and cervical, with no infection on the cerebellum or adjacent areas. Therefore, a 67h infection time was chosen for all the subsequent experiments. At this timepoint, mice exhibited the initial symptoms of RV infection like a prostrated posture and ungroomed hair.

The animals used in the first experiments performed were 8 weeks old male swiss mice. The initial choice of this strain resides in the fact that Swiss mice are bigger in size than C57BL6. This facilitated the identification of the EOMs and the isolation of the LRM. Nevertheless, to able to make the direct parallel with the in vivo and in vitro experiments, two C57BL6 mice were also submitted to this protocol. The main findings were identical between Swiss and C57BL6 mice.

Dual immunodetection of RV-infected and ChAT+ neurons

After 67h of RV incubation, animals were deeply anesthetized with ketamine (Imalgene, 60 mg/kg) and xylazine (Rompun, 10 mg/kg) and perfused intracardially with 100mL of phosphate buffer saline (PBS 0.1M) followed by 300 mL of 4% paraformaldehyde (PFA). To study the neuronal substrates of this spino-extraocular pathway, the brain was dissected coronally from the midbrain (Paxinos coordinates: Interaural 0.00, Bregma 3.8 mm) to the medulla oblongata (Paxinos coordinates: Interaural -4.44, Bregma -8.20 mm) and the spinal cord was taken entirely from the cervical to the cauda equina. Each block of tissue was fixed separately and was left for 24h at 4˚C in 4% PFA, subsequently cryoprotected in 20% sucrose during at least 6h and freeze embedded at -80ºC in Tissue Tek (Sakura, Zoeterwoude The Netherlands).

Once the tissues were properly fixed, transverse sections (30 µm thick) of the brainstem as well as cervical, thoracic and lumbar spinal cord were serially cut using a cryostat (Microm, Heidelberg, Germany) and directly collected onto poly-L-lysine-coated slides. Right after, these sections were incubated to avoid unspecific binding for 1h at room temperature in blocking solution (PBS, Triton X-100, 2% bovine-serum albumin and normal donkey serum) and then left at 4˚C for 48h with the anti-RV phosphoprotein (Coulon et al., 2011) and anti-choline acetyltransferase (ChAT) diluted 1:1000 in the

blocking solution. Once the primary antibody incubation was done, sections were rinsed thrice in PBS and then incubated at room temperature with Alexa488 anti-mouse and Alexa 546 anti-goat for 2h. Finally, sections were rinsed two times with PBS and once with tap water before being mounted (Immu-mount, Fischer Scientific) under coverslips.

Analysis of the distribution of RV-infected MNs and interneurons in the spinal cord

To analyze the distribution of RV+MNs in the brainstem and LOINs neurons in the spinal cord, the sections were visualized under an upright light microscope (Axioscope, Carl Zeiss, Germany). Images of each entire section (4x) as well as magnifications of certain areas of interest (10x and 20x) were taken using a CCD camera (AxioCam MR3, Carl Zeiss). These images were afterwards treated in ZEN (Carl Zeiss) imaging software where neurons $ChAT^+$ or RV^+ were counted. It is important to note that only neurons with a visibly infected nucleus, determined by the presence of Negri, were considered.

Technical considerations

We understand that there are limitations with the use of the CVS rabies virus strain used here. Since locomotion CPGs are located in the cervical as well as on the lumbar spinal cord initially, we were aiming at understanding whether there would be direct projections to the abducens nucleus from the cervical and from the lumbar spinal cord. This was not possible with the technique used due to the narrow migration time windows and migration pattern. When the virus was left to migrate 72h, instead of 67h, synaptic steps were up to two; there were infected neurons in the vestibulocerebellum but no infected neurons in the lumbar. Two possibilities arise with this observation: either the virus did not have enough time to reach the lumbar spinal cord or the inexistence of spino-extraocular LOINs in that region. This question could have been resolved through the use of a modified RV. See the discussion (Chapter IV, Mice in motion) to read more about experiments to be considered to further explore this matter.

Chapter III – Results

Article 1. Long-Lasting Visuo-Vestibular Mismatch in Freely Behaving Mice Reduces the Vestibulo- Ocular Reflex and Leads to Neural Changes in the Direct Vestibular Pathway

This project investigated the question of long-term retention of VOR motor learning in the brainstem. The design of the experiment allowed a system approach where *in vivo* and *in vitro* experiments were combined. A long-term visuo-vestibular mismatch protocol (VVM, see Article 2. Long-term Sensory Conflict in Freely Behaving Mice) was used to create a VOR gain-down in freely behaving mice for 14 days. Mice could behave in their cages while constantly being exposed to a VOR motor learning protocol. When the device was removed at the end of the protocol, a 50% decrease of the VOR gain was registered. Flocculus shut down experiments combined with VOR and OKR tests showed that this decrease was located outside the flocculus/paraflocculus complex. The neuronal mechanisms of this reduction were further investigated in MVN neurons of brainstem slices using afferent stimulations and patch-clamp recordings. The stimulation of the VIIIth nerve demonstrated that the amplitude of the eEPSCs were decreased in adapted mice. Additionally, the analysis of membrane properties of MVN neurons showed that a subpopulation of vestibular neurons (type A) presented a decrease in spontaneous discharge and excitability. In sum, this study shows that a long-lasting visuo-vestibular mismatch leads to changes in synaptic transmission and intrinsic properties of central vestibular neurons in the direct VOR pathway. Hence, our results provide direct evidence to the hypothesis of consolidation of long-term VOR changed in the brainstem.

eNeuro

New Research

Integrative Systems

Long-Lasting Visuo-Vestibular Mismatch in Freely-Behaving Mice Reduces the Vestibulo-Ocular Reflex and Leads to Neural Changes in the Direct Vestibular Pathway

Julie Carcaud,[1] Filipa França de Barros,[1] Erwin Idoux,[1] Daniel Eugène,[1] Lionel Reveret,[2] Lee E. Moore,[3] Pierre-Paul Vidal,[3] and Mathieu Beraneck[1]

DOI:http://dx.doi.org/10.1523/ENEURO.0290-16.2017

[1]Center for Neurophysics, Physiology, Pathology, CNRS UMR 8119, Université Paris Descartes, Sorbonne Paris Cité, Paris, France, [2]INRIA Grenoble, Rhône-Alpes, Laboratoire Jean Kuntzmann, UMR 5224, France, [3]Cognition and Action Group, CNRS UMR 8257, Université Paris Descartes, Sorbonne Paris Cité, Paris, France

Abstract

Calibration of the vestibulo-ocular reflex (VOR) depends on the presence of visual feedback. However, the cellular mechanisms associated with VOR modifications at the level of the brainstem remain largely unknown. A new protocol was designed to expose freely behaving mice to a visuo-vestibular mismatch during a 2-week period. This protocol induced a 50% reduction of the VOR. *In vivo* pharmacological experiments demonstrated that the VOR reduction depends on changes located outside the flocculus/paraflocculus complex. The cellular mechanisms associated with the VOR reduction were then studied *in vitro* on brainstem slices through a combination of vestibular afferent stimulation and patch-clamp recordings of central vestibular neurons. The evoked synaptic activity demonstrated that the efficacy of the synapses between vestibular afferents and central vestibular neurons was decreased. In addition, a long-term depression protocol failed to further decrease the synapse efficacy, suggesting that the VOR reduction might have occurred through depression-like mechanisms. Analysis of the intrinsic membrane properties of central vestibular neurons revealed that the synaptic changes were supplemented by a decrease in the spontaneous discharge and excitability of a subpopulation of neurons. Our results provide evidence that a long-lasting visuo-vestibular mismatch leads to changes in synaptic transmission and intrinsic properties of central vestibular neurons in the direct VOR pathway. Overall, these results open new avenues for future studies on visual and vestibular interactions conducted *in vivo* and *in vitro*.

Key words: multisensory; neuronal excitability; reflex; synaptic plasticity; vestibular neurons; VOR

Significance Statement

Calibration of the vestibulo-ocular reflex depends on the presence of visual feedback. *In vivo* work has suggested that cerebellar-dependent calibration of VOR is, in the long-term, consolidated in the brainstem. However, the associated cellular mechanisms remain unknown. To address these mechanisms, we present an innovative protocol in which freely behaving mice are submitted to 15 d of visuo-vestibular mismatch. We demonstrated that this protocol leads to a 50% reduction of the VOR. We also showed that in brainstem slices, long-term VOR reduction is associated with synaptic and intrinsic changes within the vestibular nuclei, in the direct VOR pathway. This study opens new avenues for future studies on visual and vestibular interactions conducted both *in vivo* and *in vitro*.

Introduction

Because of its relative simplicity, precise quantitative methods, and ease in applying experimental perturbations, gaze stabilization represents a suitable model to study motor learning that occurs when visual or vestibular sensory signals are modified (Blazquez et al., 2004; Broussard et al., 2011). In rodents, gaze stabilization depends on two complementary reflexes: the optokinetic reflex (OKR) that produces eye movements in the direction of visual motion and the vestibulo-ocular reflex (VOR) that stabilizes gaze during head motion (Stahl, 2004). Both reflexes cooperate to stabilize the visual scene on the retina in response to movement (Angelaki, 2004; Cullen, 2012).

Although the VOR operates even in the dark, its calibration depends on the presence of visual feedback. When a mismatch of visual and vestibular information occurs, retinal slip results, which blurs vision. This retinal slip serves as an error signal that is conveyed to the inferior olive and then to the cerebellum, where it is integrated with other sensory inputs (Fig. 1). The error signal indicates that eye movements are not compensatory, and thus drives motor learning to modulate the VOR (Shin et al., 2014) and restore gaze stabilization, a process known as VOR adaptation. The role of the cerebellum in the induction and short-term retention of this motor learning is clearly established (Hansel et al., 2001; Boyden et al., 2004; Carey, 2011; De Zeeuw and Ten Brinke, 2015). In contrast, long-term retention of the memory in the cerebellum itself or its transfer to downstream structures has long been a topic of debate (Broussard and Kassardjian, 2004; Broussard et al., 2011). One hypothesis was that the cerebellum is the main site of memory retention, as demonstrated by long-term depression at the synapses between parallel fibers and Purkinje cells (Fig. 1; Marr, 1969; Albus, 1971; Ito, 1982). An alternative model proposed that the cerebellum would not be the only site of retention but would also provide a teaching signal guiding the induction of plasticity within the brainstem (Miles and Lisberger, 1981; Lisberger et al., 1984). In favor of this hypothesis, experiments using cerebellum deactivation demonstrated that flocculi shutdown suppresses VOR short-term, but not long-term, adaptation (Luebke and Robinson, 1994; Pastor et al., 1994; Nagao and Kitazawa, 2003; Kassardjian et al., 2005). The retention of oculomotor memories outside the cerebellum in the long-term was further confirmed by OKR experiments (Shutoh et al., 2006; Anzai et al., 2010; Okamoto et al., 2011).

Although the hypothesis of a consolidation of long-term VOR changes in the brainstem has received support from many theoretical studies (Porrill and Dean, 2007; Masuda and Amari, 2008; Menzies et al., 2010; Medina, 2011; Clopath et al., 2014; Yamazaki et al., 2015), it has little experimental support. Studies *in vivo* have shown that some vestibular nuclei neurons changed their activity after VOR adaptation (Keller and Precht, 1979; Lisberger, 1988; Lisberger et al., 1994), even though this effect could not be dissociated from Purkinje cell activity. It was also proposed that the modification of the strength of the synapse between vestibular afferents and central vestibular neurons could be a key mechanism involved in VOR calibration (Menzies et al., 2010; Yamazaki et al., 2015).

Many of the studies on VOR motor learning have been conducted on animal models that do not allow for *in vitro* investigation. On the other hand, the use of the mouse model has its own constraints, as long-term modification of the VOR is classically achieved through passive head-fixed, iterated discontinuous training sessions interrupted by intertrial intervals of variable duration (Boyden and Raymond, 2003). Here, the neural basis of VOR plasticity was evaluated with a new long-term VOR reduction procedure in mice. Using a combination of behavioral analyses, oculomotor measurements with or without floccular deactivation, and *in vitro* electrophysiological recordings, we provide evidence that long-term VOR reduction is accompanied by synaptic and intrinsic modifications in the direct VOR pathway.

Material and Methods

Animals and surgical procedures

All animal procedures were performed in accordance with the University Paris Descartes animal care committee's regulations. A total of 116 C57BL/6J male mice (Janvier Labs; RRID: IMSR_JAX:000664) aged 6–8 weeks were included in the protocol. Gas anesthesia was induced using isoflurane. The head was shaved using an electric razor, and a 2-cm longitudinal incision of the skin was made to expose the skull. A small custom-built head holder (0.3 × 0.3 × 0.5 mm) was fixed to the skull just anterior to the lambda landmark using dental cement (C&B Metabond; Parkell). After the surgery, animals were isolated and closely monitored for 48 h. Buprenorphine (0.05 mg/kg) was provided for postoperative analgesia,

Received September 26, 2016; accepted January 10, 2017; First published January 16, 2017.

The authors declare no competing financial interests.

Author contributions: J.C. and M.B. designed research; J.C., F.F.D.B., E.I., D.E., L.R., and M.B. performed research; J.C., F.F.D.B., E.I., L.R., L.E.M., and M.B. analyzed data; J.C., F.F.D.B., E.I., D.E., L.E.M., P.-P.V., and M.B. wrote the paper.

This research was supported by the Centre National de la Recherche Scientifique and the University Paris Descartes. EI and MB receive support from the Centre National des Etudes Spatiales. JC and MB receive support from the French ANR-13-CESA-0005-02. FFB and MB receive support from the French ANR-15-CE32-0007.

Acknowledgments: We thank L. McElvain and S. Du Lac for their advice on the methodology for the vestibular afferents stimulation. We are grateful to P. Jegouzo for his technical support; this work would have not been possible without his innovative thinking in designing the VVM device. We thank M. Tagliabue for his help in developing the *in vivo* mouse experiments. We also thank C. Adou for her technical support for *in vitro* experiments. We thank J. McIntyre and J.X. Brooks for critically reading the manuscript.

Correspondence should be addressed to M. Beraneck. Center for Neurophysics, Physiology, Pathology, CNRS UMR 8119, 45 rue des St-Pères 75270, Université Paris Descartes, Paris, France. E-mail: mathieu.beraneck@parisdescartes.fr.

DOI:http://dx.doi.org/10.1523/ENEURO.0290-16.2017

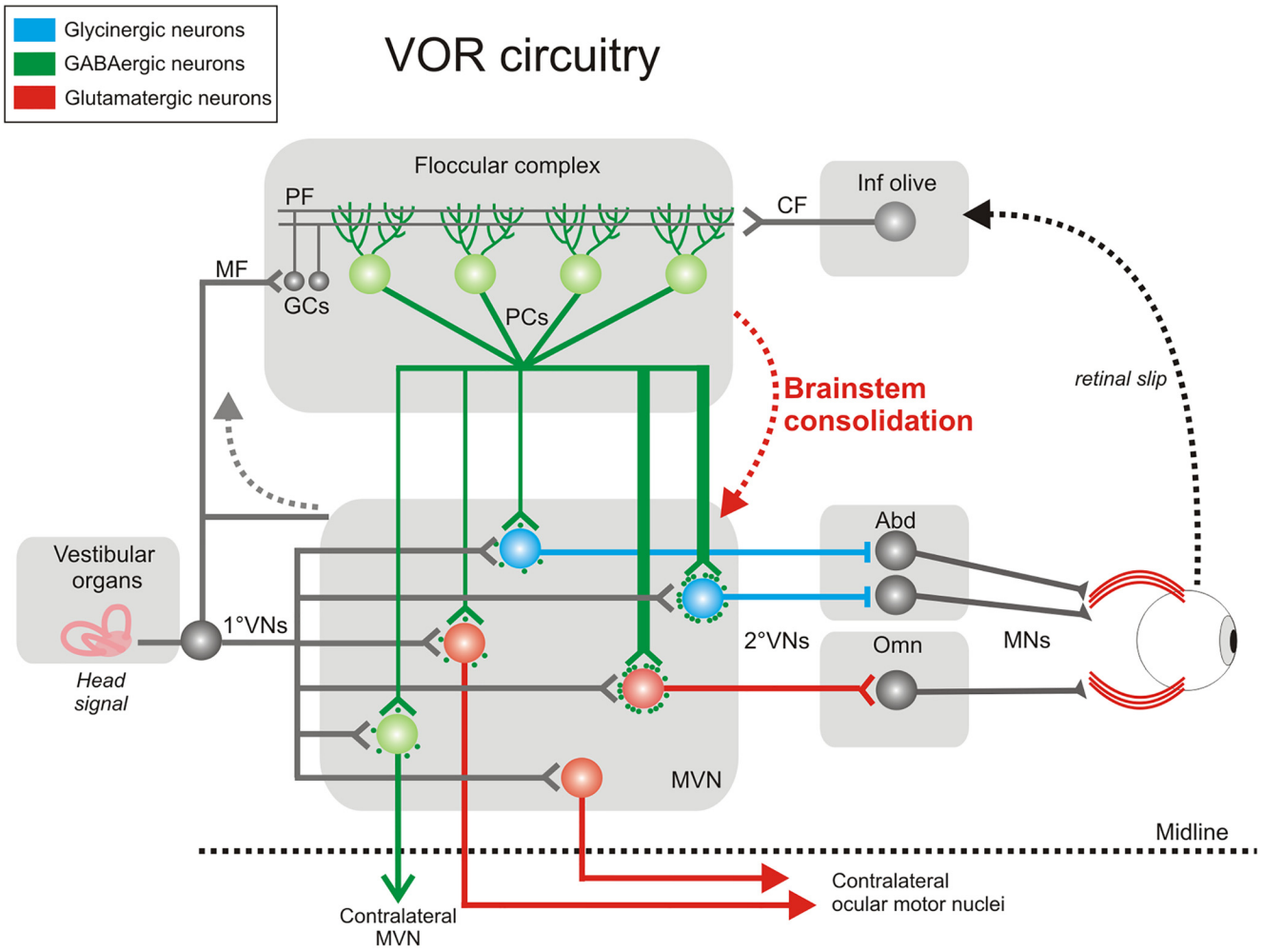

Fig. 1. Circuitry of structures implicated in VOR and its calibration. Integration of vestibular and visual inputs in the floccular complex modulates PC outputs. Floccular target neurons in the MVN are partitioned depending on the density of innervations received from the flocculi (thin or thick lines; density of synaptic contacts), on their neurotransmitter content, and projection sites. 1°VN and 2°VN, first- and second-order vestibular neuron; MN, motoneuron; CF, MF, and PF, climbing, mossy, and parallel fiber; GC, granule cell; Abd and Omn, abducens and oculomotor nucleus.

and care was taken to avoid hypothermia and dehydration.

Visuo-vestibular mismatch protocol

Two days after the surgery, a custom-built device was secured on top of the head holder. The device consisted of a helmet (2.2 cm width × 1.5 cm depth × 1.5 cm length; weight 2 g) that completely covered the mouse's head. The front of the device was adapted to the mouse anatomy so that the nose was not covered, and its width allowed for grooming and barbering behaviors. To preserve light-dependent physiology and nychthemeral rhythm, the device was made of nonopaque plastic with a thickness of 0.3 mm. In addition, 3-mm large vertical black stripes were drawn on the external surface to produce a high-contrast head-fixed visual signal during self-generated movements (Fig. 2*A*, top). A similar procedure was used on sham animals, except that the device was attached upside-down so that it did not cover the face of the mouse (Fig. 2*A*, bottom). Therefore, sham animals were exposed to the same surgical procedures and wore the same device but did not experience the visual-vestibular mismatch. Visuo-vestibular mismatch (VVM) and sham animals were housed together. Animals were housed in groups of three to stimulate social interactions. After 2 weeks with the device on the head, mice were immediately tested in behavioral experiments or used for *in vitro* electrophysiological experiments. The VOR of mice used for electrophysiology measures was not recorded to avoid relearning/extinction processes.

General observations

During the first hours of the VVM protocol, mice displayed disturbed behavior including difficulties orienting in the cage, bumping into walls, and reduction in social interactions. Initial difficulties to access food and drink were also noted, and animals therefore received intensive attention during the initial 48 h of the protocol. This early period corresponded to a decrease in the weight of the animal (Fig. 2*B*). On the other hand, sham mice did not

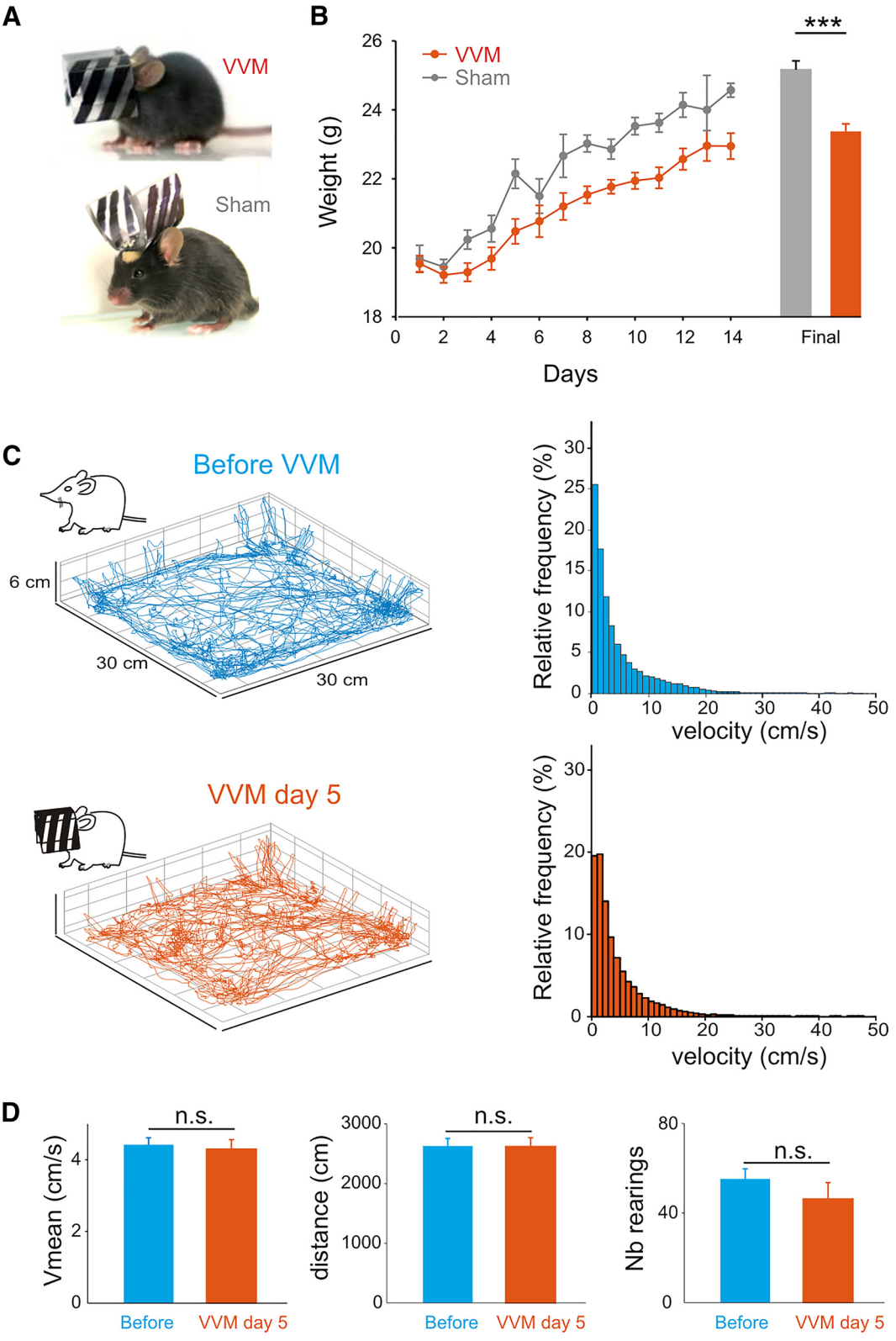

Fig. 2. VVM protocol and open-field experiments. ***A***, Pictures of a mouse during VVM (top) or sham (bottom) protocols. ***B***, Mean body weight of sham ($n = 24$, gray line) and VVM mice ($n = 57$, red) during the 2 weeks of the protocol. ***C***, Locomotion of mice before VVM (top) or after 5 d of VVM protocol (bottom) recorded while the animal explores the open field. Left panels, examples of 3D reconstruction of the path of the same animal. Right panels, distribution of velocities for the population of mice ($n = 4$) before VVM (blue) or after 5 d of VVM (red). ***D***, Plots of the mean velocity (Vmean, in cm/s), total covered distance (in cm), and vertical explorations (number of rearings) of mice ($n = 4$) before and after 5 d of VVM. Error bars represent ± SEM.

show any sign of disturbed behavior after beginning the protocol. After 2 d, the general behavior of VVM mice returned to normal, with good orientation in the cage, normal locomotion, and social interactions. The increase in weight observed thereafter was comparable to that of sham animals; still, after 2 weeks, a significant weight difference of ~1.5 g persisted between the two groups (Mann–Whitney, $z = 4.28$, $p = 0.00002$).

Behavioral measures

Open-field test

To determine how the VVM affects the way mice move, 3D tracking during open-field exploratory behavior was performed before the beginning of the protocol and 5 d after the device was implanted, i.e., once general behavior was back to normal. The setup consisted of a 30-cm cube surrounded by eight CCD cameras (synchronization frequency: 10 Hz; Point Grey Research, GRAS-03K2M). Mice were placed, one at a time, at the center of the arena and left completely undisturbed for 10 min. The 3D trajectory of the center of volume of the mouse was recovered using a multiple-view optical system. The images were electronically synchronized at the frame level using a trigger signal and a time stamp. For each camera, a calibration procedure provided the geometric projection from a 3D reference frame to the 2D image plane using a pinhole model. The 3D reference frame was oriented so that the *XY*-plane corresponds to the ground plane ($Z = 0$) and the *z*-axis to the up vertical axis. For each image, a background subtraction technique isolated the 2D silhouette of the mouse. The centroid of the silhouette provided a 2D cue of the animal's center of mass. After calibration of the cameras, the 2D centroids of each frame were triangulated using a direct linear transformation technique to compute the 3D trajectory of the center of volume. The third vertical coordinate was used to count the number of rearings. This experiment allowed analysis of the whole-body velocity, total distance traveled, and number of rearings performed during exploration of the open field.

Video-oculography and vestibulo-ocular performance

Video-oculography was performed to quantify the gaze-stabilizing reflexes. Mice were head-fixed at a ~30° nose-down position to align the horizontal canals in the yaw plane (Calabrese and Hullar, 2006; Oommen and Stahl, 2008) and placed in a custom-built Plexiglas tube secured on the superstructure of a vestibular stimulator. VOR performance was tested before and after the VVM protocol, with all sources of light turned off except for the computer screen. The turntable was further surrounded with a closed black box to isolate the animal from any remaining light, with an intensity inside the box <0.02 lux. Ten minutes before the experiment, 2% pilocarpine was applied to the eye to keep the pupil size constant (van Alphen et al., 2010). To record the effect of the VVM on the VOR, the head-fixed animal was put on the vestibular turntable immediately after the removal of the device while kept in the dark to avoid visual access in the environment.

Eye movements were recorded using an infrared video system (ETL-200, Iscan). The video-oculography calibration procedure was similar to that described by Stahl (2004). Eye and head position signals were sampled at 1 kHz, digitally recorded (CED power1401 MkII) with Spike 2 software, and later exported to Matlab for offline analysis (Matlab, The MathWorks; RRID: SCR:001622). Horizontal eye and head movement data were digitally low pass-filtered (cutoff frequency: 40 Hz), and position data were differentiated to obtain velocity traces. Segments of data with saccades were excluded from VOR slow-phase analysis. For horizontal sinusoidal rotations, at least 20 cycles were analyzed for each frequency. VOR gain and phase were determined by least-squares optimization:

$$EH_v(t) = g \times \{[HH_v \times (t - t_d)] + C^{te}\},$$

where $EH_v(t)$ is eye horizontal velocity, g (gain) is constant value, HH_v is head horizontal velocity, t_d is the dynamic lag time (in ms) of the eye movement with respect to the head movement, and C^{te} is an offset. t_d was used to calculate the corresponding phase $\varphi°$ of eye velocity relative to head velocity. The variance-accounted-for (VAF) of each fit was computed as

$$1 - \left[\frac{\mathrm{var}(est - EHv)}{\mathrm{var}(EHv)}\right],$$

where var represents variance, *est* represents the modeled eye velocity, and *EHv* represents the actual eye horizontal velocity. VAF values were typically between 0.70 and 1 (~97% of recordings), where a VAF of 1 indicates a perfect fit to the data. Trials for which the VAF was <0.5 were excluded from the analysis.

Overall, the VVM protocol was tested on 25 mice: $n = 13$ for the characterization of VOR features and $n = 12$ for VOR dependency on rotation frequency. Horizontal VOR in the dark was first tested during sinusoidal angular rotation around the vertical axis (0.5 Hz; velocity in range 20–50°/s) on 13 mice after VVM and on six sham mice. The ratio of slow-phase reduction was calculated by dividing the post-VVM measure by the pre-VVM measure. To compare how VVM affects slow phases versus quick phases, quick-phase analysis was performed at the highest tested velocity (0.5 Hz; 50°/s). A total of 20–25 cycles were analyzed in 10 of 13 VVM animals that had a VOR reduction >60%. The number of quick phases was counted, and their amplitudes were analyzed in Matlab.

To further characterize the slow-phase reduction, the dependence on the stimulation frequency on 12 additional VVM and six sham mice were tested at different frequencies of 0.2, 0.5, 1, and 2 Hz and at a fixed peak velocity of 30°/s.

Optokinetic reflex performance and flocculi shutdown experiments

To test whether the VOR reduction depends on the cerebellum or on a different brain structure, a flocculus shutdown experiment was performed. During these tests, the OKR was recorded to validate the effect of the pharmacological inhibition of the flocculus/paraflocculus complex. To record the OKR, the mouse was surrounded by a 40-cm-wide dome, and sources of light were turned off

except for the optokinetic projector. The light intensity inside the dome during OKR testing was measured at 185 lux (Luxmeter Lux-1337 Iso-tech). The optokinetic full-field stimulation was performed by projecting a dot pattern at velocities of 7.5°/s in both clockwise and counterclockwise directions. The dot pattern consisted of 25,000 white dots (max width 0.075°) randomly distributed on a black background. Optokinetic constant velocity stimulations lasted 1 min and were separated by at least 2 min of darkness. Optokinetic responses were analyzed offline after being imported into Matlab. Segments of data with saccades were excluded from the analysis. Optokinetic responses were measured as the mean eye velocities on segments longer than 1 s. Optokinetic gains were then calculated as the ratios of the mean eye velocities to the constant drum velocity.

After 2 weeks of VVM, both OKR and VOR performances were tested on seven mice. OKR and VOR were again measured 30 min after the stereotaxic injection of lidocaine ($n = 5$; 1 μL, 2% lidocaine) or sham injections of vehicle ($n = 2$) in the bilateral flocculi following a medial (3 mm medio-lateral) dorso-ventral direct approach (6 mm antero-posterior; *The Mouse Brain in Stereotaxic Coordinates*, Paxinos and Franklin) as in Shutoh et al. (2006). Injection was performed under isoflurane anesthesia to allow a rapid recovery and eye movement measurements. VOR testing was performed after OKR measures in complete darkness at frequencies of 0.2, 0.5, 1, and 2 Hz and at a fixed peak velocity of 30°/s, as described above.

To confirm the injection was made in the flocculi, fluorescent dye (1% fluorescein isothiocyanate, Invitrogen) was added to the lidocaine or saline injection and visualized using an epifluorescent microscope on subsequently cut slices, following the procedure described by Okamoto et al. (2011). After intracerebellar injections, intracardiac perfusions were performed, and the brains were removed. The brains were postfixed overnight in PFA 4% and dehydrated in 30% sucrose solution for at least 48 h. Then, 80-μm brain slices were cut using a microtome and visualized with the epifluorescent microscope (Olympus BX-61).

Electrophysiological experiments

Whole-cell patch-clamp recordings

Brain dissections and patch-clamp recordings were performed on slices taken from control ($n = 36$) or VVM ($n = 38$) animals. After decapitation under deep anesthesia (pentobarbital 100 mg/kg), the brain was quickly removed and placed in ice-cold, phosphate/bicarbonate-buffered artificial cerebrospinal fluid (ACSF), which included (in mM) 240 sucrose, 2.5 KCl, 1 NaH_2PO_4, 25 $NaHCO_3$, 3 $MgCl_2$, and 10 glucose and was supplemented with 95% O_2-5% CO_2. Brainstem slices of 220 μm containing the medial vestibular nuclei (MVN) were cut using a microslicer (Leica). To optimize the maintenance of vestibular afferent fibers in the plane of the slice, an angle of 15° was added to the standard coronal plane. Slices were then transferred into an incubating vial filled with regular ACSF containing (in mM) 120 NaCl, 2.5 KCl, 1 NaH_2PO_4, 25 $NaHCO_3$, 2.5 $CaCl_2$, 2 $MgCl_2$, and 10 glucose and oxygenated with 95% O_2-5% CO_2 (pH 7.4). The more rostral slices containing the MVN, in which the brainstem was attached to the cerebellum (5.8–6.5 mm AP; *The Mouse Brain in Stereotaxic Coordinates*, Paxinos and Franklin), were selected and placed in the recording chamber maintained at 32–34°C. Slices were superfused with regular ACSF at a constant flow rate of 3 ml/min. Patch-clamp pipettes were pulled from borosilicate glass tubing to a resistance of 4–7 MΩ. The internal solution (Sekirnjak and du Lac, 2006) contained (in mM) 140 K-gluconate, 2 $MgCl_2$, 5 KCl, 10 HEPES, 0.03 $CaCl_2$, 0.1 EGTA, 4 Na_2ATP, and 0.4 Na_2GTP (adjusted to pH 7.3 with KOH).

MVN neurons were visualized with a microscope (Olympus BX-51) using differential interference contrast illumination with Nomarski optics. Using the boundaries of the fourth ventricle as landmarks, MVN neuron recordings were restricted to the dorsal half of the nucleus (depth of 4–4.25 mm) and to the medial two thirds of the nucleus (0.25–0.8 mm lateral; *The Mouse Brain in Stereotaxic Coordinates*, Paxinos and Franklin). Neurons at the edge of the fourth ventricle were not recorded. After the surface of the soma of a neuron was approached with a pipette, suction was applied until a giga-ohm seal was made. Recordings were made with a Multiclamp 700B (Molecular Devices). Inhibitory transmission through glycine and $GABA_A$ receptors was blocked using 10 μM strychnine and 100 μM picrotoxin, respectively (Sigma-Aldrich; McElvain et al., 2010). The spontaneous discharge was first recorded in current-clamp mode for few minutes until a stable level was reached. MVN neurons that had a membrane potential less than −45 mV and a spike amplitude >45 mV were selected for current and voltage clamp experiments. The current and voltage from the amplifier were low-pass filtered at 2 kHz and digitized at 5 kHz (BNC-2090 + PCI-6052E, National Instruments). Custom-written codes in Matlab were used for acquisition and offline analysis.

Excitatory postsynaptic current and plasticity recordings

Excitatory postsynaptic current (EPSC) recordings were performed on brain slices cut from 12 control mice ($n = 17$ neurons; 13 from 8 naive mice and 4 neurons from 4 sham mice) and 19 VVM animals ($n = 31$ neurons). After recording the spontaneous discharge and action potentials at the basic membrane potential, the neuron was clamped at −70 mV. First, the vestibular afferents were stimulated with a concentric bipolar stimulating electrode (FHC) placed on the vestibular fiber bundle. Electrode placement was always made at the same optimal location 4.5 mm ventral to the horizontal plane and ~1.7 mm lateral (*The Mouse Brain in Stereotaxic Coordinates*, Paxinos and Franklin), similar to the procedure followed by McElvain et al. (2010). EPSC were evoked (eEPSC) using stimulation at a frequency of 0.067 Hz (one stimulation every 15 s). First, the stimulation amplitude was set at 300–400 pA to maximize the EPSC amplitude. Then, after 3 min of recording, a long-term depression (LTD) protocol consisting of 30 repetitions of 550-ms vestibular nerve stimulation at 100 Hz was applied according to the procedure provided by McElvain et al. (2010).

Table 1. Statistical table.

Fig.	Panel	Data structure	Type of test	*p* value
2	B	Non-normal distribution	Mann–Whitney test	0.00002
2	D left (Vmean)	Non-normal distribution	Wilcoxon test	0.46
2	D middle (distance)	Non-normal distribution	Wilcoxon test	0.14
2	D right (nb rearings)	Non-normal distribution	Wilcoxon test	0.14
3	C left (gain)	Normal distribution	ANOVA repeated measures: group effect	<0.0001
3	C left inset (gain)	Normal distribution	ANOVA repeated measures: group effect	0.046
3	C right (phase)	Normal distribution	ANOVA repeated measures: interaction group x velocity	0.022
3	C right inset (phase)	Normal distribution	ANOVA repeated measures: group effect	0.96
3	D left (occurrence)	Normal distribution	paired *t*-test	0.004
3	D right (amplitude)	Normal distribution	paired *t*-test	0.11
3	E	Correlation	Pearson correlation significance test	0.0003
3	G left (gain)	Normal distribution	ANOVA repeated measures: frequency effect	0.36
3	G right (phase)	Normal distribution	ANOVA repeated measures: frequency effect	0.002
4	A/before vs. VVM	Non-normal distribution	Wilcoxon test	0.62
4	A/VVM vs. lidocaine	Non-normal distribution	Wilcoxon test	0.001
4	A/VVM vs. sham	Non-normal distribution	Wilcoxon test	0.68
4	C left (gain)	Normal distribution	ANOVA repeated measures: before vs. after group effect	0.017
4	C left (gain)	Normal distribution	ANOVA repeated measures: after vs. shutdown group effect	0.28
4	C right (phase)	Normal distribution	ANOVA repeated measures: after vs. shutdown group effect	0.49
5	B left (AUC)	Non-normal distribution	Mann–Whitney test	0.0018
5	B middle (tau)	Non-normal distribution	Mann–Whitney test	0.26
5	B right (amplitude)	Non-normal distribution	Mann–Whitney test	0.004
5	C control	Non-normal distribution	Wilcoxon test	0.017
5	C VVM	Non-normal distribution	Wilcoxon test	0.33
6	B left (all neurons)	Normal distribution	ANOVA repeated measures: group effect	0.316
6	B middle (type A)	Normal distribution	ANOVA repeated measures: group effect	0.0004
6	B right (type B)	Normal distribution	ANOVA repeated measures: group effect	0.88

All analyses were performed offline in Matlab. eEPSC amplitude (pA), area under the curve (AUC, fC), and time constant (τ, ms) were calculated offline. For the LTD protocol, eEPSCs were normalized to the preprotocol baseline, and the mean value collected during the 15 min after the LTD protocol was calculated for graphic representation.

Electrophysiological properties of MVN neurons

Basic and firing properties of MVN neurons were investigated in current-clamp ($n = 63$ control neurons from 36 mice and $n = 60$ VVM neurons from 38 mice). Because most MVN neurons are spontaneously active in slices, the potential was low-pass filtered at 1 Hz to obtain an estimate of its average resting level that was taken as the "mean average membrane potential" (Vm, in mV) of each neuron. This membrane potential value was corrected offline by measuring and subtracting the extracellular voltage offset found after withdrawal of the electrode from each neuron. Averages of the spike shapes and following interspike interval profiles were analyzed to obtain the spontaneous firing rate (in spikes/s), the associated coefficient of variation (CV), the amplitude of the afterhyperpolarization (AHP, in mV), the spike threshold potential (in mV), the concavity, and the convexity (in mV). The AHP and interspike interval first derivative was used to quantify the amplitude of the double AHP (dAHP, in V/s) and the presence of an A-like rectification (AHPR in V/s). The classification of MVN neurons was performed based on these quantitative criteria following the procedure provided by Beraneck et al. (2003). Excitability of the neurons was tested using injection of hyperpolarizing/depolarizing steps from basic potential with steps of currents (1 s; 25pA increment, range ± 125 pA). Excitability was calculated as the mean firing frequency during the steps (in spikes/s). Membrane resistance was calculated from the hyperpolarizing step at –75 pA.

Statistical analyses

Statistical analyses were performed using Statistica 7.1 software (StatSoft). A statistical table is provided (see Table 1). Repeated-measures ANOVAs were performed on VOR gain and phase across frequencies or velocities. Nonparametric unpaired Mann–Whitney tests were performed to compare measures between control and VVM mice. Nonparametric paired Wilcoxon signed rank tests were performed to compare EPSC amplitude before and after the LTD protocol.

Results

A new protocol was developed to expose freely behaving mice to a VVM for a 2-week period. The consequences of the VVM on locomotor behavior and its effects on the efficacy of the VOR were first tested. Next, the neural changes underlying long-term VOR reduction were studied using whole-cell patch-clamp electrophysiology on brainstem slices.

Behavioral experiments

Open-field data

During the freely behaving VVM protocol, the animal generates active movements. To determine whether the implanted device modifies the way the animal moves, the exploratory behavior of four mice was analyzed using a 3D tracking video system. When placed in the open field, mice naturally explored the environment in both horizontal

and vertical planes (Fig. 2C, left). Exploratory behavior was compared for each mouse before the beginning the protocol (blue trace) and 5 d after the device was implanted (red trace), while the mouse was still wearing the device. Overall, we observed no difference in the way the mice explored the open field. The distribution and range of walking velocities were comparable (Fig. 2C, right), and there was no difference in the mean velocity ($n = 4$, Wilcoxon test, $z = 0.73$, $p = 0.46$), total covered distance ($n = 4$, Wilcoxon test, $z = 1.46$, $p = 0.14$), or number of vertical explorations (rearings; $n = 4$, Wilcoxon test, $z = 1.46$, $p = 0.14$; Fig. 2D). These data complement our general observations (see Materials and methods; Fig. 2B), which suggest that after the initial 48 h, mice wearing the VVM device display relatively normal behavior.

VVM protocol reduces the VOR

To evaluate the effects of the VVM on gaze stabilization, the VOR was quantified using video-oculography in the dark during sinusoidal rotations around a vertical axis (Fig. 3A). The VOR of 25 mice was compared before the implantation of the VVM device and immediately after its removal 2 weeks later; it was similarly measured on six sham mice. As a result of VVM, the amplitude of the eye movements observed during table rotations was greatly reduced (Fig. 3B, response of the same mouse before and after VVM). A first group of 13 mice was tested at a fixed frequency of 0.5 Hz and peak velocities from 20 to 50°/s. A decrease of the VOR gain by >50% was observed for all conditions after the 2 weeks of VVM (Fig. 3C, left, repeated-measures ANOVA, group effect, $F_{1,24} = 42.6$, $p < 0.0001$), with a shift toward phase lead at velocities <40°/s (Fig. 3C, right, repeated-measures ANOVA, group × velocity interaction effect, $F_{3,72} = 3.41$, $p = 0.022$). In contrast, sham mice ($n = 6$) exposed to a comparable experience in the absence of VVM had no reduction in VOR (slight increase in VOR gain: repeated-measures ANOVA, group effect, $F_{1,5} = 6.92$, $p = 0.046$; VOR phase: repeated-measures ANOVA, group effect, $F_{1,5} = 0;003$, $p = 0.96$; see traces in Fig. 3B, C). In addition to the slow-phase changes, quick phases were also investigated. After VVM, the occurrence (Fig. 3D, left) of the quick phases was significantly diminished ($n = 10$, paired t-test, $t = 3.77$, $p = 0.004$) and although there was a tendency of decreased amplitude of saccades after VVM, this difference did not reach statistical significance (Fig. 3D, right; $n = 10$, paired t-test, $t = 1.77$, $p = 0.11$). However, the comparison of the changes in slow phases and quick phases demonstrated a significant correlation (Fig. 3E; $R = 0.905$; $z = 1.50$, $p = 0.0003$), suggesting that both features of the vestibulo-ocular reflex were modified by the VVM.

Because the VVM was generated by an actively behaving mouse, we then questioned how this reduction affects the VOR across different frequencies. The dependence of the VOR reduction on the stimulating frequency was therefore tested on the six sham animals and 12 additional VVM mice at four different frequencies (0.2, 0.5, 1, and 2 Hz; fixed peak velocity of 30°/s). No differences were found in the VOR gain and phase of sham animals before and after the protocol (mean gain ± SD before/after: 0.2 Hz, 0.14 ± 0.05/0.16 ± 0.06; 0.5 Hz, 0.34 ± 0.05/0.32 ± 0.08; 1 Hz, 0.50 ± 0.09/0.55 ± 0.1; 2 Hz, 0.59 ± 0.18/0.55 ± 0.13; repeated-

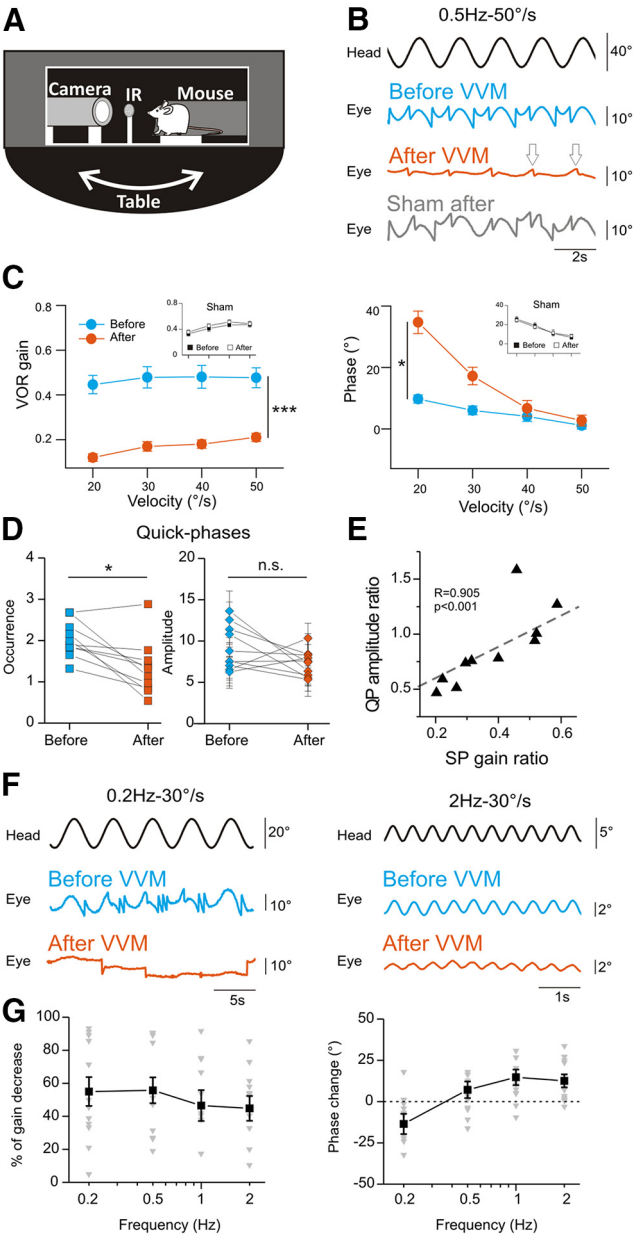

Fig. 3. VOR reduction. ***A***, Illustration of the setup used to test the VOR. IR, infrared light. ***B***, Example raw traces of the VOR in the dark recorded before (blue line) and after 2 weeks of VVM (red line) from the same animal. Gray trace, sham mouse tested after 2 weeks of wearing the helmet. White arrows indicate example of quick phases observed after VVM. Head and eye traces show rightward movements in the upward and downward directions, respectively. ***C***, Mean VOR gain (left) and corresponding phase (right) plotted as a function of tested velocity ($n = 13$ mice; fixed frequency of 0.5 Hz) measured before (blue lines) and after 2 weeks of VVM (red lines). Insets: sham ($n = 6$ mice) before (filled squares) and after (empty squares) the protocol. ***D***, Occurrence (left) and amplitude (right) of quick phases ($n = 10$ mice). ***E***, Quick-phase amplitude ratio (after/before values) is significantly correlated to slow-phase gain ratio (***$p < 0.001$). ***F***, Example raw traces of the VOR reduction at 0.2 or 2Hz stimulation. ***G***, Mean percentage of gain decrease (left, $n = 12$) or phase change (right, $n = 12$) depending on stimulating frequencies. The gray triangles represent the individual values, and the black lines represent the mean values. Error bars represent ± SEM.

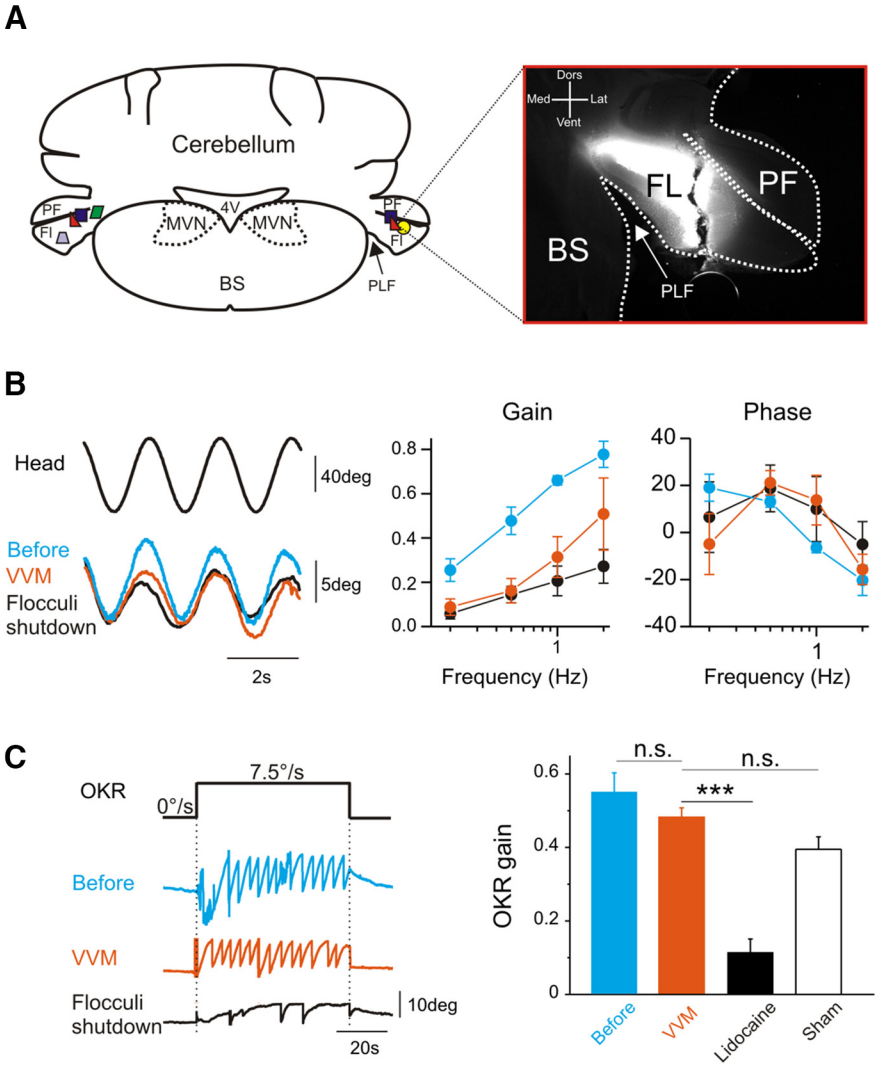

Fig. 4. Flocculi shutdown experiments. ***A***, Left, coronal section of the brainstem and cerebellum illustrating the lidocaine injections in flocculi complex. PF, paraflocculus; Fl, flocculus; PLF, posterolateral fissure; 4V, 4th ventricle; BS, brainstem. Right, example of a lidocaine injection coupled to fluorescein isothiocyanate. Dors, dorsal; Vent, ventral; Med, medial; Lat, lateral. ***B***, Left, example raw traces of VOR in the dark recorded before (blue line), after 2 weeks of VVM (red line), and after flocculi shutdown (black line). All traces are from the same animal. Right, Bode plots of VOR gain and phase (n = 5 mice). ***C***, Left, example raw traces of eye movements recorded during optokinetic stimulation (60s-long full-field stimulation at 7.5°/s constant velocity). All traces are from the same animal. Right, mean OKR gain recorded before, after VVM, after lidocaine injection, or on sham animals. Error bars represent ± SEM.

measures ANOVA, group effect; for VOR gain: $F_{1,5} = 0.007$, $p = 0.94$; for VOR phase: $F_{1,5} = 0.99$, $p = 0.36$). Fig. 3*F* shows examples traces of the VOR generated at frequencies of 0.2 Hz (left) or 2 Hz (right) before and after VVM. Again, we found a significant decrease of the gain of the VOR at all frequencies after VVM, represented by a percentage of gain decrease of ~50%. Although the average decrease of the VOR was comparable at all frequencies (repeated-measures ANOVA, frequency effect, $F_{3,33} = 1.11$, $p = 0.36$), Fig. 3*G* illustrates the variability in the amount of VOR decrease between individuals (gray triangles). The long-term VVM also had a significant effect on the phase of the VOR, with a shift toward greater phase lag at 0.2 Hz and toward greater phase lead at frequencies ≥0.5 Hz (Fig. 3*G*, right, repeated-measures ANOVA, frequency effect, $F_{3,33} = 6.30$, $p = 0.002$). Overall, video-oculography results clearly demonstrate that the 2 weeks of VVM protocol led to a strong gain-down reduction of the VOR.

Flocculus shutdown experiment

To determine whether the long-term VOR reduction depends on cellular changes located at the level of the cerebellum or in downstream structures, flocculus shutdown experiments were performed by injection of lidocaine (Fig. 4). Injections of lidocaine were coupled to fluorescent dye to validate *a posteriori* the location in the flocculi (Fig. 4*A*). As described above, VOR gain significantly decreased after 2 weeks of VVM (Fig. 4*B*, $n = 5$; repeated-measures ANOVA, before vs. after group effect, $F_{1,6} = 10.52$, $p = 0.017$). When the flocculi were inactivated, the gain and phase of the VOR remained unchanged compared to the values reached after VVM (Fig. 4*B*; repeated-measures

Table 2. Static intrinsic properties of MVN neurons.

	All		type A		type B		Statistical tests (Mann–Whitney)		
Property	Control	VVM	Control	VVM	Control	VVM	Control vs. VVM		
Number of neurons	63	60	27	17	36	43	All	type A	type B
Membrane potential (mV)	–48.28	–49.00	–47.24	–47.22	–49.07	–49.70	$z = -1.09$ NS	$z = -0.02$ NS	$z = -0.81$ NS
Spike threshold (mV)	–31.32	–32.34	–29.58	–30.73	–32.63	–32.97	$z = -1.36$ NS	$z = -0.99$ NS	$z = -0.39$ NS
Firing rate (Hz)	12.24	7.85	13.83	8.14	11.04	7.74	$z = -2.49$ $p = 0.013$	$z = -1.73$ $p = 0.08$	$z = -1.57$ NS
Coefficient of variation	0.16	0.22	0.15	0.22	0.17	0.22	$z = 1.97$ $p = 0.048$	$z = 1.40$ NS	$z = 1.11$ NS
AHPR (V/s)	0.20	0.21	0.44	0.67	0.02	0.03	$z = -1.29$ NS	$z = -0.09$ NS	$z = -0.11$ NS
dAHP (V/s)	0.71	0.69	0.00	0.00	1.24	0.96	$z = -0.07$ NS	NA NA	$z = -1.14$ NS
AHP (mV)	26.11	25.25	29.68	28.54	23.43	23.95	$z = -0.16$ NS	$z = -0.14$ NS	$z = 0.48$ NS
Concavity (mV)	–1.33	–1.50	–2.49	–3.47	–0.46	–0.73	$z = 0.002$ NS	$z = -1.49$ NS	$z = -0.59$ NS
Convexity (mV)	0.82	0.84	0.56	0.34	1.02	1.05	$z = 0.13$ NS	$z = -0.98$ NS	$z = 0.03$ NS

Parameters of the spontaneous activity of MVN neurons recorded on control and VVM slices. Static parameters are based on the analysis of the pacemaker discharge of the neurons and the quantification of the AHP and interspike interval. Neurons are pooled (all) or segmented in type A and type B. Overall, the intrinsic membrane properties recorded in controls and VVM mice show limited differences between type A and type B neurons. AHPR, dAHP, and AHP are parameters representing kinetics of the AHP and interspike interval (see Materials and methods). Statistically significant differences are highlighted in red. NS, not significant.

ANOVA, after vs. flocculi shutdown group effect, on gain measures: $F_{1,8} = 1.35$, $p = 0.28$; on phase measures: $F_{1,8} = 0.52$, $p = 0.49$). To functionally confirm the efficacy of the injection, the OKR was measured on the seven mice before and after VVM, and immediately after injection of lidocaine ($n = 5$) or saline ($n = 2$). Before VVM, optokinetic full-field stimulation performed at 7.5°/s triggered a consistent response (Fig. 4*C*, blue trace). After 2 weeks of VVM, optokinetic responses were mostly preserved (Fig. 4*C*, red trace; Wilcoxon test, $p = 0.625$). We noted, however, that OKR responses were sometimes qualitatively less robust than before VVM (not shown). After lidocaine injection in the flocculi, the OKR responses were largely abolished (Fig. 4*C*, black trace), as demonstrated by the strong reduction of the mean gain after the lidocaine injection (Wilcoxon test, $p < 0.001$). As expected, sham injection did not significantly modify the OKR responses ($n = 2$, 0.38 ± 0.13, Wilcoxon test, $p = 0.686$). The OKR tests therefore confirmed the ability of lidocaine injection to inhibit the flocculi. Overall, these experiments demonstrated that after 2 weeks of VVM, the reduction of the VOR depends on plasticity located outside the flocculus/paraflocculus complex.

In vitro electrophysiological recordings

To determine whether the VOR reduction involves plastic changes at the level of the brainstem, *in vitro* electrophysiology was performed on mice after the 2 weeks of VVM and compared with control mice. Previous studies suggested that the reduction of the VOR could depend on plastic changes in the direct horizontal VOR pathway. Therefore, we measured the synaptic and intrinsic properties of central MVN neurons after VOR reduction.

Synaptic plasticity after VVM protocol

Whole-cell patch-clamp electrophysiology was performed on central neurons recorded in brainstem slices taken from control and VVM mice. We first recorded evoked eEPSCs from second-order neurons in response to afferent stimulation (vestibular afferent fiber bundle stimulation; Fig. 5*A*, left) in control ($n = 17$ neurons) and VVM ($n = 31$ neurons) conditions. As illustrated in Fig. 5*A*, right, eEPSCs were smaller in VVM neurons compared with control neurons, a result confirmed by an AUC (Fig. 5*B*, top left) that was significantly smaller in the VVM than in control condition (Mann–Whitney test, $z = 3.13$, $p = 0.0018$). To determine whether this decrease in eEPSC AUC depends on changes in postsynaptic receptors, we explored the kinetic characteristics of the eEPSC. The eEPSC time constant (τ) was not different between the two groups (Fig. 5*B*, top middle, Mann–Whitney test, $z = -1.12$, $p = 0.26$). In contrast, the amplitude was smaller after VVM in comparison with control mice (Fig. 5*B*, top right, Mann–Whitney test, $z = 2.84$, $p = 0.004$), as shown in the distribution of eEPSC amplitude shifted toward smaller amplitudes (Fig. 5*B*, bottom). These results suggest that the receptor units involved in the eEPSC responses are qualitatively not different in VVM mice from controls. Altogether, this experiment suggests that the long-term VOR reduction is associated with a reduction of the efficacy of the synapses between vestibular afferents and central vestibular neurons.

Last, we asked whether additional down-tuning of this synapse was possible or whether the synaptic efficacy was already at its minimum. To address this question, we performed a LTD protocol in both control and VVM mice (Fig. 5*C*). As previously reported (McElvain et al., 2010), LTD could be experimentally induced in control slices, which led to a significant decrease in the eEPSC amplitude after the stimulation protocol ($n = 8$; Wilcoxon test, $z = 2.38$, $p = 0.017$). On the other hand, when neurons from VVM mice were tested, no further decrease of the synapse efficacy could be triggered ($n = 14$; Wilcoxon test, $z = 0.97$, $p = 0.33$).

Overall, these data show that the reduction in the VOR observed after VVM is correlated with a reduction in the efficacy of the synapses between the vestibular nerve and central vestibular neurons. Because no additional decrease of the synaptic efficacy could be triggered experimentally, we then explored whether these synaptic changes were supplemented by a change in the intrinsic excitability of central vestibular neurons.

Intrinsic properties of MVN neurons after VVM

To explore this hypothesis, we first characterized the membrane properties of the neurons recorded in slices of control and VVM mice (Table 2). Because vestibular neurons have a pacemaker activity in brainstem slices (Dutia

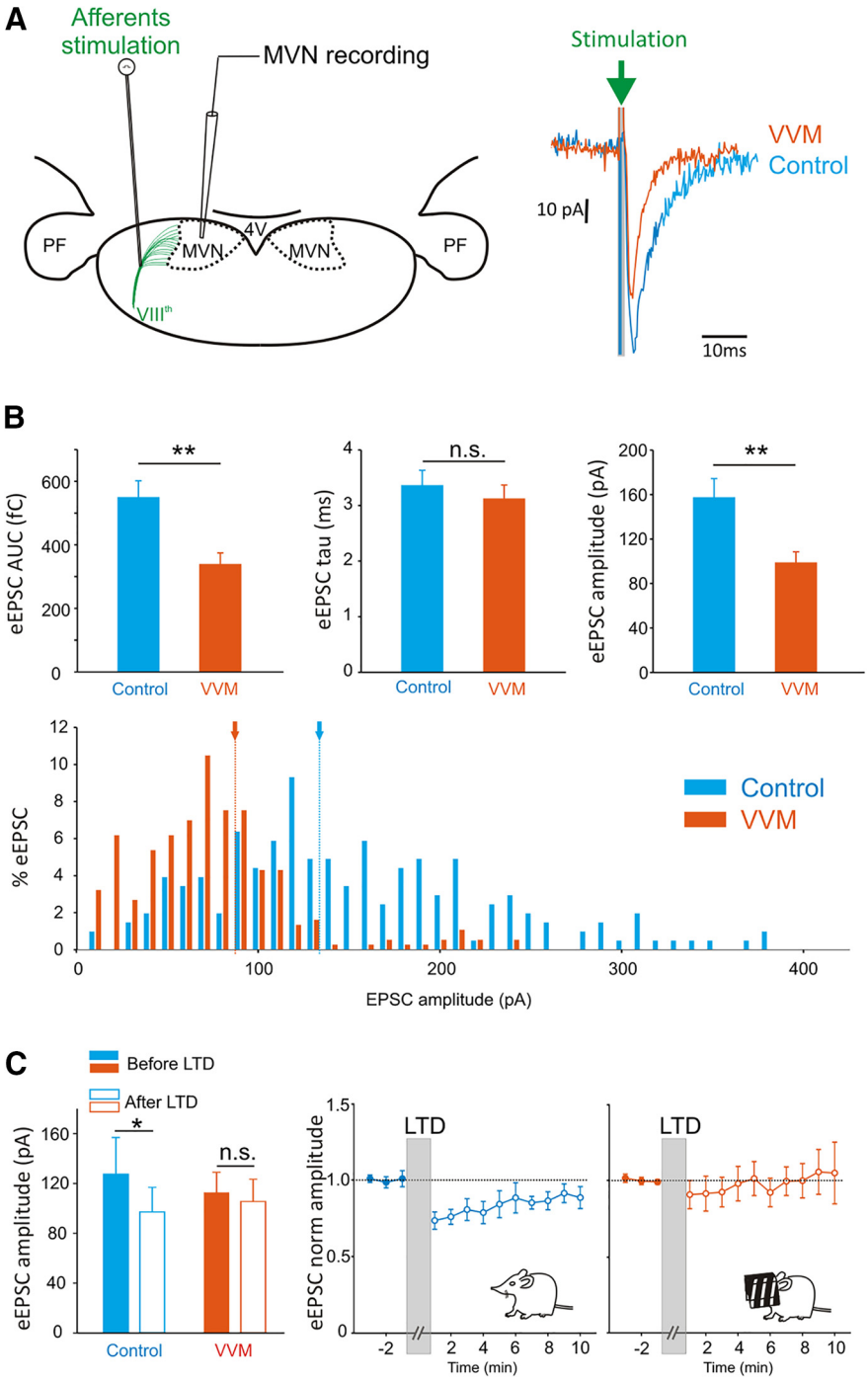

Fig. 5. Stimulation of afferents: vestibular synapses efficacy. ***A***, Left, illustration of *in vitro* patch-clamp recordings of MVN neurons on coronal brainstem slice. The stimulating electrode is placed on the central vestibular fiber bundles. PF, paraflocculus region; 4V, 4th ventricle. Right, example raw traces of superimposed eEPSC recorded from a MVN neuron of a control mouse (blue line) and from a mouse after VVM (red line). ***B***, Top, evoked EPSCs AUC (in fC), time constant (τ, in ms), and amplitude (in pA) recorded from control neurons ($n = 17$) or after VVM ($n = 31$). Bottom, distribution of eEPSC amplitude for control (blue bars) and VVM (red bars) conditions. Arrows and dashed lines indicate the medians (~135 pA for control and ~85 pA for VVM). ***C***, Plasticity of vestibular nerve synapses onto MVN neurons. Left, eEPSC amplitude recorded on control ($n = 8$) and VVM ($n = 14$) neurons before (filled bars) and after (empty bars) LTD protocol. Right, mean eEPSC peak amplitude before and after LTD protocol for control (blue line) and VVM (red line) neurons. The eEPSC values are normalized to the mean baseline value before LTD protocol (filled circles). Empty circles represent measures following LTD protocol. Error bars represent ± SEM.

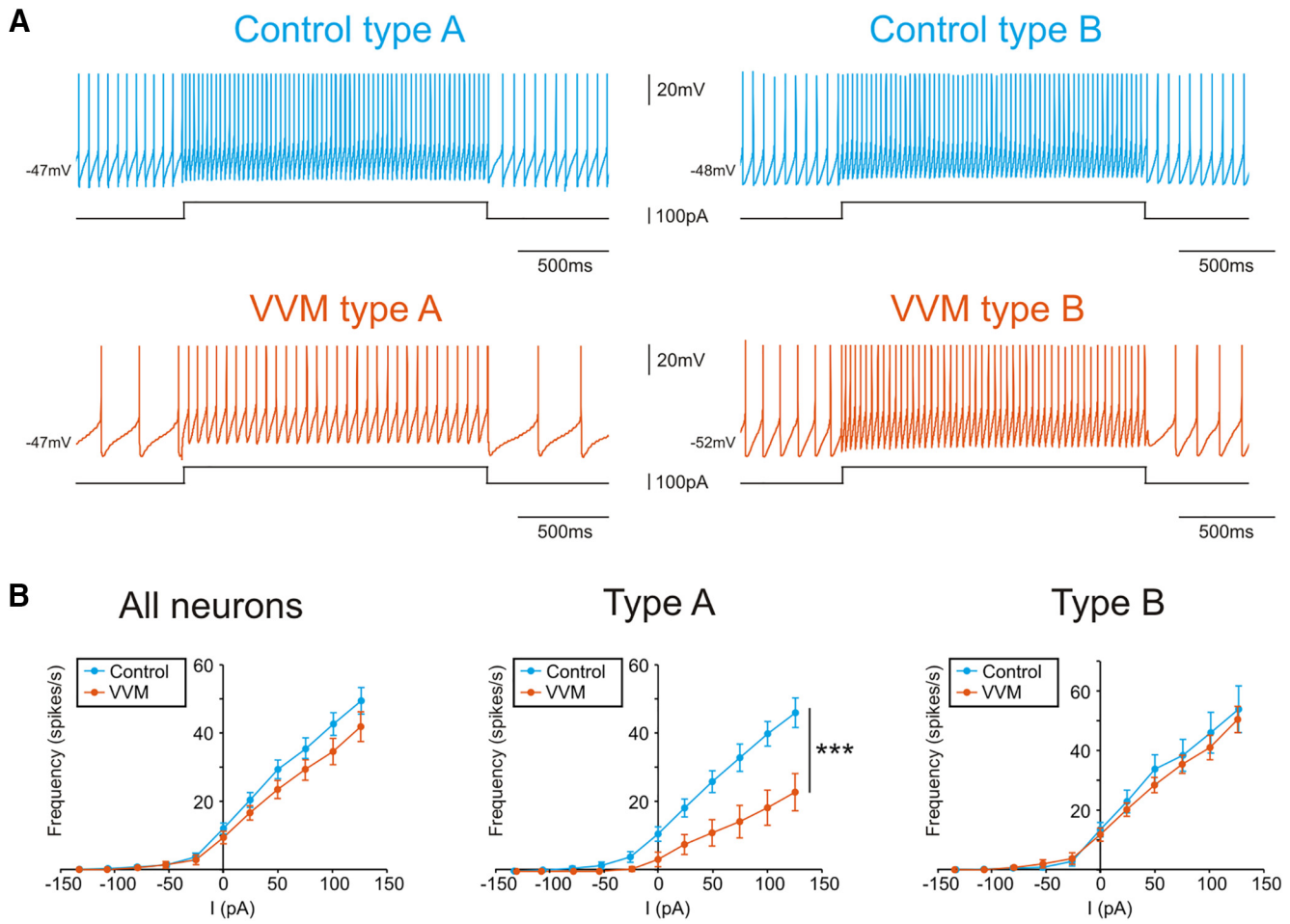

Fig. 6. Excitability of second-order vestibular neurons in response to step-like currents. ***A***, Example raw traces of MVN neurons recorded in control (top) type A (left) and type B (right), or VVM (bottom) conditions. ***B***, Relation between the injected current and the frequency of discharge (I/F curves) for all MVN neurons (left, $n = 38$ control and $n = 24$ VVM), type A (middle, $n = 23$ control and $n = 7$ VVM) and type B (right, $n = 15$ control and $n = 17$ VVM) neurons. (***$p < 0.001$).

et al., 1992, 1995), we first characterized their responses in the absence of external stimulation (Table 2). There was no difference in the spike shape parameters between control and VVM conditions ($n = 63$ control neurons vs. $n = 60$ VVM neurons). However, VVM neurons showed a decrease of their spontaneous firing rate in comparison to control neurons (Mann–Whitney test, $z = -2.49$, $p = 0.013$) and a slightly more regular spontaneous discharge than control neurons (CV of 0.16 vs. 0.22; Mann–Whitney test, $z = 1.97$, $p = 0.048$). MVN neurons were previously shown to be composed of different subpopulations that can be partly segregated using their electrophysiological signature at rest (Straka et al., 2005; Eugène et al., 2011; Beraneck and Idoux, 2012). Hence, we further divided the recorded neurons using the canonical type A and type B classification. This analysis revealed that compared with controls, type A neurons appear to be specifically modified by the VVM, with a tendency for a lower firing rate than control neurons (Mann–Whitney test, $z = -1.73$, $p = 0.08$).

We then used step-like current stimulation (Fig. 6*A*) to investigate the excitability of the neurons by assessing their current–frequency relationship (I/F curve). No significant differences in I/F curves between control ($n = 38$) and VVM ($n = 24$) conditions were found when neuronal subtypes were pooled together (Fig. 6*B*, left; on depolarizing steps, repeated-measures ANOVA, group effect: $F_{1,52} = 1.03$, $p = 0.316$). However, when neurons were segmented into type A and type B, we found a significant decrease in the excitability restricted to type A neurons ($n = 23$ control, $n = 7$ VVM; Fig. 6*B*, middle; on depolarizing steps, repeated-measures ANOVA, group effect: $F_{1,26} = 8.00$, $p = 0.009$; group × current interaction: $F_{5,130} = 4.88$, $p = 0.0004$), whereas VVM had no significant effect on the excitability of type B neurons ($n = 15$ control, $n = 17$ VVM; Fig. 6*B*, right; on depolarizing steps, repeated-measures ANOVA, group effect: $F_{1,24} = 0.02$, $p = 0.88$). We then calculated the resistance of the neurons using hyperpolarizing steps and found that the resistance of both type A neurons and type B was not different in control and VVM neurons (type A control 310 ± 33 vs. type A VVM 302 ± 46 MΩ; type B control 382 ± 54 vs. type B VVM 370 ± 47 MΩ; Mann–Whitney test, $z = -0.11$ for type A, $z = 1.10$ for type B, not significant).

Overall, these *in vitro* results demonstrate that after 14 d of VVM, long-term reduction of the VOR is accompanied

by changes occurring in the brainstem, within the direct VOR pathway. These changes consist of both a reduction of the efficacy of the vestibular afferents synapses on MVN neurons and changes in the intrinsic membrane properties of some MVN neurons.

Discussion

Using VVM in freely behaving mice, we showed neural evidence that long-term VOR reduction is correlated to plasticity within the vestibular nuclei.

A new protocol for VOR reduction through visuo-vestibular mismatch

In humans and monkeys, VOR adaptation is studied by the use of prisms that the subject wears for several days (Berthoz et al., 1981; Melvill Jones et al., 1988; Anzai et al., 2010; Nagao et al., 2013). On the other hand, traditional protocols triggering a VOR gain-down adaptation in rodents involve rotating the head-fixed animal in phase with the visual surround. This basic procedure is then repeated on several consecutive days to drive long-term adaptation (Raymond and Lisberger, 1996; Boyden and Raymond, 2003; Rinaldi et al., 2013). This methodology is time-consuming and consists of discontinuous training sessions interrupted by intertrial intervals of variable duration (Boyden and Raymond, 2003). It furthermore represents passive learning, since the vestibular stimulation is not actively generated by voluntary movements (Roy and Cullen, 2004; Cullen, 2012). VVM methodology bypasses these experimental constraints. Here, the VOR reduction occurs in response to voluntary natural head movements in an uninterrupted process. Using this approach, we report a general reduction of VOR by ~50%. Our data on open-field locomotion show that mice adapt to the device and that the animals ambulate and explore the environment relatively normally, with no indication of a generalized vestibular impairment. The results obtained on sham animals further demonstrate that the reduction of VOR is a consequence of the visuo-vestibular mismatch and not of a generalized motor impairment. This decrease is comparable to the ones observed using standard VOR gain-down adaptation protocols in head-fixed animals (Boyden et al., 2004; Kassardjian et al., 2005). Moreover, VVM was shown to differentially affect the timing (phase) of the VOR depending on the tested frequency. This result can be interpreted in the framework of frequency-selective channels for vestibular processing (Baker et al., 1981; Lisberger et al., 1983; Straka et al., 2009), and of phase crossover after classic VOR adaptation. Phase crossover after gain-down learning induces phase lags at frequencies below the training frequency and phase leads at frequencies above the training frequency (Lisberger et al., 1983; Raymond and Lisberger, 1996). We show that VVM induces a similar effect on the timing of eye movements. The crossover occurs between 0.2 and 0.5 Hz, which is compatible with the natural range of mouse head movements dominated by low frequencies (Beraneck et al., 2008). Frequencies <0.5 Hz also correspond to the range at which the visual information is most important for gaze stabilization (Faulstich et al., 2006). As the changes in eye movements after VVM are comparable to those observed after a standard head-fixed protocol driving gain down, VOR reduction observed in both cases could depend on comparable cellular mechanisms. We note, however, that the VVM constitutes a different protocol from the classic VOR adaptation performed in mice, and that caution should be taken when interpreting results obtained under different experimental conditions.

The role of brainstem changes in long-term VOR reduction

The hypothesis of a transfer of memory from the cerebellum to downstream structures has been explored using different types of cerebellar-dependent motor learning. Eyelid conditioning protocols have demonstrated that the initiation of learning in the cerebellar cortex (Ohyama and Mauk, 2001) is followed by the induction of plasticity in downstream nuclei for consolidation (Kleim et al., 2002; Ohyama et al., 2006). A comparable sequence of memory formation was demonstrated using optokinetic gain-up learning (Shutoh et al., 2006; Okamoto et al., 2011). OKR studies also suggested that long-term motor learning could depend on plastic processes within the vestibular nuclei (Shutoh et al. 2006). Adaptation of the VOR has been proposed early on to depend on several sites of plasticity in the cerebellum and the brainstem (Lisberger et al., 1981, 1994; Broussard and Lisberger, 1992; Pastor et al., 1994; du Lac et al., 1995; Dietrich and Straka, 2016). These experimental results have inspired recent theoretical studies that suggested that memory consolidation of VOR motor learning occurs in the vestibular nuclei. Here, we provide evidence of plasticity in vestibular nuclei after a long-term reduction of the VOR. The decrease of synaptic efficacy at the level of vestibular afferent synapses onto vestibular nuclei neurons is in direct line with theoretical predictions regarding VOR gain-down adaptation (Masuda and Amari, 2008; Menzies et al., 2010; Yamazaki et al., 2015). Moreover, it is consistent with a recent study showing that a change at this synapse is sufficient to induce a persistent decrease of the VOR *in vivo* (Mitchell et al., 2016). This brainstem memory raises several fundamental questions, including which subpopulations of neurons are concerned and which cellular mechanisms underlie these plastic changes.

The majority of MVN neurons are floccular target neurons

MVN neurons that receive inputs from the flocculus are named floccular target neurons (FTNs). FTNs integrate cerebellar and vestibular inputs and are key players in VOR modulation. Based on *in vivo* studies, it was proposed that two different pathways, both projecting to ocular motoneurons, would mediate the VOR: the modifiable pathway composed of FTNs and the unmodifiable pathway composed of non-FTNs (Broussard and Kassardjian, 2004). Early *in vitro* electrophysiology suggested that a relatively low proportion of MVNs are FTNs (<15%; Babalian and Vidal 2000; Sekirnjak et al. 2003). Importantly, recent anatomical studies performed on mice demonstrated that the majority of MVNs are actually FTNs (~80%; Shin et al. 2011), which segregate in subpopulations according to the amount (dense vs. sparse) and

location (somatic vs. dendritic) of cerebellar inputs received as well as their neurotransmitter content (glutamatergic, glycinergic, GABAergic; see Fig. 1; Shin et al., 2011; Matsuno et al., 2016).

Here, because FTNs were not specifically recorded, the reduction of synaptic efficacy represents the average decrease found in the entire population of second-order MVNs likely composed of densely and sparsely innervated FTNs, as well as non-FTN neurons. In line with the possibility of a widespread change in vestibular pathway, Shutoh et al. (2006) have reported an increase in the vestibular field potential, suggesting that the OKR gain-up long-term adaptation similarly concerned a majority of the vestibular neurons *in vivo*. Regardless of the actual proportion of MVN neurons receiving monosynaptic floccular inputs, cerebellar regulation of vestibular activity could, in the long-term, spread to non-FTNs through local networks. Shin et al. (2011) reported that about half of commissural neurons are sparsely contacted by FTNs, demonstrating the influence of cerebellar inputs on the regulation of bilateral vestibular activity beyond the first synaptic contact. This hypothesis is further considered below.

Synaptic plasticity: cellular and molecular mechanisms

The role of the input of Purkinje cells (PCs) in the induction of plasticity in the brainstem is well supported (Wulff et al., 2009; Zheng and Raman, 2010; Okamoto et al., 2011). How could PCs activity affect vestibular processing in FTNs? We demonstrated in this study that long-term VOR reduction is associated with a decrease in efficacy of the vestibular nerve synapses on MVNs, presumably through LTD-like mechanisms. It was shown that plasticity at this synapse can be induced by high-frequency stimulation of vestibular afferents, and that the direction of the plasticity is dependent on both developmental stage (Puyal et al., 2003) and stimulation pattern (Scarduzio et al., 2012) at basic potential (Idoux, 2015). Moreover, this plasticity is also dependent on the postsynaptic membrane potential (Pugh and Raman, 2006; McElvain et al., 2010). These *in vitro* electrophysiological data suggest that PC inhibition could guide the strengthening or weakening of vestibular nerve synapses on MVNs. The depression we report after long-term VOR reduction could be explained by a mechanism of heterosynaptic plasticity. It was theorized that this plastic process would use an anti-Hebbian input spike-timing dependent plasticity (iSTDP) mechanism, resulting from the simultaneous vestibular afferent activity and membrane hyperpolarization by PC inhibition (Menzies et al., 2010). In line with this hypothesis, a recent study demonstrated that in mouse parvocellular MVNs, inhibitory synapses from the flocculus and excitatory synapses from the vestibular nerve axons are often colocalized on distal dendrites of FTNs (Matsuno et al., 2016). Notably, the iSTDP mechanism could in theory also regulate the interaction of vestibular inputs with other, nonfloccular inhibitory inputs. In particular, the demonstration of a commissural feed-forward inhibition (Biesdorf et al. 2008; Malinvaud et al. 2010) interleaved with cerebellar inputs (Shin et al. 2011) raises the possibility of a long-term homeostatic activity-dependent regulation of vestibular synapses strengthened by local and commissural GABAergic and glycinergic neurons (Bagnall et al., 2007; Biesdorf et al., 2008; see discussion in Menzies et al. 2010; Mitchell et al. 2016). What would be the molecular mechanisms underlying the reported synaptic plasticity? The decrease in synaptic efficacy could depend on postsynaptic alterations, with changes in the glutamatergic receptors. In support of this hypothesis, it has been demonstrated that LTD at vestibular nerve synapses on vestibular nucleus neurons depends on NMDA receptors in mice (McElvain et al., 2010; Menzies et al., 2010). Because no additional decrease can be triggered in neurons from VVM mice using standard LTD protocols, NMDA receptors are likely a major player in the plastic process. Additional work will be needed to specify the molecular mechanisms involved in this long-term synaptic plasticity.

Floccular target neurons comprise both type A and type B neurons

Based on electrophysiological criteria, MVN neurons are composed of at least two subpopulations (Serafin et al., 1991). The classification used in the present study identifies type A and type B neurons based on the spike AHP and shape of the interspike interval (Beraneck et al., 2003). How are type A and type B neurons inserted into vestibular-related networks? Both types receive direct excitatory vestibular inputs (Babalian et al., 1997; Pettorossi et al., 2011) and commissural inhibition (Camp et al., 2006). The majority of type A are GABAergic neurons (Takazawa et al., 2004; Bagnall et al., 2007), which receive mostly GABAergic inhibitory inputs (Camp et al., 2006). Type A neurons likely represent the majority of local interneurons (Takazawa et al., 2004) and a significant proportion of the sparse FTNs that participate in the feed-forward local regulation of MVN activity (Biesdorf et al., 2008; Malinvaud et al., 2010; Shin et al., 2011).

On the other hand, type B neurons are glutamatergic or glycinergic output neurons that project to the ocular motor nuclei (Beraneck and Idoux, 2012). Early *in vitro* studies reported that FTNs show membrane properties specific to a subset of type B neurons (Babalian and Vidal, 2000; Sekirnjak et al., 2003). This subpopulation of FTNs with highly nonlinear properties likely corresponds to densely innervated glycinergic neurons (~10%; Shin et al., 2011; Kodama et al., 2012). In addition, the majority of glutamatergic FTNs, which project axons to the ocular motor nuclei, and of glycinergic neurons, which project to the contralateral side, are also likely to be type B neurons (Bagnall et al., 2007; Shin et al., 2011). Overall, available data suggest that FTNs are composed of both type A and type B neurons that are differentially inserted within vestibular networks and play functionally distinct roles.

In this study, the decrease of eEPSC amplitude was found on a population composed of both type A and type B neurons: the mean eEPSC amplitude was reduced by ~50% in type A and ~35% in type B. Although our available data do not allow for a definitive conclusion, they

suggest that both populations are susceptible to show synaptic plasticity after VVM, and we have therefore no evidence for a differential implication of these subpopulations in the reported synaptic plasticity.

Differential change in the intrinsic properties of type A and type B neurons

Reorganization within the vestibular pathway has been extensively studied in the context of postlesional modifications (i.e., vestibular compensation; Curthoys, 2000; Straka et al., 2005). In addition to synaptic plasticity (Vibert et al., 2000; Grassi and Pettorossi, 2001), changes in the intrinsic membrane properties of central vestibular neurons occur over the long time scale of several weeks, with differential changes in type A and type B neurons (Him and Dutia, 2001; Beraneck et al., 2003, 2004). Changes in the intrinsic excitability of MVNs were already postulated as a putative mechanism after VOR learning (du Lac, 1996; Broussard and Kassardjian, 2004; Gittis and du Lac, 2006). Pettorossi et al. (2011) demonstrated on brainstem slices that high-frequency stimulation of vestibular afferents leads to differential synaptic and intrinsic plasticity in type A or type B neurons, respectively. In particular, changes in intrinsic excitability were more consistently triggered in type A neurons than in type B neurons. Here, we report a decrease in the spontaneous discharge and the intrinsic excitability of type A MVNs. Although the electrophysiological classification we use does not differentiate the heterogeneous populations of type A neurons (Kodama et al., 2012), it identifies inhibitory GABAergic neurons as a key component in the tuning of the direct vestibular pathway following long-term VOR reduction. The precise identification of the different subpopulations of MVNs using, for instance, genetically engineered mice (Bagnall et al., 2007; Kodama et al., 2012) or tracing techniques (Sekirnjak and du Lac, 2006; Matsuno et al., 2016) will be the next step in understanding the cellular mechanisms involved in VOR long-term reduction after a visual-vestibular mismatch.

References

Albus JS (1971) A theory of cerebellar function. Math Biosci 10:25–61. CrossRef

Angelaki DE (2004) Eyes on target: what neurons must do for the vestibuloocular reflex during linear motion. J Neurophysiol 92:20–35. CrossRef Medline

Anzai M, Kitazawa H, Nagao S (2010) Effects of reversible pharmacological shutdown of cerebellar flocculus on the memory of long-term horizontal vestibulo-ocular reflex adaptation in monkeys. Neurosci Res 68:191–198. CrossRef Medline

Babalian A, Vibert N, Assie G, Serafin M, Mühlethaler M, Vidal PP (1997) Central vestibular networks in the guinea-pig: functional characterization in the isolated whole brain in vitro. Neuroscience 81:405–426. Medline

Babalian AL, Vidal PP (2000) Floccular modulation of vestibuloocular pathways and cerebellum-related plasticity: an in vitro whole brain study. J Neurophysiol 84:2514–2528.

Bagnall MW, Stevens RJ, du Lac S (2007) Transgenic mouse lines subdivide medial vestibular nucleus neurons into discrete, neurochemically distinct populations. J Neurosci 27:2318–2330. CrossRef Medline

Baker R, Evinger C, McCrea RA (1981) Some thoughts about the three neurons in the vestibular ocular reflex. Ann N Y Acad Sci 374:171–188. Medline

Beraneck M, Idoux E (2012) Reconsidering the role of neuronal intrinsic properties and neuromodulation in vestibular homeostasis. Front Neurol 3:25. CrossRef Medline

Beraneck M, McKee JL, Aleisa M, Cullen KE (2008) Asymmetric recovery in cerebellar-deficient mice following unilateral labyrinthectomy. J Neurophysiol 100:945–958. CrossRef Medline

Beraneck M, Idoux E, Uno A, Vidal PP, Moore LE, Vibert N (2004) Unilateral labyrinthectomy modifies the membrane properties of contralesional vestibular neurons. J Neurophysiol 92:1668–1684. CrossRef Medline

Beraneck M, Hachemaoui M, Idoux E, Ris L, Uno A, Godaux E, Vidal PP, Moore LE, Vibert N (2003) Long-term plasticity of ipsilesional medial vestibular nucleus neurons after unilateral labyrinthectomy. J Neurophysiol 90:184–203. CrossRef Medline

Berthoz A, Jones GM, Bégué AE (1981) Differential visual adaptation of vertical canal-dependent vestibulo-ocular reflexes. Exp Brain Res 44:19–26. CrossRef

Biesdorf S, Malinvaud D, Reichenberger I, Pfanzelt S, Straka H (2008) Differential inhibitory control of semicircular canal nerve afferent-evoked inputs in second-order vestibular neurons by glycinergic and GABAergic circuits. J Neurophysiol 99:1758–1769. CrossRef

Blazquez PM, Hirata Y, Highstein SM (2004) The vestibulo-ocular reflex as a model system for motor learning: what is the role of the cerebellum? Cerebellum 3:188–192. CrossRef Medline

Boyden ES, Raymond JL (2003) Active reversal of motor memories reveals rules governing memory encoding. Neuron 39:1031–1042. Medline

Boyden ES, Katoh A, Raymond JL (2004) Cerebellum-dependent learning: the role of multiple plasticity mechanisms. Annu Rev Neurosci 27:581–609. CrossRef Medline

Broussard DM, Lisberger SG (1992) Vestibular inputs to brain stem neurons that participate in motor learning in the primate vestibuloocular reflex. J Neurophysiol 68:1906–1909. Medline

Broussard DM, Kassardjian CD (2004) Learning in a simple motor system. Learn Mem 11:127–136. CrossRef Medline

Broussard DM, Titley HK, Antflick J, Hampson DR (2011) Motor learning in the VOR: the cerebellar component. Exp Brain Res 210:451–463. CrossRef Medline

Calabrese DR, Hullar TE (2006) Planar relationships of the semicircular canals in two strains of mice. J Assoc Res Otolaryngol 7:151–159. CrossRef Medline

Camp AJ, Callister RJ, Brichta AM (2006) Inhibitory synaptic transmission differs in mouse type A and B medial vestibular nucleus neurons in vitro. J Neurophysiol 95:3208–3218. CrossRef

Carey MR (2011) Synaptic mechanisms of sensorimotor learning in the cerebellum. Curr Opin Neurobiol 21:609–615. CrossRef Medline

Clopath C, Badura A, De Zeeuw CI, Brunel N (2014) A cerebellar learning model of vestibulo-ocular reflex adaptation in wild-type and mutant mice. J Neurosci 34:7203–7215. CrossRef Medline

Cullen KE (2012) The vestibular system: multimodal integration and encoding of self-motion for motor control. Trends Neurosci 35:185–196. CrossRef Medline

Curthoys IS (2000) Vestibular compensation and substitution. Curr Opin Neurol 13:27–30. Medline

De Zeeuw CI, Ten Brinke MM (2015) Motor learning and the cerebellum. Cold Spring Harb Perspect Biol 7:a021683. CrossRef Medline

Dietrich H, Straka H (2016) Prolonged vestibular stimulation induces homeostatic plasticity of the vestibulo-ocular reflex in larval Xenopus laevis. Eur J Neurosci 44:1787–1796. CrossRef Medline

du Lac S (1996) Candidate cellular mechanisms of vestibulo-ocular reflex plasticity. Ann N Y Acad Sci 781:489–498. Medline

du Lac S, Raymond JL, Sejnowski TJ, Lisberger SG (1995) Learning and memory in the vestibulo-ocular reflex. Annu Rev Neurosci 18:409–441. CrossRef Medline

Dutia MB, Johnston AR, McQueen DS (1992) Tonic activity of rat medial vestibular nucleus neurones in vitro and its inhibition by GABA. Exp Brain Res 88:466–472. Medline
Dutia MB, Lotto RB, Johnston AR (1995) Post-natal development of tonic activity and membrane excitability in mouse medial vestibular nucleus neurones. Acta Otolaryngol Suppl 520 (Pt 1):101–104. CrossRef
Eugène D, Idoux E, Beraneck M, Moore LE, Vidal PP (2011) Intrinsic membrane properties of central vestibular neurons in rodents. Exp Brain Res 210:423–436. CrossRef Medline
Faulstich M, van Alphen AM, Luo C, du Lac S, De Zeeuw CI (2006) Oculomotor plasticity during vestibular compensation does not depend on cerebellar LTD. J Neurophysiol 96:1187–1195. CrossRef
Gittis AH, du Lac S (2006) Intrinsic and synaptic plasticity in the vestibular system. Curr Opin Neurobiol 16:385–390. CrossRef Medline
Grassi S, Pettorossi VE (2001) Synaptic plasticity in the medial vestibular nuclei: role of glutamate receptors and retrograde messengers in rat brainstem slices. Prog Neurobiol 64:527–553. Medline
Hansel C, Linden DJ, D'Angelo E (2001) Beyond parallel fiber LTD: the diversity of synaptic and non-synaptic plasticity in the cerebellum. Nat Neurosci 4:467–475. CrossRef Medline
Him A, Dutia MB (2001) Intrinsic excitability changes in vestibular nucleus neurons after unilateral deafferentation. Brain Res 908: 58–66. Medline
Idoux E (2015) Vestibular plasticity. In: The rat nervous system, 4th Edition (Paxinos G, ed), pp 837–842: Elsevier.
Ito M (1982) Cerebellar control of the vestibulo-ocular reflex–around the flocculus hypothesis. Annu Rev Neurosci 5:275–296. CrossRef Medline
Kassardjian CD, Tan YF, Chung JY, Heskin R, Peterson MJ, Broussard DM (2005) The site of a motor memory shifts with consolidation. J Neurosci 25:7979–7985. CrossRef Medline
Keller EL, Precht W (1979) Modification of central vestibular neuron response by conflicting visual-vestibular stimulation. Prog Brain Res 50:763–770. CrossRef Medline
Kleim JA, Freeman JH, Jr., Bruneau R, Nolan BC, Cooper NR, Zook A, Walters D (2002) Synapse formation is associated with memory storage in the cerebellum. Proc Natl Acad Sci U S A 99:13228–13231. CrossRef Medline
Kodama T, Guerrero S, Shin M, Moghadam S, Faulstich M, du Lac S (2012) Neuronal classification and marker gene identification via single-cell expression profiling of brainstem vestibular neurons subserving cerebellar learning. J Neurosci 32:7819–7831. CrossRef Medline
Lisberger SG (1988) The neural basis for learning of simple motor skills. Science 242:728–735. Medline
Lisberger SG, Miles FA, Optican LM (1983) Frequency-selective adaptation: evidence for channels in the vestibulo-ocular reflex? J Neurosci 3:1234–1244. Medline
Lisberger SG, Miles FA, Zee DS (1984) Signals used to compute errors in monkey vestibuloocular reflex: possible role of flocculus. J Neurophysiol 52:1140–1153. Medline
Lisberger SG, Pavelko TA, Broussard DM (1994) Neural basis for motor learning in the vestibuloocular reflex of primates. I. Changes in the responses of brain stem neurons. J Neurophysiol 72:928–953. Medline
Lisberger SG, Miles FA, Optican LM, Eighmy BB (1981) Optokinetic response in monkey: underlying mechanisms and their sensitivity to long-term adaptive changes in vestibuloocular reflex. J Neurophysiol 45:869–890. Medline
Luebke AE, Robinson DA (1994) Gain changes of the cat's vestibulo-ocular reflex after flocculus deactivation. Exp Brain Res 98:379–390. Medline
Malinvaud D, Vassias I, Reichenberger I, Rössert C, Straka H (2010) Functional organization of vestibular commissural connections in frog. J Neurosci 30:3310–3325. CrossRef Medline
Marr D (1969) A theory of cerebellar cortex. J Physiol 202:437–470. Medline
Masuda N, Amari S (2008) A computational study of synaptic mechanisms of partial memory transfer in cerebellar vestibulo-ocular-reflex learning. J Comput Neurosci 24:137–156. CrossRef Medline
Matsuno H, Kudoh M, Watakabe A, Yamamori T, Shigemoto R, Nagao S (2016) Distribution and structure of synapses on medial vestibular nuclear neurons targeted by cerebellar flocculus Purkinje cells and vestibular nerve in mice: light and electron microscopy studies. PLoS One 11:e0164037. CrossRef Medline
McElvain LE, Bagnall MW, Sakatos A, du Lac S (2010) Bidirectional plasticity gated by hyperpolarization controls the gain of postsynaptic firing responses at central vestibular nerve synapses. Neuron 68:763–775. CrossRef Medline
Medina JF (2011) The multiple roles of Purkinje cells in sensori-motor calibration: to predict, teach and command. Curr Opin Neurobiol 21:616–622. CrossRef Medline
Melvill Jones G, Guitton D, Berthoz A (1988) Changing patterns of eye-head coordination during 6 h of optically reversed vision. Exp Brain Res 69:531–544. Medline
Menzies JR, Porrill J, Dutia M, Dean P ((2010) Synaptic plasticity in medial vestibular nucleus neurons: comparison with computational requirements of VOR adaptation. PLoS One 5. CrossRef
Miles FA, Lisberger SG (1981) Plasticity in the vestibulo-ocular reflex: a new hypothesis. Annu Rev Neurosci 4:273–299. CrossRef Medline
Mitchell DE, Della Santina CC, Cullen KE (2016) Plasticity within non-cerebellar pathways rapidly shapes motor performance in vivo. Nat Commun 7:11238. CrossRef Medline
Nagao S, Kitazawa H (2003) Effects of reversible shutdown of the monkey flocculus on the retention of adaptation of the horizontal vestibulo-ocular reflex. Neuroscience 118:563–570. Medline
Nagao S, Honda T, Yamazaki T (2013) Transfer of memory trace of cerebellum-dependent motor learning in human prism adaptation: a model study. Neural Netw 47:72–80. CrossRef Medline
Ohyama T, Mauk M (2001) Latent acquisition of timed responses in cerebellar cortex. J Neurosci 21:682–690. Medline
Ohyama T, Nores WL, Medina JF, Riusech FA, Mauk MD (2006) Learning-induced plasticity in deep cerebellar nucleus. J Neurosci 26:12656–12663. CrossRef Medline
Okamoto T, Shirao T, Shutoh F, Suzuki T, Nagao S (2011) Post-training cerebellar cortical activity plays an important role for consolidation of memory of cerebellum-dependent motor learning. Neurosci Lett 504:53–56. CrossRef Medline
Oommen BS, Stahl JS (2008) Eye orientation during static tilts and its relationship to spontaneous head pitch in the laboratory mouse. Brain Res 1193:57–66. CrossRef Medline
Pastor AM, de la Cruz RR, Baker R (1994) Cerebellar role in adaptation of the goldfish vestibuloocular reflex. J Neurophysiol 72: 1383–1394. Medline
Pettorossi VE, Dieni CV, Scarduzio M, Grassi S (2011) Long-term potentiation of synaptic response and intrinsic excitability in neurons of the rat medial vestibular nuclei. Neuroscience 187:1–14. CrossRef Medline
Porrill J, Dean P (2007) Cerebellar motor learning: when is cortical plasticity not enough? PLoS Comput Biol 3:1935–1950. CrossRef Medline
Pugh JR, Raman IM (2006) Potentiation of mossy fiber EPSCs in the cerebellar nuclei by NMDA receptor activation followed by postinhibitory rebound current. Neuron 51:113–123. CrossRef Medline
Puyal J, Grassi S, Dieni C, Frondaroli A, Demêmes D, Raymond J, Pettorossi VE (2003) Developmental shift from long-term depression to long-term potentiation in the rat medial vestibular nuclei: role of group I metabotropic glutamate receptors. J Physiol 553: 427–443. CrossRef
Raymond JL, Lisberger SG (1996) Behavioral analysis of signals that guide learned changes in the amplitude and dynamics of the vestibulo-ocular reflex. J Neurosci 16:7791–7802. Medline
Rinaldi A, Defterali C, Mialot A, Garden DL, Beraneck M, Nolan MF (2013) HCN1 channels in cerebellar Purkinje cells promote late

stages of learning and constrain synaptic inhibition. J Physiol 591:5691–5709. CrossRef Medline

Roy JE, Cullen KE (2004) Dissociating self-generated from passively applied head motion: neural mechanisms in the vestibular nuclei. J Neurosci 24:2102–2111. CrossRef Medline

Scarduzio M, Panichi R, Pettorossi VE, Grassi S (2012) The repetition timing of high frequency afferent stimulation drives the bidirectional plasticity at central synapses in the rat medial vestibular nuclei. Neuroscience 223:1–11. CrossRef Medline

Sekirnjak C, du Lac S (2006) Physiological and anatomical properties of mouse medial vestibular nucleus neurons projecting to the oculomotor nucleus. J Neurophysiol 95:3012–3023. CrossRef Medline

Sekirnjak C, Vissel B, Bollinger J, Faulstich M, du Lac S (2003) Purkinje cell synapses target physiologically unique brainstem neurons. J Neurosci 23:6392–6398. Medline

Serafin M, de Waele C, Khateb A, Vidal PP, Mühlethaler M (1991) Medial vestibular nucleus in the guinea-pig. I. Intrinsic membrane properties in brainstem slices. Exp Brain Res 84:417–425. Medline

Shin M, Moghadam SH, Sekirnjak C, Bagnall MW, Kolkman KE, Jacobs R, Faulstich M, du Lac S (2011) Multiple types of cerebellar target neurons and their circuitry in the vestibulo-ocular reflex. J Neurosci 31:10776–10786. CrossRef Medline

Shin SL, Zhao GQ, Raymond JL (2014) Signals and learning rules guiding oculomotor plasticity. J Neurosci 34:10635–10644. CrossRef Medline

Shutoh F, Ohki M, Kitazawa H, Itohara S, Nagao S (2006) Memory trace of motor learning shifts transsynaptically from cerebellar cortex to nuclei for consolidation. Neuroscience 139:767–777. CrossRef Medline

Stahl JS (2004) Using eye movements to assess brain function in mice. Vision Res 44:3401–3410. CrossRef Medline

Straka H, Lambert FM, Pfanzelt S, Beraneck M (2009) Vestibulo-ocular signal transformation in frequency-tuned channels. Ann N Y Acad Sci 1164:37-44. CrossRef Medline

Straka H, Vibert N, Vidal PP, Moore LE, Dutia MB (2005) Intrinsic membrane properties of vertebrate vestibular neurons: function, development and plasticity. Prog Neurobiol 76:349–392. CrossRef Medline

Takazawa T, Saito Y, Tsuzuki K, Ozawa S (2004) Membrane and firing properties of glutamatergic and GABAergic neurons in the rat medial vestibular nucleus. J Neurophysiol 92:3106–3120. CrossRef Medline

van Alphen B, Winkelman BH, Frens MA (2010) Three-dimensional optokinetic eye movements in the C57BL/6J mouse. Invest Ophthalmol Vis Sci 51:623–630. CrossRef Medline

Vibert N, Beraneck M, Bantikyan A, Vidal PP (2000) Vestibular compensation modifies the sensitivity of vestibular neurones to inhibitory amino acids. Neuroreport 11:1921–1927. Medline

Wulff P, Schonewille M, Renzi M, Viltono L, Sassoè-Pognetto M, Badura A, Gao Z, Hoebeek FE, van Dorp S, Wisden W, Farrant M, De Zeeuw CI (2009) Synaptic inhibition of Purkinje cells mediates consolidation of vestibulo-cerebellar motor learning. Nat Neurosci 12:1042–1049. CrossRef Medline

Yamazaki T, Nagao S, Lennon W, Tanaka S (2015) Modeling memory consolidation during posttraining periods in cerebellovestibular learning. Proc Natl Acad Sci U S A 112:3541–3546. CrossRef Medline

Zheng N, Raman IM (2010) Synaptic inhibition, excitation, and plasticity in neurons of the cerebellar nuclei. Cerebellum 9:56–66. CrossRef Medline

Article 2. Long-term Sensory Conflict in Freely Behaving Mice

My team developed a novel and unique long-term sensory conflict protocol for freely behaving mice. The motivation behind this protocol resided in enabling uninterrupted learning of gaze stabilizing reflexes product of naturally generated head movements. Mice are implanted with a headpost, in a quick and straight-forward surgery, where a helmet-like device is fixed posteriorly onto it. They're able to go about their life as they would otherwise since the device unobstructedly allows their daily routines (eating, drinking or grooming). After 2 weeks the device is removed and videoculography sessions are performed to analyze the change in the response of their reflexes.

The first publication that used this protocol (presented above, Article 1 (Carcaud et al., 2017)) was used to study the effects of this sensory-conflict in the VOR, right after the removal of the device. This study raised many inter-related questions regarding the reversal of the reflexes as well as the visual input, that were answered in the follow-up paper (Article 3, França de Barros *et tal*., submitted). However, this protocol has also been used to study its protective effect against motion sickness when mice were exposed to a provocative stimulus (Idoux et al., 2018). Therefore, protocols like this could pave the way for the development of anti-motion sickness treatments. The variety of studies for which this protocol has been useful for, proves its polyvalence. For example, by only changing the duration of the conflict (<14 days or >14days), a myriad of studies would be unlocked.

I had the opportunity of optimizing this protocol by tackling 3 issues regarding the headposts and devices: 1) production availability and cost; 2) material; 3) final weight of both components. The original version was hand-made which was slow and involved higher production costs per piece. To solve this, 3D printing was introduced to allow for an affordable mass production. Material-wise, the substitution of the originally used transparent plastic for a PLA plastic ensured that mice were restrained from visual inputs (apart from luminance). Last but not least, PLA plastic rendered lighter components thus providing the mouse a seamless experience.

The methodology article presented below states in detail the necessary materials and steps for the replication of this protocol by any other interested team. It includes how to assemble the adaptation device and the respective 3D printer files; the steps of the headpost implantation surgery; how to attach and remove the device from the animal as well as procedures for the videoculography sessions. Additionally, an illustrative video is

available online (https://www.jove.com/video/59135/long-term-sensory-conflict-in-freely-behaving-mice).

Video Article

Long-term Sensory Conflict in Freely Behaving Mice

Filipa França de Barros[1,2], Julie Carcaud[2], Mathieu Beraneck[1,2]

[1]Integrative Neuroscience and Cognition Center, UMR8002, CNRS

[2]Sorbonne Paris Cité, Université Paris Descartes

Correspondence to: Mathieu Beraneck at mathieu.beraneck@parisdescartes.fr

URL: https://www.jove.com/video/59135
DOI: doi:10.3791/59135

Keywords: Neuroscience, Issue 144, neuroscience, mouse, freely behaving mice, vestibular, VOR, adaptation, visual, sensory conflict, video-oculography, gaze stabilization, motor learning

Date Published: 2/20/2019

Citation: França de Barros, F., Carcaud, J., Beraneck, M. Long-term Sensory Conflict in Freely Behaving Mice. *J. Vis. Exp.* (144), e59135, doi:10.3791/59135 (2019).

Abstract

Long-term sensory conflict protocols are a valuable means of studying motor learning. The presented protocol produces a persistent sensory conflict for experiments aimed at studying long-term learning in mice. By permanently wearing a device fixed on their heads, mice are continuously exposed to a sensory mismatch between visual and vestibular inputs while freely moving in home cages. Therefore, this protocol readily enables the study of the visual system and multisensory interactions over an extended timeframe that would not be accessible otherwise. In addition to lowering the experimental costs of long-term sensory learning in naturally behaving mice, this approach accommodates the combination of *in vivo* and *in vitro* experiments. In the reported example, video-oculography is performed to quantify the vestibulo-ocular reflex (VOR) and optokinetic reflex (OKR) before and after learning. Mice exposed to this long-term sensory conflict between visual and vestibular inputs presented a strong VOR gain decrease but exhibited few OKR changes. Detailed steps of device assembly, animal care, and reflex measurements are hereby reported.

Video Link

The video component of this article can be found at https://www.jove.com/video/59135/

Introduction

Sensory conflicts, such as visual ones, are present in daily life, for instance, when one wears glasses or during an entire lifespan (developmental growth, changes in sensory acuity, etc.). Due to a well-described circuit anatomy, easily controlled sensory inputs, quantifiable motor outputs, and precise quantification methods[1], gaze stabilization reflexes have been used as models of motor learning in many species. In humans and monkeys, the vestibulo-ocular reflex (VOR) adaptation is studied through the use of prisms that the subject wears for several days[2,3,4,5]. Since the rodent model allows the combination of behavioral and cellular experiments, we developed a new method to create long-term sensory conflict in freely behaving mice with a helmet-like device. Inspired by the methodology used in humans and monkeys, the protocol generates a mismatch between the vestibular and visual inputs (i.e., visuo-vestibular mismatch, VVM) that leads to a decrease in VOR gain.

Classical protocols triggering a VOR gain-down adaptation in rodents consist of rotating the head-fixed animal on a turntable while rotating the visual field in phase. This paradigm creates a visuo-vestibular conflict, which makes the VOR counter-productive. Long-term adaptation protocols consist of an iteration of this procedure over the course of several consecutive days[6,7,8]. As a result, when a large group of animals needs to be tested, classical methodology requires a great amount of time. In addition, because the animal is head-fixed, the learning is mostly limited to a discrete frequency/velocity and consist of discontinuous trainings interrupted by intertrial intervals of variable duration[6]. Finally, classical protocols use passive learning, as the vestibular stimulation is not actively generated by the animal's voluntary movements, a situation that greatly shapes vestibular processing[9,10].

The aforementioned experimental constraints are surpassed by the presented innovative methodology. The required surgical approach is straightforward, and the materials used are readily available commercially. The sole part that relies on more expensive material is the quantification of the behavior; nonetheless, the fundamentals of the protocol may be used for any experiment, from *in vitro* investigations to other behavioral studies of learning. Overall, by generating a temporary visual impairment and a visuo-vestibular conflict over several days, this methodology can easily be transposed to any study concerned with sensory perturbation or motor learning.

Protocol

All animal procedures followed the Paris Descartes University animal regulations.

1. Device assembly

NOTE: The device used in this protocol is a helmet-like structure fixed on mice skulls by means of an implanted headpost.

1. Using a 3D printer and white opaque poly (lactic acid) (PLA) plastic, print using the design and specification files provided here (see **Table of Materials**) for both the device and headpost.
   NOTE: The dimensions of the device are shown in **Figure 1** and dimensions of the headpost shown in **Figure 2**.
2. A striped as well as sham device are to be tested (**Figure 2A**[11]). To obtain the striped model, using black nail polish, draw 3 mm large vertical stripes on the external surface of the device. The sham condition does not require any modification to the printed device.

2. Headpost implantation surgery

All the materials used in this protocol are detailed in the materials list in the supplementary information. Steps 2.7-2.9 use the biomaterials provided in the implantation kit (see **Table of Materials**). Ensure the use of sterile instruments and arrange surgery and recovery in different zones. Once mastered, the implantation procedure lasts about 30 min.

1. For analgesia, 30 min before the beginning of the surgery, subcutaneously inject buprenorphine (0.05 mg/kg) and put back the animal in its home cage.
   NOTE: Buprenorphine's analgesic effects last approximately 12 h, long after the end of the procedure. In our experience, mice do not show any signs of distress related to this intervention but a subsequent dose of 0.05mg/kg buprenorphine is recommended 24h after the surgery.
2. Anesthetize the animal in a chamber with 2.5%-3% isoflurane gas. Wait 3 min and check if the mouse is properly anesthetized by observing respiration and lack of movement inside the chamber. Pass the mouse to a nose cone on a surgical table with a heating pad and, by interdigital pinching, verify that there is no withdrawal reflex and lower the isoflurane to 1.5%.
3. Shave the head of the mouse using an electric razor. To obtain a sterile environment, rub the shaved area with iodine solution and after with 70% alcohol. Repeat this procedure two more times.
4. Inject lidocaine hydrochloride (2%, 2 mg/kg) under the skin of the head for local anesthesia and wait 5 min for the effects to begin. To avoid eye damage due to dryness, cover the mouse's eyes with topical ophthalmic vet ointment.
5. With a pair of blunt forceps, grab the skin at the back of the head, and with a pair of blunt scissors (or scalpel), make a longitudinal incision of about 1.5 cm to expose the skull.
6. With the help of a scalpel, scratch the periosteum. Be careful not to scratch too hard, as the fixation of the headpost can be compromised if the skull starts to bleed slightly.
7. Apply a drop of the green activator on the middle of the skull. This will improve the fixation of the cement by increasing bone permeability.
8. Prepare the cement: mix one spoon (provided in the implantation kit) of polymer with five drops of monomer and one drop of catalyzer. With the help of a brush, apply a generous amount of the cement mix between the lambda and bregma skull landmarks;
9. Quickly place the headpost on the cement with a swiping motion going from lambda to bregma. After the headpost has been placed, reapply more cement around the inferior part to ensure that the headpost properly sticks to the skull. To guarantee proper fixation, make sure the cement is applied abundantly and that it dries before continuing to the next step.
   NOTE: With this fixation procedure, the headpost will not come off and allow for long-term, repeated tests; in our hands, headpost removal is <10%.
10. Prepare the resin mix by applying a powder-to-liquid ratio that enables a smooth consistency of the mixture. Apply the resin where the cement was applied as well as around the headpost in order to protect its surface.
11. Wait 3 min for the resin to dry and close the skin at the back of the ears with monofilament suture. With a cotton swab, apply diluted (10%-20%) iodine solution to the operated area.
    NOTE: Make sure the skin does not get stuck to the resin.
12. Turn off the anesthesia and place the animal under a red warm light to avoid hypothermia. Place moistened food and hydrogel or another water source based in gel in the cage's floor. Do not leave the mouse unattended until it regains consciousness. As soon as the animal fully recovers from the procedure (usually, 30 min to 1 h after), place it in a cage with groups of three or four to stimulate social interactions.

3. Device fixation

1. 48 h following the surgery, secure the custom-built head device onto the headpost.
   1. Using a pair of 1.2 mm screws and a screwdriver (1.3 mm hex), align the holes in the striped device with the holes in the headpost, place the screws and secure them. To fix the sham condition, turn the device upside down and, with the back part (**Figure 1A**) of the device facing the rostral direction, align the holes in the device with the holes in the headpost.
      NOTE: It is recommended that this step be done by two operators, one holding the mouse with a one-handed mouse restraint, while the other securing the device to the headpost. If the fixation is done by a single operator, the device can be placed while the mouse is under gas anesthesia.
   2. Check that the device is well-secured and cannot be removed by the animal and that the device does not apply pressure directly on the mouse's nose, which could potentially cause pain, difficulty to breath, or skin injury.
      NOTE: It is also important to ensure the device is symmetrically inserted on the mouse face, so that eyes are completely covered by the head device. Check that the animal does not show any signs of abnormal pain or distress.
2. Leave the device on the mouse for 14 days.

4. Animal care and surveillance

1. Once back in their cages, mice will exhibit certain abnormalities in behavior. At first, the animal may stay prostrated and try to remove the device using its forepaws, but this should stop after the first hour. During the next following hours, the animal will usually display difficulties

orienting itself inside the cage and reaching for food and water. Therefore, during the 48 h following implantation, monitor the mice and provide easy access to water and food, by placing both directly on the cage floor, for example.
2. Keep track of mice's weights during the duration of the protocol. Weigh the mice right after implantation and again every 24 h. Special attention should be given to animals wearing the striped device, as they normally experience body weight loss (1-2 g) during the first 48 h, but start gaining weight again at a normal pace following that initial period (see **Figure 2B**[11]).
3. After 2 days, mice are expected to return to their regular faculties. Depending on the system used in animal facilities, the device might be preventing access to the food and water. Ensure the animal is at ease while eating and drinking or adapt the dispensing system accordingly.
NOTE: The range of head movements produced by the animals after a few days with the device on is not modified by the device (see **Figure 2**[11]) (i.e., the range of head movements produced remains similar to natural head movements).
4. To further ensure mice's well-being, ensure daily surveillance and apply the qualitative scale (**Table 1**) of well-being throughout the duration of the protocol.
5. Remove a mouse from the ongoing protocol if one or more of the following criteria apply:
    1. Mice that have a total score higher than 4 points on the aforementioned qualitative scale must immediately be excluded from the experiment (see **Table 1**). Regardless of the score, if the mouse does not regain its initial weight after 6 days, the procedure must be stopped.
    2. The device is not correctly fixed to the headpost if, for instance, the headpost shakes when touched or a part starts to come off. This causes the headpost to come off the mouse's head and consequently interrupts the learning, which explains why daily surveillances are necessary.
    3. When a mouse has its headpost ripped off during any part of the protocol. Due to the skull bleeding associated to this detachment, the reimplantation surgery has a low success rate and is not worth attempting.

5. Removal of the device

1. After the learning period (in this protocol 14 days), remove the device following the same instructions as for its fixation (section 3). As soon as the device is removed, test the mice with experiments such as video-oculography tests, or, for instance, with *in vitro* electrophysiology as described previously[11].
NOTE: As soon as the device is taken off, mice are exposed back to the standard, visually unobstructed environment. Therefore, perform experiments that aim to test the learning effects of this device directly after its removal.

6. Video-oculography sessions

NOTE: Video-oculography experiments are performed to record the generated eye movements while the animal is being rotated in the dark (vestibulo-ocular reflex, VOR) or by rotating the animal's surroundings while the animal is still (optokinetic reflex, OKR). Each mouse was tested for both these reflexes before and after the adaptation protocol. For more details about the video-oculography set-up, see previously published reports[12,13]. In order to habituate the mice to the restrained recording conditions, the day before the beginning of the recording, place the animal on the tube at the center of the turntable for 10minutes without performing any test.

1. Secure the mouse on the turntable by head-fixing it with the help of screws inserted into the headpost. Place a screen dome surrounding the animal and turn off all the lights in the room except for the optokinetic projector.
NOTE: Video-oculography recordings require the animal to be still and with its eyes open. Interrupt the recording session and put the animal back on its cage in case the mouse does not voluntarily keep its eyes open, or if the appearance of the eye deteriorates during the recording session. Another attempt can be made following a resting period of at least 12h.
2. Start the OKR full-field stimulation (white dot pattern projection) and record at several different velocities in both clockwise and counter clockwise directions. As soon as the recordings are over, remove the dome.
3. To be able to record the VOR in pitch dark, apply a drop of 2% pilocarpine to the eyes[14]. Wait at least 5 min for it to act and gently remove it with a cotton swab. The pilocarpine will keep the pupil constricted with a constant size throughout the measurements, allowing proper quantification of movements in the dark.
4. Turn off all the lights in the room and add a box on top of the turntable to keep the animal in pitch dark. Start the horizontal VOR using sinusoidal angular rotations around a vertical axis with different frequencies and/or different velocities.
5. Once the recording session is finished, return the mouse to a cage properly illuminated with an infrared lamp. The heat will prevent hypothermia caused by the secondary vasodilator effects of pilocarpine on the body of the mouse.
NOTE: Due to the animal being restrained, recording sessions can't last more than 90 min. When additional test sessions are needed, let the animal rest for 24h between sessions.

Representative Results

The following figures illustrate the results obtained with mice that underwent the 2 week adaptation protocol wearing either a striped or sham device. **Figure 3** shows an example of raw traces seen during recording sessions. As shown by comparing the traces, the VOR response decreases after the VVM protocol (**Figure 3A**, before vs. after striped). The VOR of sham mice remained unaltered after the adaptation (**Figure 3A**, before vs. after sham). The OKR of mice wearing the striped device (**Figure 3B**) is comparable to the period prior to the VVM protocol and to sham mice. **Figure 4** shows a quantification example of the mean VOR gains at a fixed frequency of 0.5 Hz and at 40 degrees per second, before and after the VVM protocol, for both striped and sham devices. There is a strong gain decrease after mice wore the striped device, while the sham mice did not have significant gain changes. Effects of VOR decrease tested at different velocities/frequencies have been reported by Carcaud et al.[11] and Idoux et al.[15].

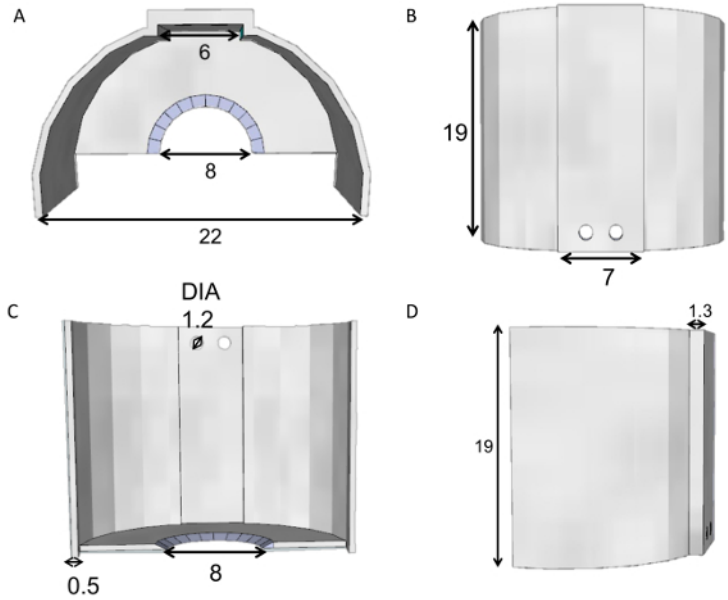

Figure 1: Head device depicted with dimensions, in millimeters. Views: (**A**) back, (**B**) side, (**C**) bottom, and (**D**) aerial. Please click here to view a larger version of this figure.

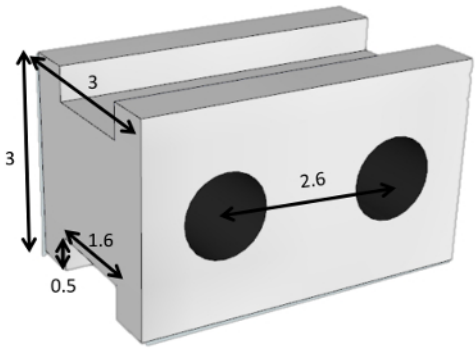

Figure 2: Headpost depicted with dimensions, in millimeters. Fixed in the implantation surgery, this light (0.2 g) poly (lactic acid) plastic headpost allows the locking of the adaptation device to the mouse and head-fixing of the animal on the turntable during the video-oculography sessions. Please click here to view a larger version of this figure.

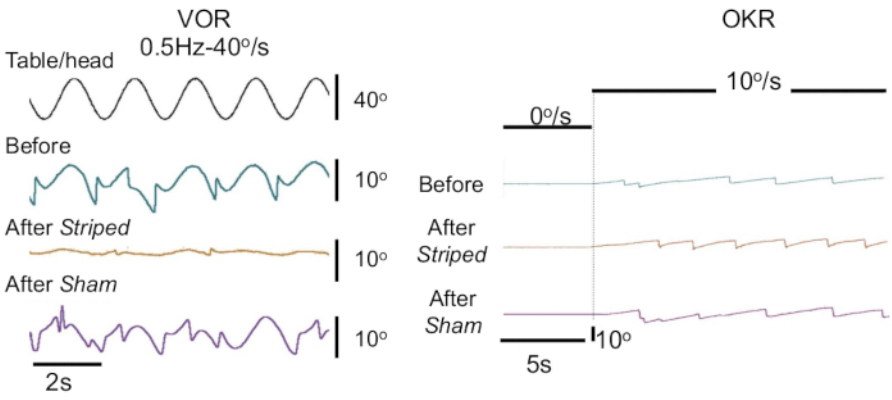

Figure 3: Example raw traces of eye movements during VOR and OKR stimulations. (**A, left**) Left: VOR performed at 0.5 Hz at 40 °/s and (**B, right**) optokinetic stimulation at a constant velocity of 10 °/s (black line), in a clockwise direction, before (green lines) and after (yellow) wearing the striped or sham (purple) device. Please click here to view a larger version of this figure.

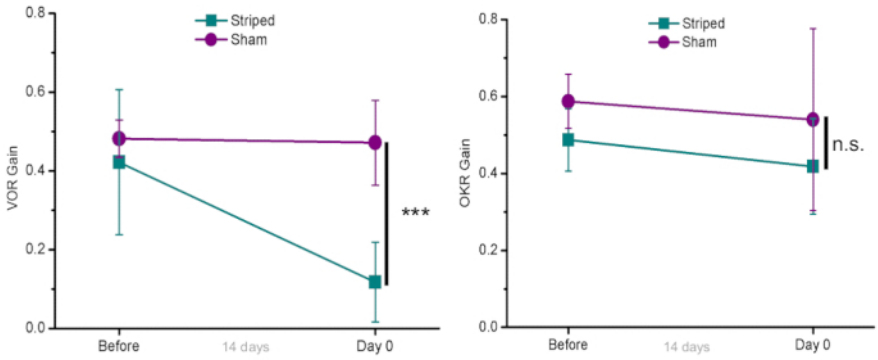

Figure 4: Example mean VOR and OKR gain values after adaptation to either striped or sham device. Gains were plotted according to time (days) for the striped (n = 10) and sham (n = 6) devices at stimulations of 40°/s and 0.5 Hz for the VOR (left), and 10 °/s clockwise direction for the OKR (right). On the timescale, "before" day represents the day immediately prior to the adaptation and "day 0" represents the day when the device is removed. Error bars represent the standard deviation, ***p < 0.001, not significant. Please click here to view a larger version of this figure.

Points	Body weight alterations	Physical appearance	Behavior
0	none or weight gain	standard	no signs of distress and normal locomotion
1	weight loss <10%	no body grooming	impaired locomotion or cage orientation
2	weight loss between 10%-20%	dehydration	--
3	weight loss >20%	wounds	nervous ticks (e.g. scratching, biting)

Table 1: Qualitative scale for the well-being assessment. Listed are the qualitative parameters that must be assessed during the duration of the protocol. The sum weight alterations, physical appearance, and behavior scores should not be greater than four points.

Supplemental File 1. Device.stl. Please click here to download this file.

Supplemental File 2. Headpost.stl. Please click here to download this file.

Discussion

The long-term sensory perturbation described here consists of a visuo-vestibular mismatch produced in freely-behaving mice. To implant the device that mice wear for 14 days, a simple and short surgery using a commercially available surgical kit is performed. Mice recover in less than 1 h from this headpost implantation procedure and show no associated signs of distress from it. Subsequently, in the given example of application of this protocol, VOR and OKR are measured using the video-oculography technique. Nonetheless, this device-induced long-term learning protocol could be used in a variety of experiments such as *in vitro* electrophysiology[1], neuronal imaging, and various behavioral assays. The rationale behind the development of this technique was inspired by the prism-based methodology used in humans and monkeys. This technique, however, differs because it impairs rather than modifies vision. Thus, it constitutes (in its current form) an extreme case of visuo-vestibular mismatch. The authors believe that the provided technical information may be useful for designing a prism-like version of the device or further developing specific feature-restricting devices[16].

Made of a light (0.9 g) poly (lactic acid) plastic, the head device was designed to fit the head of a young adult mouse, allowing protection of the snout and leaving enough space laterally to let the animal groom. The front part of this device exposes the end of the snout to permit feeding and grooming behaviors. The device is slightly opaque, so that the animal is deprived of precise vision of the surrounding but still receives luminance stimulation. The striped and sham implantations are tested to ensure that the measured effects are due primarily to the visuo-vestibular mismatch caused by the high-contrast visual signal during self-generated movements of the striped device and not by proprioceptive modification (i.e, the weight of the device applied in the mouse´s head and neck).

Experimentally, mice that wore the striped device showed a significant VOR gain decrease of 50% after the learning period; still, there can be an inter-individual variability for absolute gain values. Sham mice showed no significant VOR gain alterations, thus demonstrating that the VOR reduction is caused by the sensory conflict and not by motor impairment. Furthermore, young mice (<P26) showed VOR and OKR gain values lower than older animals[17]. For that reason, animal age has to be taken into account while planning the experiment. Finally, the aforementioned mice exclusion criteria (section 4.5) are a crucial step that should be followed to ensure well-being as well as establish reliable results.

One of the advantages of this protocol is the time that it saves experimenters during the learning period, compared to other types of VOR/OKR adaptation protocols. So far, VOR adaptation in mice has been studied by head-fixing and training the animal on a rotating turntable[6,8,18,19], which is time-consuming, especially when a lot of animals must be trained. The presented protocol allows the training of several animals at once and saves time. In addition, in these classical experiments the trainings are typically limited to 1 h per day, leaving long periods of putative unlearning that cause adaptation to be an iterated alternation of learning/unlearning with different dynamics[20]. Here, the head-fixation of the device allows for uninterrupted learning. Another advantage is that since the learning period is generated in a freely behaving head-free situation, mice are

able to learn through a range of natural head movements that are actively generated. In the classical protocols, the animal is head-fixed while being passively rotated on the turntable so that the learning occurs at a determined stimulation (one frequency, one velocity)[21] that does not reflect the natural range of head movements. It is important to note that the vestibular system encodes movements differently when they are actively generated by the subject or when externally applied[10]; thus, the cellular mechanisms triggered in both situations may also differ.

Overall, the described methodology is suitable for combined *in vivo/in vitro* studies on long-term sensory adaptations occurring after a visual conflict and/or visuo-vestibular mismatch in freely behaving mice. Sensory conflicts are a recognized cause of motion sickness, which is a field that has recently attracted use of mice[22,23]. It was recently demonstrated that the gain adaptation caused by the use of this device offers protection against motion sickness when mice are exposed to a provocative stimulus[15]. Hence, this protocol could be used to identify the cellular mechanisms underlying adaptation to a sensory conflict as well as to develop anti-motion sickness treatments.

Disclosures

The authors declare no conflicts of interest.

Acknowledgments

We thank Patrice Jegouzo for the head devices and headpost development and production. We also thank P. Calvo, A. Mialot, and E. Idoux for their help in the development of previous versions of the device and VVM protocol.

This work was funded by the Centre National des Etudes Spatiales, the CNRS, and the Université Paris Descartes. J. C. and M. B. receive support from the French ANR-13-CESA-0005-02. F. F. B. and M. B. receive support from the French ANR-15-CE32-0007.

References

1. Blazquez, P. M., Hirata, Y., Highstein, S. M. The vestibulo-ocular reflex as a model system for motor learning: what is the role of the cerebellum? *Cerebellum.* **3** (3), 188-192 (2004).
2. Berthoz, A., Jones, G. M., Begue, A. E. Differential visual adaptation of vertical canal-dependent vestibulo-ocular reflexes. *Experimental Brain Research.* **44** (1), 19-26 (1981).
3. Melvill Jones, G., Guitton, D., Berthoz, A. Changing patterns of eye-head coordination during 6 h of optically reversed vision. *Experimental Brain Research.* **69** (3), 531-544 (1988).
4. Anzai, M., Kitazawa, H., Nagao, S. Effects of reversible pharmacological shutdown of cerebellar flocculus on the memory of long-term horizontal vestibulo-ocular reflex adaptation in monkeys. *Neuroscience Research.* **68** (3), 191-198 (2010).
5. Nagao, S., Honda, T., Yamazaki, T. Transfer of memory trace of cerebellum-dependent motor learning in human prism adaptation: a model study. *Neural Networks.* **47** 72-80 (2013).
6. Boyden, E. S., Raymond, J. L. Active reversal of motor memories reveals rules governing memory encoding. *Neuron.* **39** (6), 1031-1042 (2003).
7. Raymond, J. L., Lisberger, S. G. Behavioral analysis of signals that guide learned changes in the amplitude and dynamics of the vestibulo-ocular reflex. *Journal of Neuroscience.* **16** (23), 7791-7802 (1996).
8. Rinaldi, A. *et al.* HCN1 channels in cerebellar Purkinje cells promote late stages of learning and constrain synaptic inhibition. *Journal of Physiology.* **591** (22), 5691-5709 (2013).
9. Roy, J. E., Cullen, K. E. Dissociating self-generated from passively applied head motion: neural mechanisms in the vestibular nuclei. *Journal of Neuroscience.* **24** (9), 2102-2111 (2004).
10. Cullen, K. E. The vestibular system: multimodal integration and encoding of self-motion for motor control. *Trends in Neurosciences.* **35** (3), 185-196 (2012).
11. Carcaud, J. *et al.* Long-Lasting Visuo-Vestibular Mismatch in Freely-Behaving Mice Reduces the Vestibulo-Ocular Reflex and Leads to Neural Changes in the Direct Vestibular Pathway. *eNeuro.* **4** (1), (2017).
12. Stahl, J. S. Using eye movements to assess brain function in mice. *Vision Research.* **44** (28), 3401-3410 (2004).
13. de Jeu, M., De Zeeuw, C. I. Video-oculography in mice. *Journal of Visualized Experiments.* (65), e3971 (2012).
14. van Alphen, B., Winkelman, B. H., Frens, M. A. Three-dimensional optokinetic eye movements in the C57BL/6J mouse. *Investigative Ophthalmology and Visual Science.* **51** (1), 623-630 (2010).
15. Idoux, E., Tagliabue, M., Beraneck, M. No Gain No Pain: Relations Between Vestibulo-Ocular Reflexes and Motion Sickness in Mice. *Frontiers in Neurology.* **9** (918), (2018).
16. Yoshida, T., Ozawa, K., Tanaka, S. Sensitivity profile for orientation selectivity in the visual cortex of goggle-reared mice. *PloS One.* **7** (7), e40630 (2012).
17. Faulstich, B. M., Onori, K. A., du Lac, S. Comparison of plasticity and development of mouse optokinetic and vestibulo-ocular reflexes suggests differential gain control mechanisms. *Vision Research.* **44** (28), 3419-3427 (2004).
18. Schonewille, M. *et al.* Purkinje cell-specific knockout of the protein phosphatase PP2B impairs potentiation and cerebellar motor learning. *Neuron.* **67** (4), 618-628 (2010).
19. Kimpo, R. R., Rinaldi, J. M., Kim, C. K., Payne, H. L., Raymond, J. L. Gating of neural error signals during motor learning. *eLife.* **3,** e02076 (2014).
20. Kimpo, R. R., Boyden, E. S., Katoh, A., Ke, M. C., Raymond, J. L. Distinct patterns of stimulus generalization of increases and decreases in VOR gain. *Journal of Neurophysiology.* **94** (5), 3092-3100 (2005).
21. Hubner, P. P., Khan, S. I., Migliaccio, A. A. Velocity-selective adaptation of the horizontal and cross-axis vestibulo-ocular reflex in the mouse. *Experimental Brain Research.* **232** (10), 3035-3046 (2014).
22. Wang, J. *et al.* Storage of passive motion pattern in hippocampal CA1 region depends on CaMKII/CREB signaling pathway in a motion sickness rodent model. *Scientific Reports.* **7,** 43385 (2017).

23. Wang, Z. B. *et al.* Low level of swiprosin-1/EFhd2 in vestibular nuclei of spontaneously hypersensitive motion sickness mice. *Scientific Reports.* **7,** 40986 (2017).

Article 3. Long-term visuo-vestibular mismatch in freely behaving mice differentially affects gaze stabilizing reflexes

The drive behind this project was to answer some of the questions that Article 1 opened through the use of the novel VVM device (Article 2).

The previous study mainly focused on only one of the gaze stabilizing reflexes, VOR. In fact, OKR was quantified in that paper but this test was used as a means to evaluate if the learned changes with the VVM resided on the flocculi. There, only one type of stimulation was used (7.5º/s). However, when performing the tests, we noticed that OKR responses were sometimes qualitatively less robust than before the VVM. This intrigued us to further research about the consequences of the VVM protocol on the OKR. When we carried out new tests, we found that the adaptation protocol also impacted the OKR responses by a 30% decrease in its gain. Therefore, OKR was also included in this study.

The gaze stabilization tests ran on the previous study were performed on the day of the removal of the device. Thus, in this study we aimed at understanding how strong the persistence of the learned changes in these reflexes was. To do so, we tested the VOR and OKR at 1, 2, and 6 days after the removal of the device and compared their responses. We found that VOR changes persist for at least 2 days, while OKR changes persist no more than 1 day.

Since mice are freely behaving on their cages, motor learning is evoked for the range of head/body movements naturally performed. Therefore, we wanted to know if the adaptation protocol affected more a certain range of frequencies and/or velocities and if these changes were more labile for some of them. Hence, using sinusoidally-modulated stimulations, the tests were performed at high and low ranges of frequencies and velocities. We found that, the decreases in VOR and OKR were frequency-selective with larger reductions for frequencies <0.5Hz. Constant-velocity OKR stimulation tests demonstrated that the persistent components of the OKR were not modified while the transient, initial responses were.

Classical adaptation protocols use exposure to high-contrast pattern during training sessions to evoke an error signal that will cause blur of the image on the retina and thus drive motor learning of gaze stabilizing reflexes. In this study we followed some of those classical lines by using a black and white striped device to induce adaptation. Still, we

wanted to study whether the error signal evoked by a helmet with no contrast would cause the same changes as one with high contrast. We did so by applying the exact same device that was originally used (Pattern, Article 2 Long-term Sensory Conflict in Freely Behaving Mice) but, in this group, no stripes were drawn onto its surface (No-pattern). Despite more robust in the Pattern device, reductions were largely comparable and recovered with similar time course. This result suggests that rather than an error signal (retinal slip), the absence of visual feedback would seem a most likely responsible of the reduction in OKR and VOR.

Globally, this study shows that a long-term visuo-vestibular mismatch, while affecting both gaze stabilizing reflexes, has a greater impact on the VOR. Moreover, we show evidence for a frequency-selective influence of visual signals in the tuning of mice gaze stabilizing reflexes.

The article presented below has been submitted to a peer-reviewed journal and is, on the date of this thesis' defense, under consideration.

Long term visuo-vestibular mismatch in freely behaving mice differentially affects gaze stabilizing reflexes

Authors

Filipa França de Barros[1*], Louise Schenberg[1], Michele Tagliabue[1], Mathieu Beraneck[1*]

Affiliations :

[1] Université de Paris, CNRS, Integrative Neuroscience and Cognition Center, F-75006 Paris, France.

Keywords: vestibulo ocular reflex; optokinetic reflex; long term; motor learning; visuo-vestibular mismatch; frequency dependence; gaze stabilization

***Corresponding authors:**

Filipa França de Barros: CNRS UMR 8002, Université de Paris, 45 rue des St-Pères, Paris 75270, France. E-mail: filipa.barros@parisdescartes.fr

Dr. M. Beraneck: CNRS UMR 8002, Université de Paris, 45 rue des St-Pères, Paris 75270, France. E-mail: mathieu.beraneck@parisdescartes.fr

Running title

Recovery of VOR and OKR following a visuo-vestibular mismatch

ABSTRACT

The vestibulo-ocular reflex (VOR) and the optokinetic reflex (OKR) work synergistically to stabilize gaze in response to head movements. We previously demonstrated that a 14-day visuo-vestibular mismatch (VVM) protocol applied in freely behaving mice decreased the VOR gain. Here, we first show that the OKR gain is also reduced, and report on the recovery dynamics of both VOR and OKR after the end of the VVM protocol. Using sinusoidally-modulated stimulations, the decreases in VOR and OKR were found to be frequency-selective with larger reductions for frequencies <0.5Hz. Constant-velocity OKR stimulation tests demonstrated that the persistent components of the OKR were not modified while the transient, initial responses were. To identify the signals driving VOR and OKR reductions, we compared the responses of mice exposed to a high-contrast and no-contrast VVM. Despite more robust in the high-contrast conditions, reductions were largely comparable and recovered with similar time course. A global analysis showed that, compared to the OKR, the alterations in the VOR were of significantly larger amplitude with significantly slower dynamic of recovery. Our findings are evidence for a frequency-selective influence of visual signals in the tuning of mice gaze stabilizing reflexes.

INTRODUCTION

During everyday life, natural head movements in mammals cover a large range of frequencies and velocities[1–3]. To avoid blurry vision, image displacements on the retina are minimized by compensatory eye movements. These eye-in-space movements are referred to as gaze stabilization eye movements, which result from the transformation of sensory signals into extraocular motor commands[4]. Vertebrates possess two gaze stabilizing reflexes -the optokinetic reflex (OKR) and the vestibulo-ocular reflex (VOR)- that act synergistically to compensate for environmental and self-movements. The OKR responses rely on direction-selective retinal ganglion cells that are efficient for relatively slow motions of the visual scene (± 3º/s in mice)[5,6]. Consequently, the OKR gain is inversely proportional to the velocity of the visual stimulus[7]. On the other hand, the vestibular acceleration-sensitive neurons responsible for VOR are more sensitive to mid-to-high range head motions[8]. In addition, the OKR can respond to constant-velocity visual motions while the vestibular system encodes only non-constant, transient head velocities[6]. The optokinetic and vestibulo-ocular reflexes are therefore functionally complementary, their combination enables efficient gaze stabilization and allows to discriminate self- from environmental movements in most naturally encountered situations.

The VOR works as an open-loop system[9,10]: it is completely functional in the dark, *i.e*, inner ear vestibular signals generate compensatory eye movements even in the absence of visual feedback. In rodents, the initial development of the VOR relies on the early maturation of the vestibular circuitry even before eye-opening (P12-14)[11–14]. Nevertheless, visual inputs are critical for the proper functioning of the vestibulo-ocular reflex of VOR development: its fine-tuning depends on the visual feedback that informs on the efficacy of the compensatory eye movements. In the absence of vision, such as in congenitally or adventitiously blind people, the VOR is impaired[15]. The gain of the vestibulo-ocular reflex improves after the opening of the eyes in mice, while the phase shifts toward smaller phase leads[9]. In addition, vision critically influences the time constant of the velocity storage[16], the development of vestibular nuclei neurons[17] and the acquisition of their plastic properties[14,18,19].

We recently reported a visuo-vestibular mismatch (VVM) protocol which consists in a high-contrast patterned device wore by the animal for 14 consecutive days while freely behaving in its cage [20]. Using this VVM, we demonstrated in adult mice that the long-term visual perturbation leads to neural modifications in the direct vestibulo-ocular pathway[21]. Specifically, VVM led to a drastic reduction of the VOR, associated with changes in the efficacy at the synapse between vestibular afferents and medial vestibular neurons as well as modifications of the intrinsic properties of a subpopulation of central vestibular neurons[21].

Nevertheless, our previous study let several questions unanswered. First, it remains unclear which neural signals (*e.g*. oculomotor error/retinal slip)[22–24] drive VVM plasticity. To answer to this question in the present study mice were tested either with a high- or no- contrast VVM device. If the retinal slip is among the signals driving plasticity, we expect different VOR gain reduction in the 2 conditions. Second, whether the changes in the VOR are paralleled with changes in the OKR remains elusive. To better understand the interplay between VOR and OKR, both reflexes were measured throughout the protocol. Lastly, few studies have explored the capacity of the VOR to recover following alteration in mice[25]. To determine how VOR and/or OKR recover after VVM, the gaze stabilizing reflexes were measured before the VVM protocol, right after its conclusion, and until recovery to pre-VVM levels.

RESULTS

Effect of the visuo-vestibular mismatch and recovery of the vestibulo-ocular reflex

To measure the effect of each device (Fig. 1a; see methods) on the VOR response, video-oculography was performed in darkness using sinusoidal turntable rotations (Fig. 1b). Figure 1c shows examples of the oculomotor response of mice of each of the three groups the day the device was removed during a 0.5Hz stimulation. A striking difference can be qualitatively observed between the amplitude of the eye movements of Sham mice compared to Pattern and No-Pattern mice, with smaller compensatory eye oscillation for the latter. Figure 1d quantitatively illustrates the evolution over time of the mean gain of the VOR for the three groups, which results in a statistically significant interaction between the effect of the tested *Day* and of the *VVM group* (repeated measures ANOVA, *Day x VVM group interaction effect:* $F_{8,108}=5.33$, $p<10^{-4}$). As expected, before the visuo-vestibular mismatch the gain of the reflex was the same for the three groups of mice, and the Sham group did not show significant modulations over the whole duration of the protocol. On the other hand, at day 0, Pattern and No-pattern groups showed a significant decrease of the VOR gain and both had significantly lower gains than Sham (Newman-Keuls post-hoc test: at day 0 Sham vs Pattern, $p<10^{-4}$; Sham vs No-pattern, $p<10^{-4}$). At day 1, the gain of both Pattern and No-pattern groups had significantly recovered with respect to day 0 (Newman-Keuls post-hoc test: day 0 vs day 1, No-pattern, p=0.0002; Pattern, p=0.0004), but still showed significant differences compared to Sham (Newman-Keuls post-hoc test: at day 1, Sham vs Pattern, $p<10^{-4}$; Sham vs No-pattern, p=0.019). From day 2 on, there was no significant difference between the VOR gain of the three *VVM groups*.

To determine whether the effect of the Pattern and No-pattern protocols on the VOR is modulated by the frequency of the stimulation, the VOR gain (Fig. 1e) and phase (Fig. 1f) are illustrated as bode plots for each test day. Frequency specific effects were revealed by the significant statistical interactions between the effects of the *Day*, *VVM group* and *stimulation Frequency*, on both the gain and the phase

of the VOR (repeated measures ANOVA, *Day x VVM group x stimulation Frequency interaction effect*, Gain: $F_{24,324}$=1.92, p=0.007; Phase: $F_{24,300}$=5.05, $p<10^{-5}$). More precisely, at day 0 the VOR gain of the Pattern and No-pattern groups dropped significantly compared to Sham (Fig. 1e) for all tested frequencies (Newman-Keuls post-hoc test, at day0 Sham vs Pattern at 0.2Hz, p=0.0002; at 0.5Hz, 1Hz and 2Hz, all $p<10^{-4}$; Sham vs No-Pattern at 0.2Hz, p=0.0005; 0.5Hz and 1Hz, $p<10^{-4}$; at 2Hz, p=0.007). On day 1 the VOR gain of the Pattern group remained significantly reduced (Newman-Keuls post-hoc test, at day1 Sham vs Pattern at 0.2Hz, p=0.0014; 0.5Hz, p=0.0003; 1Hz, p=0.002; 2Hz, p=0.0006) whilst for the No-pattern group only the lowest frequencies (0.2 and 0.5 Hz) remained significantly reduced (Newman-Keuls post-hoc test, at day1, Sham vs No-pattern at 0.2Hz, p=0.0177; at 0.5Hz, p=0.0026). On day 2 only the Pattern group VOR gain at 0.5Hz is still different from the Sham (Newman-Keuls post-hoc test, at day2 Sham vs Pattern at 0.5Hz, p=0.0049). At day 6 significant differences can no longer be detected between the three VVM groups. Regarding the phase, Figure 1f shows that the VVM had an effect only at day 0 and this effect is opposite for the low and high frequencies: greater phase lag at 0.2 Hz (Newman-Keuls post-hoc test, at day0: Sham vs No-pattern at 0.2Hz, $p<10^{-4}$; Sham vs Pattern at 0.2Hz, $p<10^{-4}$) and greater phase leads at 1 and 2 Hz (Newman-Keuls post-hoc test, at day0: Sham vs No-pattern and Sham vs Pattern at: 1Hz and 2Hz, all $p<10^{-4}$)
Overall, these results suggest that the VOR responses of the Pattern and No-pattern groups recovered a regular timing (phase) faster than an adequate amplitude of response (gain). Moreover, there were only limited differences in the gain reductions and recovery dynamics of the VOR responses between the Pattern and No-pattern groups. These results suggest that the high-contrast visual input of the Pattern device did not substantially influence the processes triggered by the visuo-vestibular mismatch.

Effect of the VVM and recovery during sinusoidal optokinetic stimulation

To investigate whether the visuo-vestibular mismatch affects the optokinetic reflex in the frequency domain, animals were first tested using sinusoidal rotations of a dotted pattern (Fig. 2a) at a fixed peak speed of 10°/s and at different frequencies in range 0.2-1Hz. In response to sinusoidal oscillations of the dotted pattern, all mice responded with slow phases that smoothly tracked the visual stimulation (Fig. 2b). On day 0, Pattern and No-pattern mice presented diminished amplitude of eye movements (compare traces on Fig. 2b). Figure 2c illustrates for all VVM groups the global tendency for OKR gain changes along the tested days (repeated measures ANOVA, *Day x VVM group,* $F_{6,69}$=2.2, p=0.053). On day 0, the Pattern and No-pattern groups had a significantly diminished OKR gain (Newman-Keuls post-hoc test, at day0 Sham vs Pattern p=0.0294; Sham vs No-pattern, p=0.0046). On day 1, both Pattern and No-pattern groups showed a significant OKR gain recovery (Newman-Keuls post-hoc test, day0 vs

day1: No-pattern, p=0.0001; Pattern, p=0.0002), resulting in no differences between the three groups from day 1 onwards.

To investigate if the alteration of the OKR response was dependent on the frequency tested, the gain (Fig. 2d) and phase (Fig. 2e) were plotted as a function of the stimulation frequency for each day. Frequency-specific effects were revealed by the significant statistical interactions between the effects of the *Day*, *VVM group* and *stimulation Frequency*, on both the gain and the phase of the OKR (repeated measures ANOVA, *Day x VVM group x stimulation Frequency interaction effect*, Gain: $F_{18,207}$=2.6288, p=0.0005; Phase: $F_{18,207}$=3.2987, $p<10^{-4}$). Figure 2d shows that the above-mentioned effect at day 0 is mainly due to a reduction of the OKR gain for stimulations at the lowest tested frequencies (0.2Hz and 0.33Hz) (Newman-Keuls post-hoc test, at day 0 Sham vs Pattern at 0.2Hz: p=0.006; Sham vs No-pattern at 0.2Hz: p=0.0015; at 0.33Hz: p=0.0146). On this day, a significant phase shift towards a greater phase lead was also observed across all stimulation *Frequencies* for both Pattern and No-pattern groups (Newman-Keuls post-hoc test, day0, Sham vs Pattern at all frequencies: $p<10^{-4}$; Sham vs No-pattern at 0.2Hz, 0.33 and 0.5Hz: $p<10^{-4}$; at 1Hz: p=0.0078). On day 1, for all frequencies the OKR gain of both Pattern and No-pattern groups was no longer different from the Sham group. However, the timing of the OKR responses was still affected on Pattern and No-pattern groups, with remaining significant differences between these groups and Sham at 0.2 and 0.5 Hz (Newman-Keuls post-hoc test, day1, Sham vs Pattern at 0.2Hz: p=0.0001; at 0.5Hz: p=0.0296; Sham vs No-pattern at 0.2Hz: p=0.0004; at 0.5Hz: p=0.0282;). At day 2, both gain and phase had completely recovered, and no further differences were found between the three *groups*.

In conclusion, sinusoidal stimulations at different frequencies showed that significant gain and phase changes occurred in the OKR pathway following the VVM protocols. However, the reduction of the OKR responses appeared to last no more than one day and to predominantly concern the responses to low stimulation frequencies.

Effect of the VVM in response to constant velocity optokinetic stimulation

To further investigate how the optokinetic response is affected by the visuo-vestibular mismatch protocol, we next tested the OKR using long-lasting (60s) full-field stimulations at constant velocities of 2.5, 5, 7.5 and 10°/s. Mice responded to the visual stimulations with nystagmus-like responses consisting in series of slow phases in the direction of the stimulus, interrupted by quick-phases that recenter the eye in its orbit. Figure 3a displays example raw traces at day 0 at a velocity of 7.5°/s and Temporo-Nasal direction for each group. Throughout each 60s-long stimulation, the slow phases evoked were characterized by their number, amplitude and duration (at day 0, see Supplementary Fig.

S1). For all groups, the number of slow phases significantly increased as a function of the stimulus velocity while their duration decreased (repeated measures ANOVA, *Velocity* effect, Number: $F_{3,90}=31.886$, $p<10^{-4}$; Duration: $F_{3,93}=26.846$, $p<10^{-4}$). No significant differences were found between the number and duration of slow phases between the three groups (repeated measures ANOVA, *VVM group* effect, Number: $F_{2,30}=1.3783$, p=0.27; Duration: $F_{2,31}=3.0007$, p=0.065). The amplitude of the slow phases also significantly increased with the stimulus velocity (repeated measures ANOVA, *Velocity* effect, Amplitude: $F_{3,93}=13.648$, $p<10^{-4}$). However, the amplitude of the slow phases was significantly different between Sham and Pattern groups (repeated measures ANOVA, *VVM group* effect, Amplitude: $F_{2.31}=5.4568$, p=0.0093; Newman-Keuls post-hoc test, day0, Sham vs Pattern p=0.0096).

The dynamics of the OKR response are illustrated on Figure 3b, which presents the individual traces recorded during stimulation at 7.5°/s at day-14, day0 and day1. As previously described in the mouse[26–28], before the VVM protocol (Day-14), the intensity of the optokinetic responses decreased over time during the 60 seconds duration of the optokinetic stimulation. This dynamic was quantified by comparing the mean gain of the first and last slow phases evoked during all the different stimulations (2.5-10°/s) tested (Fig. 3c). There was a significant interaction between the *VVM Groups*, *Day* and *Component* (repeated measures ANOVA, *Day x VVM group x Component interaction effect*, Gain: $F_{6,90}=4.6741$, p=0.0035). Before the VVM (day -14), the mean gain of the first slow phases was significantly higher than the mean gain of the last slow phases for all the tested groups (Fig. 3c, day-14, Newman-Keuls post-hoc test, Sham, p=0.0002; Pattern, p=0.0002; No-pattern, p=0.0013). At day 0, while this dynamic was unchanged in the Sham group, the response of Pattern and No-pattern groups showed rather different profiles. Specifically, the gain of the first slow phase was significantly reduced (day 0, Newman-Keuls post-hoc test; Sham vs Pattern, P=0.0002; Sham vs No-pattern, p=0.0008) while the gain of the last slow phase was not. At day 1, the mean gain of the first slow phases had mostly recovered for both Pattern and No-pattern groups (Newman-Keuls post-hoc test, day1, Sham vs Pattern, p=0.3802; Sham vs No-pattern, p=0.3399). However, the dynamic of their response was not yet back to normal (no significant decrease between first and last slow phase; Newman-Keuls post-hoc test, day1, First slow phase vs Last slow phase: Pattern, p=0.0754; No-pattern, p=0.0746). All these parameters had fully recovered on day 2.

Overall, the modifications of OKR responses observed during constant-velocity stimulation suggest that it was the transient, initial component of the OKR that was mostly affected by the visuo-vestibular mismatch, while the sustained, late component was not.

Comparison between VOR and OKR gain changes as a result of the VVM protocol

Results presented so far demonstrate that 2 weeks of visuo-vestibular mismatch led to a significant alteration of the vestibulo-ocular reflex (Fig. 1) which recovered in about 2 days, while alteration of optokinetic reflex recovered in about 1 day (Fig. 2). Overall, the general effects were similar between Pattern and No-pattern mice. In order to directly compare the dynamic and magnitude of the changes in VOR and OKR while taking into account the non-specific effects, for each stimulation modality and day, we subtracted the mean responses of the Sham group from those of the Pattern and No-pattern groups (ΔGain; Fig. 4). There was a significant interaction between the *Day*, and *Stimulation modality (*repeated measures ANOVA, *Day x Stimulation modality interaction effect*, $F_{3,117}$=23.579, $p<10^{-4}$*).* At day-14, ΔGain for both VOR and OKR were, as expected, not different from 0, and not significantly different from each other (Newman-Keuls post-hoc test, d-14: VOR vs OKR, p=0.1041). On day 0, day 1 and day 2, the ΔGain magnitude of VOR was significantly larger than the ΔGain for OKR at all tested days (Newman-Keuls post-hoc test, day0: VOR vs OKR p=0.0014; day1 and day2: VOR vs OKR, $p<10^{-4}$). The ΔGain of OKR was only significantly smaller than the initial d-14 value at day0 (Newman-Keuls post-hoc test, day-14 vs day0 for OKR: p=0.0001); the optokinetic responses were therefore no longer affected after the first day of recovery. On the other hand, the ΔGain of VOR was significantly different from day-14 at day 0 (Newman-Keuls post-hoc test, day-14 vs day0 for VOR, p=0.0001), day 1 (day-14 vs day1 for VOR, p=0.0001) as well as at day 2 (day-14 vs day2, p=0.0001). This shows that, globally, VOR responses of Pattern and No-pattern mice are still abnormally reduced at day 2. Overall, this comparative analysis demonstrates that alteration in the OKR and VOR pathways differ both in terms of amplitude and dynamic of recovery.

DISCUSSION

This study shows a concurrent decrease of VOR and OKR following 14 days of a visuo-vestibular mismatch protocol. This concomitant reduction of OKR and VOR efficacy differs from what was previously reported following short–term (<3 days) adaptation protocols in studies that also used mice as animal models[9,29]. These short-term VOR gain-down and gain-up adaptation protocols (1/2h learning, up to 1h follow-up) showed a moderate but significant increase in the OKR, in line with early reports in the rabbit[30]. It was suggested that, like during optokinetic learning, retinal slip might serve as a learning signal during short-term VOR adaptation[22,31] and lead to potentiation in the optokinetic pathway[9]. Here, we used 2 different devices: one whose surface was completely blank (No-pattern), that would not generate any retinal slip when the eyes move, and another one with a high-contrast (Pattern). Our results show that both devices led to a significant reduction in both OKR and VOR, and no major alterations could be specifically ascribed to one or the other. The Pattern group showed larger VOR gain reductions as well as a slightly longer recovery time, but these differences were not compelling. From these experiments, it is therefore not possible to conclude whether the presence of the Pattern effectively led to a stronger "retinal slip", which would represent an important error-signal driving the adaptation described in short-term protocols. Nonetheless, the fact that both devices showed essentially similar effects suggests that, in the present long-term VVM protocol, the absence of sensory feedback is the main determining factor driving the changes in the calibration of the VOR and OKR.

Since the early 80's, long-term visual impairment protocols have been used in mammals to study the interaction of the vestibular and visual systems for gaze stabilization. The species used in these experiments vary from humans[32] and non-human primates[33,34] to cats[35,36], rabbits [37,38], and more recently, mice[20,21]. The inspiration for our protocol lies in the long-term adaptation experiments conducted in primates, in which the use of telescopic spectacles changed the visuo-vestibular interactions during head-free movements [33,34]. Several features of our results resemble the ones on these preceding studies. First, following a fixed-field protocol (fixed images viewed through lenses, providing a field of view fixed with respect to the head), the VOR in dark was decreased by 60-70% in 3-4 days[33]. The amplitude of this decrease is comparable to the decrease of VOR reported here following the VVM. OKR was also found to decrease by up to 50%, depending on the OKR velocity tested [39]. Specifically, the OKR deficit was positively correlated with velocities and concerned the closed-loop, velocity storage-dependent, pathway, as well as the optokinetic after nystagmus (OKAN) (see below[39]). Notably, comparable results were obtained during experiments in which animals were dark-reared to understand the role of visual inputs in the development of VOR and/or OKR. In rabbits

that were dark-reared for 7 months[37], the gain of the VOR in dark decreased ~70% at low frequencies and ~50% at high frequencies. The OKR gain also decreased by ~30%. OKAN responses were not affected. After 24h in a normal light, both VOR and OKR increased and kept on improving for the next 3 months but remained permanently suboptimal[37]. In cats dark-reared until adulthood, the VOR in the dark was also found to be decreased by ~70%[35]. Again, the OKR was decreased by ~25% at low velocities, and even worsened as the velocity of the optokinetic stimulation increased. The velocity-storage dependent responses, including OKAN, were also markedly affected. It is noteworthy that, despite obvious visual and oculomotor differences, the abovementioned animal models confronted with protocols of long-term visual impairments, showed drastic reductions in VOR paralleled by a mild reduction of OKR efficacy. This observation would suggest that the basic mechanisms/circuitries involved are likely shared among mammals. Thus, the mouse model as well as VVM protocol can serve as valuable means to understand the signal-driven calibration of gaze stabilizing pathways.

While the VOR pathway constitute a 3-neuron direct reflex arc[21], several subcircuits contribute to different features of the optokinetic responses. Two distinct pathways related to different retinal ganglion cells appear, for instance, to manage the initial (transient) and late (sustained) phases of the OKR response[27]. In the following paragraph we discuss the results obtained using the transient sinusoidal and the constant-velocity lasting OKR tests, and their relations to VOR. In response to transient sinusoidal stimulation, we observed a frequency-selective decrease in the OKR responses. This decrease concerned the lowest frequencies tested (below 0.5Hz). These results mirror the frequency-selective decrease observed in the VOR: at day 0, the larger gain reduction is observed for the lower frequencies tested (0.2 and 0.5Hz). The VOR phase shift also differs between low (increased phase leads) and high (increased phase lags) frequencies. In the present freely behaving protocol, the visuo-vestibular mismatch mainly occurs in the range of natural head-movements. Previous studies have demonstrated that the mouse head movements produced during home-cage recordings or open-field active exploration are dominated by low frequencies[1,2,21]. The strongest effects observed on OKR and VOR at low frequencies could therefore relate to the statistics of the natural head-movements. Another explanation would be that the VVM mainly alters VOR/OKR in the range where visual information is the dominant sensory input signaling if eye movements are compensatory. Faulstich and colleagues[9] demonstrated that, in mice, OKR and VOR have a mutually complementary working range; the OKR accounts for most of the gaze stabilization at frequencies below 0.5Hz, while the VOR takes over above 0.5Hz (mouse[9], see also rabbit[30]). How the frequency-specific changes in OKR and VOR following VVM relates to the timing rules of plasticity in the flocculus[40,41] and to the inter-dependency of these 2 reflexes[42] should be the focus of future dedicated studies. Interestingly, other features of optokinetic response were revealed by the constant-velocity OKR tests. In particular, the

gain of the first slow phase measured after stimulus onset was smaller in Pattern and No-Pattern mice compared to Sham (Fig. 3c). As the stimulation continued, the Sham mice OKR response decreased steadily (as previously reported[26–28]) whereas, Pattern and No-Pattern mice exhibited a consistently low response (Fig. 3b) that did not show any additional decrease. A degradation of the transient pathway could explain both the difference between the Pattern and No-Pattern and Sham mice during the sinusoidal stimulation and the loss in the initial OKR response. In addition, a similar late OKR response for all mice groups suggests that the persistent pathway would be only marginally affected by the VVM protocol. Another mechanism involved in the response to a constant-velocity and lasting optokinetic stimulation is the velocity storage, which manifests in vertebrates as a build-up in the response during continued high velocity optokinetic stimulation and as a persistency in the response after stimulus offset[43,44]. However, in mice the velocity storage is considered "leaky"[45] and does not generate much after nystagmus response (OKAN)[28,45]. Because the velocity storage mechanism depends on vestibular brainstem circuitry[46–49], the difference in the OKR responses between Sham and Pattern and No-Pattern mice could relate to the decreased efficacy of the direct VOR pathway[42].

A key point in understanding the dynamic of plasticity of OKR and VOR networks, is the interaction between the cellular mechanisms located in the flocculi and the long-term consolidation of the motor learning in the brainstem[21,50–52]. Jang and colleagues[53] have recently demonstrated that the brainstem consolidation following a gain-up VOR training was dependent on the synergy of synaptic and intrinsic plasticity within Purkinje cells. In the case of an iterated VOR gain-up training, plastic brainstem modifications were reported as the combination of an increase in both the vestibular afferents-central vestibular neurons synapse as well as an increase in the excitability of central vestibular neurons. Notably, this result mirrors the results obtained by Carcaud and colleagues[21] which demonstrated that a VOR gain reduction was accompanied by a decrease of the efficacy of the synapse between the vestibular afferents and the central vestibular neurons, accompanied by a decrease in the excitability of a subpopulation of central vestibular neurons. Collectively, these studies demonstrate that VOR gain modifications depend on synaptic and intrinsic plastic changes in the brainstem.

Overall, the visuo-vestibular mismatch protocol performed in freely behaving mice led to a frequency-specific reduction of the gain of both VOR and OKR. The changes observed in the OKR were of lower intensity and recovered more rapidly than the changes in the VOR. Based on the recent findings on cellular mechanisms associated with learning in gaze stabilization networks, future experimental conducted on mouse and model studies will help to better understand the cellular mechanisms associated with OKR/VOR tuning and their interactions.

METHODS

Ethics

A total of 65 male C57/BL6J mice, age 6-10 weeks, was used for the described protocol. Animals were used in accordance with the European Communities Council Directive 2010/63/EU. All efforts were made to minimize suffering and reduce the number of animals included in the study. All procedures were approved by the ethical committee for animal research of the University of Paris (CEEA.34).

Headpost implantation surgery and animal care

Surgical procedures, postoperative care, device fixation and animal surveillance during the protocol were performed as described previously [20,21]. Briefly, mice anesthetized with isoflurane gas had their heads shaved with small clippers. Then, lidocaine hydrochloride (2%; 2mg/Kg) was injected locally before a longitudinal incision of 1.5 cm was made to expose the skull. Just anterior to the lambda landmark, a small custom-built headpost (3x3x5mm; poly lactic acid) was cemented (C&B Metabond; Parkell Inc., Edgewood, NY) and laterally covered with resin (Heraeus) for protection. Animals were fully recovered 30 min after the end of the surgery, yet buprenorphine (0.05mg/kg) was provided for postoperative analgesia and they were closely monitored for the following 48 hours.

Long-term visuo-vestibular mismatch protocol

The custom-built devices were secured on top of the mouse headpost for 14 days. The device consisted of a 0,9g helmet-like structure that completely covered the mouse's head. The front of the device was adapted to the animal's anatomy so that the nose was not covered, and its width allowed for grooming and barbering behaviors. To preserve light-dependent physiology and nychthemeral rhythm, the device was made of slightly opaque PLA so that the animal could no longer see the surrounding, but still received luminance stimulation. Design and 3D printer specifications of this device were previously detailed[20]. VOR and OKR responses were recorded before the beginning of the VVM protocol. Then, mice were designated to 1 of the 3 visuo-vestibular mismatch devices (Fig. 1a): Sham (n=14), 'No-pattern' (n=24) or 'Pattern' (n=27). 'No-pattern' devices were blank (white PLA color) while 'Pattern' ones had black 3 mm stripes drawn onto their surfaces. These stripes were previously used to create a high-contrast fixed visual signal during self-generated head movements[21]. Sham mice had the device fixed upside-down so that they were exposed to the same procedure except for the visuo-vestibular mismatch[21]. After securing the device into the headpost with a pair of screws, it was ensured that the nose of the mouse was aligned with the center of the device's snout aperture and that no pressure was being directly applied to it.

Animals were housed in groups of 5 made with at least 1 mouse of each condition. Moistened food and hydrogel were placed on the cage's floor to facilitate feeding on the first two days after the fixation

of the device. Mice were left with the implanted devices for 14 days. To ensure their well-being, mice were daily weighted and surveilled. After this two-week period, the device was removed and video-oculography was performed at different timepoints.

Video-oculography recording sessions

Eye movements were recorded using non-invasive video-oculography (Stahl et al. 2000). Eye and head position signals were sampled at 1 kHz, digitally recorded (CED power1401 MkII) with Spike 2 software and analyzed off-line in Matlab (Matlab, The MathWorks, Natick, MA, USA; RRID: SCR:001622) programming environment. The experimental set-up (see Figure 1b and 2a) and methods of data acquisition are akin to those described in[21,54]. In sum, mice were put in a custom-built Plexiglas tube and head-fixed at ~30° nose-down position to align the horizontal canals to the yaw plane[55,56]. This restraint assembly was fixed on a rotating platform on top of an extended rig with a servo-controlled motor. Recording sessions were performed in a temperature-controlled room (21°C) and lasted up to 45 min. To study the effects of the device on the gaze stabilizing reflexes, mice underwent a recording session before (*d-14*) having the device implanted, immediately after its removal (*day0*), 1 (*day1*), 2 (*day2*) and 6 (*day6*) days afterwards. To minimize the exposure to the visual scene, the recording session on *day 0* began immediately after the device was removed in a room with low luminance. Mice were then left in standard lighting and housing conditions.

Vestibulo-ocular reflex tests and analysis

VOR tests were performed with all sources of light turned off except for computer screens. The turntable was surrounded by a black box to isolate the animal from any remaining light, creating a final luminance inside the box of <0.02 lux (Luxmeter Lux-1337 Iso-tech). To prevent excessive pupil dilatation, pilocarpine 2% was instilled into the eye.

To evaluate the angular vestibulo-ocular reflex, different vestibular stimulations were used. Horizontal vestibulo-ocular reflex (VOR) recordings consisted in sinusoidal angular rotations around the vertical axis at 0.2, 0.5, 1 and 2Hz at a peak velocity of 30˚/s. The angular amplitude of the table movement was adjusted accordingly. At least 10 cycles were analyzed *per* frequency/velocity. The compensatory eye movement were studied by calculating their gain and phase in each condition. Briefly, the gain is the ratio between the response (eye) velocity and stimulus (head) velocity. The phase is the temporal shift between the eye and table rotations, expressed in degrees of the sinusoidal cycle. Detailed VOR gain and phase calculation are reported in[21].

Optokinetic reflex tests and analysis

To record the OKR, head-fixed mice were surrounded by a 40cm wide dome (see figure 2a) and all sources of light were turned off except for the optokinetic stimulus projector. Optokinetic stimulations

consisted in 25000 white dots (max width 0.075°) randomly distributed on a black background. The light intensity inside the dome during the test was around 185 lux.

Two types of visual stimuli were tested: *sinusoidal* and *constant velocity* stimulations. The *sinusoidal* one allowed a direct comparison with the VOR responses in the frequency domain[9], whilst the classical *constant velocity* stimulation allowed better discriminating between the transient and sustained responses of the OKR [27].

The *optokinetic sinusoidal stimulations* were tested *at different frequencies (0.2; 0.33, 0.5; 1HZ; peak velocity of 10°/s)* using monocular stimulation. OKR response was expressed as gain and phase determined by least-squares optimization method, similar to the VOR gain and phase[21].

Optokinetic constant velocity (2.5; 5; 7.5; 10°/s) binocular stimulations in alternated clockwise (or naso-temporal (N-T) to the recorded eye) and counterclockwise (or temporo-nasal (T-N) to the recorded eye) directions. The stimulation lasted 60 seconds and was separated by at least 60 seconds of darkness. Analysis of the generated optokinetic nystagmus (alternation of slow and quick phases[57]) was performed on the slow phases after automatic removal of the quick phases using a detection threshold set at 50°/s. Slow phases shorter than 1 second were discarded. To study the individual dynamics of slow phases, each was fitted to an exponential curve in order to reduce noise in parameter estimation. The slow phase gain was computed as the ratio between the amplitude of the interpolated eye displacement and the amplitude of the stimulus displacement, on the same time window. The ocular response was analyzed for the entire duration of the stimulation and the gain of the initial and last slow phase was used to describe its transient and persistent components respectively. The mean number, amplitude and duration of the slow phases during the stimulation were also computed.

Statistical analyses

For both VOR and OKR sinusoidal stimulation experiments the effect of the protocol on the reflex gain and phase were statistically tested by performing a mixed-model ANOVA with the *VVM group* (Sham, Pattern and No-pattern) as between-individual independent factor and the Day (d-14, day0, day1, day2, and, for VOR only, day6) and the stimulation *Frequency* (for VOR: 0.2, 0.5, 1, 2 Hz; for OKR 0.2, 0.33, 0.5, 1 Hz) as within-individual independent factors. The main effects of these factors, as well as their interactions, were tested.

For the continuous OKR stimulation a mixed-model ANOVA was used to test the effect and the interaction between the following independent variables: *VVM group* (Sham, Pattern and No-pattern), as between-individual factor, and the *Day* (d-14, day0, day1, day2), stimulation *Velocity* (2.5, 5, 7.5, 10°/sec), *Direction* (T-N, N-T) and *Component* (transient (first slow phase) and sustained (last slow

phase)) as within-individual independent factors. A mixed-model ANOVA was also used for evaluating the effects of the *VVM group, Velocity* and *Direction* on the number, amplitude and duration of the OKR slow phases at day0.

For the comparison between the OKR and VOR sinusoidal stimulation experiments, for each stimulation modality and for each day, we first subtracted the average gain of the Sham group to those of the Pattern and No-pattern group. Then, we applied a mixed-model ANOVA with the *stimulation modality* (OKR and VOR) as between-individual independent factors and the *Day* (d-14, day0, day1, day2) as within-individual independent factors. For this analysis the mice of Pattern and No-pattern groups were pooled together.

For all analyses the significance threshold was set at $p<0.05$ and Newman-Keuls post-hoc test was performed whenever a significant main effect or interaction was detected. Data were analyzed using Statistica (StatSoft Inc.) software.

REFERENCES

1. Beraneck, M., McKee, J. L., Aleisa, M. & Cullen, K. E. Asymmetric recovery in cerebellar-deficient mice following unilateral labyrinthectomy. *J. Neurophysiol.* **100**, 945–958 (2008).
2. Carriot, J., Jamali, M., Chacron, M. J. & Cullen, K. E. The statistics of the vestibular input experienced during natural self-motion differ between rodents and primates. *J Physiol* **595**, 2751–2766 (2017).
3. Carriot, J., Jamali, M., Chacron, M. J. & Cullen, K. E. Statistics of the vestibular input experienced during natural self-motion: implications for neural processing. *J. Neurosci.* **34**, 8347–8357 (2014).
4. Straka, H., Simmers, J. & Chagnaud, B. P. A New Perspective on Predictive Motor Signaling. *Current Biology* **28**, R232–R243 (2018).
5. Dhande, O. S. *et al.* Genetic Dissection of Retinal Inputs to Brainstem Nuclei Controlling Image Stabilization. *J. Neurosci.* **33**, 17797–17813 (2013).
6. Masseck, O. A. & Hoffmann, K.-P. Comparative Neurobiology of the Optokinetic Reflex. *Annals of the New York Academy of Sciences* **1164**, 430–439 (2009).
7. Stahl, J. S. Using eye movements to assess brain function in mice. *Vision Res.* **44**, 3401–3410 (2004).
8. Cullen, K. E. Vestibular processing during natural self-motion: implications for perception and action. *Nat. Rev. Neurosci.* **20**, 346–363 (2019).
9. Faulstich, B. M., Onori, K. A. & du Lac, S. Comparison of plasticity and development of mouse optokinetic and vestibulo-ocular reflexes suggests differential gain control mechanisms. *Vision Research* **44**, 3419–3427 (2004).
10. Robinson, D. A. Control of Eye Movements. in *Handbook of Physiology Section II : The Nervous System* 1275–1320 (The William and Wilkins Co, 1981).
11. Lannou, J., Cazin, L., Precht, W. & Toupet, M. Optokinetic, vestibular, and optokinetic-vestibular responses in albino and pigmented rats. *Pflugers Arch.* **393**, 42–44 (1982).

12. Curthoys, I. S. The development of function of horizontal semicircular canal primary neurons in the rat. *Brain Res.* **167**, 41–52 (1979).
13. Curthoys, I. S. The vestibulo-ocular reflex in newborn rats. *Acta Otolaryngol.* **87**, 484–489 (1979).
14. Beraneck, M., Lambert, F. M. & Sadeghi, S. G. Functional Development of the Vestibular System. in *Development of Auditory and Vestibular Systems* 449–487 (Elsevier, 2014). doi:10.1016/B978-0-12-408088-1.00015-4.
15. Sherman, K. R. & Keller, E. L. Vestibulo-ocular reflexes of adventitiously and congenitally blind adults. *Invest. Ophthalmol. Vis. Sci.* **27**, 1154–1159 (1986).
16. Seemungal, B. M., Glasauer, S., Gresty, M. A. & Bronstein, A. M. Vestibular perception and navigation in the congenitally blind. *J. Neurophysiol.* **97**, 4341–4356 (2007).
17. Puyal, J. *et al.* Developmental shift from long-term depression to long-term potentiation in the rat medial vestibular nuclei: role of group I metabotropic glutamate receptors. *J. Physiol. (Lond.)* **553**, 427–443 (2003).
18. Beraneck M. & Lambert F.M. Differential Organization of Intrinsic Membrane Properties of Central Vestibular Neurons and Interaction with Network Properties. in *The Senses: A Comprehensive Reference* (Elsevier / Academic Press, 2020).
19. Grassi, S., Dieni, C., Frondaroli, A. & Pettorossi, V. E. Influence of visual experience on developmental shift from long-term depression to long-term potentiation in the rat medial vestibular nuclei. *J. Physiol. (Lond.)* **560**, 767–777 (2004).
20. França de Barros, F., Carcaud, J. & Beraneck, M. Long-term Sensory Conflict in Freely Behaving Mice. *J Vis Exp* (2019) doi:10.3791/59135.
21. Carcaud, J. *et al.* Long-Lasting Visuo-Vestibular Mismatch in Freely-Behaving Mice Reduces the Vestibulo-Ocular Reflex and Leads to Neural Changes in the Direct Vestibular Pathway. *eNeuro* **4**, (2017).
22. Boyden, E. S., Katoh, A. & Raymond, J. L. CEREBELLUM-DEPENDENT LEARNING: The Role of Multiple Plasticity Mechanisms. *Annu. Rev. Neurosci.* **27**, 581–609 (2004).

480 23. Shin, S.-L., Zhao, G. Q. & Raymond, J. L. Signals and Learning Rules Guiding Oculomotor
481 Plasticity. *Journal of Neuroscience* **34**, 10635–10644 (2014).
482 24. Lac, S., Raymond, J. L., Sejnowski, T. J. & Lisberger, S. G. Learning and Memory in the
483 Vestibulo-Ocular Reflex. *Annual Review of Neuroscience* **18**, 409–441 (1995).
484 25. Boyden, E. S. & Raymond, J. L. Active Reversal of Motor Memories Reveals Rules
485 Governing Memory Encoding. *Neuron* **39**, 1031–1042 (2003).
486 26. Beraneck, M. & Cullen, K. E. Activity of vestibular nuclei neurons during vestibular and
487 optokinetic stimulation in the alert mouse. *J. Neurophysiol.* **98**, 1549–1565 (2007).
488 27. Sugita, Y., Miura, K., Araki, F., Furukawa, T. & Kawano, K. Contributions of retinal
489 direction-selective ganglion cells to optokinetic responses in mice. *Eur. J. Neurosci.* **38**,
490 2823–2831 (2013).
491 28. Kodama, T. & du Lac, S. Adaptive Acceleration of Visually Evoked Smooth Eye
492 Movements in Mice. *J. Neurosci.* **36**, 6836–6849 (2016).
493 29. Wakita, R. *et al.* Differential regulations of vestibulo-ocular reflex and optokinetic response
494 by β- and α2-adrenergic receptors in the cerebellar flocculus. *Sci Rep* **7**, 3944 (2017).
495 30. Collewijn, H. & Grootendorst, A. F. Adaptation of Optokinetic and Vestibulo-Ocular
496 Reflexes to Modified Visual Input in the Rabbit. in *Progress in Brain Research* (eds. Granit,
497 R. & Pompeiano, O.) vol. 50 771–781 (Elsevier, 1979).
498 31. Dean, P. & Porrill, J. Decorrelation learning in the cerebellum: computational analysis and
499 experimental questions. *Prog. Brain Res.* **210**, 157–192 (2014).
500 32. Gonshor, A. & Jones, G. M. Extreme vestibulo-ocular adaptation induced by prolonged
501 optical reversal of vision. *J Physiol* **256**, 381–414 (1976).
502 33. Miles, F. A. & Eighmy, B. B. Long-term adaptive changes in primate vestibuloocular reflex.
503 I. Behavioral observations. *J. Neurophysiol.* **43**, 1406–1425 (1980).
504 34. Miles, F. A. & Lisberger, S. G. Plasticity in the vestibulo-ocular reflex: a new hypothesis.
505 *Annu. Rev. Neurosci.* **4**, 273–299 (1981).
506 35. Harris, L. R. & Cynader, M. The eye movements of the dark-reared cat. *Exp Brain Res* **44**,
507 41–56 (1981).

508 36. Jones, G. M. & Davies, P. Adaptation of cat vestibulo-ocular reflex to 200 days of optically
509 reversed vision. *Brain Research* 551–554 (1976).
510 37. Collewijn, H. Optokinetic and vestibulo-ocular reflexes in dark-reared rabbits. *Exp Brain*
511 *Res* **27**, 287–300 (1977).
512 38. Ito, M., Jastreboff, P. J. & Miyashita, Y. Adaptive modification of the rabbit's horizontal
513 vestibulo-ocular reflex during sustained vestibular and optokinetic stimulation. *Exp Brain*
514 *Res* **37**, 17–30 (1979).
515 39. Lisberger, S. G., Miles, F. A., Optican, L. M. & Eighmy, B. B. Optokinetic response in
516 monkey: underlying mechanisms and their sensitivity to long-term adaptive changes in
517 vestibuloocular reflex. *J. Neurophysiol.* **45**, 869–890 (1981).
518 40. Suvrathan, A. & Raymond, J. L. Depressed by Learning—Heterogeneity of the Plasticity
519 Rules at Parallel Fiber Synapses onto Purkinje Cells. *Cerebellum* **17**, 747–755 (2018).
520 41. Suvrathan, A., Payne, H. L. & Raymond, J. L. Timing Rules for Synaptic Plasticity Matched
521 to Behavioral Function. *Neuron* **92**, 959–967 (2016).
522 42. Holland, P. J. *et al.* A Neuroanatomically Grounded Optimal Control Model of the
523 Compensatory Eye Movement System in Mice. *Front Syst Neurosci* **14**, 13 (2020).
524 43. Laurens, J. & Angelaki, D. E. The functional significance of velocity storage and its
525 dependence on gravity. *Exp Brain Res* **210**, 407–422 (2011).
526 44. Cohen, B., Matsuo, V. & Raphan, T. Quantitative analysis of the velocity characteristics of
527 optokinetic nystagmus and optokinetic after-nystagmus. *J. Physiol. (Lond.)* **270**, 321–344
528 (1977).
529 45. van Alphen, A. M., Stahl, J. S. & De Zeeuw, C. I. The dynamic characteristics of the mouse
530 horizontal vestibulo-ocular and optokinetic response. *Brain Res.* **890**, 296–305 (2001).
531 46. Blazquez, P. M., de Carrizosa, M. A. D.-L., Heiney, S. A. & Highstein, S. M. Neuronal
532 Substrates of Motor Learning in the Velocity Storage Generated During Optokinetic
533 Stimulation in the Squirrel Monkey. *Journal of Neurophysiology* **97**, 1114–1126 (2007).
534 47. Miki, S., Urase, K., Baker, R. & Hirata, Y. Velocity storage mechanism drives a cerebellar
535 clock for predictive eye velocity control. *Sci Rep* **10**, 6944 (2020).

48. Cohen, B., Dai, M., Yakushin, S. B. & Raphan, T. Baclofen, motion sickness susceptibility and the neural basis for velocity storage. *Prog. Brain Res.* **171**, 543–553 (2008).
49. Yakushin, S. B., Raphan, T. & Cohen, B. Coding of Velocity Storage in the Vestibular Nuclei. *Front Neurol* **8**, (2017).
50. Kassardjian, C. D. The Site of a Motor Memory Shifts with Consolidation. *Journal of Neuroscience* **25**, 7979–7985 (2005).
51. Shutoh, F., Ohki, M., Kitazawa, H., Itohara, S. & Nagao, S. Memory trace of motor learning shifts transsynaptically from cerebellar cortex to nuclei for consolidation. *Neuroscience* **139**, 767–777 (2006).
52. Raymond, J. L. & Medina, J. F. Computational Principles of Supervised Learning in the Cerebellum. *Annu. Rev. Neurosci.* **41**, 233–253 (2018).
53. Jang, D. C., Shim, H. G. & Kim, S. J. Intrinsic Plasticity of Cerebellar Purkinje Cells Contributes to Motor Memory Consolidation. *J. Neurosci.* **40**, 4145–4157 (2020).
54. Beraneck, M. & Idoux, E. Reconsidering the role of neuronal intrinsic properties and neuromodulation in vestibular homeostasis. *Front Neurol* **3**, 25 (2012).
55. Calabrese, D. R. & Hullar, T. E. Planar Relationships of the Semicircular Canals in Two Strains of Mice. *JARO* **7**, 151–159 (2006).
56. Oommen, B. S. & Stahl, J. S. Eye orientation during static tilts and its relationship to spontaneous head pitch in the laboratory mouse. *Brain Res.* **1193**, 57–66 (2008).
57. Cahill, H. & Nathans, J. The optokinetic reflex as a tool for quantitative analyses of nervous system function in mice: application to genetic and drug-induced variation. *PLoS ONE* **3**, e2055 (2008).

ACKNOWLEDGMENTS

The authors thank M. Patrice Jegouzo and Laure-Hélène Bernard, Olivia Cattaneo and Thibault Patti for their technical help during the experiments. This work was supported by the *Centre National d'Etudes Spatiales*, the *Centre National de la Recherche Scientifique* and the *Université de Paris*. FB & MB received support from the *Agence Nationale de la Recherche* (ANR-15-CE32-0007-02). This study contributes to the IdEx Université de Paris ANR-18-IDEX-0001.

AUTHOR CONTRIBUTION:

Conceptualization: FB; MT; MB

Methodology: FB; LS; MT; MB

Software: LS; MT; MB

Formal analysis: FB; LS; MT; MB

Investigation: FB; LS; MB

Writing original manuscript: FB; MB

Writing – review and editing: FB; LS; MT; MB

Visualization: FB; LS; MT; MB

Supervision: FB; MT; MB

Project administration: MB

Funding acquisition: MT; MB

COMPETING INTERESTS

The authors declare no competing interests.

DATA AVAILABILITY

The VVM protocol used in this study is explained in detail in the published article[9]. The datasets generated during the current study are available in the Mendeley Data repository, https://dx.doi.org/10.17632/r56jxvyycv.1.

588 **FIGURE LEGENDS**

589

590 **Figure 1. Effects of the VVM on the VOR. a**- 3D rendering of mice wearing the three different types of
591 devices used in the protocol; Pattern (left), No-pattern (middle) and Sham (right). **b**- Depiction of the
592 set-up to test VOR; the mouse is head-fixed and secured in a plexiglas tube during horizontal rotations
593 of the turntable at a fixed peak velocity (30º/s) and variable frequencies (0.2-2Hz). **c-** Example raw
594 traces of VOR responses recorded on day 0 at0,5Hz for Sham (grey), No-pattern (green) and Pattern
595 (orange). Head rotations in the dark evoked compensatory eye movements in the opposite direction.
596 VVM-exposed mice showed altered eye movements **d-** Sham (n=8), No-pattern (n=16) and Pattern
597 (n=15) mean VOR gain along the entire protocol (20 days). The mean VOR (**e**) gain and (**f**) phase are at
598 all tested days are plotted for the different frequencies of stimulation. The significance of the gain and
599 phase changes compared to Sham are indicated next to each point in the graph. Error bars represent
600 ±SEM; Newman Keuls post-hoc test * $p<0.05$; ** $p<0.01$; *** $p<10^{-3}$.

601

602 **Figure 2. Effects of the VVM on OKR. a**- 3D rendering of the set-up used to test OKR. A dotted
603 background was projected into a mirror while the mouse was kept head-fixed. **b**- Example raw traces
604 of the OKR response to a stimulation at 0.33Hz at peak velocity of 10°/s for each condition; Sham
605 (grey), No-pattern (green) and Pattern (orange). The eye position smoothly follows the optokinetic
606 stimulus. **c**- Kinematics of the mean OKR gain of Sham (n=6), No-pattern (n=8) and Pattern (n=12)
607 during the tested days. OKR gain (d) and phase (e) at each of the different frequencies tested along
608 each day. The significance of both gain and phase are indicated on top of each point in the graph for
609 No-pattern (first line, green) and Pattern (second line, orange). Error bars represent ±SEM; Newman
610 Keuls post-hoc test * $p<0.05$; ** $p<0.01$; *** $p<10^{-3}$.

611

612 **Figure 3. Effects of the VVM on OKR nystagmus. a**- Example raw traces for each group (Sham n=8,
613 grey; No-pattern n=16, green; Pattern n=15, orange) of the OKR response to the 60s-long stimulation
614 at 7.5º/s in temporo-nasal direction (black line). The grey rectangles mark the segments that were not
615 considered in the analysis of the eye movements (quick phases or recording artefacts). Only slow
616 phases were computed to characterize the response over the duration of the visual stimulation. **b-** To
617 illustrate the dynamic of responses over the stimulation period, the individual slow phases gains were
618 plotted over time for 7.5°/s constant velocity stimulation in temporo-nasal direction. In the VVM-
619 treated groups, the first response after stimulus onset (the first slow phase), appears lower after the
620 VVM protocol. To quantify this difference, the gains of the first and last slow phases in response to all
621 velocities and directions were averaged (**c**). When computed, the difference between the first and last
622 SP gains reveals that before the VVM, the three groups had similar first and last gains while, on day 0,

VVM-treated groups had lower first slow phase gains. On day 1, these gains have increased and at day 2, they are identical to Sham. The significant differences compared to Sham are indicated on top of each point in the graphs for No-pattern (green asterisks) and Pattern (orange asterisks) groups, respectively. Error bars represent ±SEM; Newman Keuls post-hoc test * $p<0.05$; ** $p<0.01$; *** $p<10^{-3}$.

Figure 4. Comparison of the amplitude and dynamics of VOR and OKR gain changes over time. Global gain changes in VOR (purple diamonds) and OKR (blue triangles) over time were compared by subtracting the mean responses of the Sham group from those of the VVM-exposed mice (ΔGain). Differences between VOR and OKR responses of both VVM-exposed groups are represented with black asterisks. Error bars represent ±SEM; Newman Keuls post-hoc test * $p<0.05$; ** $p<0.01$; *** $p<10^{-3}$.

Supplementary Figure S1. Features of the optokinetic nystagmus. Quantification of the slow phases evoked by the constant velocity 60s-long optokinetic stimulation. The (**a**) number, (**b**) duration and (**c**) amplitude describe the slow phases recorded at day 0 at different velocities. Differences between groups are indicated above each graph**.** Bars represent mean+/-SEM. Newman Keuls post-hoc test * $p<0.05$; ** $p<0.01$; *** $p<10^{-3}$.

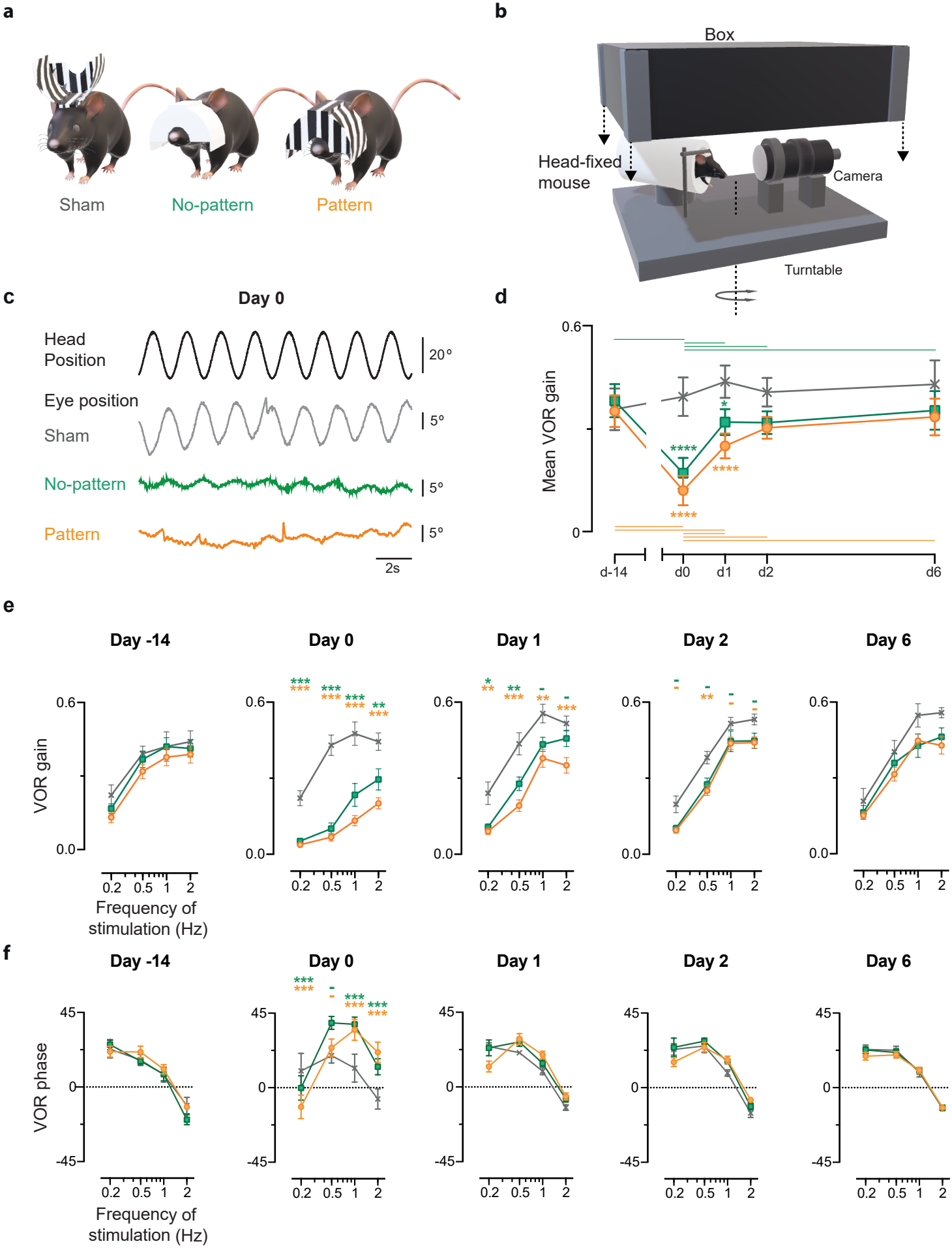
a
Sham
No-pattern
Pattern
b
Box
Head-fixed mouse
Camera
Turntable
c
Day 0
Head Position
20°
Eye position
Sham
5°
No-pattern
5°
Pattern
5°
2s
d
Mean VOR gain
0.6
0
d-14
d0
d1
d2
d6
e
Day -14
Day 0
Day 1
Day 2
Day 6
VOR gain
0.6
0.0
0.2 0.5 1 2
Frequency of stimulation (Hz)
f
Day -14
Day 0
Day 1
Day 2
Day 6
VOR phase
45
0
-45
0.2 0.5 1 2
Frequency of stimulation (Hz)

Figure 1.

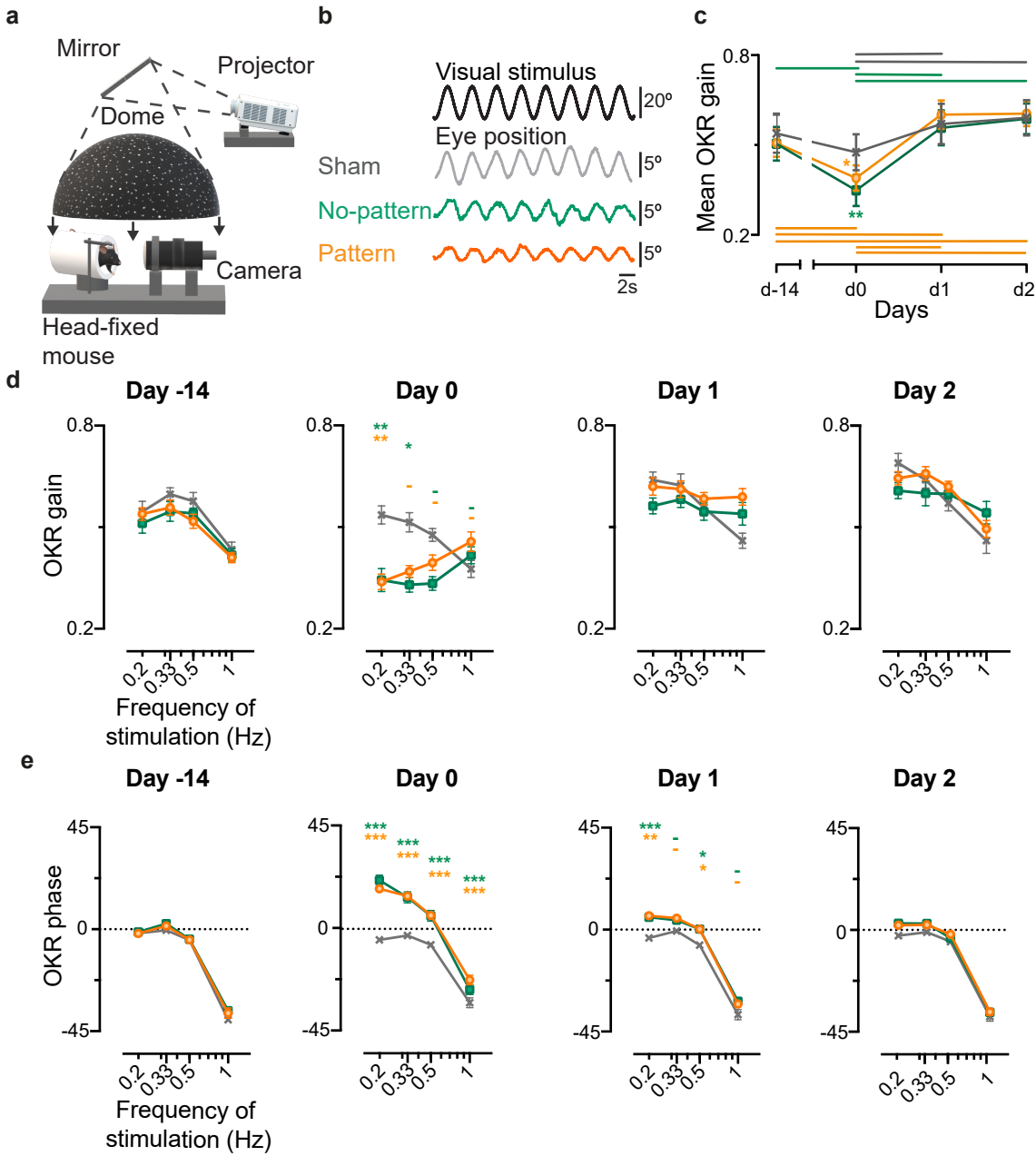
a
Mirror
Projector
Dome
Camera
Head-fixed
mouse
b
Visual stimulus
20º
Eye position
Sham
5º
No-pattern
5º
Pattern
5º
2s
c
Mean OKR gain
0.8
0.2
d-14
d0
d1
d2
Days
d
Day -14
Day 0
Day 1
Day 2
OKR gain
0.8
0.2
0.2
0.33
0.5
1
Frequency of
stimulation (Hz)
e
Day -14
Day 0
Day 1
Day 2
OKR phase
45
0
-45
0.2
0.33
0.5
1
Frequency of
stimulation (Hz)

Figure 2.

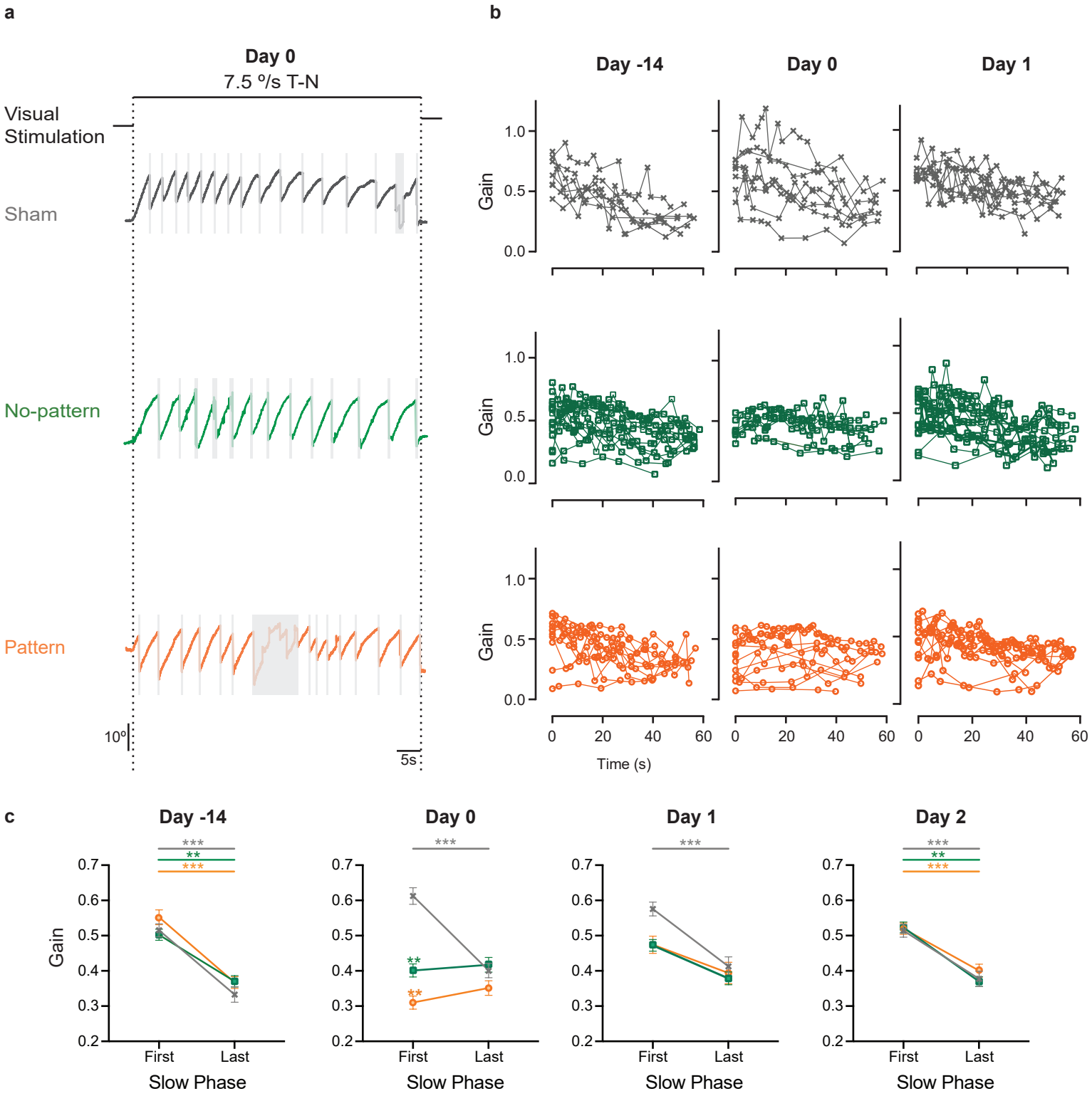
a
Day 0
7.5 °/s T-N
Visual Stimulation
Sham
No-pattern
Pattern
10°
5s
b
Day -14
Day 0
Day 1
Gain
1.0
0.5
0.0
0
20
40
60
Time (s)
c
Day -14
Day 0
Day 1
Day 2
***
**
0.7
0.6
0.5
0.4
0.3
0.2
First
Last
Slow Phase

Figure 3.

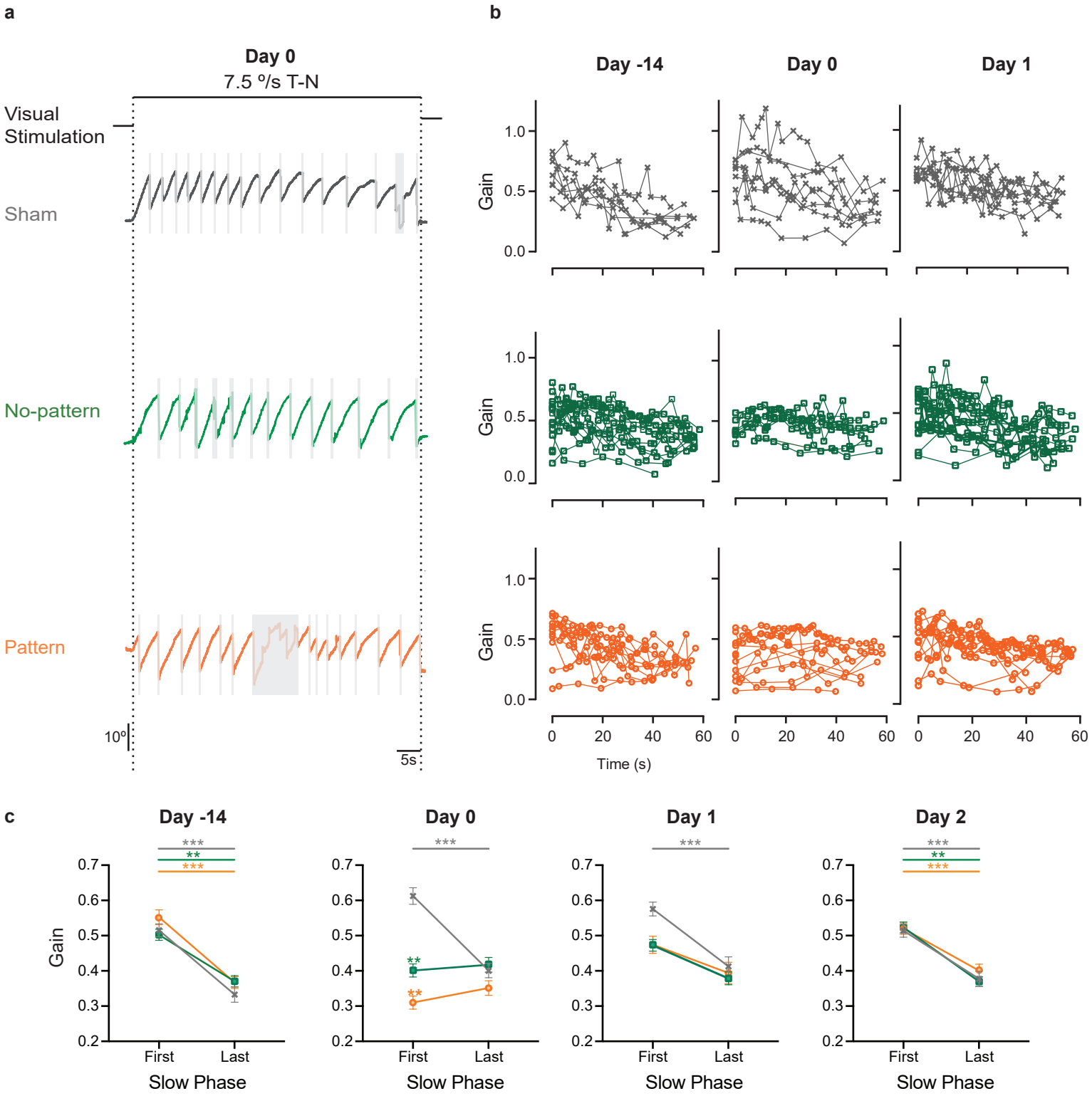
a
Day 0
7.5 °/s T-N
Visual Stimulation
Sham
No-pattern
Pattern
10°
5s
b
Day -14
Day 0
Day 1
Gain
1.0
0.5
0.0
0
20
40
60
Time (s)
c
Day -14
Day 0
Day 1
Day 2
***
**
0.7
0.6
0.5
0.4
0.3
0.2
First
Last
Slow Phase

Figure 3.

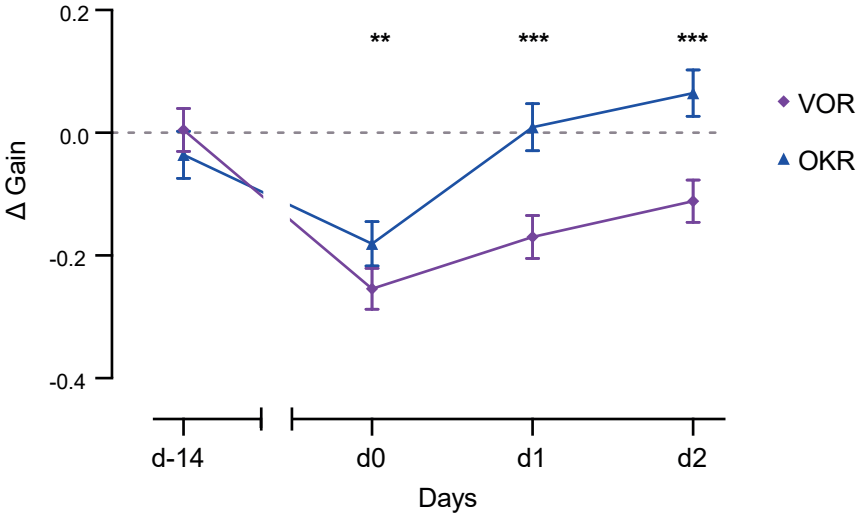

Figure 4.

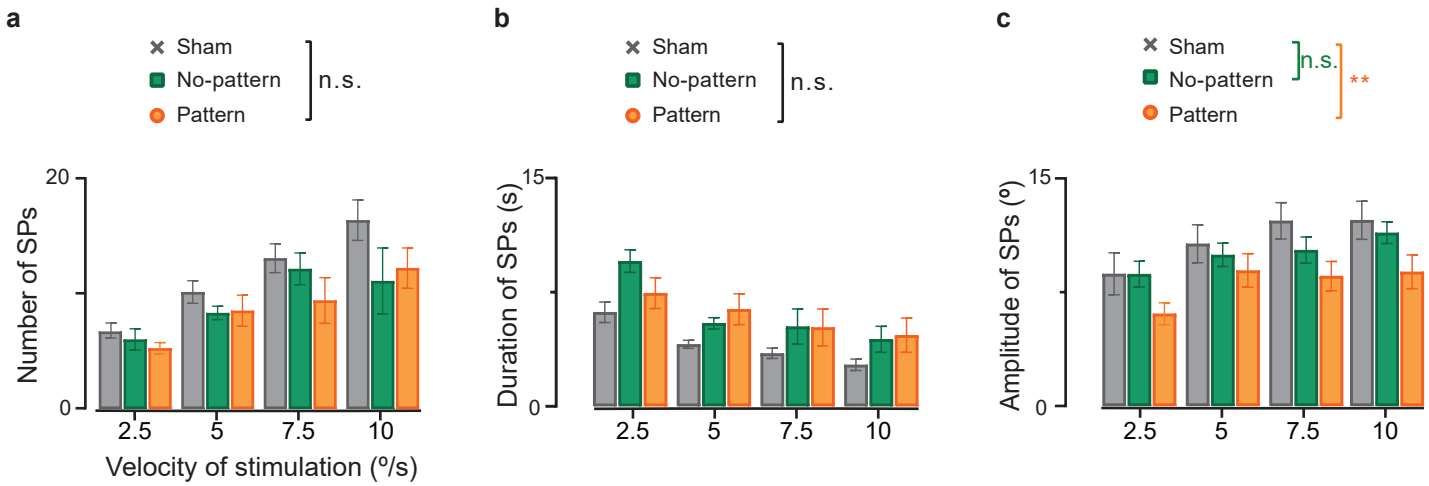
a
Sham
No-pattern
Pattern
n.s.
Number of SPs
20
0
2.5
5
7.5
10
Velocity of stimulation (°/s)
b
Sham
No-pattern
Pattern
n.s.
Duration of SPs (s)
15
0
2.5
5
7.5
10
c
Sham
No-pattern
Pattern
n.s.
**
Amplitude of SPs (°)
15
0
2.5
5
7.5
10

Article 4. Locomotor CPG-driven efferent copy couples eye movements with forelimb locomotion in mice

Accurate visual information is crucial in the life of most animals. In order to maintain visual acuity during head/body movements, several sensorimotor inputs (*e.g.* vestibular, visual and proprioceptive) converge in the brainstem nuclei. From there, a premotor output will be generated so that the eye and/or the head can be moved in space.

In addition to the aforementioned sensorimotor inputs, an efferent copy has also been proven to contribute to minimize visual disturbances during locomotion in Xenopus tadpoles. Efference copies are neural replicas of motor outputs used to anticipate the sensory consequences of a self-generated action. They are responsible for the coordination of motor behaviors as those intrinsic feed-forward signals generated by a local motor circuitry may influence a neural network involved in another behavior. This was first demonstrated by one of the 2 teams involved in this project(Combes et al., 2008; Lambert et al., 2012).

In vitro data in the Xenopus tadpole allowed to unravel a new gaze stabilization mechanism that involves a central interaction between locomotor circuits of the spinal cord and the extraocular motor nuclei of the brainstem. That work revealed that, during undulatory swimming, an efferent copy (predictive signaling) coming from the locomotor CPG, assures a first internal command of gaze stabilization, independent of the traditional visuo-vestibular reflexes (optokinetic and vestibulo-ocular). This efferent copy of the locomotor pattern, conjugated to swimming, produces conjugated eye movements that compensate for the tail's undulation (Bacqué-Cazenave et al., 2018; Combes et al., 2008; Lambert et al., 2012; Uckermann et al., 2013). Therefore, in the Xenopus tadpole, during *in vitro* fictive locomotion and in the absence of sensory inputs, a spino-extraocular motor command couples the locomotor CPG activity to the extraocular motor nerves (Combes et al., 2008; Lambert et al., 2012). This spino-extraocular command coordinates the spinal rhythmic activity with the extraocular motor activity.

However, in this model, the locomotor profiles are stage specific. Therefore, after metamorphosis the gaze stabilizing process changes from left-right head displacements to compensate to, as an adult, relying on binocular conjugate movements. However, the presence of this predictive efferent signal was not only confirmed in tadpoles but also in the juvenile frog stage. Interestingly the neural pathways mediating this spino-extraocular coupling are reorganized from contralateral to strictly ipsilateral during metamorphosis of

the amphibian so it can generate an appropriate ocular movement to compensate for the change of locomotor scheme (Uckermann et al., 2013). In a phylogenetic approach and since keeping visual acuity is a transversal characteristic in vertebrates, the presence of a similar gaze stabilizing strategy in higher vertebrates can be hypothesized.

Hence, the present project aimed at exploring whether a predictive signal, coupling eye movements to locomotion, is present in mice. This question was experimentally approached by semi-intact preparations, *ex vivo* and *in vitro*.

The first set of experiments aimed at verifying the existence of this efferent copy in mice using the same technique as applied in tadpoles. Thus, the activity of spinal and abducens motor nerves were recorded simultaneously *ex vivo* in isolated brainstem-spinal cord preparations of neonatal mice. A rhythmic coupled discharge between limb and abducens motor nerve activities during active locomotion bouts was recorded by electrical as well as pharmacological stimulation.

Next, a precollicular and premammillary decerebrated head-fixed adult mouse preparation was used to unmask this efferent copy in a behaving mouse. In this preparation, eye movements were recorded during locomotion in a motorized treadmill. Due to the absence of vestibular and visual inputs during this experiment, the recorded horizontal eye movements are coherent with the behavioral output of an efferent copy.

Finally, the neuronal pathway that couples the cervical CPG and the abducens nuclei was anatomically traced through the use of rabies virus. Injections were performed in the lateral rectus, a muscle responsible for horizontal eye movements, and mapped a direct projection from cervical spinal cord neurons to the abducens nucleus.

In conclusion, with a multi-methodological integrative approach, this study, demonstrated for the first time that a cervical CPG-driven efference copy directly couples eye movements with forelimb movement during vigorous locomotion in mice.

The article presented below is in preparation and hasn't been submitted for publication.

Title

Central pattern generator-driven efference copy couples eye movements with forelimb locomotion in mice

Authors

Filipa França de Barros[1*], Coralie Taillebuis[1,4], Marin Manuel[2], Hélène Bras[3], Julien Bacqué-Cazenave[4], Denis Combes [4], François Lambert[4], Mathieu Beraneck[1*]

[1] Université de Paris, Integrative Neuroscience and Cognition Center, CNRS UMR 8002, 75270 Paris, France.

[2]-SPPIN UMR 8003, CNRS, Paris, France

[3]-INT UMR 7289, CNRS, Marseille, France

[4]-INCIA UMR 5287, CNRS, Bordeaux, France

Keywords: efferent copy, CPG, locomotion, predictive signaling, gaze stabilization

***Corresponding authors**

Filipa Barros. E-mail: filipa.barros@parisdescartes.fr

Dr. M. Beraneck. CNRS UMR 8002, Université de Paris, 45 rue des St-Pères, Paris 75270, France. Email: mathieu.beraneck@parisdescartes.fr

Running title

Locomotor CPG-driven efferent copy couples eye movements with forelimb locomotion in mice

Author contribution:

Conceptualization: FB; FL, DC, MB

Methodology: FB; MM, JBC, HB, MB

Software: JBC, MM

Formal analysis: FB; CT; MM, FL, MB

Investigation: FB; CT, MM, HB

Writing original manuscript: FB; MB

Visualization: FB; LS; MT; MB

Supervision: FB; FL; MB

Project administration: DC, FL, MB

Funding acquisition: DC, FL; MB

Acknowledgments

This project was financed by the *Agence Nationale de la Recherche* (ANR-15-CE32-0007).

Introduction

Accurate visual information is crucial in the life of most animals. In order to maintain visual acuity during head/body movements, several sensorimotor inputs (e.g. vestibular, visual and proprioceptive) converge in the brainstem nuclei. From there, a premotor output will be generated so that the compensatory eye and/or head movements are produced. Efference copies are neural replicas of motor outputs used to anticipate the sensory consequences of a self-generated motor action. They are responsible for the coordination of motor behaviors as those intrinsic feed-forward signals, generated by a local motor circuitry, may influence a neural network involved in another behavior (Straka 2019).

In this study we characterize the implication of an efferent copy coming from the locomotor CPG, the spinal neuronal network responsible for the locomotor rhythm, in the gaze stabilization of mice. In vitro data from the Xenopus tadpole demonstrated a new mechanism of gaze stabilization that implied a central interaction between the locomotor circuits of the spinal cord and the extraocular motor nuclei of the brainstem. These experiments revealed that during tadpole swimming an efferent copy (predictive signaling) coming from the locomotor CPG ensures a first gaze stabilizing command, independent of the traditional gaze stabilizing reflexes. This efferent copy, originated by swimming, produces conjugated eye movements that compensate the tail undulation. There, during in vitro fictive locomotion and in the absence of sensory inputs, a spino-extraocular motor command couples the locomotor CPG activity to the extraocular nerves (Lambert et al., 2012). Even though amphibians, due to their metamorphosis, constitute an evolutionary bridge between tail and limb-based locomotion, this spino-extraocular coupling was never demonstrated in mammals. Here we explore whether such a predictive signal, which couples eye movements to locomotion, is preserved in phylogenesis, particularly in mammals.

Material and methods

Rabies virus inoculation

RV manipulation was done by vaccinated experimenters in a Biosafety level 2 facility. The virus (Challenge Virus Strain, CVS) was produced and concentrated as described by (Gaudin et al., 1992) Aliquots of the virus were stocked at -80ºC and thawed before use. Mice were anesthetized by an i.p. injection of ketamine (Imalgene, 60 mg/kg) and xylazine (Rompun, 10 mg/kg) and deep anesthesia was confirmed by lack of response to interdigital pinching. The left extraocular muscles were exposed through an incision

on the skin covering the mouse's eye, surrounding fatty tissue was removed and absorbable hemostatic gelatin sponges were used to curtail bleeding (Spongostan, Ethicon). After its identification, the lateral rectus muscle (LRM) was isolated using small hooks and an injector canula (gauge 33), linked to a 10µL Hamilton syringe, was inserted. 1µL of the RV were then slowly injected and the needle was left in place for an extra minute to prevent leaking. Finally, the skin was closed using monofilament suture (for a detailed description see (Bras et al., 2008; Coulon et al., 2011)) and mice were put back on their cages under a red light.

Inoculation times were narrowed down to obtain RV-infected spinal cord neurons with monosynaptic connections to the abducens nucleus. A 72h inoculation window displayed RV+ neurons (Purkinje cells) in the cerebellum, therefore disynaptic connections were already present. When the inoculation time was lowered to 67h the RV+ neurons were restricted to the brainstem and cervical, with no infection on the cerebellum or adjacent areas. Therefore, a 67h infection time was chosen for all the subsequent experiments. Mice that after 57 hours of RV infection in the LRM didn't present any infection were excluded from the experiment.

Dual immunodetection of RV and choline acetyltransferase neurons

After 67h RV incubation, animals were deeply anesthetized with ketamine (Imalgene, 60 mg/kg) and xylazine (Rompun, 10 mg/kg) and perfused intracardially with 100mL of phosphate buffer saline (PBS 0.1M) followed by 300 mL of 4% paraformaldehyde (PFA). To study the neuronal substrates of this spino-extraocular pathway, the brain was dissected coronally from the midbrain (Paxinos coordinates: Interaural 0.00, Bregma 3.8 mm) to the medulla oblongata (Paxinos coordinates: Interaural -4.44, Bregma -8.20 mm) and the spinal cord was taken entirely from the cervical to the cauda equina. Tissue fixation was let for 24h at 4˚C in 4% PFA, subsequently cryoprotected in 20% sucrose during at least 6h and freeze embedded at -80ºC in Tissue Tek (Sakura, Zoeterwoude The Netherlands).

Transverse sections (30 µm thick) of the brain and cervical, thoracic and lumbar spinal cord were serially cut in cryostat (Microm, Heidelberg, Germany) and collected onto poly-L-lysine-coated slides. These sections were first incubated to avoid unspecific binding for 1h at room temperature in blocking solution (PBS, Triton X-100, 2% bovine-serum albumin and normal donkey serum) and then left at 4˚C for 48h with the anti-RV phosphoprotein (Coulon et al., 2011) and anti-choline acetyltransferase (ChAT) diluted 1:1000 in the blocking solution. After being rinsed thrice in PBS, sections were incubated at room temperature with Alexa488 anti-mouse and Alexa546 anti-goat for 2h. Finally,

sections were rinsed two times with PBS and once with tap water before being mounted (Immu-mount, Fischer Scientific) under coverslips.

Fluorescence microscopy

To analyze the distribution of RV+MNs in the brainstem and LOINs neurons in the spinal cord, the sections were visualized under an upright light microscope (Axioscope, Carl Zeiss, Germany). Images of each entire section (4x) as well as magnifications of certain areas of interest (10x and 20x) were taken using a CCD camera (AxioCam MR3, Carl Zeiss). These images were afterwards treated in ZEN (Carl Zeiss) imaging software where neurons $ChAT^+$ or RV^+ were counted. Only neurons with a visibly infected nucleus, determined by the presence of Negri, were considered.

Treadmill locomotion in decerebrated headfixed mice

Anesthesia induction and tracheotomy

Anesthesia induction was performed in an isolation chamber with 3% isoflurane gas delivery for 4 minutes. After tilting the induction chamber to verify the righting reflex, the mouse was transferred to the surgery table on a covered heating pad. A nose cone was placed on the snout and mouth to maintain anesthesia with 1,5% (vol/vol) isoflurane with medical grade oxygen (SomnoSuite, Kent Scientific). A rectal probe was placed to ensure the temperature stayed around 38ºC (Physiosuite, Kent Scientific), the head was shaved with hair clippers and the eyes were covered with ophthalmic gel to avoid dryness. The mouse was then flipped to its dorsal side and the neck skin was shaved. The front limbs were taped to the table, a pulse oximeter and a heart rate monitor (MouseSTAT, Kent Scientific) was placed in one hindlimb, while the other was left uncovered to verify the pinching reflex along the surgery. Using a pair of fine forceps, the skin immediately below the chin was lifted and, with round scissors, an incision was made until the sternum. The salivary glands were separated as well as the skin covering the trachea and, after exposure, two 4-0 suture threads were passed underneath it. The tracheotomy was then performed, using a pair of micro-scissors, by cutting the upper half of the fibrous membrane between two cartilages. The air delivery mode was then quickly switched to ventilator mode (the respiration system, SomnoSuite, Kent Scientific) and a plastic endotracheal tube was placed, on the incision made, to allow for artificial ventilation along the rest of the procedure. The suture threads were then tied to the endotracheal tube and the isoflurane level was lowered to 1.2% after confirming that the pCO2 levels were acceptable (higher than 2.5%). To avoid excessive bleeding during decerebration, the left and right carotids were bluntly isolated and tied using 6-0 soy

suture threads; an electric cauterizer (Bovie change-a-tip) was used to cauterize the space between the two knots. The incision initially made was closed back and, to prevent dehydration, 0,3 ml of sterile lactated Ringer's solution (Braun Medical) were injected subcutaneously.

Craniotomy and decerebration

Craniotomy and decerebration procedures mainly followed as described by Meehan and collaborators (Meehan et al., 2017). Briefly, the mouse was placed within a stereotaxic frame and, using a pair of blunt scissors, an incision was made along the skin of the head to expose the skull. Using a micro-drill (Foredom, David Kopf Instruments), the skull was scored along the limitation of the temporal bones and they were removed in one piece. The midline was scored at the lambda and bregma crest and carefully removed after immediate cauterization of the superior sagittal sinus. Decerebration was performed at the confluence of the sagittal and transverse sinus, perpendicular to the midline and at a 40±5º angle. On that location, a n10 scalpel was used to perform a gentle slicing motion; the blade was plunged deep enough not to damage the mammillary bodies. The structures rostral to the incision were fully removed from the brain with a microspatula. Finally, another subcutaneous injection of Ringer's lactate (0.3 ml) was applied and the isoflurane was turned off.

Treadmill locomotion

Still on the surgery table, the pulse oximeter was removed as well as the stereotaxic frame and custom-made ear bars were placed. After the transfer to the treadmill, the ear bars were fixed onto the transparent platform and a mouthpiece was positioned on the mouth to ensure head fixation (see Figure 1A). Complete anesthesia withdrawal and muscular tonus happened 10-20 minutes after isoflurane removal; pCO_2 levels rose consequently. Body temperature was crucial for the survival of the preparation and since after the surgery the mouse was not able to autoregulate its temperature, a hairdryer was used to keep a constant temperature of 38-39ºC. In order to have a trackable eye, special care was taken to preserve its quality by gently brushing the skin surrounding it with a moistened cotton-swab and re-applying ophthalmic gel whenever the eye acquired a dry appearance. Once the experiment was completed, mice were sacrificed with an IP injection of Dolethal (Vethoquinol, France).

Videoculography during locomotion

The set up consisted of two infrared CCD cameras with a zoom lens (Zoom 6000, Navitar inc., NY), an infrared video camera (Grasshopper3, Point Grey) and a motorized

treadmill (Brand), all fixed onto a metallic platform. To ensure darkness during the experiment, a black curtain covered the set up by hanging on top of bars placed on each corner of the platform. The eyes of the mouse were illuminated with an infrared emitter attached to each camera that was placed symmetrically regarding the front part of the treadmill. The eye video signal was registered with an eye tracking system (ETL-200, ISCAN, Burlington, MA), sampled at 1kHz and recorded (CED power 1401 MkII) with Spike2 software. The IR video camera was paired to the recording software with a trigger; once the treadmill was turned on and locomotion spontaneously started, the trigger was launched to proceed with video recordings of body movements. Eye movements were analyzed offline using DataView and locomotor cycles were tracked using a markerless pose estimation (DeepLabCut (Mathis et al., 2018). Each mouse was set on the treadmill from 1-3 hours. Mice were excluded from the experiment if, during the first hour, they didn't show a sustained locomotion (walking in the treadmill for a period over 1 minute).

Spino-extraocular coupling in isolated brainstem-spinal cord preparations

Isolated brainstem-spinal cord preparations

Mice were deeply anesthetized by 4% isoflurane inhalation until the loss of the nociceptive reflexes. After being placed in a Petri dish filled with Sylgard, they were decerebrated and eviscerated while submerged in an oxygenated (95% O_2 and 5% CO_2) artificial cerebrospinal fluid (aCSF) (in mM: 128 NaCl, 4.5 KCl, 2.5 CaCl2.2H2O, 1.0 $MgSO_4.7H_2O$, 1.2 $NaH_2PO_4.H_2O$, 5 Hepes, 25 $NaHCO_3$ and 11 D-glucose) at 4°C. In a dorsal view, a craniotomy was performed to expose and remove the cerebellum and the abducens nerves were carefully cut so that they could be recorded. With a ventral approach, a full laminectomy was done to expose the spinal cord and all the dorsal and ventral roots of both cervical sides were cut so that the final brainstem-spinal cord preparation could be extracted. After removing the meninges, the preparation was fixed to the Sylgard with insect pins with the ventral side up and preserved in oxygenated aCSF fluid at room temperature.

Extraocular motor discharge modulation during fictive locomotion

To study the spino-extraocular coupling, isolated brainstem-spinal cord preparations had the distal ends of abducens nerves as well as bilateral spinal dorsal motor roots (sacral, lumbar or cervical) simultaneously recorded (A-M Systems Model 1700 AC amplifiers, Carlsborg, US) with fire-polished borosilicate glass suction recording electrodes filled with aCSF solution and with adequate sized tip diameters. Fictive locomotion was

achieved in brainstem-spinal cord preparations either through electrical or pharmacological stimulation.

Fictive locomotion through electrical stimulation of the dorsal roots

To obtain fictive locomotion through electrical stimulation, the electrodes suctioning the dorsal roots were connected to a pulse generator; this allowed the delivery of pulse trains (4Hz for 10s, inter-stimulus interval of 0,25s and at least 5 minutes between pulse trains). Signals were amplified (10000x) by differential AC amplifiers (low cut off, X Hz; high cutoff X Hz), digitized at 5 KHz (CED 1401; Cambridge Electronic Design, Cambridge, UK), displayed and stored on computer with acquisition software (Spike 2, Cambridge Electronic Design) and finally analysed off-line with customized scripts in Spike 2. The described pulse trains were delivered at the lumbar or at the cervical while the abducens nerves were recorded. To investigate if the spino-extraocular coupling varies according to the stimulated spinal cord region, the motor coupling was disrupted using a split-bath configuration (isoflex, A.M.P.I.) that allowed reversibly isolating the brainstem from different regions of the spinal cord. Isolation was obtained by partitioning the recording chamber with two custom-made plastic walls that traversed the preparation either rostrally at the obex and spinal segment 12, or caudally at spinal segments 12 and 30. Whenever the lumbar was stimulated, the cervical was immersed in an aCSF 0 Ca2+ solution, in order to completely block transmission at that level. To isolate the cervical from the rest of the preparation, a section was made at the thoracic spinal cord and the cervical was then stimulated while the abducens nerves were recorded.

Data analysis

The electrodes were connected to extracellular amplificatory and the analogic signals were scanned by and analogic/digital interface (CED). Data was acquired with Spike2 software (Spike2, Cambridge Electronic Deisgn) at a frequency of 1000Hz. The analysis of the electrophysiological data was done after rectification (each point of the signal was replaced by its absolute value) that allowed to obtain an integrated signal. The treatment of this data was done using DataView and the following parameters were quantified: i) the frequencies of the locomotor and oculomotor discharges, this is, the amount of times the activity occurs per second; ii) the latencies, i.e., the time that separates each locomotor and oculomotor activity discharge; iii) the phase relationships between the ventral roots (lumbar and cervical) and the abducens. The phase relationship corresponds to the time difference between two activity bursts from the same locomotor cycle, normalized by the period of the refence root.

Statistical Information

The number of animals used in each experiment is indicated throughout this article by 'n'. GraphPad Prism 8.2.1 and OriginPro8 (OriginLab, US) were used for statistical analysis. The respective results were expressed as the mean ± SEM and *p* values <0.05 were considered as significantly different ($^{*}p < 0.05$; $^{**}p < 0.01$; $^{***}p < 0.001$; $^{****}p < 0.0001$; ns: non-significant). When paired t test were needed for comparing paired observations first, normality was evaluated using the D'Agostino & Pearson normality test and Shapiro-Wilk in the case of smaller unpaired two-tailed samples. When testing locomotion frequency and latency as well as the integrated electrophysiological signals, differences between two results were obtained using the unpaired two-tailed Mann–Whitney *U*-test and Kolmogorov–Smirnov test to compare distributions. To compare several values, non-parametric Kruskal–Wallis test was processed with a Dunn's multiple comparisons test. To evaluate the correlations between the frequencies of discharge of the locomotor nerves and the extraocular nerves, regression tests (R) and linear regression (R^2) were performed. Regression results were expressed as (R, R2). Circular data was analysed with Oriana 4.02 (Kovach Computing Services, UK) and the phase and strength of coupling were indicated by their mean vector (μ) and its length (r), respectively.

Results

Demonstration of a coupling between locomotor cycles and eye movements in absence of visual and vestibular inputs

The first goal of this project was to verify in the mouse the existence of a motor-to-motor coupling between the locomotion (spinal nerve activity) and the eye movements (or activity of oculomotor nerves), similar to that described in amphibians. The presence of eye movement in relation to locomotor cycle was first investigated in a semi-intact mouse preparation. We recorded eye movements in a precollicular and premammillary decerebrated head-fixed mouse running on a motorized treadmill (Figure 1 A). Due to the decerebration, the locomotion evoked in these experiments was a result of the stimulation of the limbs by the treadmill belt. Consistent locomotion (epochs between 10-40 seconds) were observed in 17 mice. Among these mice, consistent eye movements were observed in 6. Figure 1A illustrates responses observed in one of these robust preparations. Binocular conjugated eye movements were observed during trot-like locomotion (limb instantaneous frequency of 2-6Hz, tight phase coupling between forepaw and hind paw; Figure 1, A2). These eye movements consisted of a quick (saccade-like) phase and a slower phase (Figure 1, B1) that were mostly restricted to

the horizontal plane (Figure 1, B2). The amplitudes of these slow phases were comprised between 2-8º (mean 4,6º) at a range of velocity typically between 20-90º/s. Hence, the presence of a spino-oculomotor coupling is for the first time reported in the decerebrated mice.

Following the original methodology used in Xenopus tadpoles that first described this efferent copy, we proceeded to record isolated spinal cord-brainstem preparations of newborn mice. Here, we demonstrate the spino-extraocular coupling *in vitro* in an isolated brainstem-spinal cord preparation. Neonate mice were used to simultaneously record the extracellular activity from the spinal ventral roots (Vr). Since the abducens nerve (CN VI) innervates the lateral rectus muscle (responsible for the movements of the eye in the horizontal plane) this muscle was also recorded while fictive locomotion was evoked through the stimulation of either the dorsal, sacral (Figure 1, C1) or cervical roots. In this figure, the stimulation of the sensory afferences of the sacral S1 activated the lumbar locomotor CPGs causing a rhythmic and coordinated discharge of the motor lumbar nerves. This rhythmic fictive locomotor pattern consisted in a paired discharge between ipsilateral Vr, in this case right L5 and left C8, as well as the alternated discharge of the ipsilateral Vr, right L5 and right C8. (Figure 1, C2, orange/yellow and blue traces). Coupled rhythmic discharges were observed between the motor activities of the locomotor Vr and the abducens nerves all along the fictive locomotion episodes. The discharge bursts of an abducens nerve were synchronized with the ipsilateral cervical root and with the contralateral lumbar root. Hence, here the presence of a spino-extraocular coupling that resembles the one observed in xenopus tadpoles during fictive swimming is confirmed *in vitro*.

The spino-extraocular efferent copy pathway is ipsilateral and monosynaptic

In order to further characterize the spino-extraocular command, the discharge relation between the spinal and abducens nerves was quantified (Figure 2A1 and 2A2). The frequency of discharge of the spinal and abducens nerves were significantly correlated (Figure 2 A3: red- C8 vs Abd: R = 0,9528, Spearman test, p <0,001 n = 7; green- L2 vs Abd: R = 0,9487, Spearman test, n = 7; blue- L5 vs Abd: R = 0,9429, Pearson test, n= 3) and there is a linear correlation between both responses (Figure 2 A4: red- C8 vs Abd: R^2 = 0,9294, s= 0,04061; green-L2 vs Abd: R^2 = 0,9073, s = 0,05867; blue- L5 vs Abd R^2 = 0,8891, s = 0,04479). The analysis of the phase relationships (Figure 2B) confirms that the discharge bursts of the abducens were in phase with the bursts of the ventral ipsilateral root C8 (μ = 354,25 ± 1,44; r= 0,897, n= 7), as well as with the bursts of the L2 ventral ipsilateral root (μ= 357,48 ± 2,16; r= 0,936, n= 8) and ipsilateral L5 (μ= 3,96 ± 3,6; r = 0,961, n = 3). Inversely, the same bursts were in phase opposition with

the contralateral C8 (μ = 168,12 ± 19,44; r = 0,930, n = 7), contralateral L2 (μ = 170,64 ± 0,01; r = 0897, n = 6) and ipsilateral L5 (μ = 198 ± 5,04; r = 0,868, n = 3). Furthermore, the activity bursts of the abducens nerve showed a weak latency (65,5 ± 6,1 ms) with the burst of the ventral roots of the spinal cord they were in phase with. Conversely, the same abducens discharge showed a significantly longer latency (755,5 ± 18,6, Mann–Whitney test, $p < 0.01$, n = 10) with the ventral roots with which it was out of phase (Figure 2C). This relatively small latency time between the discharge of the abducens and the ipsilateral spinal Vr is compatible with a mostly monosynaptic connection, like the one previously demonstrated in the Xenopus tadpole.

To reveal the pathway connecting spinal CPG and oculomotor nuclei, rabies virus (RV) transsynaptic retrograde infection was used (Figure 2D). Since it is the abducens nerve that drives the contraction of the lateral rectus (LR) muscle, to verify the success of the viral injections, a double immunohistochemical detection of RV and ChAT (a motoneurons marker) was performed on brainstem slices to confirm the infection of MNs in the nucleus abducens (Figures 2 E1 and E2). Neurons with bright somata were counted in each structure in one series out of two. Abducens MNs simultaneously RV+ and ChAT+ were found in all mice (n=3), ipsilateral to the injection site (left lateral rectus muscle). To further verify that the stated MNs were the only gateway for RV propagation, MNs innervating other eye muscles were systematically checked for no RV+ neurons as well as brainstem premotor interneurons in the afferent to abducens MNs. This guaranteed that the RV labeled neurons were specifically the ones innervating the left LR. To ensure that only the neurons with a monosynaptic connection were detected, the timeframe of the RV transfer from the abducens MNs to the cervical was determined. To further characterize the connection and organization of the neurons responsible for conveying the efferent copy, abducens motoneurons and spinal interneurons were counted all along spinal cord (Figure 2E). On average, 1 infected abducens MN rendered 6 infected neurons in the cervical (Figure 2F). Viral labeling was observed all along the cervical spinal cord, both on the rostro-caudal axis and in the transverse plane. The segments with higher neuronal infection density were C7-C8, with a mean of 5 neurons, distributed ipsilaterally, per slice. However, from C2-C6 and C8 there was a predominance of ipsilateral infection to the injection site (68%). The neurons were mainly distributed on the cervical ventral horn and around the central canal. Some neurons around the central canal were simultaneously RV and ChAT positive (Figure 2 E5). While all segments from the cervical to the lumbar spinal cord were analyzed, only the cervical had infected motoneurons. It is important to note that this doesn’t exclude the possibility of a lumbar-extraocular direct coupling since the RV tropism could be here a limiting

354 factor. Globally, these results show for the first time a direct monosynaptic connection
355 from the cervical spinal cord to the abducens nucleus.

356 *The efferent copy depends on an intact cervical relay*

357 In order to investigate the relative contribution of the two locomotor CPGs, the
358 relationships between limb and eye movement were studied in the semi-intact and in
359 vitro preparations. The instantaneous frequency of the horizontal eye movements is
360 better correlated to the forepaw instantaneous frequency (R=0.400) than to the hind paw
361 instantaneous frequency (R=0.26). Interestingly, forepaw movements were always
362 accompanied by eye movements whereas eye movements were possible without hind
363 paw movements (see zero values on the Y axis, figure 3A2). Moreover, the decerebrated
364 preparation showed a strong correlation between the locomotor cycle and the timing of
365 the eye movement (Figure 3B). We therefore compared the duration of the front limb
366 stance/swing and slow/quick phases. The duration of the swing appears to be more
367 closely related to the duration of the quick phase. Overall, these results suggest that in
368 the decerebrated preparation, eye movements are consistently observed in relation to
369 forepaw, rather than hind paw movements. The projection of the forepaw forward (swing)
370 is synchronized with the projection of the eye (quick-phase) while the swing phase
371 corresponds to the slow, compensatory phase of the eye movement.

372 The respective influence of the spinal and lumbar locomotor CPGs on the extraocular
373 nuclei was next studied *in vitro*. To do so, locomotor networks were first studied in a split-
374 bath configuration that allowed to reversibly isolate the brainstem from different regions
375 of the spinal cord. The putative direct connection between the lumbar locomotor network
376 and the abducens motoneurons was studied by interrupting the activity of the cervical
377 locomotor network (Figure 3 C). The application of a physiological solution without
378 calcium (0 Ca^{2+} mM) in a reversible and selective manner in the cervical spinal cord
379 enabled to interrupt all the synaptic connections in this region. Blocking the activity of the
380 cervical spinal locomotor network removed all the motor discharges of the C7 Vr as well
381 as the activity of the abducens. During this inhibition, the motor activity of the L2
382 persisted, since it was immersed in a standard physiological liquid. When the no calcium
383 solution was washed away and the cervical cord was re-exposed to a standard
384 physiological solution, even if a bit altered by the previous exposure, the synaptic
385 connections and activity in the abducens were re-established. This result shows that
386 there is no direct connection between the lumbar locomotor network and the abducens
387 motoneurons and that the efferent copy passes through the cervical locomotor network.
388 This constitutes a necessary relay for the efferent copy to reach the extraocular structure.

This result also suggests that the efferent copy could potentially originate from the locomotor circuits of the cervical region.

The cervical locomotor network, more than the lumbar, seems responsible for the coupling between the spinal motor roots and the extraocular motor nerves. The motor coupling between the abducens and spinal nerves was then studied by a transverse section of the thoracic spinal cord. This section allowed cutting the coupling between the lumbar and cervical locomotor networks while minimally affected their activities. When the lumbar and cervical were independently stimulated after the transection on the thoracic spinal cord, the motor activities of the cervical and lumbar Rvs were conserved. Moreover, the spino-extraocular motor coupling between the cervical ventral roots and the abducens motoneurons persisted after the section of the thoracic spinal cord. The mean absolute latency between the discharges of the left C8 motor nerve and the left abducens was not significantly different after the section either (t test, $p > 0,05$ (p-value = 0,1038), n =3). However, the locomotor frequency was significantly lowered after the section (-0,24 Hz ± 0,1; Mann-Whitney test, p-value < 0,0001); this decrease could be explained by the damaging of the spine after the section. Despite this fact, the frequency of discharge of the abducens was linearly correlated with the ventral spinal C8 before (R =0,9817, Pearson test, p <0,001 n = 3 ; $R2$ = 0,9637, s = 0,03399) and after the section (R = 0,9983, Pearson test, n =3 ; $R2$ = 0,9966, s = 0,002200).

Overall, these experiments show that there is no evidence for a direct lumbar-extraocular connection. These results demonstrate that the spino-ocular command is dependent of the cervical spinal cord, that is either relaying or generating the efferent copy that tightly couples the locomotion and eye movements.

Discussion

This study demonstrates for the first time the existence a spino-extraocular locomotor efference copy in mice. Such motor-to-motor coupling had been previously proven in the Xenopus tadpole, where it was shown to produce conjugated eye movements that compensate for the tail's undulation during swimming (Bacqué-Cazenave et al., 2018; Combes et al., 2008; Lambert et al., 2012). The presence of this efferent copy of the locomotor pattern in both amphibians and mammals reveals that this gaze stabilization strategy is well preserved in phylogeny, emphasizing the importance of maintaining visual acuity during locomotion in vertebrates.

The discussion segment of this paper is currently in preparation. Please see the discussion (chapter IV; Mice in motion: gaze stabilization during locomotion) of the thesis manuscript for some of the topics that will be here included.

Figure Legends

Figure 1. Existence of a CPG-driven efferent copy in mice. **A-** Depiction of the set up used for recording eye movements in decerebrated mice. **A1**- Left (blue) and right (red) eye horizontal movements coupled to the swing (blue bars) and stance (black bars) phases of the locomotor cycles performed for 30 seconds. **A2**- Right- Instantaneous frequencies of the forepaw (x axis) and hind paw (y axis) movements. Left- polar plot of the phase coupling between forepaw and hind paw frequency. **A3**- Amplitude (left panel) and velocity (right panel) of the recorded eye movements (occurrence) of all the robust preparations (n=6). **B**- Segment (8 seconds) of the raw eye movement traces in the vertical and horizontal plane. **B2**- Oculograms of the right (blue) and left (red) eyes illustrating the magnitudes (in degrees) of the vertical (y axis) and horizontal (x axis) positions. **C**- Isolated brainstem and spinal cord *in vitro* preparation of neonatal mice with the stimulation and recording electrodes. **C1**- Simultaneous recording of the activities of the left (red) and right (blue) abducens nerves (CN VI), the 8^{th} cervical roots (right C8-green, left C8-yellow) and the 5^{th} lumbar ventral root (right L5, orange) during a fictive locomotion episode produced by the stimulation of the lumbar S1. **C2**- Mean discharge of the recorded nerves during a fictive locomotor cycle. The activity of the right abducens (blue) is in phase with the locomotor activities of the right C8 (green) and in phase opposition with right L5(orange) and left C8 (yellow). The pattern is inverted for the activity of the left abducens-

Figure 2. The spino-extraocular efferent copy pathway is ipsilateral and monosynaptic. A1- Schematic of the stimulated and recorded nerves in the brainstem and spinal cord preparation of new-born mice. **A2**- Linear regressions of the frequencies of the discharge of the abducens in regard to the frequency of discharge of motor ventral roots. **A3**- the frequency of discharge of the abducens were strongly correlated to the C8, L2 and L5 ventral roots during fictive locomotion episodes. **A4**- the frequencies f activity of the abducens were linearly correlated to the discharge of C8, L2 and L5. **B**- Circular plots of the phase relationships between the different ventral roots and the abducens, allowing a phase analysis of the spino-extraocular coupling. **C**- Mean latency time between the ventral roots and the abducens nerves. The mean absolute latency between the discharge of the abducens and the ipsilateral C8 and L2 and contralateral L5 was weak and significatively inferior to the mean latency time between the abducens an the contralateral C8, L2 and contralateral L5. **D**-Depiction of the rabies virus injections

protocol in the lateral rectus extraocular muscle where the virus was left for 55h to migrate and reached approximately 7000µm down the cervical. **E**- Images of the RV+ neurons in different sections of the spinal cord. **F**- Neurons were counted and their location was pointed (red dots) in the different segments of the cervical spinal cord. **G**- Number of infected abducens motoneurons (x axis) and the consequently infected interneurons (y axis) in the cervical. **H**- Number of infected interneurons per each cervical segment.

Figure 3. Cervical dominance of the spino-extraocular efference copy. A and **B-** Relationship between the limb and eye horizontal movements of the decerebrated preparation. **A1-** Instantaneous step frequency between the forepaw and the horizontal eye movements. The absence of data points in the x axis (eye horizontal IF) demonstrated that forepaw movements were needed to evoke horizontal eye movements. **A2-** The correlation (R=0.400) was higher between forepaw and eye movements than between hind paw and eye movements (R=0.26). **B1-** Example traces of eye movements in regard to the phase of the locomotor cycle (grey bars- swing; white bars- stance). The slow phase appears to be occurring simultaneously to the stance and the quick phase seems paired to the swing. **B2**- Relationship between the duration of the locomotor cycle and the quick/slow eye phase. Red- stance and the slow phase of the eye movements and Blue- swing and quick phase of the eye movements. **C-** Split bath configuration that enabled the 0 Ca2+ experiments. Recordings of the spontaneous activities of the right abducens (blue) and the C7 (green), L2 (grey), L5 (orange) during fictive locomotion episodes. **D-** Mean discharge during a fictive locomotor cycle of the different nerves recorded in the control condition (left), in the presence of a 0Ca2+ aCSF (middle) and after washout (right). **E-** Mid-thoracic cut experiments; spontaneous activities of the abducens nerves and the C8 and L2 ventral roots. **F-** Linear regression of the frequencies of discharge of the abducens and C8 before and after the thoracic cut. **G-** Polar plots of the phase relationships between the C8 and abducens. **H**- Mean latency between the spinal ventral roots and the abducens nerves before and after the section.

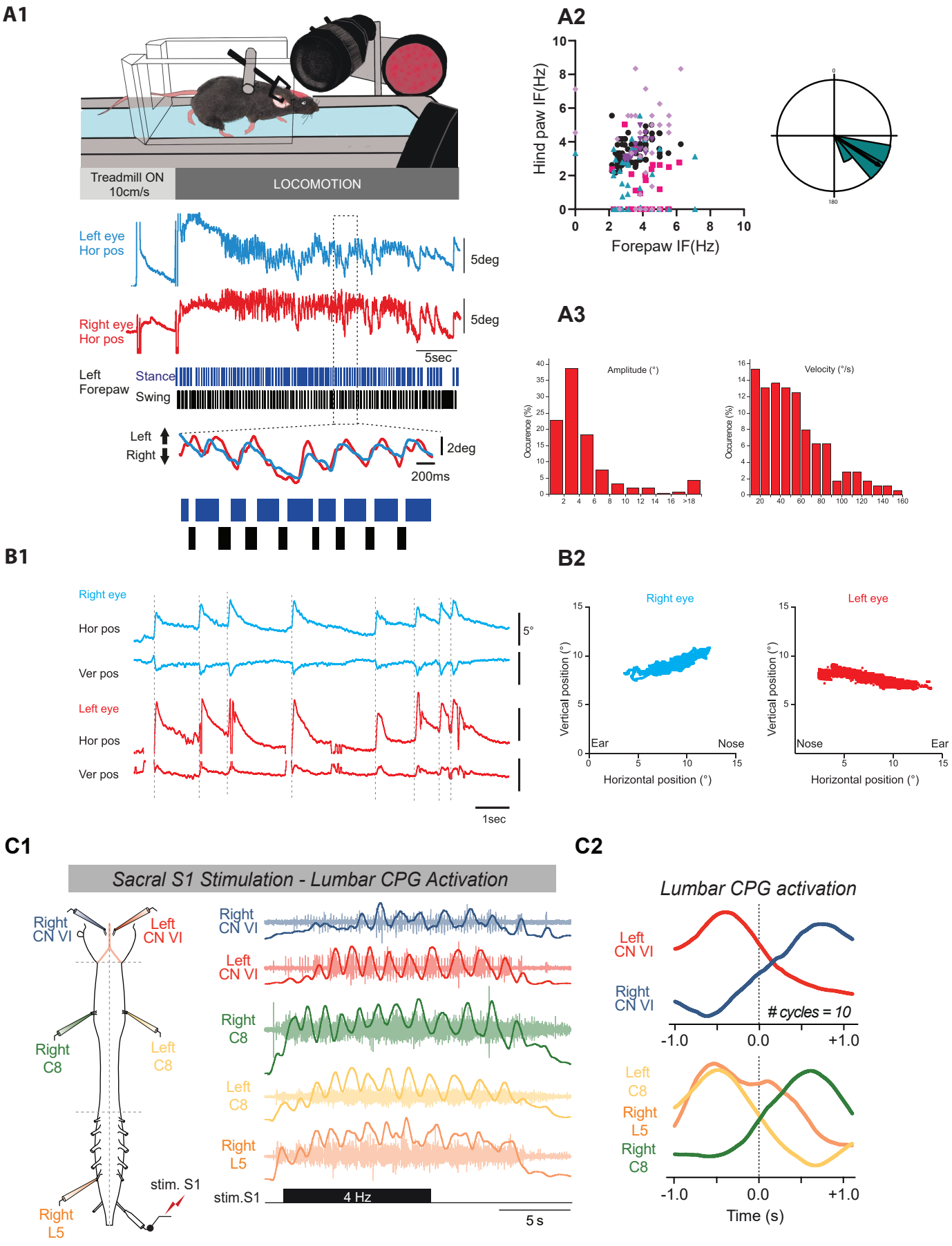

Figure 1. Existence of a CPG-driven efferent copy

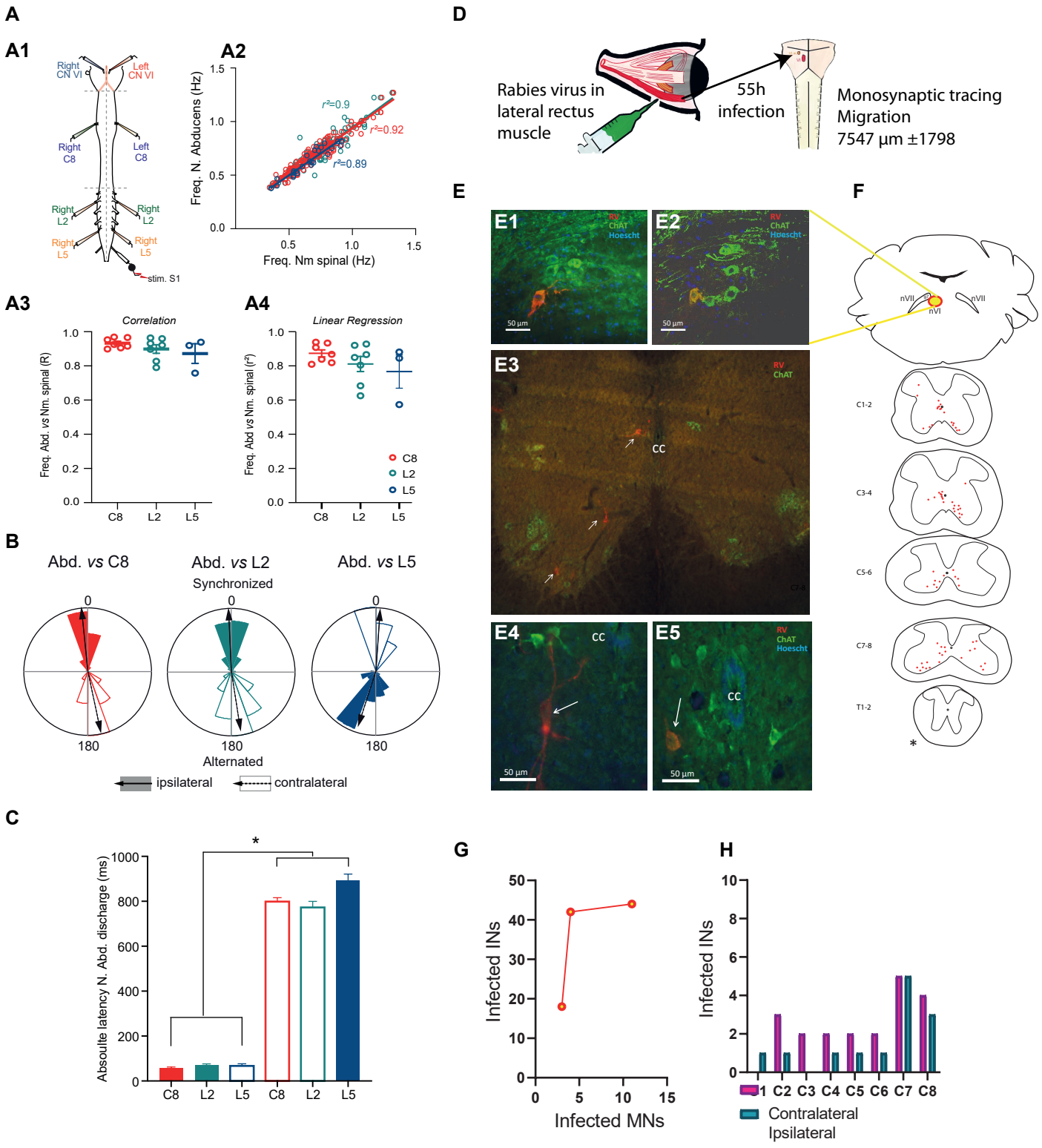

Figure 2. The spino-extraocular efferent copy pathway is ipsilateral and monosynaptic

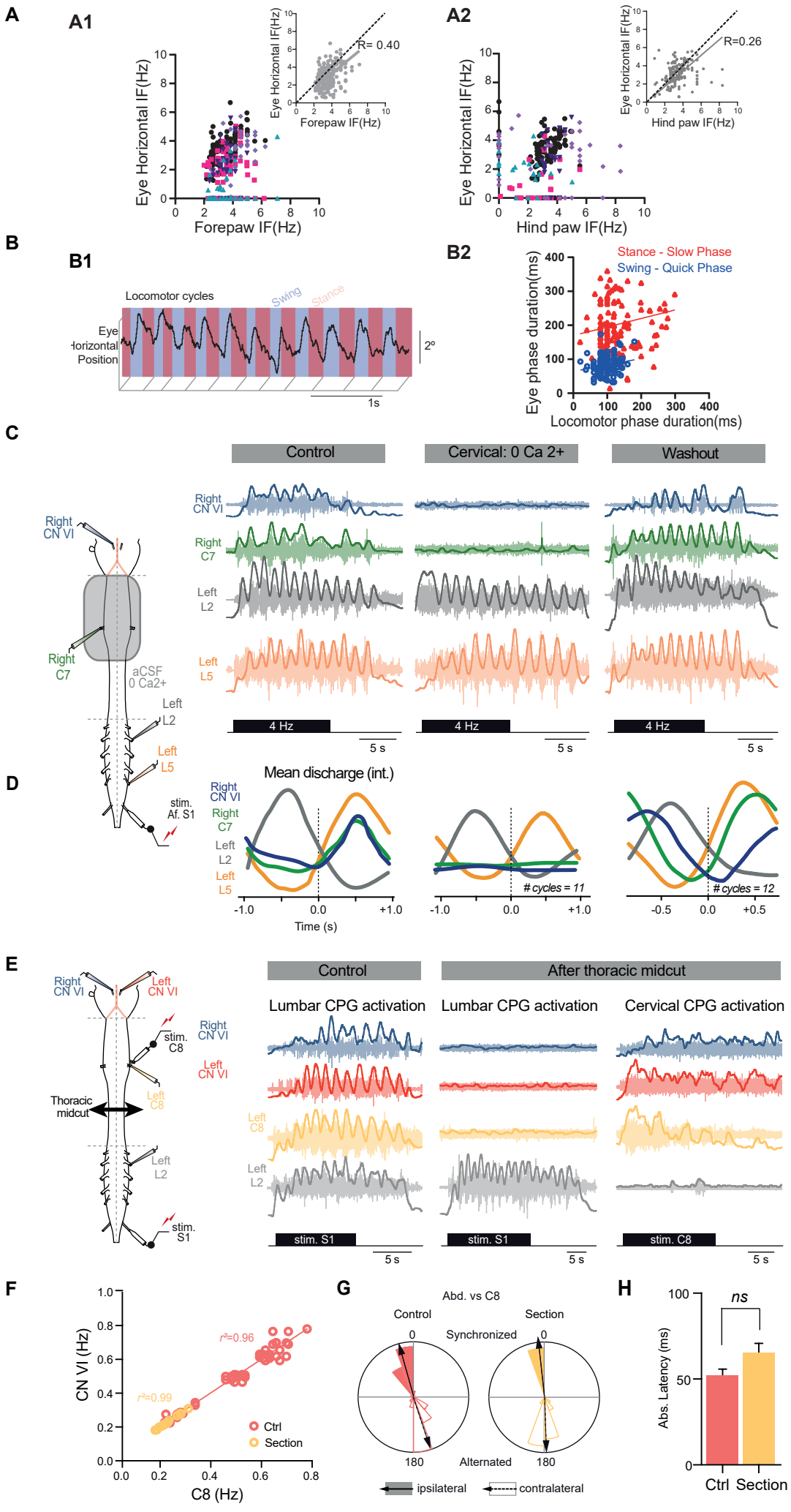

Figure 3. Cervical dominance of the spino-extraocular efference copy.

Article 5. Local gene therapy durably restores vestibular function in a mouse model of Usher syndrome type 1G

The present paper was a collaboration with the *Institut Pasteur, Genetics & Physiology of Hearing team*.

The Usher syndrome is one of the most common inherited (autosomal recessive; prevalence up to 1/10.000) pathologies simultaneously affecting vision, audition and balance (El-Amraoui & Petit, 2014). There are 3 types of Usher syndrome but the most common and the one that has the strongest vestibular impairments is type 1. Specifically, patients with USH1 suffer from congenital profound deafness and vestibular dysfunction and later in life, blindness. Naturally, the progressive visual loss is accompanied by an increase in the severeness of the vestibular symptoms because vision participates to balance.

Mutations of the USH1 gene affect the hair bundle morphogenesis and tip-link maintenance overall in the inner ear (Friedman et al., 2005). Tip links are actin filaments that join the tips of the smaller stereocilia to the body of neighboring bigger ones. They have a key role in the synaptic message generation since they regulate the mechanoelectrical transduction (MET) channels at the summit of the smaller stereocilia. When motion bends the tip link towards the stereocilia, the tension on the tip link increases resulting in the opening of the MET channels, depolarization of the hair cell and consequent increase of the firing rate of the vestibular nerve. Contrarily, if the stereocilia are dragged away from the kinocilium the tip link reduces its tension which will close the MET channel. Thus, hyperpolarizing the hair cell, closing the Ca2+ channels and decreasing the firing rate of vestibular afferents. When tip links are missing or defective, the vestibular synaptic message can’t be generated. Sans proteins are one of three USH1 proteins that anchor tip links to the stereocilia (El-Amraoui & Petit, 2014).

Despite being a very common medical complaint, the treatment that patients with vertigo receive can be inappropriate or inadequate (Bittar et al., 2013). In the case of Usher1, there is currently no available cure, only the auditory symptoms are treated with a cochlear implant and the success is variable from one patient to another. Research laboratories are now focusing on resolving this issue by using the latest technologies available, like adenoassociated virus (AAV)-mediated gene transfer. Inner ear is an area that can specifically and be safely targeted with injections due to its relative isolation and systemic dissemination. Additionally, due to the similarity between the anatomy of the

inner ear and vestibular system between mice and humans, these tools could serve as potential USH1 patients. Even though AAV-mediated gene transfer is currently being tested in patients with Parkinson's and retinal diseases, they have not yet been used in inner ear disorders (Hudry & Vandenberghe, 2019).

AAVs are currently rising as the gene therapy tool of choice. It was first identified because it often contaminated laboratory adenovirus preparations, hence its designation. AAVs belong to the *Parvoviridae* family and consist in a non-enveloped (no phospholipid coat) icosahedral protein capsid surrounding and carrying a small (4.8 kilo bases in length) single-stranded DNA (Naso et al., 2017). For its successful replication, it requires co-infection by a helper virus like adenovirus or herpes virus. In this study the murine cDNA, sans, corresponding to the spliced transcript of Ush1g together with the cDNA sequence of the GFP was inserted into AAV8 capsid. The fluorescent reported was added so the. AAV are endemic in humans and has a very low pathogenicity with a very mild immune response.

In our study, AAV-mediated gene therapy was aimed at restoring *sans* proteins, submembrane scaffold proteins involved in the delivery of cDNA. Sans proteins are key in the maintenance of hair cell bundles and tip-links and are one of the main affected proteins in this pathology. Since these proteins are ubiquitous in the neuroepithelia of the inner ear, restoring them would not only treat deafness but also regain the vestibular functions that are impaired in this disease.

After the delivery of the sans cDNA by AAV8 in newborn mice, the effects on both the auditory and vestibular system were tested in adult mice. The first test performed was on the hearing responses which demonstrated a partial hearing rescue (5-15kHz). However, the question of whether the vestibular function was restored remained open. Mice demonstrated an improved locomotor behavior, but not vestibular specific tests had been performed. Our team tackled this question by phenotyping the complete vestibular endorgans with the use of video-oculography. The semicircular canals were evaluated using the vestibulo-ocular reflex (VOR) test and the otolithic organs by the maculo-ocular reflex (MOR) responses in both USH1$^{-/-}$, treated USH1$^{-/-}$ and control mice (total of 15 mice, 5 *per* group). The off vertical axis rotation (OVAR) test served to evaluate the detection of linear acceleration by the otolithic organs. The OVAR tests require the turntable to be 17º tilted in respect to the vertical axis and consists in rotations at a constant speed at clockwise and counterclockwise directions. The first few rotations provoke both canalar and otolithic responses but only the otolithic component remains

after that and allow to isolate the response of the macula to the acceleration (Mathieu Beraneck et al., 2012).

It was striking to register the complete absence of compensatory eye movements in USH1$^{-/-}$ mice during all the range of performed tests: VOR (30º/s at 0.1 – 2Hz) and OVAR (50 º/s). From the treated USH1$^{-/-}$ group, 2/5 of the mice had fully recovered both otolithic and canalar responses and 3/5 had fully recovered semicircular but not otolithic responses. Interestingly, injected mice received treatment at P3 and were only tested for vestibular (and auditory) responses 10-12 months after. Thus, showing that the treatment, besides being efficient, is durable. Our contribution in this article was essential as it provided the definitive quantitative evidence of the behavioral recovery specific of the vestibular function, and therefore of the efficacy of the treatment.

Several AAV-mediated therapies have currently ongoing clinical trials to potentially cure several diseases, for example, neuromuscular and (Aguti et al., 2018) neurodegenerative disorders (Hudry & Vandenberghe, 2019). However, inner ear diseases aren’t yet on that list. Studies like this could represent hope for AAV-mediated treatments becoming recurring tools for curing inner ear diseases.

Local gene therapy durably restores vestibular function in a mouse model of Usher syndrome type 1G

Alice Emptoz[a,b,c], Vincent Michel[a,b,c], Andrea Lelli[a,b,c], Omar Akil[d], Jacques Boutet de Monvel[a,b,c], Ghizlene Lahlou[a,b,c], Anaïs Meyer[a,b], Typhaine Dupont[a,b,c], Sylvie Nouaille[a,b,c], Elody Ey[e], Filipa Franca de Barros[f], Mathieu Beraneck[f], Didier Dulon[g], Jean-Pierre Hardelin[a,b,c], Lawrence Lustig[h], Paul Avan[i], Christine Petit[a,b,c,j,1,2], and Saaid Safieddine[a,b,c,1,2]

[a]INSERM, UMR 1120, Paris, France; [b]Génétique et Physiologie de l'Audition, Institut Pasteur, 75015 Paris, France; [c]Complexité du Vivant, Sorbonne Universités, Université Pierre-et-Marie-Curie, Université Paris VI, 75015 Paris, France; [d]Otolaryngology-Head & Neck Surgery, University of California, San Francisco, CA 94117; [e]Unité de Génétique Humaine et Fonctions Cognitives, Institut Pasteur, CNRS UMR 3571, 75015 Paris, France; [f]Centre de Neurophysique, Physiologie, et Pathologie, CNRS UMR 8119, Université Paris-Descartes, 75006 Paris, France; [g]Laboratoire de Neurophysiologie de la Synapse Auditive, Bordeaux Neurocampus, INSERM, UMR 1120, Université de Bordeaux, 33076 Bordeaux, France; [h]Columbia University School of Medicine and New York Presbyterian Hospital, New York, NY 10034; [i]Laboratoire de Biophysique Sensorielle, Faculté de Médecine, Université d'Auvergne, Biophysique Médicale, Centre Jean Perrin, 63000 Clermont-Ferrand, France; and [j]Collège de France, 75005 Paris, France

Contributed by Christine Petit, July 27, 2017 (sent for review June 26, 2017; reviewed by Karen B. Avraham and Deniz Dalkara)

Our understanding of the mechanisms underlying inherited forms of inner ear deficits has considerably improved during the past 20 y, but we are still far from curative treatments. We investigated gene replacement as a strategy for restoring inner ear functions in a mouse model of Usher syndrome type 1G, characterized by congenital profound deafness and balance disorders. These mice lack the scaffold protein sans, which is involved both in the morphogenesis of the stereociliary bundle, the sensory antenna of inner ear hair cells, and in the mechanoelectrical transduction process. We show that a single delivery of the sans cDNA by the adenoassociated virus 8 to the inner ear of newborn mutant mice reestablishes the expression and targeting of the protein to the tips of stereocilia. The therapeutic gene restores the architecture and mechanosensitivity of stereociliary bundles, improves hearing thresholds, and durably rescues these mice from the balance defects. Our results open up new perspectives for efficient gene therapy of cochlear and vestibular disorders by showing that even severe dysmorphogenesis of stereociliary bundles can be corrected.

gene | therapy | balance | mouse | Usher

Patients affected by both sensorineuronal hearing impairment and balance disorders due to inner ear defects are currently fitted with auditory prostheses (hearing aids or cochlear implants) and can benefit from balance rehabilitation therapy, but the outcomes are different from one patient to another. Some individuals with congenital profound deafness are able to have phone conversations thanks to cochlear implants, whereas others obtain little or no benefit from these devices, beyond becoming aware of environmental sounds (1, 2). Such variability has been reported in patients with Usher syndrome type 1 (USH1) (Online Mendelian Inheritance in Man no. 276900) (3, 4). Patients with USH1 suffer from congenital profound deafness and balance defects, and they subsequently undergo sight loss leading to blindness. The loss of visual input impedes lip reading and greatly limits vestibular defect compensation.

We tested local gene replacement as an alternative approach to cure deafness and balance disorders of USH1. The anatomy of the human inner ear is suitable for gene therapy. Its relatively isolated fluid-filled compartments allow one to deliver recombinant viral particles locally while minimizing the risk of systemic dissemination. The inner ear contains the hearing organ (the cochlea) and five vestibular end organs devoted to equilibration (the utricle and saccule, which detect linear acceleration, and three semicircular canals, each housing an ampulla, which detect angular accelerations of head rotation) (Fig. 1*A*). Sound and acceleration are detected by the mechanosensory receptor cells (hair cells) through deflection of their hair bundles, an array of modified microvilli known as stereocilia, organized into rows of graduated heights forming a staircase pattern. The tip link, a fibrous link connecting the tip of each transducing stereocilium to the side of its taller neighbor, gates the mechanoelectrical transduction channel(s) located at the tip of the shorter stereocilium (Fig. 2*A*). Mutations of USH1 genes affect hair bundle morphogenesis and tip-link maintenance in the inner ear hair cells (5).

Adenoassociated virus (AAV)-mediated gene transfer has emerged as a promising strategy for treating hereditary diseases (6, 7). AAV vectors have different cell tropisms, and can mediate high levels of transgene expression. These properties have led to their use in preclinical and clinical trials for several inherited disorders, including genetic forms of Parkinson's disease, metabolic disorders, and retinal diseases, but they have not yet been used for inner ear diseases (6–10). Various viral vectors containing *GFP* as a reporter gene have been shown to transduce inner ear hair cells (11–15), and several studies have investigated the use of gene therapy to restore hearing and balance in animal models, with different degrees of success. However, to date, partial hearing improvement was only obtained for mouse models without severe dysmorphogenesis of the inner ear hair cells (16–22). Here, we focused on the genetic form of USH1 caused by mutations of *USH1G*, encoding the submembrane scaffold protein sans (23, 24). *Ush1g*$^{-/-}$ mutant mice display profound deafness and vestibular dysfunction, characterized by circling behavior and head

Significance

Hearing and balance impairments are major concerns and a serious burden for public health, but still lack an effective curative therapy. We assessed inner ear functions in a mouse model of Usher syndrome type 1, a developmental disorder characterized by profound congenital deafness and balance deficit, after local gene therapy. Viral transfer of the wild-type cDNA to the inner ear of the mutant mice shortly after birth resulted in a partial restoration of hearing and a long-lasting, almost complete, removal of the balance defect. The present results provide a basis for future clinical trials in humans.

Author contributions: C.P. and S.S. designed research; A.E., V.M., A.L., O.A., J.B.d.M., G.L., A.M., T.D., S.N., F.F.d.B., M.B., D.D., L.L., P.A., and S.S. performed research; C.P. and S.S. contributed new reagents/analytic tools; A.E., V.M., J.B.d.M., E.E., and S.S. analyzed data; and A.E., V.M., J.B.d.M., J.-P.H., C.P., and S.S. wrote the paper.

Reviewers: K.B.A., Tel Aviv University; and D.D., Université Pierre-et-Marie-Curie.

Conflict of interest statement: A patent involving A.E., C.P., and S.S. (PCT/EP2016/053613) has been deposited by the Institut Pasteur, INSERM, and CNRS.

Freely available online through the PNAS open access option.

[1]C.P. and S.S. contributed equally to this work.

[2]To whom correspondence may be addressed. Email: christine.petit@pasteur.fr or saaid.safieddine@pasteur.fr.

This article contains supporting information online at www.pnas.org/lookup/suppl/doi:10.1073/pnas.1708894114/-/DCSupplemental.

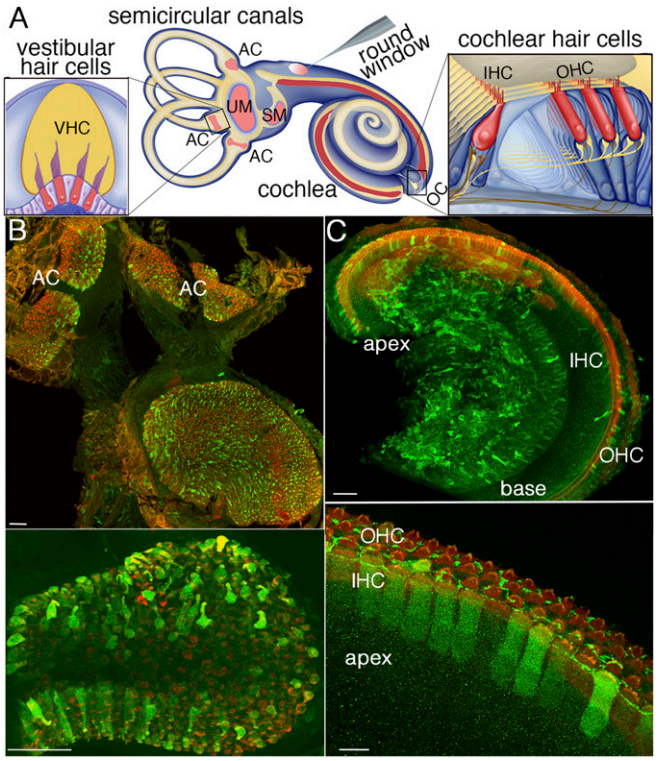

Fig. 1. AAV8 vector (Penn Vector Core) transduces vestibular and cochlear hair cells with different efficiencies. (*A*) Diagram of the mouse inner ear and viral injection through the round window of the cochlea. The vestibular sensory epithelia [AC, ampullar crista(e) of the three semicircular canals; SM, saccular macula; UM, utricular macula] and cochlear sensory epithelium (OC, organ of Corti) are drawn in pink and in red, respectively. Details of an AC and the OC are presented on the left side and right side of this diagram, respectively, with the hair cells (IHCs, OHCs, and VHCs) drawn in red. The AAV8-*Sans-IRES-GFP* (Penn Vector Core) recombinant virus injected through the cochlear round window of a mouse on P2.5 transduces the vast majority of VHCs (*B*, *Upper*) and transduces cochlear IHCs and OHCs more efficiently in the apical region than in the basal region of the cochlea (*C*, *Upper*), as shown by the GFP labeling (green) on P8.5. All hair cells are stained red by an anti-myosin VI antibody. Higher magnification views of the AC (*B*, *Lower*) and the OC (*C*, *Lower*) from the cochlear apical region are shown. (Scale bars: *Upper*, 50 μm; *Lower*, 10 μm.)

tossing. The hair bundles of their cochlear hair cells and vestibular hair cells (VHCs) undergo abnormal morphogenesis and lack functional tip links (24, 25). We explored the feasibility, reliability, and long-term efficacy of local gene therapy in these mice.

Results

Viral cDNA Transfer Restores Sans Expression and Targeting in Cochlear and VHCs of *Ush1g*$^{-/-}$ Mice. A number of AAV serotypes and over 100 naturally occurring AAV variants have been isolated from adenovirus stocks or from human/nonhuman primate tissues. They display different cell tropisms (14), but there are some discrepancies in their reported transduction efficiencies and cell tropisms in the inner ear (26–29). We thus investigated the ability of several AAV vectors to transduce the inner ear hair cells. We tested recombinant AAV1, AAV2, AAV5, and AAV8 vectors containing the green fluorescent protein (GFP) reporter gene driven by a hybrid promoter (CAG) consisting of the CMV enhancer fused to the chicken β-actin gene promoter. A single viral injection through the round window membrane separating the middle ear from the inner ear was performed in C57BL/6 wild-type mice on postnatal day 2.5 (P2.5) (Fig. 1*A*). The sensory epithelium of the cochlea (organ of Corti) and the vestibular end organs were microdissected on P8.5, and immunolabeled for otoferlin or myosin VI to visualize the inner ear hair cells, as well as for GFP. These recombinant AAV vectors transduced the inner ear cell types with different cell tropisms and transduction rates. In the cochlea, AAV1 (SignaGen) and AAV2 and AAV5 (Penn Vector Core) mostly transduced supporting cells of the organ of Corti, namely, Deiters' cells and inner phalangeal cells (Fig. S1 *A*–*C*). AAV8 from SignaGen (with the CAG promoter) mainly transduced cochlear ganglion neurons (Fig. S1*D*), whereas AAV8 from Penn Vector Core (with the same promoter) efficiently transduced hair cells and supporting cells (Fig. S1*E*). There are two types of cochlear hair cells: the inner hair cells (IHCs), which are the genuine auditory sensory cells that transmit the encoded sensory signal to the central nervous system, and the outer hair cells (OHCs), which function as fine-tuned amplifiers of the sound stimulus (30) (Fig. 1*A*). After injection of AAV8 from Penn Vector Core, more IHCs expressed GFP at the apex of the cochlea (84 ± 3%) than at the base (40% ± 0.5%), whereas OHCs were transduced with roughly the same efficiency at the base (28 ± 3%) and at the apex (24 ± 2%) (n = 23 mice; Fig. S1 *E* and *F*). Surgery and intracochlear injection of the virus did not affect auditory brainstem responses (ABRs) tested from 2 to 12 wk after injection (see Fig. 4*A* and Fig. S4; Mann–Whitney test, P = 0.7).

We then investigated the efficiency with which the recombinant AAV8-*Sans*-internal ribosome entry site (*IRES*)-*GFP* virus (Penn Vector Core) containing the murine cDNA *Sans*, encoding the unique spliced transcript of *Ush1g*, transduced inner ear hair cells. *Ush1g*$^{+/-}$ mice were injected with the recombinant virus on P2.5, and 6 d later, the sensory epithelia of the cochlea and vestibular end organs were microdissected and immunolabeled either for GFP and myosin VI or for GFP and sans. The hair cell transduction efficacy of AAV8-*Sans-IRES-GFP* was similar to that of AAV8-*GFP* (Fig. 1 *B* and *C*). The rate of IHC transduction (i.e., *GFP*-expressing IHCs) was 87 ± 4% at the cochlear apex, gradually decreasing to 45 ± 6% at the cochlear base, and the rate of OHC transduction was 33 ± 6% at the apex, gradually decreasing to 25 ± 5% at the base (n = 24 mice; Fig. 1*C*). Surprisingly, in the vestibular end organs of the injected ears, the hair cells were transduced at a much higher rate, 91 ± 24% (n = 17 mice; Fig. 1*B*). Moreover, the injection of AAV8-*Sans-IRES-GFP* into the cochlea of *Ush1g*$^{-/-}$ mice restored a normal targeting of the sans protein to the tips of the stereocilia of transduced IHCs, OHCs, and VHCs on P8.5 (24, 25) (Fig. 2).

Viral Transfer of the *Sans* cDNA to the Hair Cells Rescues *Ush1g*$^{-/-}$ Mice from Hair Bundle Defects. From embryonic day 17.5 (E17.5) onward, cochlear hair cells of *Ush1g*$^{-/-}$ mice display fragmented hair bundles with reduced numbers of stereocilia and mispositioned kinocilia (24, 25), and nearly all VHCs have collapsed hair bundles. The degeneration of the middle and short rows of stereocilia in IHCs and OHCs and the collapse of the VHC hair bundles are even more pronounced at P2.5 (Fig. 3*A* and Fig. S2). We investigated whether the viral expression of the *Sans* cDNA in the hair cells rescued the mice from these defects by scanning electron microscopy analysis. In the injected *Ush1g*$^{-/-}$ mice, the vast majority of hair bundles of IHCs, OHCs of the cochlear apex, and VHCs displayed a typical staircase pattern (81 ± 3% for cochlear hair cells, n = 72 cells and 70 ± 1% for VHCs, n = 304 cells from 10 mice). Notably, the stereocilia of the short and middle rows in most IHCs (93 ± 2%, n = 27 cells) and OHCs (68 ± 5%, n = 55 cells) in the apical region of the injected cochlea had prolate tips pointing toward their taller neighbors, just like in *Ush1g*$^{+/-}$ control mice. The stereocilia tips of most VHCs had their characteristic prolate shape too. Prolate tips are considered a hallmark of the presence of functional tip links resulting from the pulling force exerted by these links on the tips of the stereocilia (31). By contrast, the stereocilia tips had

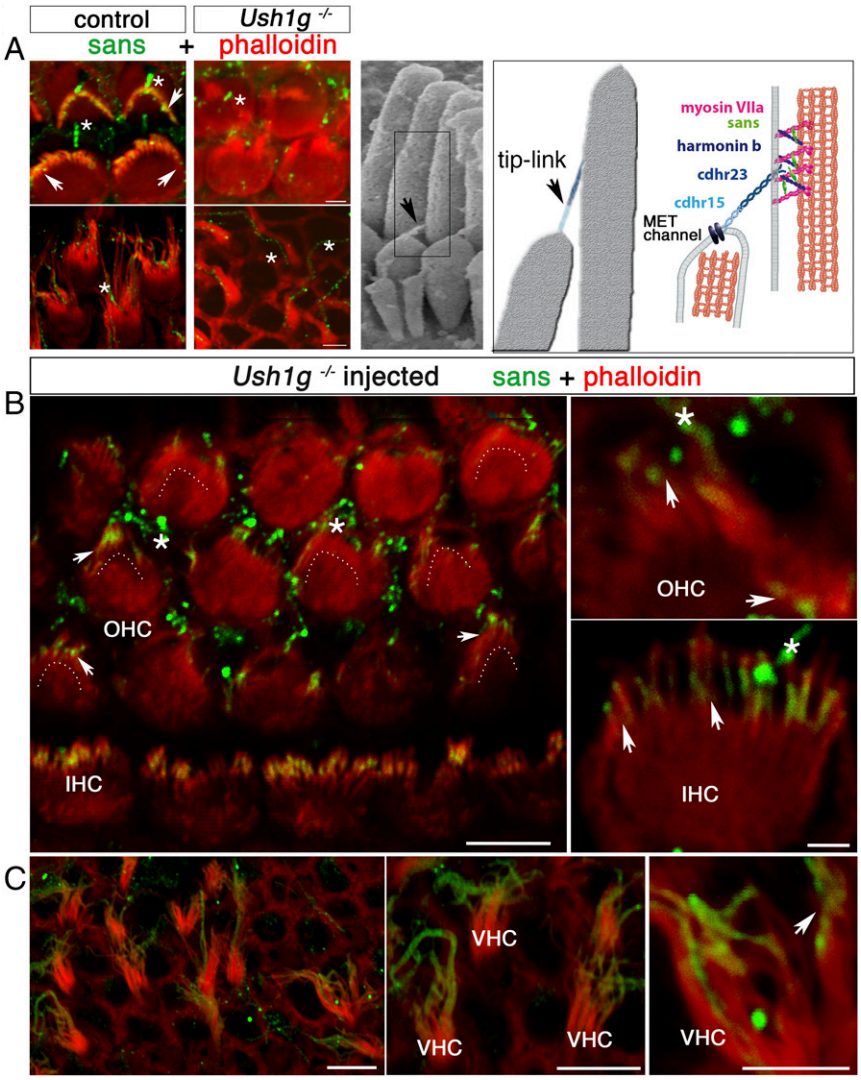

Fig. 2. AAV8-*Sans-IRES-GFP* restores sans expression and targeting in the inner ear hair cells of *Ush1g*$^{-/-}$ mice. (*A*, *Left*) OHC (*Upper*) and VHC (*Lower*) hair bundles from P8.5 wild-type (control) and *Ush1g*$^{-/-}$ mice, immunostained for sans (green) and stained for F-actin with phalloidin (red). Sans is detected at the tips of the stereocilia in the wild-type mouse (white arrowheads), but not in the *Ush1g*$^{-/-}$ mouse. A nonspecific staining of the kinocilium is present both in the wild-type and *Ush1g*$^{-/-}$ mice (asterisks). (*A*, *Center*) Scanning electron micrograph of the IHC hair bundle, showing the tip links between adjacent stereocilia of different rows (black arrowhead). (*A*, *Right*) Diagram showing the tip-link lower and upper insertion points, the position of the mechanoelectrical transduction (MET) channel(s) at the tip of the shorter stereocilium, and the locations of the five USH1 proteins forming the tip link [cadherin-related proteins 15 (cdhr15) and 23 (cdhr23)] or presumably involved in its anchoring to the actin filaments of the taller stereocilium (harmonin b, sans, and myosin VIIa). The submembrane scaffold protein sans belongs to the tip-link upper insertion point molecular complex. Top views of the organ of Corti in the cochlear apical region (*B*) and of the utricular macula (*C*) of an injected *Ush1g*$^{-/-}$ mouse on P8.5 and high-magnification photographs of OHC, IHC, and VHC hair bundles are shown. Sans is targeted to the tips of the stereocilia in all hair cell types (arrowheads). The image in *B* is extracted from a larger tile scan and contains two tiles stitched together at the upper part of the image. Dashed lines in *B* indicate the position of the hair bundle base (V shape) in OHCs expressing the transgene. (Scale bars: 5 μm.)

prolate shapes in only 4% of the VHCs (n = 204 cells) and none of the cochlear hair cells (n = 147 cells, from seven mice) of uninjected *Ush1g*$^{-/-}$ mice (Fig. 3*A*, *Insets*; Mann–Whitney test, $P < 10^{-4}$ for all comparisons between injected and uninjected *Ush1g*$^{-/-}$ mice), which is consistent with the loss of tip links in these mice (24). Finally, we estimated the numbers of stereocilia per hair bundle, their projected heights, and their spacing, based on our scanning electron micrographs (Table S1). We found no significant differences in any of these parameters between the injected *Ush1g*$^{-/-}$ mice and *Ush1g*$^{+/-}$ mice (Table S1). Of note, the cochlear and vestibular hair bundles of injected and uninjected wild-type mice did not differ in appearance either, suggesting that the injection through the round window membrane did not impair the morphological development of the hair bundles.

In keeping with the morphological rescue of the hair bundles, the transduced IHCs and OHCs of injected *Ush1g*$^{-/-}$ P8.5 mice, identified on the basis of GFP fluorescence, displayed mechanoelectrical transduction currents of much higher peak amplitudes (424 ± 69.4 pA in IHCs, n = 11 and 641 ± 35 pA in OHCs, n = 12) than IHCs and OHCs of uninjected *Ush1g*$^{-/-}$ mice (110.8 ± 30.8 pA in IHCs, n = 5 and 47.3 ± 5.7 pA in OHCs, n = 4; Student's t test, $P < 0.01$ for each comparison; Fig. 3*B*). In addition, the sensitivity of the transduction current response to hair bundle displacement was similar in injected *Ush1g*$^{-/-}$ mice and injected *Ush1g*$^{+/-}$ (control) mice (calculated mean sensitivity values: 1.12 ± 0.19 μm^{-1} and 1.30 ± 0.14 μm^{-1} for IHCs, and 1.73 ± 0.2 μm^{-1} and 2.24 ± 0.15 μm^{-1} for OHCs of injected *Ush1g*$^{+/-}$ and injected *Ush1g*$^{-/-}$ mice, respectively; unpaired t test, $P > 0.1$ for both comparisons) (24) (Fig. 3*B* and Fig. S3*A*).

Partial Restoration of Hearing. *Ush1g*$^{-/-}$ mice are profoundly deaf and show no identifiable ABRs, even in response to sounds of intensities up to 110 dB sound pressure level (SPL) (24) (Fig. 4*A*). After gene transfer, ABR waves could be recorded in 2- to 12-wk-old *Ush1g*$^{-/-}$ mice for sound intensities exceeding 75 dB SPL, indicating a substantial improvement in cochlear function. For sounds in the low-frequency range (5–15 kHz), the hearing threshold elevation was about 50 dB on P30, instead of a complete hearing loss in the uninjected mutant mice (n = 18 injected mice; one-way ANOVA test, $P < 0.01$; Fig. 4*A*). The improvement of hearing thresholds was less noticeable at higher frequencies (20–40 kHz), which is consistent with the decrease in cochlear hair cell transduction rates from the apical region to the basal region of the cochlea, where high-frequency tones are analyzed (32) (Fig. S1*F*). It is noteworthy that a partial hearing rescue was still present at the age of 12 wk, the oldest age at which the mice were tested (33) (Fig. S4). Thus, a single intracochlear injection of the transgene during the neonatal period

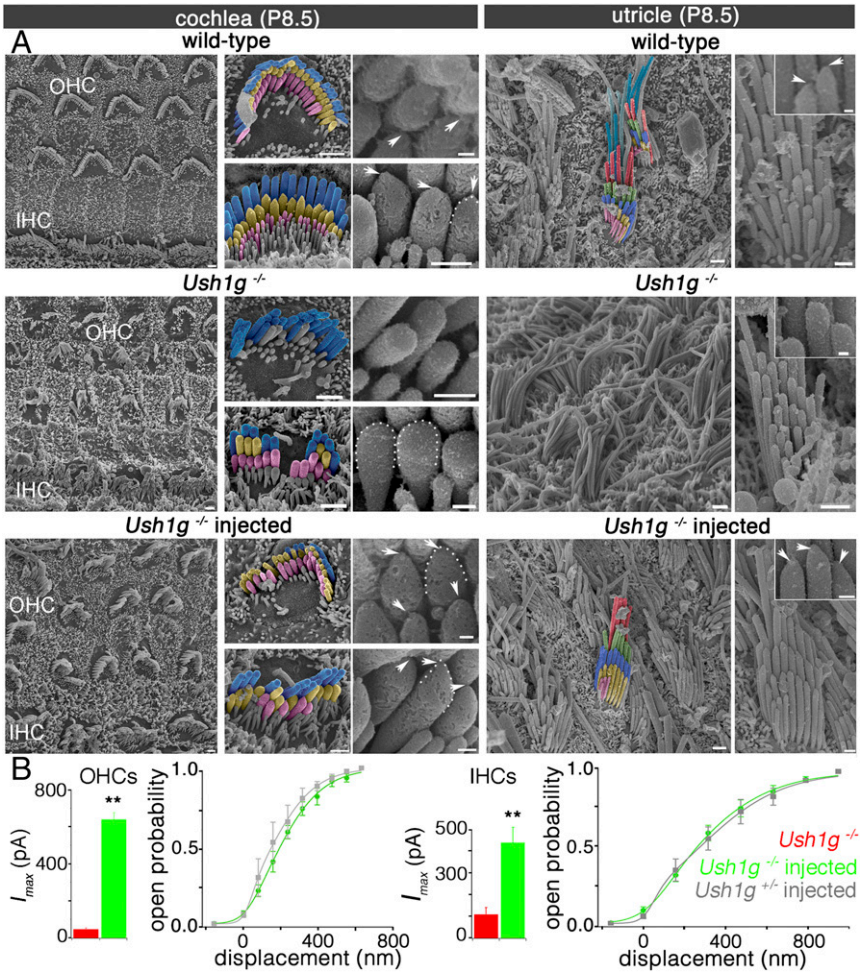

Fig. 3. *Sans* cDNA transfer to inner ear hair cells rescues *Ush1g*$^{-/-}$ mice from hair bundle structural defects. (*A*) Low-, intermediate-, and high-magnification scanning electron micrographs showing the architecture of the hair bundles in cochlear OHCs and IHCs (*Left*) and in VHCs (utricle, *Right*) of a control wild-type mouse, an *Ush1g*$^{-/-}$ mouse, and an *Ush1g*$^{-/-}$ mouse injected with the *Sans* cDNA, on P8.5. In the wild-type mouse, the stereocilia tips have prolate shapes, which is the hallmark of functional tip links (arrowheads and dashed lines) (31), whereas they have rounded shapes in the *Ush1g*$^{-/-}$ mouse (dashed lines), in keeping with the loss of the tip links (24). Note the fragmentation of the hair bundles and the degeneration of some stereocilia in this mouse. In the injected *Ush1g*$^{-/-}$ mouse, the hair bundles have recovered their normal staircase architecture and the prolate shapes of stereocilia tips (arrowheads and dashed line). (Scale bars: 2 μm.) (*B*) Mechanoelectrical transduction (MET) currents recorded ex vivo in IHCs and OHCs of uninjected *Ush1g*$^{-/-}$ (red), injected *Ush1g*$^{-/-}$ (green), and injected *Ush1g*$^{+/-}$ (control, gray) P8.5 mice. Bar charts show the peak amplitudes of the MET currents (I_{max}) recorded in the hair cells of uninjected or injected *Ush1g*$^{-/-}$ mice (110.8 ± 30.8 pA in IHCs and 47.3 ± 5.7 pA in OHCs of uninjected *Ush1g*$^{-/-}$ mice vs. 424 ± 70 pA in IHCs and 641 ± 35 pA in OHCs of injected *Ush1g*$^{-/-}$ mice). Note the marked increase of I_{max} in the injected *Ush1g*$^{-/-}$ mice compared with the noninjected mice (Student's *t* test, $^{**}P < 0.01$ for both IHCs and OHCs*)*. Line graphs show the MET channel opening probability plotted as a function of hair bundle displacement for IHCs and OHCs of injected *Ush1g*$^{+/-}$ (gray) and *Ush1g*$^{-/-}$ (green) mice. For both cell types, the two curves are superimposed.

was able to restore the hearing of loud sounds (≥75 dB) of low frequency in *Ush1g*$^{-/-}$ mice.

Complete Restoration of Vestibular Function. Video-tracking in an open-field chamber showed that injected *Ush1g*$^{-/-}$ mice explored the field in a manner similar to control mice, without circling behavior (1.5 ± 0.4 turn in 2 min for injected *Ush1g*$^{-/-}$ mice, $n = 10$, vs. 20.3 ± 2.8 turns in 2 min for uninjected *Ush1g*$^{-/-}$ mice, $n = 7$; Student's *t* test, $P < 0.01$; Fig. 4*B*, Fig. S3*B*, and Movies S1–S4). Additional behavioral tests were carried out to assess the vestibular functions in these mice, up to 53 wk after injection (31). In the balance platform test (*SI Materials and Methods*), the uninjected *Ush1g*$^{-/-}$ mice ($n = 7$) were unable to stay on the platform, whereas the injected *Ush1g*$^{-/-}$ mice ($n = 10$), like the *Ush1g*$^{+/-}$ control mice ($n = 9$), were able to spend about 1 min on the platform (58.4 ± 0.9 s vs. 27.6 ± 10.6 s for injected *Ush1g*$^{-/-}$ mice and uninjected mutant mice, respectively; Student's *t* test, $P < 0.01$). Likewise, the injected *Ush1g*$^{-/-}$ mice responded normally in the trunk curl test, and were able to reach a horizontal landing surface rapidly when suspended by the tail, without curling the trunk toward their tail, whereas the uninjected mutant mice were unable to land on the horizontal surface, instead curling toward the base of the tail when suspended (Pearson's χ^2 test, $P < 0.01$). In a contact righting test, the injected *Ush1g*$^{-/-}$ mice could reorient their bodies rapidly upon inversion of the tube in which they were held, whereas the uninjected *Ush1g*$^{-/-}$ mice could not (Pearson's χ^2 test, $P < 0.01$). In the swim test described by Hardisty-Hughes et al. (34), the injected *Ush1g*$^{-/-}$ mice behaved just like the wild-type mice, whereas the uninjected *Ush1g*$^{-/-}$ mice displayed underwater tumbling, and had to be lifted out and rescued at once (Pearson's χ^2 test, $P < 0.01$). These results suggest that gene replacement therapy by early postnatal injection of AAV8-*Sans* into the inner ear restores the vestibular function in *Ush1g*$^{-/-}$ mice. Notably, this effect persisted in the long term, as no difference was found between the *Ush1g*$^{+/-}$ and injected *Ush1g*$^{-/-}$ mice when these tests were carried out 53 wk after treatment (platform test: Student's *t* test, $P > 0.1$; swim

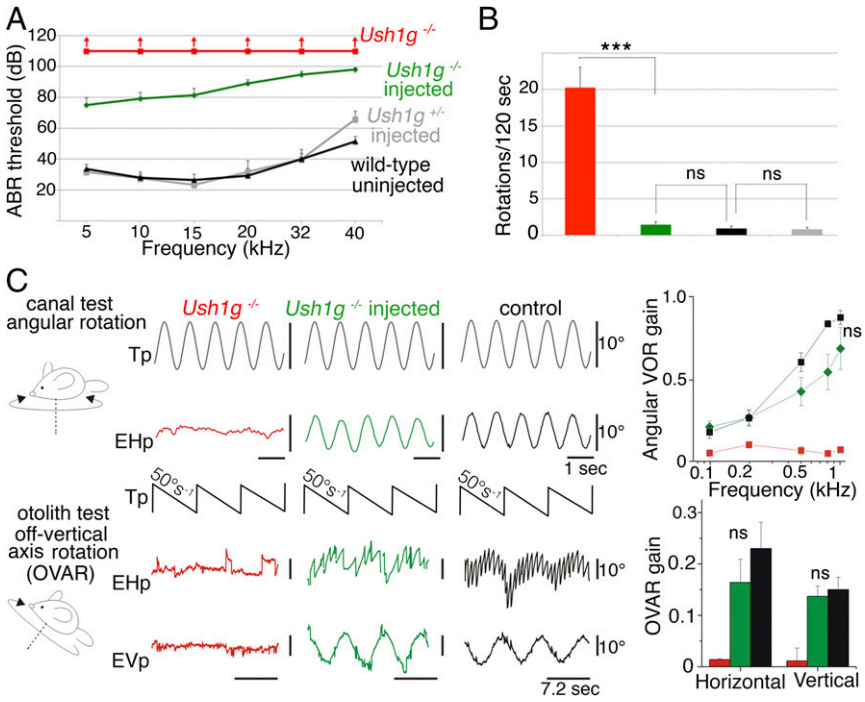

Fig. 4. *Sans* cDNA transfer improves hearing thresholds of injected *Ush1g*$^{-/-}$ mice and almost completely restores their vestibular functions. (*A*) ABR thresholds in P30 wild-type mice (not injected) and P30 *Ush1g*$^{+/-}$ and *Ush1g*$^{-/-}$ mice injected or not injected with AAV8-*Sans-IRES-GFP* on P2.5. ABRs were recorded in response to 5- to 40-kHz tone bursts, and for sound intensities between 10 and 110 dB SPL. The ABR threshold elevation is about 50 dB for low-frequency sounds (5–15 kHz) in injected *Ush1g*$^{-/-}$ mice ($n = 18$ mice), instead of a complete hearing loss in the uninjected mutant mice ($n = 3$ mice). Note that the viral injection did not affect the ABR thresholds of *Ush1g*$^{+/-}$ heterozygous mice ($n = 7$), compared with the uninjected wild-type (control) mice ($n = 6$). (*B*) Bar chart showing the number of rotations in open-field recordings of mouse displacements over a period of 2 min (120 s) in 33-wk-old *Ush1g*$^{+/-}$ (control) and *Ush1g*$^{-/-}$ mice injected or not injected with the transgene on P2.5. ***$P < 0.001$. (*C*) Vestibulo-ocular recordings done between 10 and 12 mo after injection of the transgene. (*Upper*) Semicircular canal test. An angular VOR (aVOR) was recorded during horizontal sinusoidal rotations of the turntable (the representation of the table signal, Tp, is inverted for easy comparison). No aVOR is detected in the uninjected *Ush1g*$^{-/-}$ mouse (EHp, red trace), whereas the injected *Ush1g*$^{-/-}$ mouse (green trace) displays an aVOR response similar to that of the control mouse (black trace). The line graph shows the responses for stimuli of different speeds (from 0.1 to 1 Hz) (mean ± SEM, $n = 5$ mice in each group; ANOVA, $P = 0.2$). (*Lower*) Otolithic organ test using off-vertical axis rotation (OVAR). No eye response is detected in the *Ush1g*$^{-/-}$ mouse (EHp and EVp, red traces), whereas the injected *Ush1g*$^{-/-}$ mouse (green traces) and the control mouse (black traces) display compensatory eye movements. The bar chart shows the horizontal and vertical responses (mean ± SEM, $n = 5$ mice in each group; Mann–Whitney test, $P = 0.3$ and $P = 0.5$ for the comparison of the horizontal and vertical responses between the control and injected *Ush1g*$^{-/-}$ mice, respectively). EHp, eye horizontal position (eye movements to the right are represented upward); EVp, eye vertical position; ns, statistically not significant; Tp, table position.

test: Pearson's χ^2 test, $P > 0.1$; $n = 5$ mice for each genotype). We then evaluated the long-term contributions of the different vestibular end organs to the improvement in equilibration up to 67 wk. The functions of the semicircular canals and otolith organs (saccule and utricle) were assessed by recording vestibulo-ocular reflexes (VORs) and macula-ocular reflexes (MORs) in response to specific turntable movements, respectively (35). No compensatory eye movements in response to turntable rotation could be detected in *Ush1g*$^{-/-}$ mice, indicating a complete loss of function for both the semicircular canals and otolith organs, as expected. By contrast, all of the injected *Ush1g*$^{-/-}$ mice showed compensatory eye movements in the VOR and MOR tests (Fig. 4*C*). Vestibulo-ocular responses were indistinguishable from those of wild-type mice in two of the five injected mice. In the other three mice, semicircular canal organ responses were restored to a lesser degree than otolith organ responses, which were not significantly different from those of controls, demonstrating that a single intracochlear injection of the transgene results in a long-lasting complete restoration of the vestibular function in *Ush1g*$^{-/-}$ mice.

Discussion

We demonstrate a long-term restoration of inner ear functions in a mouse model of USH1 by using a single AAV-mediated local gene therapy at an early postnatal stage. The recombinant AAV8, with the CAG promoter driving transgene expression, was found to be the most efficient of the AAV vectors tested for the transduction of inner ear hair cells. Virus injection through the round window membrane on P2.5 had no deleterious effect on inner ear development in wild-type mice. Furthermore, no adverse side effects were detected in the mice for up to 63 wk after virus injection. This approach therefore appears as a promising one to attempt in future extension to human patients.

Our results demonstrate that *Sans* cDNA delivery restores the production and localization of the sans protein in the IHCs, OHCs, and VHCs, suggesting that the exogenous protein was correctly targeted to the tip-link insertion points (24, 36) (Fig. 2). Moreover, the transduced cochlear hair cells of injected *Ush1g*$^{-/-}$ mice displayed markedly improved mechanoelectrical transduction currents in ex vivo experiments on P8.5 cochlear explants, which indicates that expression of the *Sans* cDNA in these cells effectively compensates for the absence of the native protein. From these results, we can infer that the exogenous protein most probably interacts with the other members of the USH1 protein complex (i.e., cadherin-related protein 23, cadherin-related protein 15, myosin VIIA, harmonin), as required for the correct functioning of the mechanoelectrical transduction channels (24) (Fig. 2*A*). Transduction currents can first be recorded on P0 and P2 in the hair cells of the cochlear basal and apical regions, respectively (37),

whereas the transduction apparatus of VHCs is already functional on E17 (37, 38). In this study, the *Sans* cDNA was delivered by a viral vector on P2.5, and expression of the cDNA was first detected 48 h later (i.e., about 10 d after the normal onset of *Ush1g* expression on E14.5). Despite this delay, gene replacement therapy efficiently restored the structure and function of inner ear hair cells in *Ush1g*$^{-/-}$ mice and prevented the balance deficit while limiting the hearing impairment for low sound frequencies. The time window for treating deafness and balance disorders by gene transfer in patients with USH1 may therefore be larger than initially thought. In addition, the almost complete restoration of vestibular functions reported here reveals unanticipated temporal flexibility for the effective treatment of other early-onset balance disorders of genetic origin. Further studies are required to determine why the transgene injection did not fully restore cochlear function in *Ush1g*$^{-/-}$ mice. The higher rates of hair cell transduction in the vestibular end organs than in the cochlea raise the hope of a full restoration of hearing by increasing the transduction rates in the cochlear hair cells (22). It is worthy of note that hearing thresholds were significantly improved for sounds in the low-frequency range (5–15 kHz), which are analyzed in a cochlear apical region that, owing to its high curvature, cannot be reached by the electrode arrays of cochlear implants (39). Therefore, this gene therapy approach might be effective in association with current cochlear implants by partly restoring the tonotopic information that these implants cannot provide, and thus allowing for better sound perception.

This study constitutes a significant step toward the virus-mediated cure of a form of genetic deafness in humans. However, before considering translation to clinical trials, these results must be reproduced in larger animal models that are better predictors of responses in humans than rodents, based on the size and the kinetics of maturation of their cochlea.

Materials and Methods

Detailed information is provided in *SI Materials and Methods*. Animal experiments were carried out in accordance with INSERM and Institut Pasteur welfare guidelines. Animals were housed in the Institut Pasteur animal facilities accredited by the French Ministry of Agriculture for experiments on live mice. The intracochlear viral injection procedure, approved by the Animal Care and Use Committee of the Institut Pasteur, was carried out as described by Akil et al. (16). Immunofluorescence analyses were carried out as described elsewhere (40, 41). Scanning electron microscopy analysis was done as described elsewhere (24). Electrophysiological whole-cell patch-clamp recordings of hair cell mechanoelectrical transduction currents were carried out in cochlear explants from P8.5 mice, as described by Michalski et al. (42). ABRs to sound stimuli were recorded and analyzed as previously described (43). The various tests to assess vestibular function were carried out as previously reported (34, 35).

ACKNOWLEDGMENTS. We thank Jean-Marc Panaud (Reprography Service, Institut Pasteur) for assistance with SEM image colorization. This work was supported by Fondation pour la Recherche Médicale (A.E.); the European Union Seventh Framework Programme under the grant agreement HEALTH-F2-2010-242013 (TREATRUSH); the European Commission (ERC-2011-ADG_294570); French state funds managed by Agence Nationale de la Recherche within the Investissements d'Avenir Programme (ANR-15-RHUS-0001); LabEx Lifesenses (ANR-10-LABX-65); and grants from the BNP Paribas Foundation, the FAUN-Stiftung, the LHW-Stiftung, and Errera Hoechstetter.

1. Jeon EK, Turner CW, Karsten SA, Henry BA, Gantz BJ (2015) Cochlear implant users' spectral ripple resolution. *J Acoust Soc Am* 138:2350–2358.
2. Vivero RJ, Fan K, Angeli S, Balkany TJ, Liu XZ (2010) Cochlear implantation in common forms of genetic deafness. *Int J Pediatr Otorhinolaryngol* 74:1107–1112.
3. Friedman TB, Schultz JM, Ahmed ZM (2005) Usher syndrome type 1: Genotype-phenotype relationships. *Retina* 25(Suppl):S40–S42.
4. Liu XZ, et al. (2008) Cochlear implantation in individuals with Usher type 1 syndrome. *Int J Pediatr Otorhinolaryngol* 72:841–847.
5. Petit C, Richardson GP (2009) Linking genes underlying deafness to hair-bundle development and function. *Nat Neurosci* 12:703–710.
6. Collins M, Thrasher A (2015) Gene therapy: Progress and predictions. *Proc Biol Sci* 282: 20143003.
7. Simonato M, et al. (2013) Progress in gene therapy for neurological disorders. *Nat Rev Neurol* 9:277–291.
8. Asokan A, Schaffer DV, Samulski RJ (2012) The AAV vector toolkit: Poised at the clinical crossroads. *Mol Ther* 20:699–708.
9. Kotterman MA, Schaffer DV (2014) Engineering adeno-associated viruses for clinical gene therapy. *Nat Rev Genet* 15:445–451.
10. Mingozzi F, High KA (2011) Therapeutic in vivo gene transfer for genetic disease using AAV: Progress and challenges. *Nat Rev Genet* 12:341–355.
11. Iizuka T, et al. (2008) Noninvasive in vivo delivery of transgene via adeno-associated virus into supporting cells of the neonatal mouse cochlea. *Hum Gene Ther* 19: 384–390.
12. Kilpatrick LA, et al. (2011) Adeno-associated virus-mediated gene delivery into the scala media of the normal and deafened adult mouse ear. *Gene Ther* 18:569–578.
13. Konishi M, Kawamoto K, Izumikawa M, Kuriyama H, Yamashita T (2008) Gene transfer into guinea pig cochlea using adeno-associated virus vectors. *J Gene Med* 10: 610–618.
14. Wu Z, Asokan A, Samulski RJ (2006) Adeno-associated virus serotypes: Vector toolkit for human gene therapy. *Mol Ther* 14:316–327.
15. Xia L, Yin S, Wang J (2012) Inner ear gene transfection in neonatal mice using adeno-associated viral vector: A comparison of two approaches. *PLoS One* 7:e43218.
16. Akil O, et al. (2012) Restoration of hearing in the VGLUT3 knockout mouse using virally mediated gene therapy. *Neuron* 75:283–293.
17. Askew C, et al. (2015) Tmc gene therapy restores auditory function in deaf mice. *Sci Transl Med* 7:295ra108.
18. Chang Q, et al. (2015) Virally mediated Kcnq1 gene replacement therapy in the immature scala media restores hearing in a mouse model of human Jervell and Lange-Nielsen deafness syndrome. *EMBO Mol Med* 7:1077–1086.
19. Chien WW, et al. (2016) Gene therapy restores hair cell stereocilia morphology in inner ears of deaf whirler mice. *Mol Ther* 24:17–25.
20. Isgrig K, et al. (2017) Gene therapy restores balance and auditory functions in a mouse model of Usher syndrome. *Mol Ther* 25:780–791.
21. Landegger LD, et al. (2017) A synthetic AAV vector enables safe and efficient gene transfer to the mammalian inner ear. *Nat Biotechnol* 35:280–284.
22. Pan B, et al. (2017) Gene therapy restores auditory and vestibular function in a mouse model of Usher syndrome type 1c. *Nat Biotechnol* 35:264–272.
23. Weil D, et al. (2003) Usher syndrome type I G (USH1G) is caused by mutations in the gene encoding SANS, a protein that associates with the USH1C protein, harmonin. *Hum Mol Genet* 12:463–471.
24. Caberlotto E, et al. (2011) Usher type 1G protein sans is a critical component of the tip-link complex, a structure controlling actin polymerization in stereocilia. *Proc Natl Acad Sci USA* 108:5825–5830.
25. Lefèvre G, et al. (2008) A core cochlear phenotype in USH1 mouse mutants implicates fibrous links of the hair bundle in its cohesion, orientation and differential growth. *Development* 135:1427–1437.
26. Derby ML, Sena-Esteves M, Breakefield XO, Corey DP (1999) Gene transfer into the mammalian inner ear using HSV-1 and vaccinia virus vectors. *Hear Res* 134:1–8.
27. Raphael Y, Frisancho JC, Roessler BJ (1996) Adenoviral-mediated gene transfer into guinea pig cochlear cells in vivo. *Neurosci Lett* 207:137–141.
28. Sacheli R, Delacroix L, Vandenackerveken P, Nguyen L, Malgrange B (2013) Gene transfer in inner ear cells: A challenging race. *Gene Ther* 20:237–247.
29. Wang Y, et al. (2013) Early postnatal virus inoculation into the scala media achieved extensive expression of exogenous green fluorescent protein in the inner ear and preserved auditory brainstem response thresholds. *J Gene Med* 15:123–133.
30. Fettiplace R, Hackney CM (2006) The sensory and motor roles of auditory hair cells. *Nat Rev Neurosci* 7:19–29.
31. Prost J, Barbetta C, Joanny JF (2007) Dynamical control of the shape and size of stereocilia and microvilli. *Biophys J* 93:1124–1133.
32. Kandler K, Clause A, Noh J (2009) Tonotopic reorganization of developing auditory brainstem circuits. *Nat Neurosci* 12:711–717.
33. Johnson KR, Erway LC, Cook SA, Willott JF, Zheng QY (1997) A major gene affecting age-related hearing loss in C57BL/6J mice. *Hear Res* 114:83–92.
34. Hardisty-Hughes RE, Parker A, Brown SD (2010) A hearing and vestibular phenotyping pipeline to identify mouse mutants with hearing impairment. *Nat Protoc* 5:177–190.
35. Romand R, et al. (2013) Retinoic acid deficiency impairs the vestibular function. *J Neurosci* 33:5856–5866.
36. Grati M, Kachar B (2011) Myosin VIIa and sans localization at stereocilia upper tip-link density implicates these Usher syndrome proteins in mechanotransduction. *Proc Natl Acad Sci USA* 108:11476–11481.
37. Géléoc GS, Holt JR (2014) Sound strategies for hearing restoration. *Science* 344: 1241062.
38. Denman-Johnson K, Forge A (1999) Establishment of hair bundle polarity and orientation in the developing vestibular system of the mouse. *J Neurocytol* 28:821–835.
39. Van Abel KM, et al. (2015) Hearing preservation among patients undergoing cochlear implantation. *Otol Neurotol* 36:416–421.
40. Roux I, et al. (2009) Myosin VI is required for the proper maturation and function of inner hair cell ribbon synapses. *Hum Mol Genet* 18:4615–4628.
41. Roux I, et al. (2006) Otoferlin, defective in a human deafness form, is essential for exocytosis at the auditory ribbon synapse. *Cell* 127:277–289.
42. Michalski N, et al. (2009) Harmonin-b, an actin-binding scaffold protein, is involved in the adaptation of mechanoelectrical transduction by sensory hair cells. *Pflugers Arch* 459:115–130.
43. Delmaghani S, et al. (2015) Hypervulnerability to sound exposure through impaired adaptive proliferation of peroxisomes. *Cell* 163:894–906.

Chapter IV –
Discussion and Perspectives

1. Motion in mice: vestibulo-ocular and optokinetic pathways through time

The following discussion includes the work presented in the first 3 articles of this thesis. There, two gaze stabilizing reflexes were studied in response to a long-term visuo-vestibular mismatch (VVM) protocol. Properties of MVN neurons were studied in vitro right after the end of the protocol and, behaviorally, the recovery of the VOR and OKR responses was measured over time. This section features the discussion of these works by mentioning points that were not treated on the respective articles as well as further elaborating on some of them.

1.1. The visuo-vestibular mismatch as a long-term motor learning protocol

Three of the works of this thesis were based on the use of the VVM protocol. This protocol consists in a long-term sensory perturbation that consisted in a visuo-vestibular mismatch in freely behaving mice.

Experimentally, there are several advantages that make this protocol an attractive choice for studying motor learning. Regarding the surgery; the required surgery for the headpost implantation is straightforward, it can be performed with a commercial surgery kit, it's a brief (±30min) procedure. Additionally, the yield of success (death or post-surgical removal of the headpost) is quite high and it has a short post-operative recovery time (between 30min and 1h). Yet, it is primordial to ensure every set of the surgery is correctly performed so that the headpost is well attached and it doesn't fall off once the protocol has begun. In that case, mice have to be excluded from the protocol which is unfortunate since the protocol requires 2 weeks. In the perspective of the experimenter; this protocol is less time consuming than other VOR gain-down protocols that require mice to be head-fixed and trained daily for several hours on a rotating turntable. This protocol enables groups of mice to be trained simultaneously since each one of them has its own adaptation device fixed onto their heads.

In other long-term protocols aiming at changing the VOR gain, the animal is head-fixed and rotated in phase (gain-down) or out of phase (gain-up) with the visual surrounding and this is repeated during several days (Boyden & Raymond, 2003; Raymond & Lisberger, 1996). Moreover, these protocols are limited to only some hours per day of training, leaving several hours of putative unlearning in between. The paradigm of the VVM protocol offers a VOR (and OKR) reduction that is a product of voluntary head movements in an uninterrupted process. Additionally, the time frame of

execution of the protocol can freely be adjusted hence, both short-term and long-term protocols can be easily achieved. For example, a possible experiment would be to change the timeframe of adaptation of the protocol and test whether a shorter/longer time would make a smaller/bigger VOR and OKR decrease. The recovery of the response of these reflexes could also be tested to confirm if a stronger/weaker decrease produces a more durable/transient change in the gain.

Most in vivo motor learning studies are performed in monkeys and cats while in vitro studies are done in rodents. This disparity denies the possibility of studying, in a sole organism, the complete mechanisms of motor learning in gaze stabilizing reflexes. The VVM protocol surpasses this obstacle since it allows performing both types of experiments in the same animal.

It must be emphasized that, our VVM protocol differs from traditional VOR or OKR adaptation protocol. Traditional VOR adaptation protocols used controlled and quantified inputs to create the adaptation during iterative training sessions. Contrarily, our protocol creates a 'decalibration' of the VOR by imposing a constant visual and vestibular mismatch (black and white pattern or no-pattern) for 2 weeks and therefore can't be directly compared to VOR adaptation protocols.

The retinal slip is the movement of the visual relative to the eye and it is believed to be the error signal that drives VOR motor learning (Boyden & Raymond, 2003). Classical adaptation protocols often apply retinal slips during training by moving the turntables at a determined frequency and by oscillating the drum that presents the image (Katoh et al., 1998; Shutoh et al., 2006). It can be calculated by extracting the amplitude and phase from the averaged difference between drum velocity and eye movement velocity. In our protocol, we can't measure retinal slip since it does not consist in training sessions were the input given is controlled; mice are freely behaving in their cages. This is a disadvantage of our protocol since it prevents directs comparisons to results where the retinal slip is measured.

1.2. The influence of visual inputs in the motor learning of gaze stabilizing reflexes

In one of the studies (Article 3), a 'blank' or 'no-pattern' device was used besides the patterned device with stripes drawn onto its surface. The concept behind this choice was to compare the effect of the visual input on the decalibration of the gaze stabilizing reflexes. The patterned device was thought to induce a strong error message since, the high contrast produced with the stripes would cause great retinal blur. On the other hand, in the no-pattern device, the uniform 'white' canvas perceived as the visual input would

hypothetically produce a minimal error message. Surprisingly, even though they weren't identical, both devices yielded similar results. Both the magnitude of the gain decrease and the kinematics of the recovery of the gaze stabilization responses were comparable between pattern and no-pattern groups. This result raises several questions that will be now discussed.

The first question one might ask is: how important is the type of visual input when creating an error signal? Hypothetically, in the pattern device, retinal ganglion cells would more easily detect motion by using the stripes as a reference point for movement and would readily convey an error signal that would modulate the VOR and OKR responses. On the other hand, in the no-pattern device, there is hardly any reference from movement since the background is all the same color. Thus, this would hypothetically create a disparity, between both responses. However, the kind of visual environment was different between both devices, but this difference wasn't translated into the output of these responses. This fact implies that the alteration of the 'normal' visual surroundings is the principal factor that determines the "decalibration" of the reflexes.

This being said, would the traditional VOR adaptation training sessions, that use high-contrast patterns, work if a white background would be used? The effect of a 'blank' canvas as the visual stimulus during iterative training sessions would be interesting to test if the same VOR adaptation is attained.

Nonetheless, in our study, the kinematics of decalibration were not study. After 14 days, when the VVM devices are removed, both devices present a comparable amount of decalibration. However, the difference between both devices could lie in the amount of time needed for that decalibration to occur. This could be investigated by submitting mice to a protocol in which the adaptation period, still in the long-term timeframe, would be shortened to find how many days are needed for each condition to reach the >60% VOR gain decrease registered in our study. This would help determine whether the 'type' of visual input plays a role in the speed of decalibration of gaze stabilizing reflexes.

Another possible experiment to study the influence of the visual input on the decalibration of the gaze stabilization reflexes would be to use an all-black device. This device would elaborate on the no-pattern one since, apart from not having a visual contrast, it wouldn't receive any light. By using a completely dark device, where no image or light could be perceived, would allow studying how does the complete absence of visual inputs affects the magnitude of decalibration and the kinematics of recovery of these reflexes. Hypothetically, in this case, the OKR would have a stronger decalibration

(or even extinction) since this reflex depends on the visual system that, in this paradigm, would be shut down.

1.3. The VVM differentially affects OKR and VOR

In Article 3, additionally to the VOR, the OKR responses were also measured. The VVM protocol is a purely visual modification that is able to produce changes in both the visual and vestibular pathways. It is so because, when the head moves with the device fixed onto it, the VOR that is produced, is no longer compensatory and is consequently suppressed. Nevertheless, it's interesting that, the most drastic changes were registered for the vestibular and not for the visual reflex. Globally, a 30% decrease in the gain of the OKR was registered while the VOR decreased >60%. The contrasting gain decreases could be explained by the difference in the storage site of the long-term memory in each reflex.

As seen in Article 1, the long-term reduction of the VOR, driven by the VVM, is associated with changes in MVN neurons, i.e., in the direct VOR pathway. The changes in MVN neurons are reflected in the decrease of the efficiency of the vestibular nerve synapse onto these neurons, probably through an LTD mechanism. In that study, OKR was tested in VVM-adapted mice after the flocculus had been shut down (lidocaine injections). The OKR gain in these mice was largely abolished, suggesting that the neural actors for this OKR decalibration could reside in the floccular site. If this is so, the responsible neurons would be floccular Purkinje cells (PCs), the only cells that directly project into the vestibular nuclei. Hypothetically, alterations to these cells could be due to a modification of the input that they receive either from climbing fibers or from parallel fibers.

1.4. A frequency-dependent decalibration

In Article 3, the frequency- dependence of OKR and VOR responses was analyzed by testing both reflexes at different frequencies. For the VOR, at the end of the VVM protocol, the decrease of the gain was different at each tested frequency. The intermediate frequencies (0,5 and 1Hz) were the ones that demonstrated a bigger decrease after the protocol: the lowest frequency (0,2 Hz) was the one that had the lowest decrease and the highest frequency (2Hz) followed right after. Furthermore, the retention of the learned changes was more persistent at the lower frequencies since the decrease was still present two days after the end of the VVM protocol. These observations go in line with the frequency-dependent differential role of the visual inputs in the tuning of the vestibular and optokinetic systems. Furthermore, the selectivity of a stronger adaptation to intermediate frequencies could be explained by the range of head

movements naturally evoked in a behaving mouse in the yaw plane, usually <3-4 Hz (Beraneck et al., 2008; Carriot et al., 2017). On the other hand, for the OKR, the decalibration was only registered at the lowest frequencies (0,2 and 0,33Hz) and not at the highest (0,5 and 1Hz). This observation can be explained by the fact that OKR is functional mostly at low frequency movements (Faulstich et al., 2004) and thus, it's at those ranges that the motor learning would have occurred.

1.5. Influence of the visual surroundings in the recovery

The VVM disrupts the common visual environment subsequently lowering the VOR and OKR response for at least 2 days after the end of the protocol. Moreover, in the case of VOR, the recovery can take up to 6 days. Hence, it would be exciting to think that this recovery time could be manipulated. A way to do so, could be to study the influence of the visual surroundings in the recovery of gaze stabilizing reflexes.

In our experiments, during the recovery period mice were housed in their usual lab-standard cages. A possibility to test this would be to adapt the visual surroundings during this period. By controlling the visual input that mice perceive during recovery, there wouldn't be such an abrupt visual environment (VVM to no-VVM) transition. A cage with little visual information could produce a different recovery than the standard used cages that unlock a myriad of visual inputs. To test this hypothesis, right after the VVM protocol, mice could be left in a cage whose walls would imitate the no-pattern device. This is, instead of being transparent, the walls of the cage could be made of the white PLA. In this way, the only visual cues that the mouse would have would be the interior of the cage but not the outside environment. Right after the end of the protocol, mice would have their devices removed and transferred to one of these cages for several hours (for example, 3-6 hours) and then transferred back to a regular cage. Potentially, this smoother transition in the visual environment could allow for a faster recovery of the gaze stabilizing reflexes.

In sum, the work discussed in this section contributed with electrophysiological and behavioral data to the understanding of the adaptation of gaze stabilizing reflexes in mice. Nevertheless, more experiments for a deeper understanding of this modulation have been here suggested.

2. Mice in motion: gaze stabilization during locomotion

The experiments performed in this project demonstrate the existence of a cervical CPG-driven efferent copy that directly couples eye movements with forelimb movement during high-frequency locomotion in mice. The following paragraphs discuss the findings of Article 4.

2.1. Locomotion in the decerebrated preparations

During the decerebration experiments, evoking and maintaining locomotion was often an issue. In these experiments, we attempted at pharmacologically stimulating locomotion. Monoamines have been known to have a strong effect in the initiation of locomotion (Schmidt & Jordan, 2000). Thus, we performed a laminectomy that exposed segments of the cervical and thoracic spinal cord and poured serotonin (5HT) to try evoking locomotion in decerebrated preparations that didn't locomote (n=4). However, these experiments were not successful in evoking a sustained locomotion; only very short locomotion were evoked (3-5 seconds). The overall condition of the mouse in some of these preparations was even getting worse, probably because of the additional surgery time (30min) as well as the debilitation of an already delicate preparation that this procedure involved.

2.2. Need for speed

The locomotion registered in our preparations was characterized by a step frequency (2-8Hz) and phase (anti-phase coupling of hindlimb and forelimb) of the limbs consistent with a trot-like classification. Trot is the preferential gait used during treadmill locomotion and is, apart from full-bound, the fastest attractor gait (Lemieux et al., 2016). It is known that trained mice can sustain a trot gait to speeds up to 85 cm/s (Herbin et al., 2004). Nevertheless, different treadmill speeds were tested (between 15-30cm/s) and consistently evoked the same locomotor gait and the same profile of associated eye movements.

An important point to note is that this speed was needed to evoke the recorded eye movements in the decerebrated preparations. Also, preparations where mice had a lack of postural and muscular tonus, were uncapable of sustaining this vigorous locomotion and hence, no eye movements were induced. There are recent experiments in humans that support that predictive gaze stabilizing efferent copies have a 'need for speed', *i.e.*, they were only registered when a high velocity locomotion was evoked. Our observations are in line with this hypothesis.

Recently, Dietrich and Wuehr (H. Dietrich & Wuehr, 2019) studied the influence of locomotor speed on gaze stabilization in healthy subjects. They recorded eye movements during a range of velocities (0.4 to 2.4 m/s) during treadmill locomotion. Vertical aVOR responded better (more in phase), becoming more automated and independent of visual feedback with increasing locomotor speeds. This suggests that vertical gaze stabilization switches to an automated feed-forward control at fast locomotion (H. Dietrich & Wuehr, 2019). Furthermore, in a consequent study this team recently (Haike Dietrich & Wuehr, 2019) confirmed that the VOR is selectively suppressed during faster walking and running in humans. They did so by recording the eye and head movements at different locomotor speeds to measure the horizontal and vertical angular VOR. Here, horizontal VOR was persevered at all tested locomotor speed. On the other hand, the eye and head compensation elicited in response to the vertical movements during higher-speed locomotion, changed from having a VOR-based coordination to a synergistic behavior were head and eye move in phase. Hence, an internal feed-forward command acts to predict and mediate gaze stabilization in the vertical plane in response to faster walking and running in humans (Haike Dietrich & Wuehr, 2019).

Brandt (Brandt et al., 1999) and colleagues studied gait deviation in patients with unilateral vestibular failure. This pathology is characterized by a spontaneous nystagmus towards the affected contralateral side and postural imbalance. They asked the subjects to either walk or run a corridor. During walking, patients deviated gaze towards the lesioned side and it was hard for them to walk without touching the walls of the corridor for support. On the other hand, while running, they were able to maintain their trajectory and felt that the task was easier. Therefore, the gaze stabilization strategies of these patients were excelling when the locomotor speed was increased (Brandt et al., 1999). This study suggests that a predictive feedforward efferent copy could also be present during running in vestibular impaired patients. However, in humans, the origin of this motor efferent copy is still unknown. Perhaps, it could arise, like in the Xenopus (Combes et al., 2008) and mice (França de Barros et al., in preparation), from the spinal CPGs. Furthermore, due to the similarities in gaze stabilization mechanisms between mice and humans, the present observation of a velocity-dependent mechanism by Dietrich and Wuehr goes in line with our observations.

Being so, these examples illustrate that gaze stabilization strategies are closely related to the type of locomotion performed. A slow locomotion allows for on-time integration of sensory inputs while ongoing. However, gaze stabilization strategies must also respond while the locomotor speed is increased. Due to its predictive nature, this

feedforward efferent copy is crucial for maintaining visual acuity since it would counteract the head/body movements elicited during fast locomotion. In this context, different speeds elicit different mechanisms that are yet to be fully explained and investigated.

2.3. The adjustment of eye movements to the running speed

In our experiments, a locomotion speed buildup was needed for the eye movements to start, *i.e.*, the eyes began to move only a few seconds (2s) after the mouse began running and stopped as soon as the mouse began decelerating. Therefore, it seems that once the desirable speed has been reached, the mouse turns on a sort of 'cruise control' that maintains the eye movements that are expected to counteract the head movements that would normally be generated during the corresponding running speed. However, in physiological conditions, mice don't always run in straight courses; they often need to adjust their speeds as a response to the terrain (*e.g.*, slopes or type of terrain) or to the obstacles encountered. Given that, one could wonder if the triggered eye movements would be automatically adjusted in response to changes in the running speed.

Our mice ran under laboratorial conditions, *i.e.*, head-fixed locomoting in a flat-surfaced motorized treadmill with imposed speeds. These challenging conditions only enabled us to control the locomotion by changing the speed of the treadmill belt. However, when we did so (treadmill speeds between 10-30cm/s), no major changes were seen in the running speed of the mice. A way to surpass this obstacle and acquire more control on the locomotion would be to use genetically engineered mice that would allow for the optogenetic activation of spinal neurons responsible for locomotor speed. However, this would create and even more challenging experimental condition since it would involve the addition of an optogenetic stimulation set up as well as a laminectomy for the exposure and accessibility of the spinal neurons.

2.4. Eye movement directionality

In the decerebrated preparations, the eyes moved in a conjugated fashion but each mouse always seemed to make the saccades towards the same side. This observation contradicts the idea of a direct "compensatory" role of these patterns of eye movements. One would have expected that quick phases would be in alternating direction and/or different direction for right and left eyes. Since this is not the case in decerebrated mice in the absence of visual and vestibular inputs, how this efferent copy is integrated to exafference signals remains an open question.

In vitro experiments also revealed that the distribution of infected RV+ neurons along the cervical spinal cord was mainly ipsilateral to the lateral rectus injection.

Moreover, spinal cord preparations revealed that the abducens nerve fired simultaneously with its ipsilateral cervical ventral root. This fact questions the reason for the unidirectionality of the saccades. A possible explanation would be that saccades are linked to the paw leading the locomotor pattern/gait. This paw would be the right or left front limb that is initiating the locomotor cycle and being projected first.

Since our data in vitro and in decerebrated preparations do not match any simple hypothesis regarding the direction of gaze, no clear conclusion can be drawn at this point.

2.5. The spino-extraocular efferent copy as a predictor for eye movements during locomotion

With our study, we prove that, like in the Xenopus (Combes et al., 2008; Lambert et al., 2012), mammalian brains also use efference copies of motor commands that help stabilize gaze during locomotion. However, if gaze stabilization during locomotion can be achieved by sensory inputs (visual, proprioceptive and vestibular) that compute the resulting eye and body/head movements, why and when is this motor coupling needed?

A standing hypothesis is that this motor-to-motor signaling would be more efficient in predicting the eye movements that need to be generated during stereotyped locomotion. In 2007, a probabilistic model was designed to quantify the predictability of head movements during human locomotion (MacNeilage & Glasauer, 2017). The highest head movement predictability was found while running. Moreover, by correlating this parameter with the weight of sensory inputs, it was also found that different head movement predictabilities give different weights to vestibular inputs (MacNeilage & Glasauer, 2017). That is, locomotion patterns that produced very stereotyped head movements rely less on vestibular inputs. Following this work, this year, another study focused on whether activity-dependent modulations of vestibular reflexes are explained by changes in head movement predictability (H. Dietrich et al., 2020). By quantifying body sway (center of pressure) while galvanic stimulation was applied during different walking speeds, this team found that the influence of the galvanic stimulation in the center of pressure dropped significantly when higher speeds were reached by the tested subject (H. Dietrich et al., 2020). Thus, in faster locomotor gaits, the sensitivity of the subject to vestibular input was decreased. Again, these findings corroborate the idea that locomotor efference copies have a high impact on stereotyped locomotion (*i.e.*, locomotion gaits with high head predictability).

Our experiments in mice go in line with these studies performed in humans; our spino-extraocular motor-to-motor coupling only appeared when mice have a stereotyped

locomotor gait (trot-like), triggered when the CPGs were activated at higher frequencies. Therefore, a possible physiological explanation for the role of the locomotor efference copy is that it overrides other sensory inputs during high-speed gaits due to the predictable nature of the eye movements associated to those particular gaits. This sort of 'automatic pilot' would ensure optimal motor control by excluding the need for an active assessment of sensory cues since, through a feedforward mechanism, it generates compensatory eye movements in phase with the solicited gait.

2.6. A cross-phyla mechanism

The inspiration for this project began in 2008 with the findings of our colleagues in the Xenopus tadpole (Combes et al., 2008; Lambert et al., 2012). The Xenopus *laevis* (tadpole), is an amphibian that experience a metamorphosis in its locomotion strategy along its life cycle; it switches from tail-base undulatory swimming to tetrapodal locomotion. Being performed in its larval stage, the studies of our colleagues left an interesting evolutionary bridge uncrossed: is this gaze stabilization mechanism present, not only in axial-based locomotion, but also in limb-based locomotion? By using mice as a model system, the presented study (Article 4) was able to prove that this spino-extraocular motor system coupling is also present in quadrupedal locomotion.

As it was discussed above, humans have been the subjects for the study of the presence of such gaze stabilizing strategies and several evidences have been found in favor of gaze stabilization being driven by spinal locomotor efference copies (H. Dietrich et al., 2020; H. Dietrich & Wuehr, 2019; MacNeilage & Glasauer, 2017).

The Drosophila melanogaster (fruit fly) has also been used as a model to study the predictive function of efference copies for visuomotor processing during locomotion (Cruz et al., 2019; A. J. Kim et al., 2015; L. H. Kim et al., 2017). Much like vertebrates, flies largely rely on vision for the control of self-generated locomotion (Robie et al., 2010). Moreover, flies provide interesting contributions to this topic since they enable the study in 2 different, but equally important (Busse et al., 2017), locomotor strategies in the same model - walking and flying. Despite its small size, this animal model has a brain that is numerically simple and allows for complex optogenetic and pharmacological manipulations which also allow the identification of the neuronal pathways.

A recent study states that the locomotor context (walking/flying or saccadic/non-saccadic movements) is the key for gaze stabilization (Cruz et al., 2019). This team found that, the locomotor network is able to dynamically tune its sensitivity to visual feedback in response to the locomotor context. The HS cells, a group of cells that respond to the rotational flow generated during locomotion, receive non-visual information about the

fly's walking behavior and have been hypothesized as controllers of forward walking (Fujiwara et al., 2017). In their recent experiments, this group recorded HS cells activity of tethered flies during walking in the dark (no visual inputs) and found that it is highly correlated to the fly's walking speed: the higher the forward velocity, the higher the activity of HS cells (Cruz et al., 2019). Therefore, when a particular velocity is attained for a locomotor context, apart from the visual inputs resulting from self-generated locomotion, flies also receive a motor command to help stabilize gaze.

Another team used behavioral and electrophysiological experiments in tethered flying flies to study how efference copies cancel the visual input/flow from the environment to suppress the optokinetic reflex (A. J. Kim et al., 2015). They found direct evidence that, during a fly's voluntary body turns (saccades), visual neurons receive motor inputs that were in the same magnitude but opposite direction of the expected (reafference) visual inputs.

The discovery of motor-to-motor coupling mechanisms across a wide variety of animal phyla demonstrates the importance of the conservation of their efference copies for gaze stabilization along evolution.

2.7. Possible contribution of the lumbar CPG

In our neuroanatomy experiments, after 57h post-infection, we only identified RV^+ in the cervical and the lumbar spinal cord didn't reveal any infected neurons. When more than 67 hours post-infection were attained, the tracing was at a disynaptic (infected neurons in the cerebellum: abducens nucleus; central vestibular nuclei neurons; flocculi) stage. Moreover, this timepoint didn't infect any lumbar spinal cord neurons. With the experiments we performed, it can't be stated if this result is really due to the absence of LOINs directly projecting from the lumbar to the abducens nucleus or if this is a false negative. The explanation for a false negative could be that, due to lack of time for the virus to migrate since, the lumbar spinal cord is further away than the marked cervical and could need longer than 67h to reach it. Secondly, the 'horizontal' migrating profile of the RV could also explain the incapacity of reaching the lumbar without first infecting several other structures. That is, after the first monosynaptic infection, the virus would infect what is structurally closer.

In our experiments, both in decerebrated preparations and in electrophysiological recordings, the cervical spinal cord was sufficient to produce the spino-extraocular coupling. However, the role of the lumbar CPG isn't neglectable since a coordinated locomotion was also crucial for eliciting eye movements. Therefore, a weaker direct synaptic connection could be present. To verify this, more experiments could be done

using a modified RV. Modified RV are monosynaptically restricted and the tropism only occurs in genetically specified neuronal population (Wickersham et al., 2007). In this situation, the virus could be left to migrate for multiple days or weeks, knowing that it would only cross one synapse and thus, the putatively infected lumbar neurons would be certain to be monosynaptically connections from lumbar to the abducens nucleus.

2.8. The neurotransmitter content of the RV infected LOINs

Part of the experiments performed in this project aimed at mapping the spino-extraocular pathway using rabies virus (RV). The RV injection in the lateral rectus muscle monosynaptically infected neurons in the cervical spinal cord. The location of RV+ neurons was mainly in laminas VII, VIII and IX of the cervical spinal cord.

In these experiments, a systematic ChAT staining was performed to identify the motoneurons of the abducens nucleus. Surprisingly, there were a few ChAT+ neurons in the cervical spinal cord (See figure 2 E5 of the results section of Article 4) that were, unlike the rest of the infected neurons, positive for ChAT. The location of these cholinergic interneurons was bound to the area immediately contouring the central canal hence, Rexed's lamina X. The spinal cord has cholinergic interneurons that are thought to modulate sensory and motor output. One of the main cholinergic inputs to motoneurons are C-boutons, synaptic terminals onto motoneuron cell bodies and proximal dendrites. The source of these C-bouton synapses was identified as V0c neurons. V0c neurons are known to have the Pitx2 transcription factor (Zagoraiou et al., 2009) and to be located around the central canal, on lamina X. Therefore, our cholinergic interneurons could putatively be V0c. Therefore, experiments could be done using Pitx2 antibodies to detect if our cervical cholinergic interneurons are in fact V0c neurons.

In situ hybridization (ISH) experiments would allow to unravel the neurotransmitter content of the RV+ neurons in the spinal cord. We performed preliminary fluorescent ISH experiments that aimed at identifying inhibitory (GABA) and excitatory (glutamate) neurons in cervical spinal cord slices (**Figure 36**). This technique was preferred instead of standard immunohistochemistry experiments due to the lack of antibodies that detect properly glutamate and GABA inside the soma of neurons. However, this technique proved to be rather challenging since, due to technical limitations, it wasn't possible to do an *en masse* detection of these neurons in all the slices (approximately 200 slices, 200 µm-thick) that make up the cervical spinal cord. A way to overcome this obstacle would be to only perform the ISH protocol in slices that have infected neurons. To do so, slices with RV+ neurons would need to be identified without being mounted on a slide (free floating) and selected for the ISH experiments.

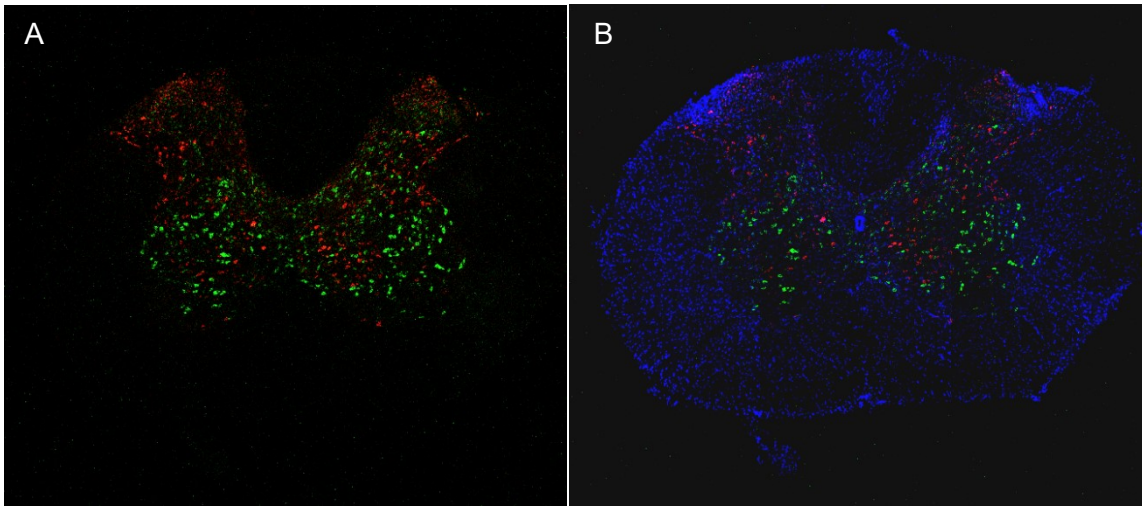

Figure 36. *In situ* hybridization of glutamatergic and GABAergic neurons of a cervical spinal cord segment. Red- vglut2 positive neurons; green- vesicular GABA transporter (VGAT) positive neurons of a C4 slice without (A) and with DAPI (B).

3. Therapies for inner ear pathologies

In the study presented in this thesis, AAV-mediated gene therapy was used to treat a mouse model of Ush1 syndrome, a congenital pathology that causes profound deafness and vestibular troubles. The used approach was able to partially restore hearing and completely restore the vestibular function in almost all mice. The following paragraphs discuss the results of Article 5.

Gene therapy was first conceptualized by Keeler in 1947 (Clyde E. Keeler, 1947). The author identified the capacity of applying an enduring, or possibly permanent, correction of the targeted pathology as one of the characteristics that could differentiate gene therapy from the therapies existing at the time. Nowadays, this is still one of the driving forces for the advance of gene therapy. Neurological diseases, including inner ear ones, can greatly benefit from this therapy since this approach targets the root cause of the pathology by reestablishing the function of the damaged or absent gene (Hudry & Vandenberghe, 2019).

The delivery route is a crucial factor for a successful gene therapy. This virus, unlike others (*e.g.*, rabies virus) isn't transsynaptic. Hence, it will only cross one synapse from the injection site. Therefore, the injection has to be directly applied in the desired organ. The virus can only target a specific cell type since the vector constructs have a recombinant promoter that codes for a gene that will only be expressed in the desired cells.

In the study presented in this thesis (Emptoz et al., 2017), the AAV was delivered in the round window of the cochlea. There, the difficulty of the delivery surgery was facilitated by the fact that this injection was performed in neonatal mice, whose tissues are very labile, and bones are yet matured, allowing the needle to easily access the inner ear. The access to the cochlea required the puncture of the, still malleable, temporal bone with a pair of sharp forceps, a much easier process than perforating a fully formed bone with a drill. Leakage of the virus was also a critical step of the procedure due to the inner ear fluids. When translating this therapy to humans, this therapy would involve more invasive surgical procedures so that the cochlea could be reached.

What also dictates a successful gene delivery is the serotype and capsid of the chosen AAV. To date, from the known AAV serotypes isolated from stock of human and primate tissue, at least 10 of them have been modified to recombinant viral vectors (Burger et al., 2005). They differ in the inverted terminal repeats that constitute the genome of the virus, the proteins of the capsids and consequently display different cell

tropisms in the host (Naso et al., 2017). AAV2 has been the virus of choice for most of the CNS injections of the studies performed so far (Burger et al., 2005). In our study, we tested 4 different serotypes: AAV1, AAV2, AAV5 and AAV8. From those, AAV8 was the one that successfully transduced hair cells and supporting cells of the cochlea. One of the obstacles of the current recombinant AAV viruses are the relatively small packaging capacity; they can hold a gene that is made of up to 5kb (Drouin & Agbandje-McKenna, 2013). Therefore, the insertion of bigger genes will be a point to overcome.

In addition to pathologies affecting the inner ear/vestibular endorgans, vestibular pathologies of the central nervous system could also be strong candidates for the use of AAV-mediated gene therapies. During my PhD, I had the opportunity of performing the delivery of AAV to the central vestibular system through the VIIIth nerve. I experimented with both AAV5 and AAV9 (Figure 37). However, the capsid that worked best for this delivery was AAV5 since the migration of the virus was closely restrained to the vestibulocochlear nerve. When AAV9 was used, the virus tendentially leaked outside the nerve (**Figure 37**). Thus, the type of AAV must be chosen according to the targeted area so that an optimal infection is attained. Nevertheless, this technique exhibits great potential and gene therapies have been the study of several recent studies (Delmaghani & El-Amraoui, 2020) and exhibit great potential as a therapeutic tool. Hopefully, AAV-mediated therapies will become a feasible clinical answer for auditory and vestibular restoration.

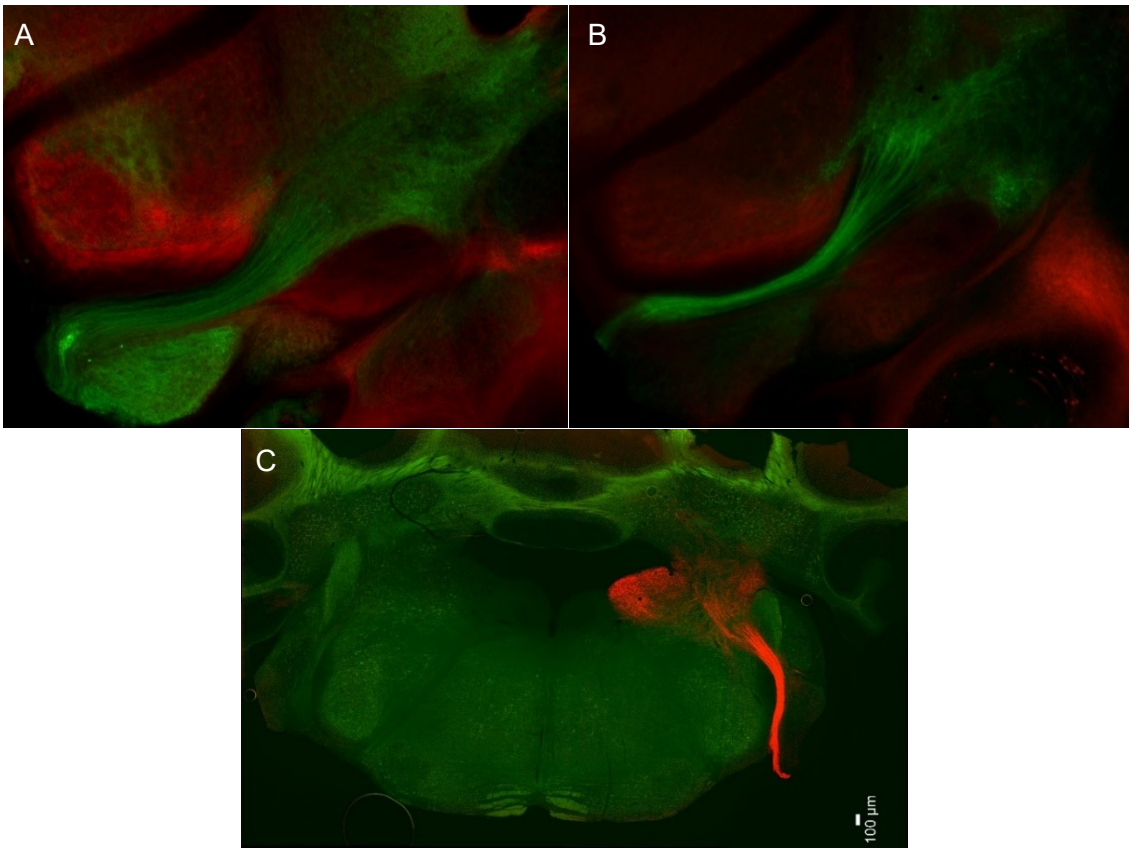

Figure 37. VIIIth nerve marked with fluorescent AAV. AAV9 (A) and AAV5 (B) were used to mark the vestibulocochlear nerve (green) in a mouse strain expressing the red fluorescent protein tdTomato in GABAergic neurons. C- Vestibulocochlear nerve (red) was traced using AAV5 in a mouse strain with green fluorescent proteins expressed in Thy1 neuronal cells. Images obtained with a fluorescence microscope with 10x (C) and 20x (A, B) magnification.

References

Abourachid, A. (2003). A new way of analysing symmetrical and asymmetrical gaits in quadrupeds. *Comptes Rendus Biologies*, *326*(7), 625–630. https://doi.org/10.1016/s1631-0691(03)00170-7

Abourachid, A., Herbin, M., Hackert, R., Maes, L., & Martin, V. (2007). Experimental study of coordination patterns during unsteady locomotion in mammals. *Journal of Experimental Biology*, *210*(2), 366–372. https://doi.org/10.1242/jeb.02632

Aguti, S., Malerba, A., & Zhou, H. (2018). The progress of AAV-mediated gene therapy in neuromuscular disorders. *Expert Opinion on Biological Therapy*, *18*(6), 681–693. https://doi.org/10.1080/14712598.2018.1479739

Andreas Vesalius. (1543). *De Humani Corporis Fabrica* (Vol. 1–7). Lugduni: Apud Joan. Tornaesium.

Angelaki, D. E. (2004). Eyes on Target: What Neurons Must do for the Vestibuloocular Reflex During Linear Motion. *Journal of Neurophysiology*, *92*(1), 20–35. https://doi.org/10.1152/jn.00047.2004

Angelaki, D. E., & Cullen, K. E. (2008). Vestibular System: The Many Facets of a Multimodal Sense. *Annual Review of Neuroscience*, *31*(1), 125–150. https://doi.org/10.1146/annurev.neuro.31.060407.125555

Babalian, A. L., & Vidal, P.-P. (2000). Floccular Modulation of Vestibuloocular Pathways and Cerebellum-Related Plasticity: An In Vitro Whole Brain Study. *Journal of Neurophysiology*, *84*(5), 2514–2528. https://doi.org/10.1152/jn.2000.84.5.2514

Bacqué-Cazenave, J., Courtand, G., Beraneck, M., Lambert, F. M., & Combes, D. (2018). Temporal Relationship of Ocular and Tail Segmental Movements Underlying Locomotor-Induced Gaze Stabilization During Undulatory Swimming in Larval Xenopus. *Frontiers in Neural Circuits*, *12*, 95. https://doi.org/10.3389/fncir.2018.00095

Badea, T. C., Cahill, H., Ecker, J., Hattar, S., & Nathans, J. (2009). Distinct Roles of Transcription Factors Brn3a and Brn3b in Controlling the Development, Morphology, and Function of Retinal Ganglion Cells. *Neuron*, *61*(6), 852–864. https://doi.org/10.1016/j.neuron.2009.01.020

Bahill, A. T., Clark, M. R., & Stark, L. (1975). The main sequence, a tool for studying human eye movements. *Mathematical Biosciences*, *24*(3), 191–204. https://doi.org/10.1016/0025-5564(75)90075-9

Ballion, B., Morin, D., & Viala, D. (2001). Forelimb locomotor generators and quadrupedal locomotion in the neonatal rat. *The European Journal of Neuroscience*, *14*(10), 1727–1738. https://doi.org/10.1046/j.0953-816x.2001.01794.x

Bankoul, S., & Neuhuber, W. L. (1990). A cervical primary afferent input to vestibular nuclei as demonstrated by retrograde transport of wheat germ agglutinin-horseradish peroxidase in the rat. *Experimental Brain Research*, *79*(2), 405–411. https://doi.org/10.1007/bf00608252

Barnes, G. R., & Collins, C. J. S. (2008). Internally generated smooth eye movement: Its dynamic characteristics and role in randomised and predictable pursuit. *Progress in Brain Research*, *171*, 441–449. https://doi.org/10.1016/S0079-6123(08)00665-1

Beraneck, M., & Cullen, K. E. (2007). Activity of vestibular nuclei neurons during vestibular and optokinetic stimulation in the alert mouse. *Journal of Neurophysiology*, *98*(3), 1549–1565. https://doi.org/10.1152/jn.00590.2007

Beraneck, Mathieu, Bojados, M., Le Séac'h, A., Jamon, M., & Vidal, P.-P. (2012). Ontogeny of Mouse Vestibulo-Ocular Reflex Following Genetic or Environmental Alteration of Gravity Sensing. *PLoS ONE*, *7*(7), e40414. https://doi.org/10.1371/journal.pone.0040414

Beraneck, Mathieu, Lambert, F. M., & Sadeghi, S. G. (2014). Functional Development of the Vestibular System. In *Development of Auditory and Vestibular Systems* (pp. 449–487). Elsevier. https://doi.org/10.1016/B978-0-12-408088-1.00015-4

Beraneck, Mathieu, Pfanzelt, S., Vassias, I., Rohregger, M., Vibert, N., Vidal, P.-P., Moore, L. E., & Straka, H. (2007). Differential intrinsic response dynamics determine synaptic signal processing in frog vestibular neurons. *The Journal of Neuroscience: The Official Journal of the Society for Neuroscience*, *27*(16), 4283–4296. https://doi.org/10.1523/JNEUROSCI.5232-06.2007

Beraneck, Mathieu, & Straka, H. (2011). Vestibular signal processing by separate sets of neuronal filters. *Journal of Vestibular Research: Equilibrium & Orientation*, *21*(1), 5–19. https://doi.org/10.3233/VES-2011-0396

Bittar, R. S. M., Oiticica, J., Bottino, M. A., Ganança, F. F., Dimitrov, R., Bittar, R. S. M., Oiticica, J., Bottino, M. A., Ganança, F. F., & Dimitrov, R. (2013). Population epidemiological study on the prevalence of dizziness in the city of São Paulo. *Brazilian Journal of Otorhinolaryngology*, *79*(6), 688–698. https://doi.org/10.5935/1808-8694.20130127

Blakemore, S. J., Wolpert, D. M., & Frith, C. D. (1998). Central cancellation of self-produced tickle sensation. *Nature Neuroscience*, *1*(7), 635–640. https://doi.org/10.1038/2870

Blanks, R. H., Curthoys, I. S., & Markham, C. H. (1975). Planar relationships of the semicircular canals in man. *Acta Oto-Laryngologica*, *80*(3–4), 185–196. https://doi.org/10.3109/00016487509121318

Bohlen, M. O., Bui, K., Stahl, J. S., May, P. J., & Warren, S. (2019). Mouse Extraocular Muscles and the Musculotopic Organization of Their Innervation. *The Anatomical Record*, *302*(10), 1865–1885. https://doi.org/10.1002/ar.24141

Boyden, E. S., Katoh, A., & Raymond, J. L. (2004). CEREBELLUM-DEPENDENT LEARNING: The Role of Multiple Plasticity Mechanisms. *Annual Review of Neuroscience*, *27*(1), 581–609. https://doi.org/10.1146/annurev.neuro.27.070203.144238

Boyden, E. S., & Raymond, J. L. (2003). Active Reversal of Motor Memories Reveals Rules Governing Memory Encoding. *Neuron*, *39*(6), 1031–1042. https://doi.org/10.1016/S0896-6273(03)00562-2

Brandt, T., Strupp, M., & Benson, J. (1999). You are better off running than walking with acute vestibulopathy. *The Lancet*, *354*(9180), 746. https://doi.org/10.1016/S0140-6736(99)03179-7

Bras, H., Gaytán, S. P., Portalier, P., Zanella, S., Pásaro, R., Coulon, P., & Hilaire, G. (2008). Prenatal activation of 5-HT $_{2A}$ receptor induces expression of 5-HT $_{1B}$ receptor in phrenic motoneurons and alters the organization of their premotor network in newborn mice. *European Journal of Neuroscience*, *28*(6), 1097–1107. https://doi.org/10.1111/j.1460-9568.2008.06407.x

Brodal, A., & Pompeiano, O. (1957). The vestibular nuclei in the cat. *Journal of Anatomy*, *91*(Pt 4), 438-454.1.

Brown, T. G. (1911). The Intrinsic Factors in the Act of Progression in the Mammal. *Proceedings of the Royal Society B: Biological Sciences*, *84*(572), 308–319. https://doi.org/10.1098/rspb.1911.0077

Burger, C., Nash, K., & Mandel, R. J. (2005). Recombinant adeno-associated viral vectors in the nervous system. *Human Gene Therapy*, *16*(7), 781–791. https://doi.org/10.1089/hum.2005.16.781

Busse, L., Cardin, J. A., Chiappe, M. E., Halassa, M. M., McGinley, M. J., Yamashita, T., & Saleem, A. B. (2017). Sensation during Active Behaviors. *The Journal of Neuroscience: The Official Journal of the Society for Neuroscience*, *37*(45), 10826–10834. https://doi.org/10.1523/JNEUROSCI.1828-17.2017

Büttner, U., & Büttner-Ennever, J. A. (2006). Present concepts of oculomotor organization. In *Progress in Brain Research* (Vol. 151, pp. 1–42). Elsevier. https://doi.org/10.1016/S0079-6123(05)51001-X

Büttner, U., & Lang, W. (1979). The vestibulocortical pathway: Neurophysiological and anatomical studies in the monkey. *Progress in Brain Research*, *50*, 581–588. https://doi.org/10.1016/S0079-6123(08)60856-0

Büttner-Ennever, J. A. (2006). The extraocular motor nuclei: Organization and functional neuroanatomy. In *Progress in Brain Research* (Vol. 151, pp. 95–125). Elsevier. https://doi.org/10.1016/S0079-6123(05)51004-5

Büttner-ennever, J. A., & Gerrits, N. M. (2004). CHAPTER 33—Vestibular System. In G. Paxinos & J. K. Mai (Eds.), *The Human Nervous System (Second Edition)* (pp. 1212–1240). Academic Press. https://doi.org/10.1016/B978-012547626-3/50034-X

Calabrese, D. R., & Hullar, T. E. (2006). Planar Relationships of the Semicircular Canals in Two Strains of Mice. *Journal of the Association for Research in Otolaryngology*, *7*(2), 151–159. https://doi.org/10.1007/s10162-006-0031-1

Carcaud, J., França de Barros, F., Idoux, E., Eugène, D., Reveret, L., Moore, L. E., Vidal, P.-P., & Beraneck, M. (2017). Long-Lasting Visuo-Vestibular Mismatch in Freely-Behaving Mice Reduces the Vestibulo-Ocular Reflex and Leads to Neural Changes in the Direct Vestibular Pathway. *ENeuro*, *4*(1). https://doi.org/10.1523/ENEURO.0290-16.2017

Carey, M. R. (2011). Synaptic mechanisms of sensorimotor learning in the cerebellum. *Current Opinion in Neurobiology*, *21*(4), 609–615. https://doi.org/10.1016/j.conb.2011.06.011

Carleton, S. C., & Carpenter, M. B. (1984). Distribution of primary vestibular fibers in the brainstem and cerebellum of the monkey. *Brain Research*, *294*(2), 281–298. https://doi.org/10.1016/0006-8993(84)91040-0

Carpenter, M. B. (1988). Chapter 1 Vestibular nuclei: Afferent and efferent projections. In O. Pompeiano & J. H. J. Allum (Eds.), *Progress in Brain Research* (Vol. 76, pp. 5–15). Elsevier. https://doi.org/10.1016/S0079-6123(08)64487-8

Carriot, J., Jamali, M., Chacron, M. J., & Cullen, K. E. (2017). The statistics of the vestibular input experienced during natural self-motion differ between rodents and primates. *The Journal of Physiology*, *595*(8), 2751–2766. https://doi.org/10.1113/JP273734

Cazalets, J., Borde, M., & Clarac, F. (1995). Localization and organization of the central pattern generator for hindlimb locomotion in newborn rat. *The Journal of Neuroscience*, *15*(7), 4943–4951. https://doi.org/10.1523/JNEUROSCI.15-07-04943.1995

Chalupa, L. M., & Williams, R. W. (Eds.). (2008). *Eye, retina, and visual system of the mouse*. MIT Press.

Clyde E. Keeler. (1947). *Gene therapy*.

Cohen, B., Matsuo, V., & Raphan, T. (1977). Quantitative analysis of the velocity characteristics of optokinetic nystagmus and optokinetic after-nystagmus. *The*

Journal of Physiology, *270*(2), 321–344. https://doi.org/10.1113/jphysiol.1977.sp011955

Cohen, H., Cohen, B., Raphan, T., & Waespe, W. (1992). Habituation and adaptation of the vestibuloocular reflex: A model of differential control by the vestibulocerebellum. *Experimental Brain Research*, *90*(3), 526–538. https://doi.org/10.1007/bf00230935

Collewijn, H., & Grootendorst, A. F. (1979). Adaptation of Optokinetic and Vestibulo-Ocular Reflexes to Modified Visual Input in the Rabbit. In R. Granit & O. Pompeiano (Eds.), *Progress in Brain Research* (Vol. 50, pp. 771–781). Elsevier. https://doi.org/10.1016/S0079-6123(08)60874-2

Combes, D., Le Ray, D., Lambert, F. M., Simmers, J., & Straka, H. (2008). An intrinsic feed-forward mechanism for vertebrate gaze stabilization. *Current Biology*, *18*(6), R241–R243. https://doi.org/10.1016/j.cub.2008.02.018

Coulon, P., Bras, H., & Vinay, L. (2011). Characterization of last-order premotor interneurons by transneuronal tracing with rabies virus in the neonatal mouse spinal cord. *The Journal of Comparative Neurology*, *519*(17), 3470–3487. https://doi.org/10.1002/cne.22717

Cruz, T., Fujiwara, T., Varela, N., Mohammad, F., Claridge-Chang, A., & Chiappe, M. E. (2019). Motor context coordinates visually guided walking in Drosophila. *BioRxiv*, 572792. https://doi.org/10.1101/572792

Cullen, K. E. (2012). The vestibular system: Multimodal integration and encoding of self-motion for motor control. *Trends in Neurosciences*, *35*(3), 185–196. https://doi.org/10.1016/j.tins.2011.12.001

Cullen, K. E. (2019). Vestibular processing during natural self-motion: Implications for perception and action. *Nature Reviews. Neuroscience*, *20*(6), 346–363. https://doi.org/10.1038/s41583-019-0153-1

Delmaghani, S., & El-Amraoui, A. (2020). Inner Ear Gene Therapies Take Off: Current Promises and Future Challenges. *Journal of Clinical Medicine*, *9*(7). https://doi.org/10.3390/jcm9072309

Dhande, O. S., Estevez, M. E., Quattrochi, L. E., El-Danaf, R. N., Nguyen, P. L., Berson, D. M., & Huberman, A. D. (2013). Genetic Dissection of Retinal Inputs to Brainstem Nuclei Controlling Image Stabilization. *Journal of Neuroscience*, *33*(45), 17797–17813. https://doi.org/10.1523/JNEUROSCI.2778-13.2013

Dhande, O. S., & Huberman, A. D. (2014). Retinal ganglion cell maps in the brain: Implications for visual processing. *Current Opinion in Neurobiology*, *24*, 133–142. https://doi.org/10.1016/j.conb.2013.08.006

Dickman, J. D., & Angelaki, D. E. (2002). Vestibular convergence patterns in vestibular nuclei neurons of alert primates. *Journal of Neurophysiology*, *88*(6), 3518–3533. https://doi.org/10.1152/jn.00518.2002

Dietrich, H., Heidger, F., Schniepp, R., MacNeilage, P. R., Glasauer, S., & Wuehr, M. (2020). Head motion predictability explains activity-dependent suppression of vestibular balance control. *Scientific Reports*, *10*(1), 668. https://doi.org/10.1038/s41598-019-57400-z

Dietrich, H., & Wuehr, M. (2019). Strategies for Gaze Stabilization Critically Depend on Locomotor Speed. *Neuroscience*, *408*, 418–429. https://doi.org/10.1016/j.neuroscience.2019.01.025

Dietrich, Haike, & Wuehr, M. (2019). Selective suppression of the vestibulo-ocular reflex during human locomotion. *Journal of Neurology*, *266*(Suppl 1), 101–107. https://doi.org/10.1007/s00415-019-09352-7

Dodge, R. (1903). Five types of eye movement in the horizontal meridian plane of the field of regard. *American Journal of Physiology-Legacy Content*, *8*(4), 307–329. https://doi.org/10.1152/ajplegacy.1903.8.4.307

Drager, U. C. (1978). Observations on monocular deprivation in mice. *Journal of Neurophysiology*, *41*(1), 28–42. https://doi.org/10.1152/jn.1978.41.1.28

Drouin, L. M., & Agbandje-McKenna, M. (2013). Adeno-associated virus structural biology as a tool in vector development. *Future Virology*, *8*(12), 1183–1199. https://doi.org/10.2217/fvl.13.112

Eatock, R. A. (2000). Adaptation in Hair Cells. *Annual Review of Neuroscience*, *23*(1), 285–314. https://doi.org/10.1146/annurev.neuro.23.1.285

Eatock, R. A., & Songer, J. E. (2011). Vestibular Hair Cells and Afferents: Two Channels for Head Motion Signals. *Annual Review of Neuroscience*, *34*(1), 501–534. https://doi.org/10.1146/annurev-neuro-061010-113710

El-Amraoui, A., & Petit, C. (2014). The retinal phenotype of Usher syndrome: Pathophysiological insights from animal models. *Comptes Rendus Biologies*, *337*(3), 167–177. https://doi.org/10.1016/j.crvi.2013.12.004

Emptoz, A., Michel, V., Lelli, A., Akil, O., Boutet de Monvel, J., Lahlou, G., Meyer, A., Dupont, T., Nouaille, S., Ey, E., Franca de Barros, F., Beraneck, M., Dulon, D., Hardelin, J.-P., Lustig, L., Avan, P., Petit, C., & Safieddine, S. (2017). Local gene therapy durably restores vestibular function in a mouse model of Usher syndrome type 1G. *Proceedings of the National Academy of Sciences of the United States of America*, *114*(36), 9695–9700. https://doi.org/10.1073/pnas.1708894114

Epema, A. H., Gerrits, N. M., & Voogd, J. (1988). Commissural and intrinsic connections of the vestibular nuclei in the rabbit: A retrograde labeling study. *Experimental Brain Research*, *71*(1), 129–146. https://doi.org/10.1007/bf00247528

Ernst Mach. (1873). Physikalische Versuche ¨uber den Gleichgewichtssinn desMenschen. *Ber Akad Wiss Wien Mathnaturw Kl*, 124–140.

Falgairolle, M., de Seze, M., Juvin, L., Morin, D., & Cazalets, J.-R. (2006). Coordinated network functioning in the spinal cord: An evolutionary perspective. *Journal of Physiology-Paris*, *100*(5), 304–316. https://doi.org/10.1016/j.jphysparis.2007.05.003

Faulstich, B. M., Onori, K. A., & du Lac, S. (2004). Comparison of plasticity and development of mouse optokinetic and vestibulo-ocular reflexes suggests differential gain control mechanisms. *Vision Research*, *44*(28), 3419–3427. https://doi.org/10.1016/j.visres.2004.09.006

Fedirchuk, B., Stecina, K., Kristensen, K. K., Zhang, M., Meehan, C. F., Bennett, D. J., & Hultborn, H. (2013). Rhythmic activity of feline dorsal and ventral spinocerebellar tract neurons during fictive motor actions. *Journal of Neurophysiology*, *109*(2), 375–388. https://doi.org/10.1152/jn.00649.2012

Fernández, C., Baird, R. A., & Goldberg, J. M. (1988). The vestibular nerve of the chinchilla. I. Peripheral innervation patterns in the horizontal and superior semicircular canals. *Journal of Neurophysiology*, *60*(1), 167–181. https://doi.org/10.1152/jn.1988.60.1.167

Fernandez, C., & Goldberg, J. M. (1976). Physiology of peripheral neurons innervating otolith organs of the squirrel monkey. I. Response to static tilts and to long-duration centrifugal force. *Journal of Neurophysiology*, *39*(5), 970–984. https://doi.org/10.1152/jn.1976.39.5.970

França de Barros, F., Carcaud, J., & Beraneck, M. (2019). Long-term Sensory Conflict in Freely Behaving Mice. *Journal of Visualized Experiments: JoVE*, *144*. https://doi.org/10.3791/59135

Friedman, T. B., Schultz, J. M., & Ahmed, Z. M. (2005). Usher syndrome type 1: Genotype-phenotype relationships. *Retina (Philadelphia, Pa.)*, *25*(8 Suppl), S40–S42. https://doi.org/10.1097/00006982-200512001-00016

Fuchs, A. F., & Kimm, J. (1975). Unit activity in vestibular nucleus of the alert monkey during horizontal angular acceleration and eye movement. *Journal of Neurophysiology*, *38*(5), 1140–1161. https://doi.org/10.1152/jn.1975.38.5.1140

Fujiwara, T., Cruz, T. L., Bohnslav, J. P., & Chiappe, M. E. (2017). A faithful internal representation of walking movements in the Drosophila visual system. *Nature Neuroscience*, *20*(1), 72–81. https://doi.org/10.1038/nn.4435

Fukuda, T., & Tokita, T. (1957). [Relation of the direction of optical stimulation to the type of reflex of the oculomotor muscles]. *Acta Oto-Laryngologica*, *48*(5–6), 415–424. https://doi.org/10.3109/00016485709126902

Gaudin, Y., Ruigrok, R. W. H., Tuffereau, C., Knossow, M., & Flamand, A. (1992). Rabies virus glycoprotein is a trimer. *Virology*, *187*(2), 627–632. https://doi.org/10.1016/0042-6822(92)90465-2

Goldberg, J. M., & Fernandez, C. (1975). Responses Of Peripheral Vestibular Neurons To Angular And Linear Accelerations In The Squirrel Monkey. *Acta Oto-Laryngologica*, *80*(1–6), 101–110. https://doi.org/10.3109/00016487509121307

Goldberg, J. M., & Fernández, C. (1980). Efferent vestibular system in the squirrel monkey: Anatomical location and influence on afferent activity. *Journal of Neurophysiology*, *43*(4), 986–1025. https://doi.org/10.1152/jn.1980.43.4.986

Goldberg, J. M., Highstein, S. M., Moschovakis, A. K., & Fernandez, C. (1987). Inputs from regularly and irregularly discharging vestibular nerve afferents to secondary neurons in the vestibular nuclei of the squirrel monkey. I. An electrophysiological analysis. *Journal of Neurophysiology*, *58*(4), 700–718. https://doi.org/10.1152/jn.1987.58.4.700

Goldberg, Jay M. (2000). Afferent diversity and the organization of central vestibular pathways. *Experimental Brain Research. Experimentelle Hirnforschung. Experimentation Cerebrale*, *130*(3), 277–297.

Goldberg, Jay M., Wilson, V. J., Cullen, K. E., Angelaki, D. E., Broussard, D. M., Büttner-Ennever, J. A., Fukushima, K., & Minor, L. B. (2012a). *Historical transformation: Ancillary Material for Chapter 1*. Oxford University Press. https://www.oxfordscholarship.com/view/10.1093/acprof:oso/9780195167085.001.0001/acprof-9780195167085-chapter-001

Goldberg, Jay M., Wilson, V. J., Cullen, K. E., Angelaki, D. E., Broussard, D. M., Büttner-Ennever, J. A., Fukushima, K., & Minor, L. B. (2012b). *Structure of the Vestibular Labyrinth*. Oxford University Press. https://www.oxfordscholarship.com/view/10.1093/acprof:oso/9780195167085.001.0001/acprof-9780195167085-chapter-002

Goldberg, Jay M., Wilson, V. J., Cullen, K. E., Angelaki, D. E., Broussard, D. M., Büttner-Ennever, J. A., Fukushima, K., & Minor, L. B. (2012c). *The Vestibular System: A Sixth Sense*. Oxford University Press. https://www.oxfordscholarship.com/view/10.1093/acprof:oso/9780195167085.001.0001/acprof-9780195167085-chapter-001

Goldberg, Jay M., Wilson, V. J., Cullen, K. E., Angelaki, D. E., Broussard, D. M., Büttner-Ennever, J. A., Fukushima, K., & Minor, L. B. (2012d). *The Vestibular System in*

Everyday Life. Oxford University Press. https://www.oxfordscholarship.com/view/10.1093/acprof:oso/9780195167085.001.0001/acprof-9780195167085-chapter-001

Goulding, M. (2009). Circuits controlling vertebrate locomotion: Moving in a new direction. *Nature Reviews Neuroscience*, *10*(7), 507–518. https://doi.org/10.1038/nrn2608

Grantyn, A., Brandi, A.-M., Dubayle, D., Graf, W., Ugolini, G., Hadjidimitrakis, K., & Moschovakis, A. (2002). Density gradients of trans-synaptically labeled collicular neurons after injections of rabies virus in the lateral rectus muscle of the rhesus monkey. *The Journal of Comparative Neurology*, *451*(4), 346–361. https://doi.org/10.1002/cne.10353

Gray, P. A., Janczewski, W. A., Mellen, N., McCrimmon, D. R., & Feldman, J. L. (2001). Normal breathing requires preBötzinger complex neurokinin-1 receptor-expressing neurons. *Nature Neuroscience*, *4*(9), 927–930. https://doi.org/10.1038/nn0901-927

Grillner, S. (2003). The motor infrastructure: From ion channels to neuronal networks. *Nature Reviews Neuroscience*, *4*(7), 573–586. https://doi.org/10.1038/nrn1137

Gustafsson, B., & Lindström, S. (1973). Recurrent control from motor axon collaterals of Ia inhibitory pathways to ventral spinocerebellar tract neurones. *Acta Physiologica Scandinavica*, *89*(4), 457–481. https://doi.org/10.1111/j.1748-1716.1973.tb05541.x

Hain, T. C. (2007). Chapter 12 - Cranial Nerve VIII: Vestibulocochlear System. In C. G. Goetz (Ed.), *Textbook of Clinical Neurology (Third Edition)* (pp. 199–215). W.B. Saunders. https://doi.org/10.1016/B978-141603618-0.10012-8

Heesy, C. P. (2004). On the relationship between orbit orientation and binocular visual field overlap in mammals. *The Anatomical Record Part A: Discoveries in Molecular, Cellular, and Evolutionary Biology*, *281A*(1), 1104–1110. https://doi.org/10.1002/ar.a.20116

Herbin, M., Gasc, J.-P., & Renous, S. (2004). Symmetrical and asymmetrical gaits in the mouse: Patterns to increase velocity. *Journal of Comparative Physiology A*, *190*(11), 895–906. https://doi.org/10.1007/s00359-004-0545-0

Highstein, S. M., & Holstein, G. R. (2006). The Anatomy of the vestibular nuclei. In J. A. Büttner-Ennever (Ed.), *Progress in Brain Research* (Vol. 151, pp. 157–203). Elsevier. https://doi.org/10.1016/S0079-6123(05)51006-9

Hückesfeld, S., Schoofs, A., Schlegel, P., Miroschnikow, A., & Pankratz, M. J. (2015). Localization of Motor Neurons and Central Pattern Generators for Motor Patterns

Underlying Feeding Behavior in Drosophila Larvae. *PLOS ONE*, *10*(8), e0135011. https://doi.org/10.1371/journal.pone.0135011

Hudry, E., & Vandenberghe, L. H. (2019). Therapeutic AAV Gene Transfer to the Nervous System: A Clinical Reality. *Neuron*, *101*(5), 839–862. https://doi.org/10.1016/j.neuron.2019.02.017

Hultborn, H., & Kiehn, O. (1992). Neuromodulation of vertebrate motor neuron membrane properties. *Current Opinion in Neurobiology*, *2*(6), 770–775. https://doi.org/10.1016/0959-4388(92)90132-5

Idoux, E., Tagliabue, M., & Beraneck, M. (2018). No Gain No Pain: Relations Between Vestibulo-Ocular Reflexes and Motion Sickness in Mice. *Frontiers in Neurology*, *9*, 918. https://doi.org/10.3389/fneur.2018.00918

Inoue, Y., Takemura, A., Kawano, K., Kitama, T., & Miles, F. A. (1998). Dependence of short-latency ocular following and associated activity in the medial superior temporal area (MST) on ocular vergence. *Experimental Brain Research*, *121*(2), 135–144. https://doi.org/10.1007/s002210050445

Ito, M. (2006). Cerebellar circuitry as a neuronal machine. *Progress in Neurobiology*, *78*(3), 272–303. https://doi.org/10.1016/j.pneurobio.2006.02.006

Johnston, J. L., & Sharpe, J. A. (1994). The initial vestibulo-ocular reflex and its visual enhancement and cancellation in humans. *Experimental Brain Research*, *99*(2), 302–308. https://doi.org/10.1007/bf00239596

Joseph Breuer. (1873). ¨ Uber die Bogeng¨ange das Labyrinths: Vorl¨aufige Mitteilung. *Anz Ges d ¨ Arzte*, *7*, 15–18.

Josset, N., Roussel, M., Lemieux, M., Lafrance-Zoubga, D., Rastqar, A., & Bretzner, F. (2018). Distinct Contributions of Mesencephalic Locomotor Region Nuclei to Locomotor Control in the Freely Behaving Mouse. *Current Biology*, *28*(6), 884-901.e3. https://doi.org/10.1016/j.cub.2018.02.007

Kassardjian, C. D. (2005). The Site of a Motor Memory Shifts with Consolidation. *Journal of Neuroscience*, *25*(35), 7979–7985. https://doi.org/10.1523/JNEUROSCI.2215-05.2005

Kelley, D. B., & Bass, A. H. (2010). Neurobiology of vocal communication: Mechanisms for sensorimotor integration and vocal patterning. *Current Opinion in Neurobiology*, *20*(6), 748–753. https://doi.org/10.1016/j.conb.2010.08.007

Khan, S., & Chang, R. (2013). Anatomy of the vestibular system: A review. *NeuroRehabilitation*, *32*(3), 437–443. https://doi.org/10.3233/NRE-130866

Kim, A. J., Fitzgerald, J. K., & Maimon, G. (2015). Cellular evidence for efference copy in Drosophila visuomotor processing. *Nature Neuroscience*, *18*(9), 1247–1255. https://doi.org/10.1038/nn.4083

Kim, L. H., Sharma, S., Sharples, S. A., Mayr, K. A., Kwok, C. H. T., & Whelan, P. J. (2017). Integration of Descending Command Systems for the Generation of Context-Specific Locomotor Behaviors. *Frontiers in Neuroscience*, *11*. https://doi.org/10.3389/fnins.2017.00581

Kodama, T., & du Lac, S. (2016). Adaptive Acceleration of Visually Evoked Smooth Eye Movements in Mice. *The Journal of Neuroscience: The Official Journal of the Society for Neuroscience*, *36*(25), 6836–6849. https://doi.org/10.1523/JNEUROSCI.0067-16.2016

Lambert, F. M., Combes, D., Simmers, J., & Straka, H. (2012). Gaze Stabilization by Efference Copy Signaling without Sensory Feedback during Vertebrate Locomotion. *Current Biology*, *22*(18), 1649–1658. https://doi.org/10.1016/j.cub.2012.07.019

Land, M. (2019). Eye movements in man and other animals. *Vision Research*, *162*, 1–7. https://doi.org/10.1016/j.visres.2019.06.004

Land, M. F. (2013). Animal Vision: Rats Watch the Sky. *Current Biology*, *23*(14), R611–R613. https://doi.org/10.1016/j.cub.2013.06.015

Laurens, J., & Angelaki, D. E. (2011). The functional significance of velocity storage and its dependence on gravity. *Experimental Brain Research*, *210*(3–4), 407–422. https://doi.org/10.1007/s00221-011-2568-4

Lemieux, M., Josset, N., Roussel, M., Couraud, S., & Bretzner, F. (2016). Speed-Dependent Modulation of the Locomotor Behavior in Adult Mice Reveals Attractor and Transitional Gaits. *Frontiers in Neuroscience*, *10*. https://doi.org/10.3389/fnins.2016.00042

Lim, R., & Brichta, A. M. (2012). Chapter 27—Vestibular System. In C. Watson, G. Paxinos, & L. Puelles (Eds.), *The Mouse Nervous System* (pp. 661–681). Academic Press. https://doi.org/10.1016/B978-0-12-369497-3.10027-5

Lindeman, H. H. (1969). Regional differences in structure of the vestibular sensory regions. *The Journal of Laryngology and Otology*, *83*(1), 1–17. https://doi.org/10.1017/s0022215100070018

Lisberger, S. G. (1984). The latency of pathways containing the site of motor learning in the monkey vestibulo-ocular reflex. *Science*, *225*(4657), 74–76. https://doi.org/10.1126/science.6610214

Lisberger, S. G., & Fuchs, A. F. (1978). Role of primate flocculus during rapid behavioral modification of vestibuloocular reflex. I. Purkinje cell activity during visually guided horizontal smooth-pursuit eye movements and passive head rotation. *Journal of Neurophysiology*. https://doi.org/10.1152/jn.1978.41.3.733

Lisberger, S. G., & Miles, F. A. (1980). Role of primate medial vestibular nucleus in long-term adaptive plasticity of vestibuloocular reflex. *Journal of Neurophysiology*, *43*(6), 1725–1745. https://doi.org/10.1152/jn.1980.43.6.1725

Lorente de Nó. (1933). Vestibulo-ocular reflex arc. *Arch. Neurol. Psychiatry*, 245–291.

Machado, A. S., Darmohray, D. M., Fayad, J., Marques, H. G., & Carey, M. R. (2015). A quantitative framework for whole-body coordination reveals specific deficits in freely walking ataxic mice. *ELife*, *4*. https://doi.org/10.7554/eLife.07892

MacNeilage, P. R., & Glasauer, S. (2017). Quantification of Head Movement Predictability and Implications for Suppression of Vestibular Input during Locomotion. *Frontiers in Computational Neuroscience*, *11*. https://doi.org/10.3389/fncom.2017.00047

Masseck, O. A., & Hoffmann, K.-P. (2009). Comparative Neurobiology of the Optokinetic Reflex. *Annals of the New York Academy of Sciences*, *1164*(1), 430–439. https://doi.org/10.1111/j.1749-6632.2009.03854.x

Mathis, A., Mamidanna, P., Cury, K. M., Abe, T., Murthy, V. N., Mathis, M. W., & Bethge, M. (2018). DeepLabCut: Markerless pose estimation of user-defined body parts with deep learning. *Nature Neuroscience*, *21*(9), 1281. https://doi.org/10.1038/s41593-018-0209-y

McKelvey-Briggs, D. K., Saint-Cyr, J. A., Spence, S. J., & Partlow, G. D. (1989). A reinvestigation of the spinovestibular projection in the cat using axonal transport techniques. *Anatomy and Embryology*, *180*(3), 281–291. https://doi.org/10.1007/bf00315886

Mebatsion, T., König, M., & Conzelmann, K.-K. (1996). Budding of Rabies Virus Particles in the Absence of the Spike Glycoprotein. *Cell*, *84*(6), 941–951. https://doi.org/10.1016/S0092-8674(00)81072-7

Medina, J. F. (2011). The multiple roles of Purkinje cells in sensori-motor calibration: To predict, teach and command. *Current Opinion in Neurobiology*, *21*(4), 616–622. https://doi.org/10.1016/j.conb.2011.05.025

Meehan, C. F., Mayr, K. A., Manuel, M., Nakanishi, S. T., & Whelan, P. J. (2017). Decerebrate mouse model for studies of the spinal cord circuits. *Nature Protocols*, *12*(4), 732–747. https://doi.org/10.1038/nprot.2017.001

Menzies, J. R. W., Porrill, J., Dutia, M., & Dean, P. (2010). Synaptic Plasticity in Medial Vestibular Nucleus Neurons: Comparison with Computational Requirements of VOR Adaptation. *PLoS ONE*, *5*(10), e13182. https://doi.org/10.1371/journal.pone.0013182

Miles, F. A. (1998). The neural processing of 3-D visual information: Evidence from eye movements. *The European Journal of Neuroscience*, *10*(3), 811–822. https://doi.org/10.1046/j.1460-9568.1998.00112.x

Miles, F. A., & Lisberger, S. G. (1981). Plasticity in the vestibulo-ocular reflex: A new hypothesis. *Annual Review of Neuroscience*, *4*, 273–299. https://doi.org/10.1146/annurev.ne.04.030181.001421

Mitsacos, A., Reisine, H., & Highstein, S. M. (1983). The superior vestibular nucleus: An intracellular HRP study in the cat. I. Vestibulo-ocular neurons. *The Journal of Comparative Neurology*, *215*(1), 78–91. https://doi.org/10.1002/cne.902150107

Naso, M. F., Tomkowicz, B., Perry, W. L., & Strohl, W. R. (2017). Adeno-Associated Virus (AAV) as a Vector for Gene Therapy. *BioDrugs*, *31*(4), 317–334. https://doi.org/10.1007/s40259-017-0234-5

Nikolic, J., Lagaudrière-Gesbert, C., Scrima, N., Blondel, D., & Gaudin, Y. (2019). Structure and Function of Negri Bodies. *Advances in Experimental Medicine and Biology*, *1215*, 111–127. https://doi.org/10.1007/978-3-030-14741-9_6

Ohio, D. of N. R. J. L. P., Neuroscience Otolaryngology and Biomedical Engineering Case Western Reserve University University Hospitals and Veterans Affairs Medical Center Cleveland, & Neuroscience, D. of N. D. S. Z. P., Ophthalmology Otolaryngology Head and Neck Surgery and. (1999). *The Neurology of Eye Movements: Text and CD-ROM: Text and CD-ROM*. Oxford University Press, USA.

Orlovsky, G., Deliagina, T. G., & Grillner, S. (1999). *Neuronal Control of Locomotion: From Mollusc to Man*. Oxford University Press. https://www.oxfordscholarship.com/view/10.1093/acprof:oso/9780198524052.001.0001/acprof-9780198524052

Oyster, C. W., Takahashi, E., & Collewijn, H. (1972). Direction-selective retinal ganglion cells and control of optokinetic nystagmus in the rabbit. *Vision Research*, *12*(2), 183–193. https://doi.org/10.1016/0042-6989(72)90110-1

Panek, I., Bui, T., Wright, A. T. B., & Brownstone, R. M. (2014). Cutaneous afferent regulation of motor function. *Acta Neurobiologiae Experimentalis*, *74*(2), 158–171.

Peterka, R. J., Black, F. O., & Schoenhoff, M. B. (1990). Age-related changes in human vestibulo-ocular and optokinetic reflexes: Pseudorandom rotation tests. *Journal of Vestibular Research: Equilibrium & Orientation*, *1*(1), 61–71.

Picton, L. D., Sillar, K. T., & Zhang, H.-Y. (2018). Control of Xenopus Tadpole Locomotion via Selective Expression of Ih in Excitatory Interneurons. *Current Biology*, *28*(24), 3911-3923.e2. https://doi.org/10.1016/j.cub.2018.10.048

Porrill, J., & Dean, P. (2007). Cerebellar Motor Learning: When Is Cortical Plasticity Not Enough? *PLoS Computational Biology*, *3*(10), e197. https://doi.org/10.1371/journal.pcbi.0030197

Purves, D. (Ed.). (2004). *Neuroscience* (3rd ed). Sinauer Associates, Publishers.

Rabbitt, R. D. (1999). Directional coding of three-dimensional movements by the vestibular semicircular canals. *Biological Cybernetics*, *80*(6), 417–431. https://doi.org/10.1007/s004220050536

Rapaport, D. H., & Stone, J. (1984). The area centralis of the retina in the cat and other mammals: Focal point for function and development of the visual system. *Neuroscience*, *11*(2), 289–301. https://doi.org/10.1016/0306-4522(84)90024-1

Robert Bárány. (1907). *Physiologie und Patholgie des Bogengang- Apparates beim Menschen*. Vienna: Deuticke.

Robie, A. A., Straw, A. D., & Dickinson, M. H. (2010). Object preference by walking fruit flies, Drosophila melanogaster, is mediated by vision and graviperception. *Journal of Experimental Biology*, *213*(14), 2494–2506. https://doi.org/10.1242/jeb.041749

Roseberry, T. K., Lee, A. M., Lalive, A. L., Wilbrecht, L., Bonci, A., & Kreitzer, A. C. (2016). Cell-Type-Specific Control of Brainstem Locomotor Circuits by Basal Ganglia. *Cell*, *164*(3), 526–537. https://doi.org/10.1016/j.cell.2015.12.037

Rossignol, S., Dubuc, R., & Gossard, J.-P. (2006). Dynamic Sensorimotor Interactions in Locomotion. *Physiological Reviews*, *86*(1), 89–154. https://doi.org/10.1152/physrev.00028.2005

Roy, J. E., & Cullen, K. E. (2001). Selective processing of vestibular reafference during self-generated head motion. *The Journal of Neuroscience: The Official Journal of the Society for Neuroscience*, *21*(6), 2131–2142.

Ruigrok, T. J. H., Pijpers, A., Goedknegt-Sabel, E., & Coulon, P. (2008). Multiple cerebellar zones are involved in the control of individual muscles: A retrograde transneuronal tracing study with rabies virus in the rat. *The European Journal of Neuroscience*, *28*(1), 181–200. https://doi.org/10.1111/j.1460-9568.2008.06294.x

Ryczko, D., & Dubuc, R. (2013). The multifunctional mesencephalic locomotor region. *Current Pharmaceutical Design*, *19*(24), 4448–4470. https://doi.org/10.2174/1381612811319240011

Sadeghi, S. G., Goldberg, J. M., Minor, L. B., & Cullen, K. E. (2009). Efferent-Mediated Responses in Vestibular Nerve Afferents of the Alert Macaque. *Journal of Neurophysiology*, *101*(2), 988–1001. https://doi.org/10.1152/jn.91112.2008

Samonds, J. M., Choi, V., & Priebe, N. J. (2019). Mice Discriminate Stereoscopic Surfaces Without Fixating in Depth. *Journal of Neuroscience*, *39*(41), 8024–8037. https://doi.org/10.1523/JNEUROSCI.0895-19.2019

Schiller, P. H. (2010). Parallel information processing channels created in the retina. *Proceedings of the National Academy of Sciences*, *107*(40), 17087–17094. https://doi.org/10.1073/pnas.1011782107

Schmidt, B. J., & Jordan, L. M. (2000). The role of serotonin in reflex modulation and locomotor rhythm production in the mammalian spinal cord. *Brain Research Bulletin*, *53*(5), 689–710. https://doi.org/10.1016/s0361-9230(00)00402-0

Schweigart, G., Mergner, T., Evdokimidis, I., Morand, S., & Becker, W. (1997). Gaze stabilization by optokinetic reflex (OKR) and vestibulo-ocular reflex (VOR) during active head rotation in man. *Vision Research*, *37*(12), 1643–1652. https://doi.org/10.1016/s0042-6989(96)00315-x

Scudder, C. A., & Fuchs, A. F. (1992). Physiological and behavioral identification of vestibular nucleus neurons mediating the horizontal vestibuloocular reflex in trained rhesus monkeys. *Journal of Neurophysiology*, *68*(1), 244–264. https://doi.org/10.1152/jn.1992.68.1.244

Sengul, G., & Watson, C. (2012). Chapter 13—Spinal Cord. In C. Watson, G. Paxinos, & L. Puelles (Eds.), *The Mouse Nervous System* (pp. 424–458). Academic Press. https://doi.org/10.1016/B978-0-12-369497-3.10013-5

Sherrington, C. S. (1906). Observations on the scratch-reflex in the spinal dog. *The Journal of Physiology*, *34*(1–2), 1–50. https://doi.org/10.1113/jphysiol.1906.sp001139

Shin, S.-L., Zhao, G. Q., & Raymond, J. L. (2014). Signals and Learning Rules Guiding Oculomotor Plasticity. *Journal of Neuroscience*, *34*(32), 10635–10644. https://doi.org/10.1523/JNEUROSCI.4510-12.2014

Shutoh, F., Ohki, M., Kitazawa, H., Itohara, S., & Nagao, S. (2006). Memory trace of motor learning shifts transsynaptically from cerebellar cortex to nuclei for consolidation. *Neuroscience*, *139*(2), 767–777. https://doi.org/10.1016/j.neuroscience.2005.12.035

Simpson, J. I., & Graf, W. (1985). The selection of reference frames by nature and its investigators. *Reviews of Oculomotor Research*, *1*, 3–16.

Slonaker, J. R. (1897). A comparative study of the area of acute vision in vertebrates. *Journal of Morphology*, *13*(3), 445–502. https://doi.org/10.1002/jmor.1050130304

Smith, J. C., Ellenberger, H. H., Ballanyi, K., Richter, D. W., & Feldman, J. L. (1991). Pre-Botzinger complex: A brainstem region that may generate respiratory rhythm

in mammals. *Science*, *254*(5032), 726–729. https://doi.org/10.1126/science.1683005

Smith, R. S., John, S. W. M., Nishina, P. M., & Sundberg, J. P. (2001). *Systematic Evaluation of the Mouse Eye: Anatomy, Pathology, and Biomethods*. CRC Press.

Soodak, R. E., & Simpson, J. I. (1988). The accessory optic system of rabbit. I. Basic visual response properties. *Journal of Neurophysiology*, *60*(6), 2037–2054. https://doi.org/10.1152/jn.1988.60.6.2037

Spencer, R. F., & Porter, J. D. (2006). Biological organization of the extraocular muscles. In *Progress in Brain Research* (Vol. 151, pp. 43–80). Elsevier. https://doi.org/10.1016/S0079-6123(05)51002-1

Squire, L. R. (Ed.). (2008). *Fundamental neuroscience* (3rd ed). Elsevier / Academic Press.

Stahl, J. S., van Alphen, A. M., & De Zeeuw, C. I. (2000). A comparison of video and magnetic search coil recordings of mouse eye movements. *Journal of Neuroscience Methods*, *99*(1–2), 101–110. https://doi.org/10.1016/s0165-0270(00)00218-1

Stahl, John S. (2004). Using eye movements to assess brain function in mice. *Vision Research*, *44*(28), 3401–3410. https://doi.org/10.1016/j.visres.2004.09.011

Straka, H., Biesdorf, S., & Dieringer, N. (1997). Canal-Specific Excitation and Inhibition of Frog Second-Order Vestibular Neurons. *Journal of Neurophysiology*, *78*(3), 1363–1372. https://doi.org/10.1152/jn.1997.78.3.1363

Straka, Hans, & Chagnaud, B. P. (2017). Moving or being moved: That makes a difference. *Journal of Neurology*, *264*(S1), 28–33. https://doi.org/10.1007/s00415-017-8437-8

Straka, Hans, Simmers, J., & Chagnaud, B. P. (2018). A New Perspective on Predictive Motor Signaling. *Current Biology*, *28*(5), R232–R243. https://doi.org/10.1016/j.cub.2018.01.033

Straka, Hans, Zwergal, A., & Cullen, K. E. (2016). Vestibular animal models: Contributions to understanding physiology and disease. *Journal of Neurology*, *263*(S1), 10–23. https://doi.org/10.1007/s00415-015-7909-y

Tauber, E. S., & Atkin, A. (1968). Optomotor Responses to Monocular Stimulation: Relation to Visual System Organization. *Science*, *160*(3834), 1365–1367. https://doi.org/10.1126/science.160.3834.1365

Ter Braak, J.W. (1936). Untersuchung ¨uber optokinetischen Nystagmus. *Arch. Neer. Physiol*, 309–376.

Tomlinson, R. D., & Robinson, D. A. (1984). Signals in vestibular nucleus mediating vertical eye movements in the monkey. *Journal of Neurophysiology*, *51*(6), 1121–1136. https://doi.org/10.1152/jn.1984.51.6.1121

Uchino, Y., Sasaki, M., Sato, H., Bai, R., & Kawamoto, E. (2005). Otolith and canal integration on single vestibular neurons in cats. *Experimental Brain Research*, *164*(3), 271–285. https://doi.org/10.1007/s00221-005-2341-7

Uckermann, G. von, Ray, D. L., Combes, D., Straka, H., & Simmers, J. (2013). Spinal Efference Copy Signaling and Gaze Stabilization during Locomotion in Juvenile Xenopus Frogs. *Journal of Neuroscience*, *33*(10), 4253–4264. https://doi.org/10.1523/JNEUROSCI.4521-12.2013

Ugolini, G. (1995). Specificity of rabies virus as a transneuronal tracer of motor networks: Transfer from hypoglossal motoneurons to connected second-order and higher order central nervous system cell groups. *The Journal of Comparative Neurology*, *356*(3), 457–480. https://doi.org/10.1002/cne.903560312

Ugolini, Gabriella. (2010). Advances in viral transneuronal tracing. *Journal of Neuroscience Methods*, *194*(1), 2–20. https://doi.org/10.1016/j.jneumeth.2009.12.001

Ugolini, Gabriella. (2011). Rabies virus as a transneuronal tracer of neuronal connections. *Advances in Virus Research*, *79*, 165–202. https://doi.org/10.1016/B978-0-12-387040-7.00010-X

Ugolini, Gabriella, Klam, F., Doldan Dans, M., Dubayle, D., Brandi, A.-M., Büttner-Ennever, J., & Graf, W. (2006). Horizontal eye movement networks in primates as revealed by retrograde transneuronal transfer of rabies virus: Differences in monosynaptic input to “slow” and “fast” abducens motoneurons. *The Journal of Comparative Neurology*, *498*(6), 762–785. https://doi.org/10.1002/cne.21092

van Alphen, A. M., Stahl, J. S., & De Zeeuw, C. I. (2001). The dynamic characteristics of the mouse horizontal vestibulo-ocular and optokinetic response. *Brain Research*, *890*(2), 296–305. https://doi.org/10.1016/s0006-8993(00)03180-2

Wada, N., Funabiki, K., & Nakanishi, S. (2014). Role of granule-cell transmission in memory trace of cerebellum-dependent optokinetic motor learning. *Proceedings of the National Academy of Sciences of the United States of America*, *111*(14), 5373–5378. https://doi.org/10.1073/pnas.1402546111

Walls, G. L. (1962). The evolutionary history of eye movements. *Vision Research*, *2*(1), 69–80. https://doi.org/10.1016/0042-6989(62)90064-0

Wang, L., Liu, M., Segraves, M. A., & Cang, J. (2015). Visual Experience Is Required for the Development of Eye Movement Maps in the Mouse Superior Colliculus.

Journal of Neuroscience, *35*(35), 12281–12286. https://doi.org/10.1523/JNEUROSCI.0117-15.2015

Warwick, R. A., Kaushansky, N., Sarid, N., Golan, A., & Rivlin-Etzion, M. (2018). Inhomogeneous Encoding of the Visual Field in the Mouse Retina. *Current Biology*, *28*(5), 655-665.e3. https://doi.org/10.1016/j.cub.2018.01.016

Whelan, P. J., Hiebert, G. W., & Pearson, K. G. (1995). Stimulation of the group I extensor afferents prolongs the stance phase in walking cats. *Experimental Brain Research*, *103*(1), 20–30. https://doi.org/10.1007/bf00241961

Whitford, T. J., Jack, B. N., Pearson, D., Griffiths, O., Luque, D., Harris, A. W., Spencer, K. M., & Le Pelley, M. E. (2017). Neurophysiological evidence of efference copies to inner speech. *ELife*, *6*, e28197. https://doi.org/10.7554/eLife.28197

Wickersham, I. R., Lyon, D. C., Barnard, R. J. O., Mori, T., Finke, S., Conzelmann, K.-K., Young, J. A. T., & Callaway, E. M. (2007). Monosynaptic Restriction of Transsynaptic Tracing from Single, Genetically Targeted Neurons. *Neuron*, *53*(5), 639–647. https://doi.org/10.1016/j.neuron.2007.01.033

Wiest, G. (2015). The origins of vestibular science: The origins of vestibular science. *Annals of the New York Academy of Sciences*, *1343*(1), 1–9. https://doi.org/10.1111/nyas.12706

Yildirim, F. B., & Sarikcioglu, L. (2007). Marie Jean Pierre Flourens (1794–1867): An extraordinary scientist of his time. *Journal of Neurology, Neurosurgery & Psychiatry*, *78*(8), 852–852. https://doi.org/10.1136/jnnp.2007.118380

Zagoraiou, L., Akay, T., Martin, J. F., Brownstone, R. M., Jessell, T. M., & Miles, G. B. (2009). A Cluster of Cholinergic Premotor Interneurons Modulates Mouse Locomotor Activity. *Neuron*, *64*(5), 645–662. https://doi.org/10.1016/j.neuron.2009.10.017

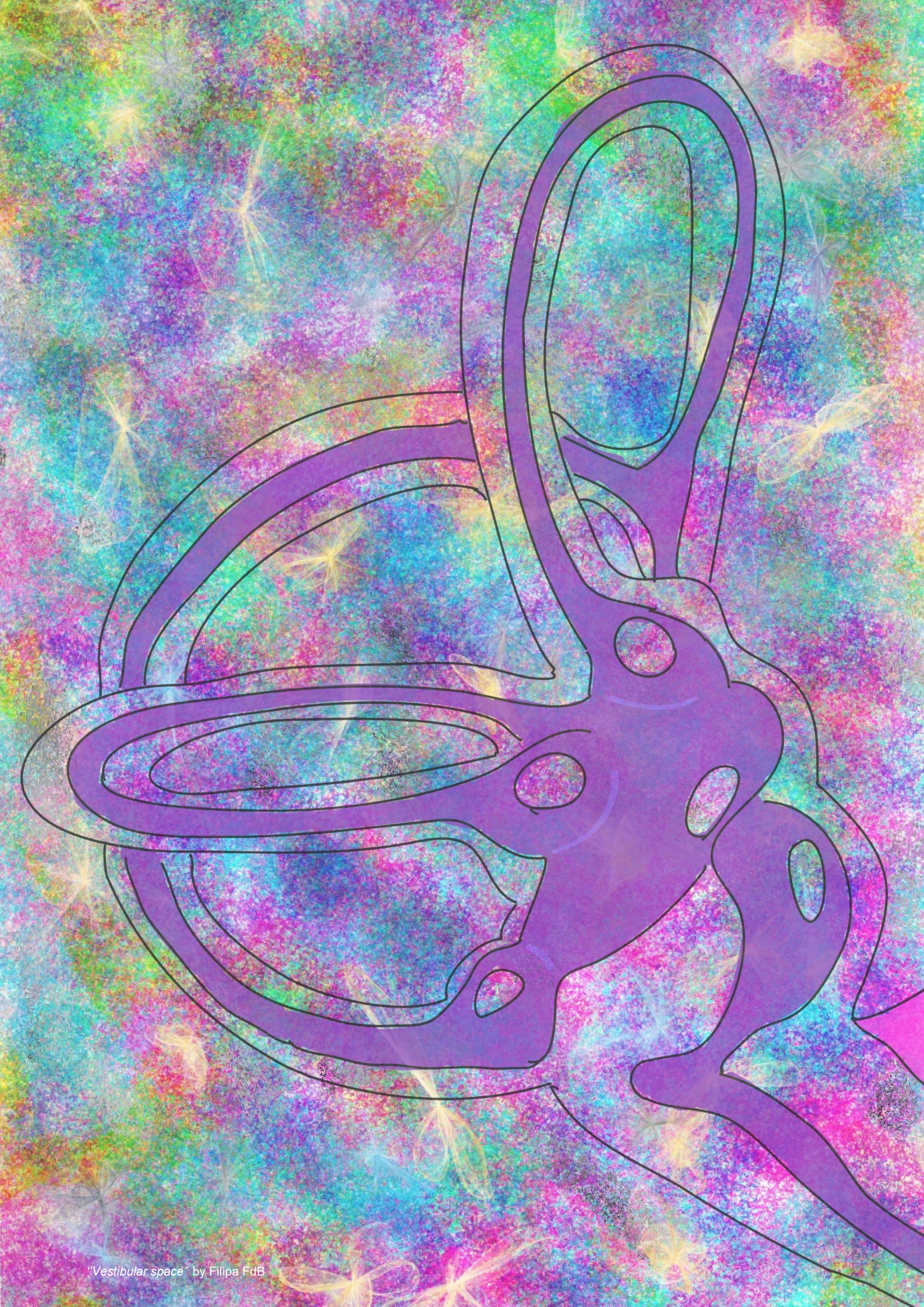

"Vestibular space" by Filipa FdB

THÈSE DE DOCTORAT

UNIVERSITÉ DE PARIS

Spécialité Neurosciences

École Doctorale Cerveau Cognition Comportement nº158

Présentée par

Filipa França de Barros

Pour obtenir le grade de

Docteure de Université de Paris

Sujet de la thèse

Stabilisation du regard chez la souris : adaptation visuo-vestibulaire et signalisation prédictive pendant la locomotion

Soutenue publiquement le 04 Septembre 2020

Devant le jury composé de

Pr. Thérèse Collins	Université de Paris	Présidente du jury
Dr. Megan Carey	Fondation Champalimaud	Rapporteure
Dr. Muriel Thoby-Brisson	Université de Bordeaux	Rapporteure
Dr. Andrew Murray	Sainsbury Wellcome Center	Examinateur
Pr. Hans Straka	Ludwig Maximilian University of Munich	Examinateur
Dr. Pierre Pouget	Institut du Cerveau et de la Moelle épinière	Examinateur
Dr. Mathieu Beraneck	Université de Paris	Directeur de thèse

Sommaire

Résumé

L'information visuelle est cruciale pour que les espèces animales agissent, interagissent et s'orientent dans leur environnement. La stabilisation du regard permet une acuité visuelle adéquate en garantissant que la scène visuelle est maintenue immobile sur la rétine, même pendant le mouvement. Les systèmes sensorimoteurs sont responsables de la stabilisation du regard grâce à l'utilisation d'entrées complémentaires qui finissent par déplacer l'œil dans l'espace et / ou la tête dans l'espace.

Cette thèse présente toute d'abord des études qui concernent les deux voies sensorimotrices convergentes du tronc cérébral qui permettent la stabilisation du regard chez la souris. Plus précisément, nous étudions comment les réflexes d'origine visuelle (réflexe optocinétique ou OKR) et vestibulaire (réflexe vestibulo-oculaire ou VOR) s'adaptent en réponse à une perturbation visuelle persistante. Cela a été réalisé au moyen d'un protocole de conflit visuo-vestibulaire de 2 semaines chez des souris libres de leurs mouvements (França de Barros et al., 2019). Dans un premier temps, nous avons démontré que le protocole de conflit visuo-vestibulaire à long terme conduit à une plasticité en dehors du cervelet, notamment dans la voie directe du VOR (Carcaud et al., 2017). Des modifications plastiques ont été mises en évidence dans la transmission synaptique entre les afférents vestibulaires et les neurones vestibulaires centraux d'une part, et dans les propriétés intrinsèques de certains neurones vestibulaires centraux d'autre part. Ensuite, la dynamique d'adaptation et de récupération des réflexes OKR et VOR a été comparée dans deux mésappariements qui différaient dans la quantité de glissement rétinien (França de Barros et al., 2020). Nous avons constaté que les deux conditions étaient comparables, entraînant toutes deux des changements plus importants dans le VOR que dans l'OKR. La dynamique de ces changements plastiques est très largement dépendante de la fréquence, avec une récupération retardée pour les fréquences inférieures à 1 Hz. Dans l'ensemble, ces données fournissent des données expérimentales concernant les cascades séquentielles de plasticité dans les voies réflexes de stabilisation du regard et montrent les interdépendances fonctionnelles entre le VOR et l'OKR.

En plus des voies sensorimotrices classiques, des preuves récentes ont démontré chez les têtards de Xénope le rôle de la signalisation motrice prédictive dans la réduction des perturbations visuelles pendant la locomotion. Nous avons exploré si ce signal prédictif, couplant les mouvements oculaires à la locomotion, est phylogénétiquement conservé chez les mammifères (França de Barros et al., en préparation 1). En utilisant une préparation précolliculaire et prémamillaire décérébrée de souris adultes,

maintenues tête fixe, nous avons montré que la locomotion entraînée par le tapis roulant provoque des mouvements des yeux bilatéraux et conjugués. Pour déterminer l'influence des CPG (Central Pattern Generator) locomoteurs des rachis cervical et lombaire sur les noyaux moteurs de l'œil, l'activité des nerfs moteurs rachidiens et abducens a été enregistrée simultanément ex vivo dans des préparations isolées de tronc cérébral et de moelle épinière de souris néonatales. Une décharge couplée rythmique a été trouvée entre les activités du membre et du nerf moteur abducens lors d'épisodes locomoteurs fictifs provoqués par une stimulation électrique ou pharmacologique. Pour cartographier la voie neuronale qui couple le CPG cervical et les noyaux abducens, le virus de la rage (RV) a été injecté dans le muscle droit latéral des souris adultes. Nous avons trouvé des motoneurones infectés (RV+) (révélés par le marquage ChAT) dans le noyau abducens ipsilatéral ainsi que des interneurones RV + le long de la moelle épinière cervicale. Cette étude a pour la première fois démontré qu'une copie d'efférence pilotée par le CPG cervical couple directement les mouvements oculaires avec le mouvement des membres antérieurs pendant une locomotion soutenue chez la souris.

Additionellement, cette thèse présente une collaboration avec le groupe de Saaid Safieddine de l'Institut Pasteur où la thérapie génique médiée par l'AAV a été utilisée pour restaurer durablement les fonctions auditives et vestibulaires d'un modèle murin du syndrome d'Usher 1. Les souris USH1- / - présentent une surdité profonde et un dysfonctionnement locomoteur suggérant des troubles vestibulaires. Dans cette étude, notre équipe a mesuré par vidéo-oculographie les réflexes vestibulo-oculaires d’origine canalaire et otolitique de souris Knock-out USH1- / -. Alors que les souris USH1- / - non injectées n'ont pas réussi à évoquer des mouvements oculaires compensatoires, les souris USH1- / - injectées ont présenté des réponses proches de celles de type sauvage. Par conséquent, la thérapie génique médiée par AVV a pu restaurer la fonction vestibulaire. Cette étude a conduit à plusieurs collaborations avec groupes de l'Institut Pasteur visant tous à développer de nouvelles lignes thérapeutiques pour les patients souffrant de pathologies de l'oreille interne.

Globalement, les travaux présentés dans cette thèse permettent de mieux comprendre les complémentarités fonctionnelles des voies réflexes impliquées dans les mécanismes de stabilisation du regard ainsi que leurs adaptations à différents contextes comportementaux et à des changements de l’environnement.

Mots-clés : stabilisation du regard, réflexe vestibulo-oculaire, réflexe optocinétique, tronc cérébral, sensorimoteur, copie d’efférence, générateur central du patron locomoteur, couplage moteur.

Projet de thèse et objectifs

La stabilisation du regard aide à assurer l'acuité visuelle en maintenant la scène visuelle stationnaire sur la rétine. La convergence des entrées visuelles, vestibulaires et proprioceptives et leur intégration dans les structures du tronc cérébral sont connues pour générer une stabilisation active du regard.

Dans ce cadre, cette thèse vise deux objectifs distincts mais complémentaires : 1) étudier l'adaptabilité et la cinématique des réflexes de stabilisation du regard après que les entrées visuelles et vestibulaires subissent une perturbation à long terme ; 2) pour déchiffrer si les mammifères, en plus des voies sensorimotrices classiques, utilisent la signalisation motrice prédictive pendant la locomotion pour stabiliser le regard.

Le premier objectif est à l'origine de trois projets. Lors de ma première année au laboratoire, en tant que stagiaire à la maîtrise, l'équipe avait un projet en cours qui consistait à étudier les effets d'une perturbation visuo-vestibulaire à long terme sur la voie directe du VOR (Carcaud et al., 2017). La conception de ce protocole a permis non seulement pour les enregistrements de vidéo-oculographie in vivo des réflexes de stabilisation du regard, mais aussi pour les enregistrements électrophysiologiques in vitro des neurones vestibulaires centraux. Cet ensemble de données, auquel j'ai contribué à la fois avec des données comportementales et électrophysiologiques, a été finalisé dans les premiers mois de ma thèse. Pour cette étude, les souris ont été exposées pendant 2 semaines à une discordance visuo-vestibulaire (VVM) qui consistait en un dispositif en forme de casque fixé sur leur tête. Avec cet appareil VVM, les souris peuvent se comporter librement dans leurs cages tout en étant constamment exposées à un protocole d'apprentissage moteur VOR. Lorsque l'appareil a été retiré à la fin du protocole, une diminution de 50% du gain VOR a été enregistrée. Les expériences d'arrêt de flocculus combinées aux tests VOR et OKR ont montré que cette diminution était localisée à l'extérieur du complexe flocculus / paraflocculus. Les mécanismes neuronaux de cette réduction ont été étudiés plus en détail dans les neurones MVN de tranches de tronc cérébral en utilisant des stimulations afférentes et des enregistrements patch-clamp. La stimulation du nerf VIII a démontré que l'amplitude des EPSC évoqués était diminuée chez les souris adaptées. De plus, l'analyse des propriétés membranaires des neurones MVN a montré qu'une sous-population de neurones vestibulaires (type A) présentait une diminution de la décharge spontanée et de l'excitabilité. En somme, cette étude montre qu'une discordance visuo-vestibulaire de longue durée entraîne des changements dans la transmission synaptique et les propriétés intrinsèques des neurones vestibulaires centraux dans la voie directe du VOR. Par conséquent, nos

résultats fournissent une preuve directe de l'hypothèse d'une consolidation du VOR à long terme modifié dans le tronc cérébral.

Les protocoles de conflit sensoriel à long terme sont un moyen précieux d'étudier l'apprentissage moteur. Par conséquent, le prochain objectif de cette thèse était d'optimiser davantage le protocole VVM utilisé dans l'étude susmentionnée (França de Barros et al., 2019). En étant fixé sur des têtes de souris, cet appareil crée un conflit sensoriel durable, ce qui en fait un excellent outil pour les expériences d'apprentissage à long terme. Cette structure en forme de casque respecte l'anatomie du museau des souris et permet donc des comportements de barbier, d'alimentation et de boisson. Plusieurs aspects tels que la production, le coût, le matériau et le poids final de l'appareil ont été optimisés pour rendre une méthodologie améliorée. La production est passée du manuel à la série grâce à l'utilisation d'une imprimante 3D qui a par conséquent abaissé le coût de production ainsi qu'un plus grand taux de reproductibilité entre les différents expérimentateurs et laboratoires. Le matériau utilisé pour sa production a également été remplacé par un plastique poly lactique qui a permis un poids plus léger. Par la suite, les étapes d'assemblage du dispositif et de soins aux animaux en chirurgie liées à ce protocole VVM innovant ont été détaillées et publiées sous une forme écrite et audiovisuelle afin qu'il soit mis à la disposition de tout autre laboratoire qui pourrait en bénéficier (article 2. Conflit sensoriel à long terme dans Souris à comportement libre).

Le projet de conclusion du premier objectif de cette thèse a étudié la cinématique de récupération des réflexes stabilisateurs du regard après un conflit sensoriel de longue durée. Dans ce projet, les réflexes optocinétique et vestibulo-oculaire ont été testés sur le retrait du dispositif VVM ainsi que 1, 2 et 6 après. Nous avons constaté que les changements VOR persistent pendant au moins 2 jours après la fin du protocole VVM. De plus, nous signalons pour la première fois que l'OKR est également affecté ; ses réponses souffrent d'une diminution de 30% le jour de la fin du protocole, et rendent compte de la dynamique de récupération à la fois du VOR et de l'OKR après la fin du protocole VVM. En utilisant des stimulations à modulation sinusoïdale, les diminutions de VOR et OKR se sont avérées sélectives en fréquence avec des réductions plus importantes pour les fréquences <0,5 Hz. Néanmoins, la diminution de l'OKR est plus transitoire puisque toutes les conditions testées récupèrent rapidement leurs gains initiaux. Ainsi, nos données sont compatibles avec l'hypothèse de cascades séquentielles de plasticité dans les voies OKR / VOR.

Pour identifier les signaux entraînant des réductions VOR et OKR, nous avons comparé les réponses de souris exposées à un contraste élevé et sans contraste VVM.

Le protocole VVM de Carcaud et al., 2017 a utilisé l'exposition à un motif à contraste élevé pendant les séances d'entraînement pour évoquer un signal d'erreur fort qui entraînerait l'apprentissage moteur du VOR. Dans cette étude, mis à part ce périphérique VVM à motif de contraste élevé, nous avons également appliqué un modèle sans motif de ce périphérique sans aucun motif. Étonnamment, nous n'avons trouvé aucune différence majeure entre les deux types de dispositifs ni dans l'ampleur de la diminution de la réponse ni dans la dynamique de récupération. Le dispositif sans motif avait tendance à produire une adaptation plus douce, mais peu de ces différences atteignaient une signification. Ce résultat suggère que plutôt qu'une signal d'erreur (glissement rétinien), c'est plutôt l'absence de décorrélation de rétroaction visuelle qui serait responsable de la diminution de l'OKR et du VOR.

Le deuxième objectif de cette thèse est rendu dans le projet intitulé «LOCOGAZE», acronyme de «Substrats neurophysiologiques évolutifs et développementaux pour les stratégies de stabilisation du regard lors de la locomotion chez les vertébrés». Ce travail, accordé par l'Agence Nationale de la Recherche (ANR), a impliqué dans un premier temps 2 laboratoires collaborateurs : l'Institut de Neurosciences Cognitives et Intégratives d'Aquitaine (INCIA, Bordeaux) et notre laboratoire, le Centre Intégratif de Neurosciences et Cognition (INCC, Paris). Une collaboration a également été établie avec l'Institut de Neurosciences de la Timone (INT, Marseille), où j'ai mené les expériences sur le virus de la rage. Ces équipes ont travaillé à caractériser, chez la souris, l'influence d'une copie d'efférence générée dans le réseau locomoteur rachidien sur la stabilisation du regard (França de Barros et al, en préparation). C'est l'équipe INCIA qui, en 2008 (Combes et al., 2008), a signalé pour la première fois chez les têtards Xenopus une signalisation prédictive en aval des CPG locomoteurs rachidiens engagés dans le mouvement des yeux lors de la nage fictive. Comme cela a été découvert chez des têtards à tête fixe semi-intacts, cela a soulevé la question de savoir si cette voie spino-extraoculaire est conservée par phylogénie chez les mammifères. Cette thèse visait à enquêter sur l'existence de cette voie chez la souris et à la caractériser (Article 4. Copie efférente locomotrice CPG couple mouvements oculaires et locomotion des membres antérieurs chez la souris). Nous l'avons fait grâce à une approche multiméthodologique combinant des préparations semi-intactes, des expériences ex vivo et in vivo.

Une préparation de souris adulte décérébrée précolliculaire et prémammillaire à tête fixe a été utilisée pour démasquer cette copie efférente chez une souris qui se comporte. Nous avons trouvé une corrélation cohérente entre la locomotion sur tapis roulant évoquée dans les mouvements oculaires sombres et conjugués. Les combats de

locomotion en forme de trot ont duré entre 10 et 40 secondes et ont évoqué des mouvements oculaires horizontaux conjugués avec des phases lentes entre une amplitude de 5 à 10 ° et une plage de fréquences de 1 à 5 Hz. En outre, pour déterminer l'influence des CPG locomoteurs cervicaux et lombaires sur les noyaux moteurs de l'œil, l'activité des nerfs moteurs rachidiens et abducens a été enregistrée simultanément ex vivo dans des préparations isolées de tronc cérébral-moelle épinière de souris nouveau-nés. Une décharge couplée rythmique a été trouvée entre les activités nerveuses motrices du membre et de l'abducens au cours d'épisodes locomoteurs fictifs provoqués par une stimulation électrique ou pharmacologique. L'activation isolée de l'activité CPG cervicale ou lombaire a révélé que la sortie du réseau cervical mais non lombaire est suffisante pour entraîner la décharge nerveuse abducens. Nous avons utilisé le virus de la rage pour cartographier la voie neuronale qui associe le CPG cervical aux noyaux abducens. Des injections dans le muscle droit latéral de souris adultes marquées motoneurones dans le noyau abducens ipsilatéral et interneurones dans la moelle épinière cervicale ont révélé une voie directe reliant la colonne cervicale aux neurones oculomoteurs.

Dans l'ensemble, les études menées par notre équipe au cours de cette thèse permettent de mieux comprendre la complémentarité fonctionnelle des voies réflexives participant à la stabilisation du regard ainsi que leur adaptation à différents contextes comportementaux et environnementaux.

Enfin, cette thèse bénéficie d'une collaboration avec l'Institut Pasteur (article 5. La thérapie génique locale restaure durable la fonction vestibulaire dans un modèle murin du syndrome d'Usher de type 1G) où la thérapie génique médiée par un virus adéno-associé (AAV) a été utilisée pour restaurer l'audition et le vestibule. fonctions d'un modèle murin du syndrome d'Usher de type 1 (USH1) (Emptoz et al., 2017). Les patients USH1 souffrent de surdité profonde congénitale et de troubles de l'équilibre et, actuellement, il n'existe pas de traitement disponible pour cette pathologie. Dans cette étude, la protéine d'échafaudage sans, qui est impliquée dans la morphogenèse des cellules ciliées de l'oreille interne, a été restituée chez des souris USH1 par la délivrance de son ADNc via un AAV. Cela a restauré la fonctionnalité des faisceaux stéréociliaires et par conséquent amélioré les seuils d'audition et a retrouvé les comportements locomoteurs et posturaux. Cependant, la démonstration de la restauration de la fonction vestibulaire faisait défaut. À cette fin, la restauration de la fonction vestibulaire a été évaluée en mesurant les réponses vestibulo-oculaires spécifiques. Aucun mouvement oculaire compensatoire n'a été enregistré chez les souris USH1 - / -, et divers tests ont indiqué une perte totale de fonction des canaux semi-circulaires et des organes

otolithiques. D'autre part, les réponses des souris USH1 - / - traitées par AAV aux mêmes tests étaient impossibles à distinguer des souris de type sauvage, ce qui indique que la fonction vestibulaire avait été restaurée. Ce résultat, basé sur la vidéo-oculographie, a fourni la preuve définitive de l'efficacité du traitement sur les voies vestibulaires spécifiques. Nous avons pu en outre montrer que cette restauration persistait pendant plus d'un an après l'injection unique de traitement, indiquant le potentiel de cette thérapie pour la guérison à long terme. Cette étude fondamentale a depuis conduit à plusieurs collaborations en cours entre mon groupe et des groupes de l'Institut Pasteur. Il démontre comment l'expertise développée pour acquérir des connaissances de base sur la fonction vestibulaire peut être traduite en études visant à développer de nouvelles lignes thérapeutiques pour les patients souffrant de pathologies de l'oreille interne.

Résultats

Article 1 : Conflit visuo-vestibulaire de longue durée chez les souris réduit le réflexe vestibulo-oculaire et entraîne des changements neuronaux dans la voie vestibulaire directe

Ce projet a étudié la question de la rétention à long terme de l'apprentissage moteur VOR dans le tronc cérébral. La conception de l'expérience a permis une approche systémique où les expériences in vivo et in vitro ont été combinées. Un protocole de mésappariement visuo-vestibulaire à long terme (VVM, voir l'article 2. Conflit sensoriel à long terme chez les souris à comportement libre) a été utilisé pour créer un gain de VOR vers le bas chez des souris à comportement libre pendant 14 jours. Les souris pouvaient se comporter dans leurs cages tout en étant constamment exposées à un protocole d'apprentissage moteur VOR. Lorsque l'appareil a été retiré à la fin du protocole, une diminution de 50% du gain VOR a été enregistrée. Les expériences d'arrêt de Flocculus combinées aux tests VOR et OKR ont montré que cette diminution était localisée à l'extérieur du complexe flocculus / paraflocculus. Les mécanismes neuronaux de cette réduction ont été étudiés plus en détail dans les neurones MVN de tranches de tronc cérébral en utilisant des stimulations afférentes et des enregistrements patch-clamp. La stimulation du nerf VIII a démontré que l'amplitude des eEPSC était diminuée chez les souris adaptées. De plus, l'analyse des propriétés membranaires des neurones MVN a montré qu'une sous-population de neurones vestibulaires (type A) présentait une diminution de la décharge spontanée et de l'excitabilité. En somme, cette étude montre qu'une discordance visuo-vestibulaire de longue durée entraîne des changements dans la transmission synaptique et les propriétés intrinsèques des neurones vestibulaires centraux dans la voie directe du VOR. Par conséquent, nos résultats fournissent une preuve directe de l'hypothèse d'une consolidation du VOR à long terme modifié dans le tronc cérébral.

Cet article a été publié en 2017 sur le journal eNeuro.

Article 2 : Conflit sensoriel à long terme chez des souris à comportement libre

Mon équipe a développé un protocole de conflit sensoriel à long terme novateur et unique pour les souris qui se comportent librement. La motivation derrière ce protocole résidait dans permettre l'apprentissage ininterrompu des réflexes de stabilisation du regard produit des mouvements de la tête générés naturellement. Les souris sont implantées avec un pilier, dans une chirurgie rapide et simple, où un dispositif en forme de casque est fixé postérieurement dessus. Ils sont capables de vivre leur vie comme ils le feraient autrement, car l'appareil permet sans obstruction à leurs routines quotidiennes (manger, boire ou se toiletter). Après 2 semaines, l'appareil est retiré et des enregistrements par vidéo-oculographie sont effectués pour analyser le changement de la réponse de leurs réflexes.

La première publication utilisant ce protocole (présentée ci-dessus, article 1 (Carcaud et al., 2017)) a permis d'étudier les effets de ce conflit sensoriel dans le VOR, juste après le retrait du dispositif. Cette étude a soulevé de nombreuses questions interdépendantes concernant l'inversion des réflexes ainsi que l'apport visuel, auxquelles ont répondu le document de suivi (article 3, França de Barros et tal., 2020). Cependant, ce protocole a également été utilisé pour étudier son effet protecteur contre le mal des transports lorsque les souris étaient exposées à un stimulus provocateur (Idoux et al., 2018). Par conséquent, des protocoles comme celui-ci pourraient ouvrir la voie au développement de traitements anti-mal des transports. La variété des études pour lesquelles ce protocole a été utile, prouve sa polyvalence. Par exemple, en ne modifiant que la durée du conflit (<14 jours ou> 14 jours), une myriade d'études serait débloquée.

J'ai eu l'opportunité d'optimiser ce protocole en abordant 3 problématiques concernant les poteaux et les appareils : 1) disponibilité et coût de production; 2) matériel; 3) poids final des deux composants. La version originale était faite à la main, ce qui était lent et impliquait des coûts de production plus élevés par pièce. Pour résoudre ce problème, l'impression 3D a été introduite pour permettre une production de masse abordable. Du point de vue matériel, la substitution du plastique transparent utilisé à l'origine par un plastique PLA a permis de retenir les souris des entrées visuelles (à l'exception de la luminance). Enfin, le plastique PLA a rendu les composants plus légers, offrant ainsi à la souris une expérience transparente.

L'article sur la méthodologie présenté ci-dessous indique en détail le matériel et les étapes nécessaires à la réplication de ce protocole par toute autre équipe intéressée.

Il comprend comment assembler le dispositif d'adaptation et les fichiers d'imprimante 3D respectifs ; les étapes de la chirurgie d'implantation de la tête ; comment attacher et retirer l'appareil de l'animal ainsi que les procédures pour les séances de vidéoculographie. De plus, une vidéo illustrative est disponible en ligne (https://www.jove.com/video/59135/long-term-sensory-conflict-in-freely-behaving-mice).

Cet article a été publié en 2019 sur le journal Journal of visualized experiments (JOVE).

Article 3 : Conflit visuo-vestibulaire à long terme chez la souris affecte différemment le regard réflexes stabilisants

La motivation derrière ce projet était de répondre à certaines des questions posées par l'article 1 grâce à l'utilisation du nouveau dispositif VVM (article 2, França de Barros et al 2019).

L'étude précédente portait principalement sur un seul des réflexes de stabilisation du regard, le VOR. En fait, l'OKR a été quantifié dans cet article, mais ce test a été utilisé comme un moyen d'évaluer si les changements appris avec le VVM résidaient sur les floculi. Là, un seul type de stimulation a été utilisé (7,5º / s). Cependant, lors de la réalisation des tests, nous avons remarqué que les réponses OKR étaient parfois qualitativement moins robustes qu'avant la VVM. Cela nous a incités à approfondir nos recherches sur les conséquences du protocole VVM sur l'OKR. Lorsque nous avons effectué de nouveaux tests, nous avons constaté que le protocole d'adaptation avait également un impact sur les réponses OKR par une diminution de 30% de son gain. Par conséquent, OKR a également été inclus dans cette étude.

Les tests de stabilisation du regard réalisés sur l'étude précédente ont été réalisés le jour du retrait de l'appareil. Ainsi, dans cette étude, nous avons cherché à comprendre la force de la persistance des changements appris dans ces réflexes. Pour ce faire, nous avons testé le VOR et l'OKR 1, 2 et 6 jours après le retrait de l'appareil et comparé leurs réponses. Nous avons constaté que les changements VOR persistent pendant au moins 2 jours, tandis que les changements OKR ne persistent pas plus d'un jour.

Puisque les souris se comportent librement sur leurs cages, l'apprentissage moteur est évoqué pour la gamme des mouvements tête / corps naturellement exécutés. Par conséquent, nous avons voulu savoir si le protocole d'adaptation affectait plus une

certaine gamme de fréquences et / ou de vitesses et si ces changements étaient plus labiles pour certains d'entre eux. Par conséquent, en utilisant des stimulations à modulation sinusoïdale, les tests ont été effectués à des gammes de fréquences et de vitesses élevées et basses. Nous avons constaté que les diminutions de VOR et OKR étaient sélectives en fréquence avec des réductions plus importantes pour les fréquences <0,5 Hz. Les tests de stimulation OKR à vitesse constante ont démontré que les composants persistants de l'OKR n'étaient pas modifiés alors que les réponses initiales transitoires l'étaient.

Les protocoles d'adaptation classiques utilisent l'exposition à un motif à contraste élevé pendant les séances d'entraînement pour évoquer un signal d'erreur qui provoquera un flou de l'image sur la rétine et entraînera ainsi l'apprentissage moteur des réflexes de stabilisation du regard. Dans cette étude, nous avons suivi certaines de ces lignes classiques en utilisant un dispositif rayé noir et blanc pour induire l'adaptation.

Néanmoins, nous voulions étudier si le signal d'erreur évoqué par un casque sans contraste provoquerait les mêmes changements qu'un casque à contraste élevé. Nous l'avons fait en appliquant exactement le même dispositif que celui utilisé à l'origine (modèle, article 2. Conflit sensoriel à long terme chez les souris à comportement libre) mais, dans ce groupe, aucune bande n'a été dessinée sur sa surface (sans motif). Bien que le dispositif Pattern soit plus robuste, les réductions étaient largement comparables et récupérées avec une évolution temporelle similaire. Ce résultat suggère que plutôt qu'un signal d'erreur (glissement rétinien), l'absence de rétroaction visuelle semblerait être un responsable le plus probable de la réduction de l'OKR et du VOR.

Globalement, cette étude montre qu'une discordance visuo-vestibulaire à long terme, tout en affectant les deux réflexes de stabilisation du regard, a un impact plus important sur le VOR. De plus, nous montrons des preuves d'une influence sélective en fréquence des signaux visuels dans le réglage des réflexes de stabilisation du regard des souris.

Cet article a été publié en 2020 sur le journal Scientific Reports.

Article 4 : La copie efférente pilotée par le CPG locomoteur couple les mouvements oculaires avec la locomotion des membres antérieurs chez la souris

Des informations visuelles précises sont essentielles dans la vie de la plupart des animaux. Afin de maintenir l'acuité visuelle pendant les mouvements de la tête / du corps, plusieurs entrées sensori-motrices (par exemple vestibulaire, visuelle et proprioceptive)

convergent dans les noyaux du tronc cérébral. À partir de là, une sortie prémotrice sera générée afin que l'œil et / ou la tête puissent être déplacés dans l'espace.

En plus des entrées sensorimotrices susmentionnées, une copie efférente a également été prouvée pour contribuer à minimiser les perturbations visuelles lors de la locomotion chez les têtards Xenopus. Les copies d'efférence sont des répliques neuronales de sorties motrices utilisées pour anticiper les conséquences sensorielles d'une action auto-générée. Ils sont responsables de la coordination des comportements moteurs car ces signaux de réaction intrinsèques générés par un circuit moteur local peuvent influencer un réseau neuronal impliqué dans un autre comportement. Cela a été démontré pour la première fois par l'une des 2 équipes impliquées dans ce projet (Combes et al., 2008 ; Lambert et al., 2012).

Les données in vitro sur le têtard Xenopus ont permis de démêler un nouveau mécanisme de stabilisation du regard qui implique une interaction centrale entre les circuits locomoteurs de la moelle épinière et les noyaux moteurs extraoculaires du tronc cérébral. Ces travaux ont révélé que, lors de la nage ondulatoire, une copie efférente (signalisation prédictive) provenant du CPG locomoteur, assure une première commande interne de stabilisation du regard, indépendante des réflexes visuo-vestibulaires traditionnels (optocinétique et vestibulo-oculaire). Cette copie efférente du schéma locomoteur, conjuguée à la nage, produit des mouvements oculaires conjugués qui compensent l'ondulation de la queue (Bacqué-Cazenave et al., 2018; Combes et al., 2008; Lambert et al., 2012; Uckermann et al., 2013). Ainsi, chez le têtard Xenopus, lors de la locomotion fictive in vitro et en l'absence d'entrées sensorielles, une commande motrice spino-extraoculaire couple l'activité locomotrice CPG aux nerfs moteurs extraoculaires (Combes et al., 2008; Lambert et al., 2012). Cette commande spino-extraoculaire coordonne l'activité rythmique spinale avec l'activité motrice extraoculaire.

Cependant, dans ce modèle, les profils locomoteurs sont spécifiques à l'étape. Par conséquent, après la métamorphose, le processus de stabilisation du regard change des déplacements de la tête gauche-droite pour compenser, à l'âge adulte, en s'appuyant sur les mouvements conjugués binoculaires. Cependant, la présence de ce signal efférent prédictif a été confirmée non seulement chez les têtards mais également au stade de grenouille juvénile. Il est intéressant de noter que les voies neuronales médiatisant ce couplage spino-extraoculaire sont réorganisées de controlatéral à strictement ipsilatéral pendant la métamorphose de l'amphibien afin qu'il puisse générer un mouvement oculaire approprié pour compenser le changement de schéma locomoteur (Uckermann et al., 2013). Dans une approche phylogénétique, et comme le

maintien de l'acuité visuelle est une caractéristique transversale chez les vertébrés, la présence d'une stratégie similaire de stabilisation du regard chez les vertébrés supérieurs peut être émise.

Par conséquent, le présent projet visait à explorer si un signal prédictif, couplant les mouvements oculaires à la locomotion, est présent chez la souris. Cette question a été abordée expérimentalement par des préparations semi-intactes, ex vivo et in vitro.

La première série d'expériences visait à vérifier l'existence de cette copie efférente chez la souris en utilisant la même technique que celle appliquée aux têtards. Ainsi, l'activité des nerfs moteurs de la colonne vertébrale et de l'abducens a été enregistrée simultanément ex vivo dans des préparations isolées de tronc cérébral-moelle épinière de souris néonatales. Une décharge couplée rythmique entre les activités nerveuses motrices du membre et de l'abducens pendant les épisodes de locomotion active a été enregistrée par stimulation électrique et pharmacologique.

Ensuite, une préparation de souris adulte décérébrée précolliculaire et prémammillaire à tête fixe a été utilisée pour démasquer cette copie efférente chez une souris se comportant. Dans cette préparation, les mouvements oculaires ont été enregistrés pendant la locomotion sur un tapis roulant motorisé. En raison de l'absence d'entrées vestibulaires et visuelles au cours de cette expérience, les mouvements oculaires horizontaux enregistrés sont cohérents avec la sortie comportementale d'une copie efférente.

Enfin, la voie neuronale qui couple le CPG cervical et les noyaux abducens a été tracée anatomiquement grâce à l'utilisation du virus de la rage. Les injections ont été effectuées dans le rectus latéral, un muscle responsable des mouvements oculaires horizontaux, et ont cartographié une projection directe des neurones de la moelle épinière cervicale vers le noyau abducens.

En conclusion, avec une approche intégrative multi-méthodologique, cette étude a démontré pour la première fois qu'une copie d'efférence cervicale pilotée par CPG couple directement les mouvements oculaires avec le mouvement des membres antérieurs lors d'une locomotion vigoureuse chez la souris.

Cet article est en cours de finalisation.

Article 5 : La thérapie génique locale restaure durablement la fonction vestibulaire dans un modèle murin du syndrome d'Usher de type 1G

Le syndrome d'Usher est l'une des pathologies héréditaires les plus courantes (autosomique récessive ; prévalence jusqu'à 1/10 000) affectant simultanément la vision, l'audition et l'équilibre (El-Amraoui & Petit, 2014). Il existe 3 types de syndrome d'Usher, mais le plus courant et celui qui présente les plus fortes déficiences vestibulaires est le type 1. Plus précisément, les patients atteints d'USH1 souffrent de surdité profonde congénitale et de dysfonctionnement vestibulaire et plus tard dans la vie, de cécité. Naturellement, la perte visuelle progressive s'accompagne d'une augmentation de la sévérité des symptômes vestibulaires car la vision participe à l'équilibre.

Les mutations du gène USH1 affectent la morphogenèse du faisceau capillaire et le maintien de la liaison de la pointe en général dans l'oreille interne (Friedman et al., 2005) Les liens de pointe sont des filaments d'actine qui relient les pointes des stéréocils plus petits au corps des plus gros voisins. Ils ont un rôle clé dans la génération de messages synaptiques car ils régulent les canaux de transduction mécanoélectrique (MET) au sommet des plus petites stéréocils. Lorsque le mouvement plie le lien de pointe vers les stéréocils, la tension sur le lien de pointe augmente, ce qui entraîne l'ouverture des canaux MET, la dépolarisation de la cellule ciliée et l'augmentation conséquente de la cadence de déclenchement du nerf vestibulaire. Au contraire, si les stéréocils sont éloignés du kinocilium, le lien de pointe réduit sa tension, ce qui fermera le canal MET. Ainsi, hyperpolariser la cellule ciliée, fermer les canaux Ca2 + et diminuer la cadence de tir des afférents vestibulaires. Lorsque les liens de pointe sont manquants ou défectueux, le message synaptique vestibulaire ne peut pas être généré. Les protéines sans sont l'une des trois protéines USH1 qui ancrent les liens de pointe aux stéréocils (El-Amraoui & Petit, 2014).

Bien qu'il s'agisse d'une plainte médicale très courante, le traitement que reçoivent les patients souffrant de vertiges peut être inapproprié ou inadéquat (Bittar et al., 2013). Dans le cas d'Usher1, il n'existe actuellement aucun remède disponible, seuls les symptômes auditifs sont traités avec un implant cochléaire et le succès est variable d'un patient à l'autre. Les laboratoires de recherche se concentrent désormais sur la résolution de ce problème en utilisant les dernières technologies disponibles, telles que le transfert de gène induit par un virus adéno-associé (AAV). L'oreille interne est une zone qui peut être ciblée spécifiquement et en toute sécurité avec des injections en raison de son isolement relatif et de sa dissémination systémique. De plus, en raison de

la similitude entre l'anatomie de l'oreille interne et système vestibulaire entre souris et humains, ces outils pourraient servir de patients potentiels USH1. Même si le transfert de gène médié par l'AAV est actuellement testé chez des patients atteints de la maladie de Parkinson et de la rétine, ils n'ont pas encore été utilisés dans les troubles de l'oreille interne (Hudry et Vandenberghe, 2019).

Les AAV sont actuellement en train de devenir l'outil de thérapie génique de choix. Il a d'abord été identifié car il contamina souvent des préparations d'adénovirus de laboratoire, d'où sa désignation. Les AAV appartiennent à la famille des Parvoviridae et consistent en une capside protéique icosaédrique non enveloppée (sans enveloppe phospholipidique) entourant et portant un petit ADN simple brin (4,8 kilos de bases) (Naso et al., 2017). Pour sa réplication réussie, il nécessite une co-infection par un virus auxiliaire comme l'adénovirus ou le virus de l'herpès. Dans cette étude, l'ADNc murin, sans, correspondant au transcrit épissé d'Ushlg avec la séquence d'ADNc de la GFP a été inséré dans la capside d'AAV8. Le fluorescent signalé a été ajouté de sorte que le. Les AAV sont endémiques chez l'homme et ont une très faible pathogénicité avec une réponse immunitaire très légère.

Dans notre étude, la thérapie génique médiée par l'AAV visait à restaurer les protéines sans protéines, des protéines d'échafaudage sous-membranaire impliquées dans la délivrance d'ADNc. Les protéines sans sont essentielles dans le maintien des faisceaux de cellules ciliées et des liaisons de pointe et sont l'une des principales protéines affectées dans cette pathologie. Étant donné que ces protéines sont omniprésentes dans le neuroépithélium de l'oreille interne, leur restauration permettrait non seulement de traiter la surdité, mais également de retrouver les fonctions vestibulaires qui sont altérées dans cette maladie.

Après l'injection du ADNc par AAV8 chez des souris nouveau-nées, les effets sur le système auditif et vestibulaire ont été testés chez des souris adultes. Le premier test effectué portait sur les réponses auditives qui démontraient un sauvetage auditif partiel (5-15 kHz). Cependant, la question de savoir si la fonction vestibulaire a été restaurée est restée ouverte. Les souris ont démontré un comportement locomoteur amélioré, mais aucun test spécifique vestibulaire n'avait été effectué. Notre équipe s'est attaquée à cette question en phénotypant les organes vestibulaires complets à l'aide de la vidéo-oculographie. Les canaux semi-circulaires ont été évalués en utilisant le test du réflexe vestibulo-oculaire (VOR) et les organes otolithiques par les réponses du réflexe maculo-oculaire (MOR) chez les souris USH1 - / -, traitées USH1 - / - et témoins (total de 15 souris, 5 par groupe). Le test de rotation hors axe vertical (OVAR) a permis d'évaluer la

détection de l'accélération linéaire par les organes otolithiques. Les tests OVAR exigent que le plateau tournant soit incliné à 17 °par rapport à l'axe vertical et consiste en des rotations à vitesse constante dans le sens horaire et antihoraire. Les premières rotations provoquent à la fois des réponses canalaires et otolithiques mais il ne reste que la composante otolithique après les premières stimulations et permettent d'isoler la réponse de la macula à l'accélération (Beraneck et al., 2012).

Il était frappant d'enregistrer l'absence complète de mouvements oculaires compensatoires chez les souris USH1 - / - pendant toute la gamme des tests effectués : VOR (30º / s à 0,1 - 2Hz) et OVAR (50º / s). Dans le groupe traité USH1 - / -, 2/5 des souris avaient complètement récupéré les réponses otolithiques et canalaires et 3/5 avaient complètement récupéré les réponses semi-circulaires mais pas otolithiques. Fait intéressant, les souris injectées ont reçu un traitement à P3 et n'ont été testées que pour les réponses vestibulaires (et auditives) 10 à 12 mois après. Ainsi, montrer que le traitement, en plus d'être efficace, est durable. Notre contribution à cet article a été essentielle car elle a fourni la preuve quantitative définitive de la récupération comportementale spécifique de la fonction vestibulaire, et donc de l'efficacité du traitement.

Plusieurs thérapies médiées par l'AAV font actuellement l'objet d'essais cliniques en cours pour potentiellement guérir plusieurs maladies, par exemple les troubles neuromusculaires et (Aguti et al., 2018) neurodégénératifs (Hudry & Vandenberghe, 2019). Cependant, les maladies de l’oreille interne ne figurent pas encore sur cette liste. Des études comme celle-ci pourraient représenter l'espoir que les traitements médiés par l'AAV deviennent des outils récurrents pour guérir les maladies de l'oreille interne.

Cet article a été publié en 2019 dans le journal Proceedings of the National Academy of Sciences of the United States of America (PNAS).

Conclusion

Dans cette thèse, la stabilisation du regard chez la souris a été étudiée en expérimentant sur deux voies classiques, les voies optocinétiques et vestibulo-oculaires, et en déchiffrant une nouvelle voie de la moelle épinière cervicale au tronc cérébral où une copie efférente prédictive est relayée. En utilisant une approche multiméthodologique, cette thèse vise à comprendre comment le cerveau combine différentes entrées sensori-motrices pour assurer l'homéostasie de la stabilisation du regard dans différents contextes.

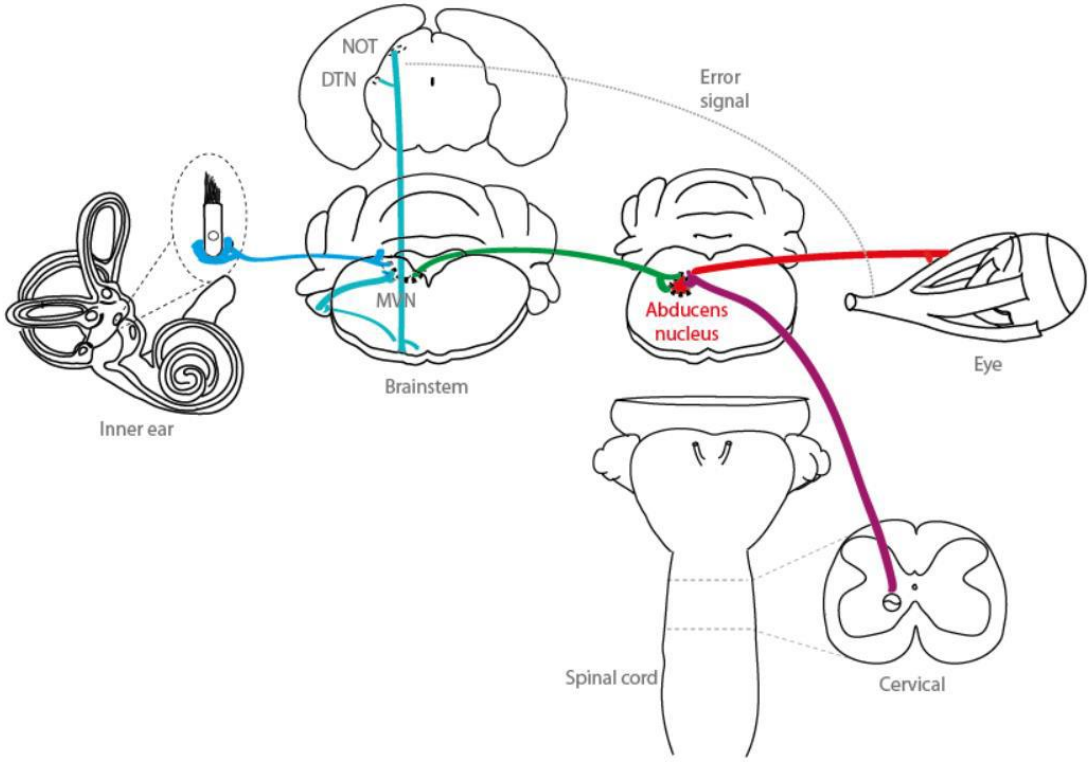

Figure 1. Schéma conceptuel des parcours étudiés dans cette thèse. VOR (ligne bleu clair et verte), OKR (lignes turquoise et verte), copie efférente des CPG locomoteurs (ligne violette) convergent sur les abducens noyau (rouge) pour qu'une commande prémotrice qui déplacera l'œil puisse être générée.

L'un des principaux objectifs était d'étudier comment les entrées visuelles et vestibulaires se complètent, et comment le cerveau s'adapte à des signaux sensoriels conflictuels. Nous voulions comprendre les effets d'une perturbation de discordance visuo-vestibulaire à long terme sur les réflexes de stabilisation du regard (OKR et VOR). Nous l'avons fait en utilisant un protocole innovant d'inadéquation visuo-vestibulaire (VVM) conçu par mon équipe où les souris ont un appareil en forme de casque fixé sur leur tête pendant 14 jours. Tout d'abord, avec ce protocole VVM, nous avons cherché à

quantifier la diminution du VOR ainsi qu'à étudier les mécanismes neuronaux de cette réduction (article 1). Pour y parvenir, nous avons utilisé l'électrophysiologie patch-clamp ainsi que des expériences de vidéo-oculographie. En raison de la polyvalence de ce protocole, nous nous sommes sentis obligés de partager la méthodologie détaillée pour son utilisation pour d'autres études (article 2).

Pour la dernière étude de ce projet, nous avons cherché à étudier l'influence des signaux visuels dans le réglage des réflexes de stabilisation du regard de la souris (article 3. Inadéquation visuo-vestibulaire à long terme chez des souris au comportement libre affecte différemment les réflexes de stabilisation du regard). Pour ce faire, nous avons étudié les conséquences de la VVM sur : 1) les réponses OKR; 2) la cinématique de l'OKR et du VOR jusqu'à 10 jours après le retrait de l'appareil (période de récupération); 3) la dépendance en fréquence de la récupération des réponses et 4) la comparaison entre la récupération d'OKR et de VOR.

Le deuxième projet de ma thèse étudie comment ces voies sensorielles pourraient, dans le contexte d'un comportement actif, être soutenues par une signalisation motrice prédictive non sensorielle. Dans cette étude, nous défions la compréhension traditionnelle selon laquelle la stabilisation du regard pendant la locomotion est exclusivement atteinte par des entrées sensorielles. Plus précisément, cette thèse visait à déchiffrer et à caractériser l'existence d'une voie spino-extraoculaire qui minimise les perturbations visuelles lors de la locomotion chez la souris. Les expériences réalisées pour ce projet étaient une collaboration entre 3 équipes à travers la France (Bordeaux, Marseille et Paris) qui a permis l'utilisation d'un éventail de techniques différentes (préparations semi-intactes, enregistrements ex vivo et in vivo). Les résultats de ce projet sont présentés dans Article 4. La copie efférente entraînée par CPG locomotrice couple les mouvements oculaires avec la locomotion des membres antérieurs chez la souris.

L'expertise acquise au cours de ces projets de recherche fondamentale a été appliquée dans une étude collaborative visant à traiter les troubles auditifs et vestibulaires à l'aide de la thérapie génique à virus adéno-associé (AAV). Ici, nous avons mesuré les mouvements oculaires compensatoires chez les souris de type 1 (USH1) traitées par AAV et non traitées avec le syndrome d'Usher. Comme leurs homologues humains, les souris USH1 souffrent de surdité congénitale profonde et de troubles de l'équilibre. Grâce à la vidéo-oculographie, nous avons pu évaluer le succès de ce traitement en mesurant leur fonction vestibulaire. Des études comme celle-ci aideront à explorer de nouvelles possibilités de traitement des pathologies de l'oreille interne.

Références

Aguti, S., Malerba, A., & Zhou, H. (2018). The progress of AAV-mediated gene therapy in neuromuscular disorders. *Expert Opinion on Biological Therapy*, *18*(6), 681–693. https://doi.org/10.1080/14712598.2018.1479739

Bacqué-Cazenave, J., Courtand, G., Beraneck, M., Lambert, F. M., & Combes, D. (2018). Temporal Relationship of Ocular and Tail Segmental Movements Underlying Locomotor-Induced Gaze Stabilization During Undulatory Swimming in Larval Xenopus. *Frontiers in Neural Circuits*, *12*, 95. https://doi.org/10.3389/fncir.2018.00095

Beraneck, M., Bojados, M., Le Séac'h, A., Jamon, M., & Vidal, P.-P. (2012). Ontogeny of Mouse Vestibulo-Ocular Reflex Following Genetic or Environmental Alteration of Gravity Sensing. *PLoS ONE*, *7*(7), e40414. https://doi.org/10.1371/journal.pone.0040414

Bittar, R. S. M., Oiticica, J., Bottino, M. A., Ganança, F. F., Dimitrov, R., Bittar, R. S. M., Oiticica, J., Bottino, M. A., Ganança, F. F., & Dimitrov, R. (2013). Population epidemiological study on the prevalence of dizziness in the city of São Paulo. *Brazilian Journal of Otorhinolaryngology*, *79*(6), 688–698. https://doi.org/10.5935/1808-8694.20130127

Carcaud, J., França de Barros, F., Idoux, E., Eugène, D., Reveret, L., Moore, L. E., Vidal, P.-P., & Beraneck, M. (2017). Long-Lasting Visuo-Vestibular Mismatch in Freely-Behaving Mice Reduces the Vestibulo-Ocular Reflex and Leads to Neural Changes in the Direct Vestibular Pathway. *ENeuro*, *4*(1). https://doi.org/10.1523/ENEURO.0290-16.2017

Combes, D., Le Ray, D., Lambert, F. M., Simmers, J., & Straka, H. (2008). An intrinsic feed-forward mechanism for vertebrate gaze stabilization. *Current Biology*, *18*(6), R241–R243. https://doi.org/10.1016/j.cub.2008.02.018

El-Amraoui, A., & Petit, C. (2014). The retinal phenotype of Usher syndrome: Pathophysiological insights from animal models. *Comptes Rendus Biologies*, *337*(3), 167–177. https://doi.org/10.1016/j.crvi.2013.12.004

França de Barros, F., Carcaud, J., & Beraneck, M. (2019). Long-term Sensory Conflict in Freely Behaving Mice. *Journal of Visualized Experiments: JoVE*, *144*. https://doi.org/10.3791/59135

França de Barros, F., Schenberg, L., Tagliabue, M., & Beraneck, M. (2020). Long term visuo-vestibular mismatch in freely behaving mice differentially affects gaze stabilizing reflexes. *Scientific Reports*, *10*(1), 20018. https://doi.org/10.1038/s41598-020-77026-w

Friedman, T. B., Schultz, J. M., & Ahmed, Z. M. (2005). Usher syndrome type 1: Genotype-phenotype relationships. *Retina (Philadelphia, Pa.)*, *25*(8 Suppl), S40–S42. https://doi.org/10.1097/00006982-200512001-00016

Hudry, E., & Vandenberghe, L. H. (2019). Therapeutic AAV Gene Transfer to the Nervous System: A Clinical Reality. *Neuron*, *101*(5), 839–862. https://doi.org/10.1016/j.neuron.2019.02.017

Lambert, F. M., Combes, D., Simmers, J., & Straka, H. (2012). Gaze Stabilization by Efference Copy Signaling without Sensory Feedback during Vertebrate Locomotion. *Current Biology*, *22*(18), 1649–1658. https://doi.org/10.1016/j.cub.2012.07.019

Naso, M. F., Tomkowicz, B., Perry, W. L., & Strohl, W. R. (2017). Adeno-Associated Virus (AAV) as a Vector for Gene Therapy. *BioDrugs*, *31*(4), 317–334. https://doi.org/10.1007/s40259-017-0234-5

Uckermann, G. von, Ray, D. L., Combes, D., Straka, H., & Simmers, J. (2013). Spinal Efference Copy Signaling and Gaze Stabilization during Locomotion in Juvenile Xenopus Frogs. *Journal of Neuroscience*, *33*(10), 4253–4264. https://doi.org/10.1523/JNEUROSCI.4521-12.2013

Dernière page